DISCLAIMER NOTICE

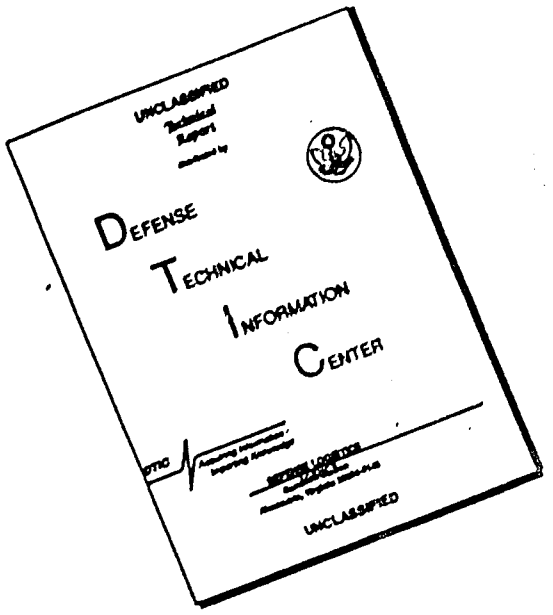

THIS DOCUMENT IS BEST QUALITY AVAILABLE. THE COPY FURNISHED TO DTIC CONTAINED A SIGNIFICANT NUMBER OF PAGES WHICH DO NOT REPRODUCE LEGIBLY.

ASD-TDR-62-728
PART 1

DESIGN CRITERIA FOR HIGH-SPEED POWER-TRANSMISSION SHAFTS

Part 1. Analysis of Critical Speed Effects and Damper Support Location

TECHNICAL DOCUMENTARY REPORT NO. ASD-TDR-62-728
PART 1

January 1963

Flight Accessories Laboratory
Directorate of Aeromechanics
Aeronautical Systems Division
Air Force Systems Command
Wright-Patterson Air Force Base, Ohio

Project No. 8128, Task No. 812802

(Prepared under Contract No. AF 33(616)-8290
by the Battelle Memorial Institute, Columbus 1, Ohio;
R. G. Dubensky, C. C. Mellor, Jr., and J. E. Voorhees, authors)

FOR ERRATA

AD 299 027

THE FOLLOWING PAGES ARE CHANGES

TO BASIC DOCUMENT

Battelle Memorial Institute

505 KING AVENUE COLUMBUS 1, OHIO

AREA CODE 614, TELEPHONE 299-3191

June 20, 1963

Defense Documentation Center
Arlington Hall Station
Arlington 12, Virginia

Gentlemen:

Enclosed are errata sheets prepared for "Design Criteria for High-Speed Power-Transmission Shafts", Part 1, Analysis of Critical Speed Effects and Damper Support Location, Technical Documentary Report No. ASD-TDR-62-728, Part 1, August 1962. All organizations on the distribution list furnished to Battelle Memorial Institute have been sent copies of the errata.

Very truly yours,

John E Voorhees

John E. Voorhees
Group Director
Machine Dynamics

JEV:jb

Encs.

Errata Sheet

for

"Design Criteria for High-Speed Power-Transmission Shafts"

Part 1. Analysis of Critical Speed Effects and Damper Support Location.

Technical Documentary Report No. ASD-TDR-62-728

Part 1, August 1962.

The first phase report of a research program titled "Design Criteria for High-Speed Power Transmission Shafts" was issued in December, 1962. This report is titled "Part 1. Analysis of Critical Speed Effects and Damper Support Location" and is designated as Technical Documentary Report No. ASD-TDR-62-728, Part 1. It was prepared under Contract No. AF 33(616)-8290, and was Project No. 8128, Task No. 812802. Since this report was issued, the following Errata has been compiled.

ERRATA

(1) Page XIV, Line 11; Add X

(2) Page XV, Line 3; Add k

(3) Page 10, Equation (14); should be

$$\frac{\text{rpm}_{\text{tube}}}{\text{rpm}_{\text{solid}}} = \frac{\sqrt{D^2 + d^2}}{\left(\frac{D^4 - d^4}{D}\right)^{1/3}}$$

(4) Page 14, Equation (16); should be

$$W_s = \frac{\pi}{4} (D^2 - d^2) \text{ LP, lb.}$$

(5) Page 42, Figure 15; Change to Figure 16.

(6) Page 49, Figure 16; Change to Figure 15.

(7) Page 73, Equation (103); should be

$$H = \alpha_k$$

(8) Page 95, Equation (111); should be

$$C_c = 2\sqrt{\frac{WK}{g}}$$

(9) Page 137, Line 10; Change from rev/sec to revolutions per minute.

NOTICES

When Government drawings, specifications, or other data are used for any purpose other than in connection with a definitely related Government procurement operation, the United States Government thereby incurs no responsibility nor any obligation whatsoever; and the fact that the Government may have formulated, furnished, or in any way supplied the said drawings, specifications, or other data, is not to be regarded by implication or otherwise as in any manner licensing the holder or any other person or corporation, or conveying any rights or permission to manufacture, use, or sell any patented invention that may in any way be related thereto.

Qualified requesters may obtain copies of this report from the Armed Services Technical Information Agency, (ASTIA), Arlington Hall Station, Arlington 12, Virginia.

This report has been released to the Office of Technical Services, U.S. Department of Commerce, Washington 25, D.C., in stock quantities for sale to the general public.

Copies of this report should not be returned to the Aeronautical Systems Division unless return is required by security considerations, contractual obligations, or notice on a specific document.

B

22-515M, 200, 3-19-63

Aeronautical Systems Division, Dir/Aeromechanics, Flight Accessories Lab, Wright-Patterson AFB, Ohio.
Rpt Nr ASD-TDR-62-728, Part I. DESIGN CRITERIA FOR HIGH-SPEED POWER-TRANSMISSION SHAFTS: Analysis of Critical Speed Effects and Damper Support Location. Final report, Jan 63, 161p incl illus., tables, 16 refs.
Unclassified Report

Repeated successful operation of high-speed power-transmission shafts at and far above their first critical speeds has been achieved. A basic new analytical technique for the design and analysis of high-speed shafting has been developed using electrical transmission line theory. Limited experimental work has shown the technique to predict successfully the damper parameters necessary to high-speed shaft operation. Equations relating full-scale and model shaft configurations to produce similar dynamic behavior have been formulated. The experimental application of torque on high-speed shafting did not change lateral critical speed. This is not in agreement with theory, which predicts a decrease in critical speed. Damping coatings applied continuously along the length of high-speed shafts controlled vibration amplitudes to a slight degree at the lowest critical speeds. At higher order criticals the coatings had no desirable effects.

(over)

1. Shafts
2. Power transmissions
I. Project 8128, Task 812802
II. Contract AF 33 (616)-8290
III. Battelle Memorial Institute, Columbus, Ohio
IV. R. G. Dubensky, C. C. Mellor, Jr., J. E. Vorhees
V. Secondary Rpt Nr G-4869
VI. Aval fr CTS
VII. In ASTIA collection

Aeronautical Systems Division, Dir/Aeromechanics, Flight Accessories Lab, Wright-Patterson AFB, Ohio.
Rpt Nr ASD-TDR-62-728, Part I. DESIGN CRITERIA FOR HIGH-SPEED POWER-TRANSMISSION SHAFTS: Analysis of Critical Speed Effects and Damper Support Location. Final report, Jan 63, 161p incl illus., tables, 16 refs.
Unclassified Report

Repeated successful operation of high-speed power-transmission shafts at and far above their first critical speeds has been achieved. A basic new analytical technique for the design and analysis of high-speed shafting has been developed using electrical transmission line theory. Limited experimental work has shown the technique to predict successfully the damper parameters necessary to high-speed shaft operation. Equations relating full-scale and model shaft configurations to produce similar dynamic behavior have been formulated. The experimental application of torque on high-speed shafting did not change lateral critical speed. This is not in agreement with theory, which predicts a decrease in critical speed. Damping coatings applied continuously along the length of high-speed shafts controlled vibration amplitudes to a slight degree at the lowest critical speeds. At higher order criticals the coatings had no desirable effects.

(over)

1. Shafts
2. Power transmissions
I. Project 8128, Task 812802
II. Contract AF 33 (616)-8290
III. Battelle Memorial Institute, Columbus, Ohio
IV. R. G. Dubensky, C. C. Mellor, Jr., J. E. Vorhees
V. Secondary Rpt Nr G-4869
VI. Aval fr CTS
VII. In ASTIA collection

Aeronautical Systems Division, Dir/Aeromechanics, Flight Accessories Lab, Wright-Patterson AFB, Ohio.
Rpt Nr ASD-TDR-62-728, Part I. DESIGN CRITERIA FOR HIGH-SPEED POWER-TRANSMISSION SHAFTS: Analysis of Critical Speed Effects and Damper Support Location. Final report, Jan 63, 161p incl illus., tables, 16 refs.
Unclassified Report

Repeated successful operation of high-speed power-transmission shafts at and far above their first critical speeds has been achieved. A basic new analytical technique for the design and analysis of high-speed shafting has been developed using electrical

(over)

transmission line theory. Limited experimental work has shown the technique to predict successfully the damper parameters necessary to high-speed shaft operation. Equations relating full-scale and model shaft configurations to produce similar dynamic behavior have been formulated. The experimental application of torque on high-speed shafting did not change lateral critical speed. This is not in agreement with theory, which predicts a decrease in critical speed. Damping coatings applied continuously along the length of high-speed shafts controlled vibration amplitudes to a slight degree at the lowest critical speeds. At higher order criticals the coatings had no desirable effects.

1. Shafts
2. Power transmissions
I. Project 8128, Task 812802
II. Contract AF 33 (616)-8290
III. Battelle Memorial Institute, Columbus, Ohio
IV. R. G. Dubensky, C. G. Mellor, Jr., J. E. Vorhees
V. Secondary Rpt Nr G-4869
VI. Aval fr CTS
VII. In ASTIA collection

Aeronautical Systems Division, Dir/Aeromechanics, Flight Accessories Lab, Wright-Patterson AFB, Ohio.
Rpt Nr ASD-TDR-62-728, Part I. DESIGN CRITERIA FOR HIGH-SPEED POWER-TRANSMISSION SHAFTS: Analysis of Critical Speed Effects and Damper Support Location. Final report, Jan 63, 161p incl illus., tables, 16 refs.
Unclassified Report

Repeated successful operation of high-speed power-transmission shafts at and far above their first critical speeds has been achieved. A basic new analytical technique for the design and analysis of high-speed shafting has been developed using electrical

(over)

transmission line theory. Limited experimental work has shown the technique to predict successfully the damper parameters necessary to high-speed shaft operation. Equations relating full-scale and model shaft configurations to produce similar dynamic behavior have been formulated. The experimental application of torque on high-speed shafting did not change lateral critical speed. This is not in agreement with theory, which predicts a decrease in critical speed. Damping coatings applied continuously along the length of high-speed shafts controlled vibration amplitudes to a slight degree at the lowest critical speeds. At higher order criticals the coatings had no desirable effects.

1. Shafts
2. Power transmissions
I. Project 8128, Task 812802
II. Contract AF 33 (616)-8290
III. Battelle Memorial Institute, Columbus, Ohio
IV. R. G. Dubensky, C. G. Mellor, Jr., J. E. Vorhees
V. Secondary Rpt Nr G-4869
VI. Aval fr CTS
VII. In ASTIA collection

FOREWORD

This report was prepared by Battelle Memorial Institute, Columbus, Ohio, on Air Force Contract AF 33(616)-8290, under Task No. 812802 of Project No. 8128, "Design Criteria for High-Speed Power-Transmission Shafts". The work was administered under the direction of Flight Accessories Laboratory, Aeronautical Systems Division. Mr. Bruce P. Brooks was project engineer for the laboratory.

The studies presented began in May, 1961, and were concluded in July, 1962. Group Director John E. Voorhees was the engineer responsible for research activity of Battelle Memorial Institute.

This report is the Final Technical Report of Phase I activities. The contractor's report number is G-4869.

This report is unclassified.

ABSTRACT

Repeated successful operation of high-speed power-transmission shafts at and far above their first critical speeds has been achieved. A basic new analytical technique for the design and analysis of high-speed shafting has been developed using electrical transmission line theory. Limited experimental work has shown the technique to predict successfully the damper parameters necessary to high-speed shaft operation. Equations relating full-scale and model shaft configurations to produce similar dynamic behavior have been formulated. The experimental application of torque on high-speed shafting did not change lateral critical speed. This is not in agreement with theory, which predicts a decrease in critical speed. Damping coatings applied continuously along the length of high-speed shafts controlled vibration amplitudes to a slight degree at the lowest critical speeds. At higher order criticals the coatings had no desirable effects.

TABLE OF CONTENTS

TABLE OF CONTENTS
(Continued)

TABLE OF CONTENTS
(Continued)

LIST OF ILLUSTRATIONS

LIST OF ILLUSTRATIONS
(Continued)

LIST OF ILLUSTRATIONS
(Continued)

LIST OF ILLUSTRATIONS
(Continued)

LIST OF ILLUSTRATIONS
(Continued)

LIST OF TABLES

LIST OF SYMBOLS

A = area, $in.^2$

A^* = torque constant, dimensionless

$B_{1, 2, etc.}$ = constants

B^* = force constant, dimensionless

C = damping value, lb-sec/in.

C_c = critical damping value, lb-sec/in.

C_e = unit capacitance

C_s = characteristic shaft critical damping value, lb-sec/in.

C^* = frequency constant, dimensionless

D = outside diameter, in.

D_s = diameter of a solid shaft which is torsionally of equal strength as a tubular shaft of given dimensions, in.

E = modulus of elasticity, $lb/in.^2$

F = force, lb

F_s = characteristic shaft unbalance, lb

G = shear modulus of elasticity, $lb/in.^2$

H = dimensionless parameter

I = section moment of inertia, $in.^4$

K = spring rate, lb/in.

K_s = characteristic shaft lateral stiffness, lb/in.

L = over-all shaft length, in.

L_e = unit inductance

M = moment, lb-in.

N = shaft speed, rpm

N = ratio of modulus of elasticity to shear yield stress, dimensionless

P = density, $lb/in.^3$

LIST OF SYMBOLS
(Continued)

O = constant

R = crank throw, in.

S_s = shear stress, lb/in.^{2}

S_{se} = endurance limit stress in shear, lb/in.^{2}

S_{sy} = shear yield stress, lb/in.^{2}

T = torque, in-lb

V = shear force, lb

W = weight, lb

W_s = characteristic shaft weight, lb

X = support or node position

$$= \frac{\text{shaft length between support or node and shaft end, in.}}{\text{over-all shaft length, in.}}$$

$\mathbf{X}$ = a function of length

Z_s = characteristic shaft impedance

Z^* = polar section modulus = $\frac{4I}{D}$, in.^{3}

a_c = centrifugal force constant, lb/in.

b_c = damping constant, lb/in.

c = critical speed proportionality constant

d = inside diameter, in.

e = eccentricity, in.

f = frequency, cps

f_c = influence coefficient, 1/lb

g = acceleration of gravity, 386 in./sec^2

h = number of equal-length spans in a multisupported shaft

h_c = deflection influence coefficient for shear force, in./lb

i = number of the vibration speed in the critical speed sequence where shaft span lengths are equal

LIST OF SYMBOLS
(Continued)

j = $\sqrt{-1}$

k = geometric factor relating span lengths of multisupported shafts

$$= \frac{\text{shaft length between most closely spaced supports, in.}}{\text{shaft length between next most closely spaced supports, in.}}$$

k = numerical index when used as a subscript

ℓ = shaft length between supports, in.

ℓ_c = shaft length between computer stations, in.

m = mass, lb-sec^2/in.

m_u = mass per unit length of shaft, lb-sec^2/in.^{2}

n = number of principal mode of vibration

n_i = critical speed proportionality constant where shaft span lengths are equal

p_c = support weight constant, lb/in.

q_c = slope influence coefficient for a moment, 1/in-lb

r = number of computer calculation stations

t = time, sec

v = velocity, in./sec

w = unit weight of shaft, lb/in.

x = position along shaft, in.

y = deflection, in.

y_s = shaker deflection, in.

α = torque function, dimensionless

β = frequency function, dimensionless

f_{ck} = inertia force constant, lb/in.

λ = wavelength, in.

ϕ = slope of deflected shaft, rad

ω = shaft critical speed, rad/sec

ω^*	= shaft critical speed with external load, rad/sec
ω_s	= characteristic shaft natural frequency, rad/sec
θ	= angular windup in total shaft length, degrees
cpm	= cycles per minute
cps	= cycles per second
hp	= horsepower
hp_s	= characteristic shaft power transmission ability, horsepower
rpm	= revolutions per minute
rps	= revolutions per second
(VSWR)	= Voltage Standing Wave Ratio

INTRODUCTION AND SUMMARY

In connection with the need for light-weight components in military helicopters and STOL and VTOL aircraft, a research program sponsored by the Aeronautical Systems Division has been conducted by Battelle to determine the merits of hypercritical-speed power-transmission shafts. The research program has produced considerable information which confirms the feasibility of such shafts, and relates their design to practical applications.

For any rotating shaft there exists a series of discrete speeds at which the centrifugal force resulting from unbalance causes progressively greater shaft deflection. The elastic restoring forces developed as the shaft deflects are overcome by the centrifugal force developed by the deflected shaft. Extremely large deflections and even destruction of the shaft and its bearings can result from operation at these speeds, called critical speeds. For this reason designers of power-transmission equipment normally avoid the problem by operating shafts below their first critical speed.

There are of course, disadvantages to restricting operation to below the first critical speed. For transmitting a given horsepower, torque and consequently shaft size must be increased as operating speed is reduced. In case of long shafts, the shaft size may be increased above that size required to transmit the torque simply to raise the first critical speed above the operating speed range. Alternatively, the shaft size may be determined by the torque loading, but additional bearings may be installed to support the shaft and thereby raise its first critical speed. The major disadvantage of these conventional practices applied to aircraft is the weight penalty.

The research program has shown that shafting can be operated consistently far above its first critical speed, with consequent savings in shaft and support weight, through the use of one or two damped supports. Methods have been developed to predict necessary damping values and support locations to provide satisfactory operation at any range of speed at and above the first critical. Methods are also included to relate the parameters which provide good operation of one shaft to any other shaft, no matter what the shaft dimensions or material. In short, hypercritical-speed shafting, with its associated advantage in weight, is a very practical and feasible means of transmitting power. With today's high-speed power sources it is especially attractive, since considerable weight could be pared from engines and gearing by transmitting power at the same speed as it is produced.

Manuscript released by the authors July 1962 for publication as an ASD Technical Documentary Report.

TECHNICAL WORK

Relationships Between Power, Speed, Torque, Shaft Size, and Critical Speed

Solid Shafts

The power-transmission properties of high-speed-shaft sizes studied in this research program can be most easily visualized upon consideration of some basic relationships.

Torque transmitted by a shaft is given by:

$$T = \frac{\pi D^3 S_s}{16}, \tag{1}$$

where

T = torque, in-lb

S_s = shear stress, psi

D = shaft diameter, in.

Horsepower transmitted by a shaft is given by:

$$hp = \frac{2\pi\, T(rpm)}{12 \times 33{,}000}, \tag{2}$$

where

hp = horsepower

(rpm) = revolutions per minute.

Substituting Equation (1) in Equation (2) gives

$$hp = \frac{2\pi^2 S_s\, (rpm) D^3}{12 \times 16 \times 33{,}000}. \tag{3}$$

This relationship may be further simplified if a given stress level is assumed. For high-quality, heat-treated steel shafting the highest torsional endurance limit that may be expected is around 50,000 psi. Substituting this value for S_s in Equation (3) gives the following result:

$$hp = 0.1557(rpm)D^3. \tag{4}$$

In Figure 1 the above relationship between shaft diameter and speed is shown for various horsepowers. It may be seen from this figure that relatively small-diameter shafts will transmit large powers at high speeds. The area in the figure bounded by the solid heavy line denotes the range of speed and shaft diameters for which the shaft test machine was designed. By interpolating between the constant horsepower lines it is seen that a 0.5-inch-diameter shaft running at 50,000 rpm can transmit nearly 1000 horsepower.

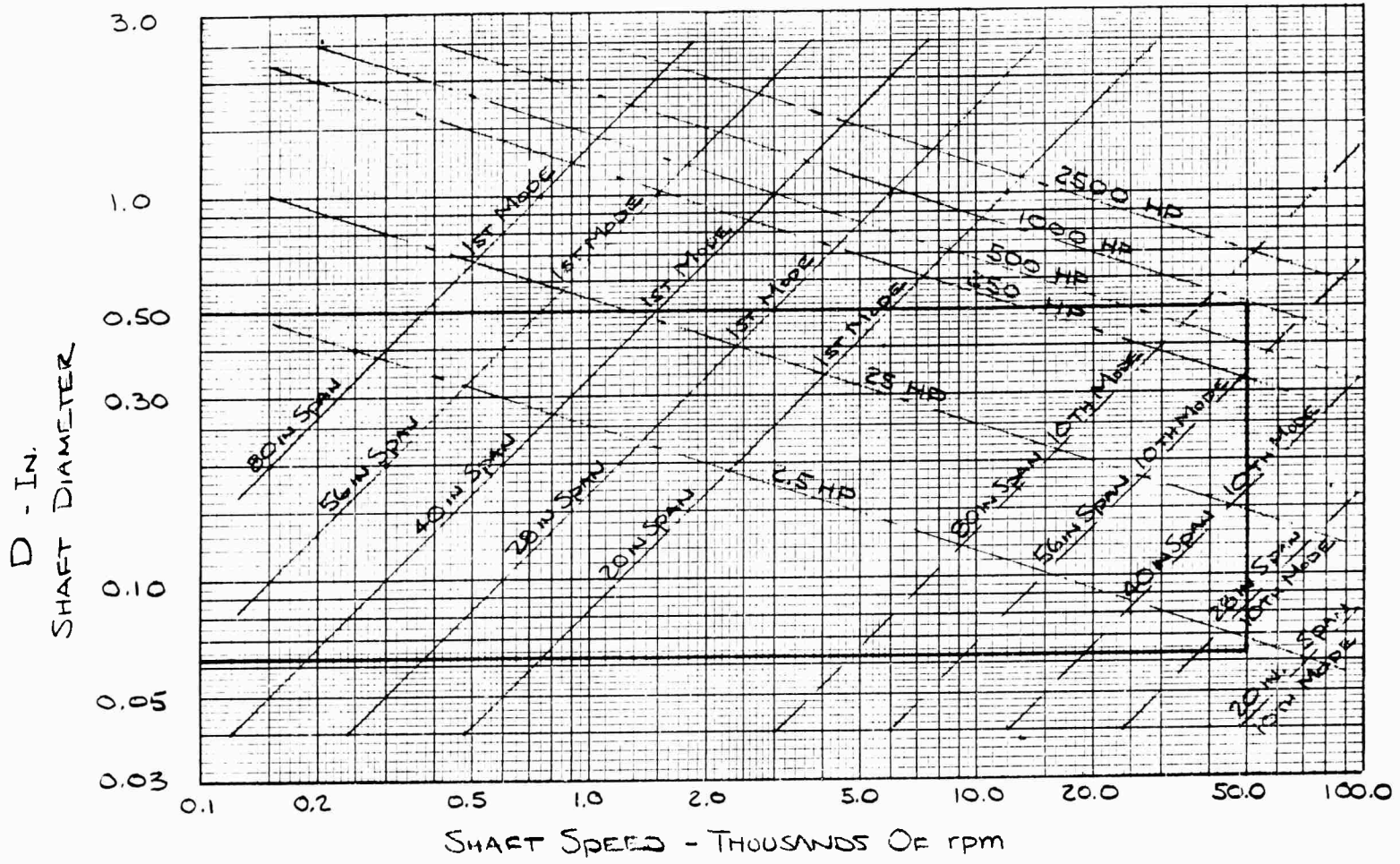

FIGURE 1. RELATIONSHIP BETWEEN SHAFT DIAMETER, SHAFT SPEED, SUPPORT SPACING, AND HORSEPOWER FOR A SINGLE-SPAN SHAFT OR A CONTINUOUS SHAFT ON FLEXIBLY SUPPORTED BEARINGS

Transmitting large horsepowers with small-diameter shafts presents the problem of controlling shaft vibration at the critical speeds. The shaft speed at which the first principal mode of vibration or first critical speed would occur can be calculated from the following equation [Ref. (1)]*:

$$\text{rpm} = 60 \times 1.57\sqrt{\frac{gEI}{w\ell^4}} = 60 \times 1.57\sqrt{\frac{386E}{\ell^4}\,\frac{\pi D^4}{64}\,\frac{4}{\pi D^2}\,\frac{1}{P}} = \frac{467D}{\ell^2}\sqrt{\frac{E}{P}}, \qquad (5)$$

where

g = acceleration of gravity, 386 in./sec^2

E = modulus of elasticity, lb/in.^{2} (30×10^6 for steel)

I = section moment of inertia, in.^{4}

w = unit weight of shaft, lb/in.

ℓ = shaft length between supports, in.

P = shaft density, lb/in.^{3} (0.283 for steel).

For a steel shaft, Equation (5) may be reduced to the following:

$$\text{rpm} = \frac{4.8 \times 10^6 D}{\ell^2}. \qquad (6)$$

Equation (6) gives the first critical speed of a simply supported shaft or a continuous shaft on equally spaced simple bearing supports for any shaft diameter and length. Solutions of this equation for various spans between bearings are plotted in solid lines on Figure 1. The second principal mode of vibration of the shaft would occur at a speed four times that computed from Equation (6). The third principal mode of vibration would occur at a speed nine times that computed using Equation (6), and the nth principal mode of vibration would occur at a speed n^2 times the speed computed from Equation (6). It can be seen, therefore, that a whole family of curves for higher modes of vibration would exist for each curve plotted in solid lines on Figure 1. Besides the curves representing the first principal mode of vibration, only the curves for the tenth principal mode are shown in dotted lines to prevent confusion.

Referring to Figure 1, a 0.5-inch-diameter shaft turning at 50,000 rpm would be running at the tenth critical speed, if the span length between bearings were approximately 70 inches. As mentioned, nearly 1000 horsepower could be transmitted by such a shaft. But without suitable means to damp lateral vibrations the shaft would be useless, unless ten or more intermediate supports were installed to decrease the span length to below that of the first critical speed.

For a simply supported steel shaft, Equation (6) gives the first critical speed for any shaft length and diameter. If n denotes the first, second, or nth mode of vibration, the critical speed for any vibration mode can be found by the following:

* References are given on page 142.

$$\text{rpm} = \frac{4.8 \times 10^6 n^2 D}{\ell^2} . \qquad (7)$$

Figure 2 is a graph of this equation with a family of curves of n^2D equal to various constants, plotted against speed and shaft length. Figure 2 also shows the maximum length and speed capabilities of the test machine as indicated within the dotted lines. From the figure, a 70-inch 50,000-rpm shaft has an n^2D constant of approximately 50. Then the value of n for a 0.5-inch-diameter shaft equals 10, meaning that the shaft is running at its tenth critical speed. A number of intermediate supports could be added to reduce the order of the vibration mode to one, or even less than one to completely avoid critical speeds. The distance between supports to reduce operation to the first critical speed for the 0.5-inch shaft running at 50,000 rpm can be calculated easily. At the first critical n = 1 and $n^2D = 0.5$. On Figure 2 the intersection of the n^2D curve equal to 0.5, and 50,000 rpm, shows the distance between supports to be about 7 inches. For operation of the shaft below the first critical speed, ten or more supports must be added to reduce support spacing below 7 inches.

Figure 2 shows graphically another interesting relation between vibration mode and diameter of simply supported shafts. Suppose the installation using a 70-inch-long shaft running at 50,000 rpm had no framework on which to mount intermediate supports along its length. A shaft diameter could be chosen to operate at or below the first critical speed. From Figure 2 the value of n^2D for the 70-inch-long, 50,000-rpm shaft is 50. If n is made equal to 1, then d must equal 50 inches. A diameter somewhat larger than 50 inches would permit operation below the first critical. Although this example is ridiculous from a practical standpoint, it illustrates the application of Figure 2 in situations where the distance between driving and driven members is fixed.

Probably most of the situations to which high-speed power-transmission shafts might be adapted would be those with considerable shaft-end fixity. Rather than being freely supported, the shaft ends would be built-in or cantilevered. Due to the increased stiffness of such shafts, their critical speeds are higher than indicated by Equations (6) and (7) and Figures 1 and 2.

The critical-speed equation for any fixed-end solid steel shaft, and for any vibration mode is:

$$\text{rpm} = \frac{3.07\,(1.25n + 0.637)^2 10^6 D}{\ell^2} . \qquad (8)$$

Equation (8) was derived from material in Reference 1. Dividing Equation (7) by Equation (8) produces the critical-speed ratio of simple to fixed-ended shafts for any vibration mode n. The critical-speed ratio is:

$$\frac{\text{rpm}_{\text{simple}}}{\text{rpm}_{\text{fixed}}} = \frac{1.57n^2}{(1.25n + 0.637)^2} , \qquad (9)$$

and is plotted in Figure 3 for the first 20 critical speeds.

At the higher criticals there is less difference in speed due to the decreasing prominence of the two end vibration loops compared to the total number of loops along the shaft. Referring to Figure 3 the critical-speed ratio for the tenth mode is about 0.9.

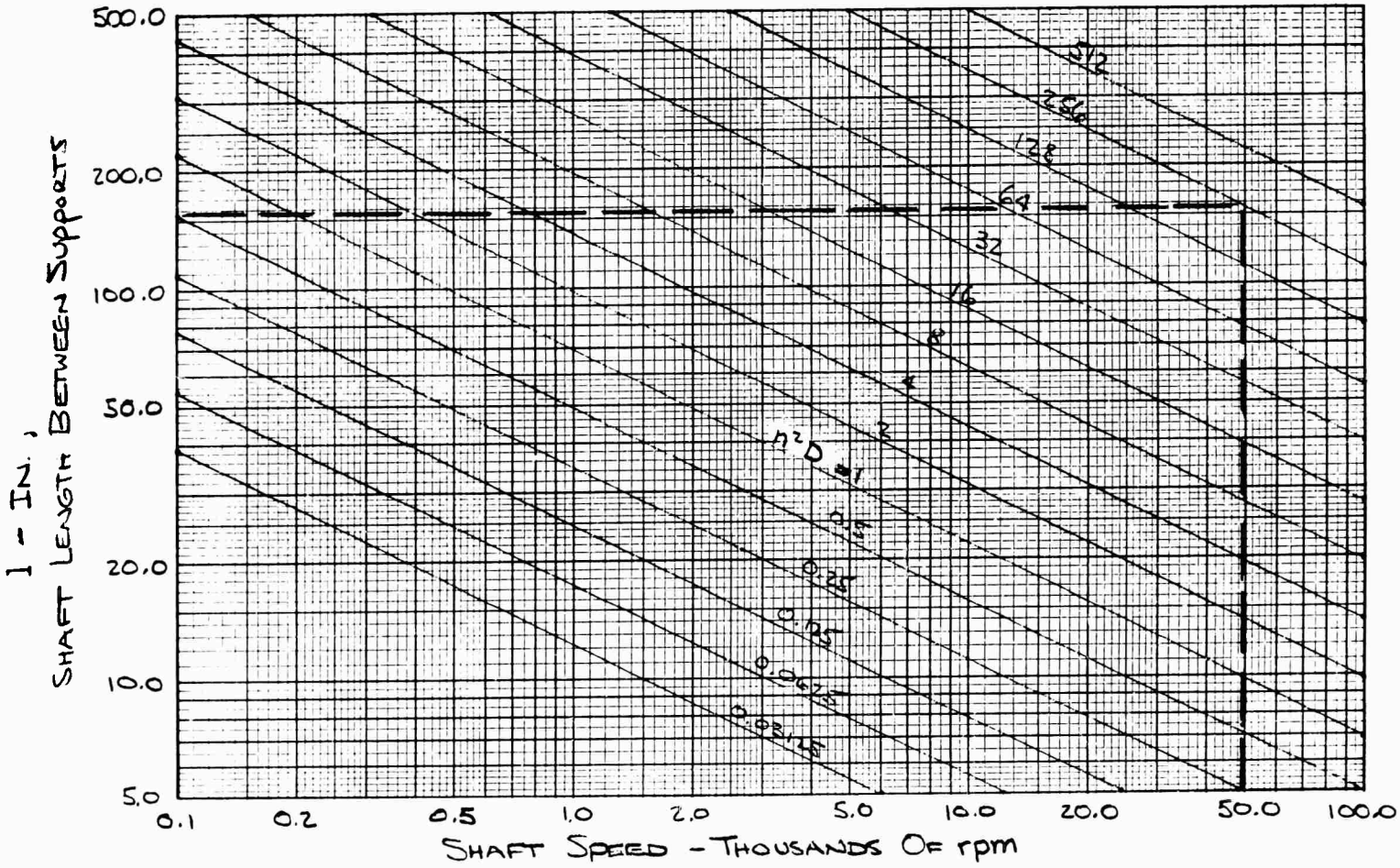

FIGURE 2. RELATIONSHIP BETWEEN LENGTH, DIAMETER, CRITICAL VIBRATION MODE, AND SPEED FOR A SIMPLY SUPPORTED STEEL SHAFT

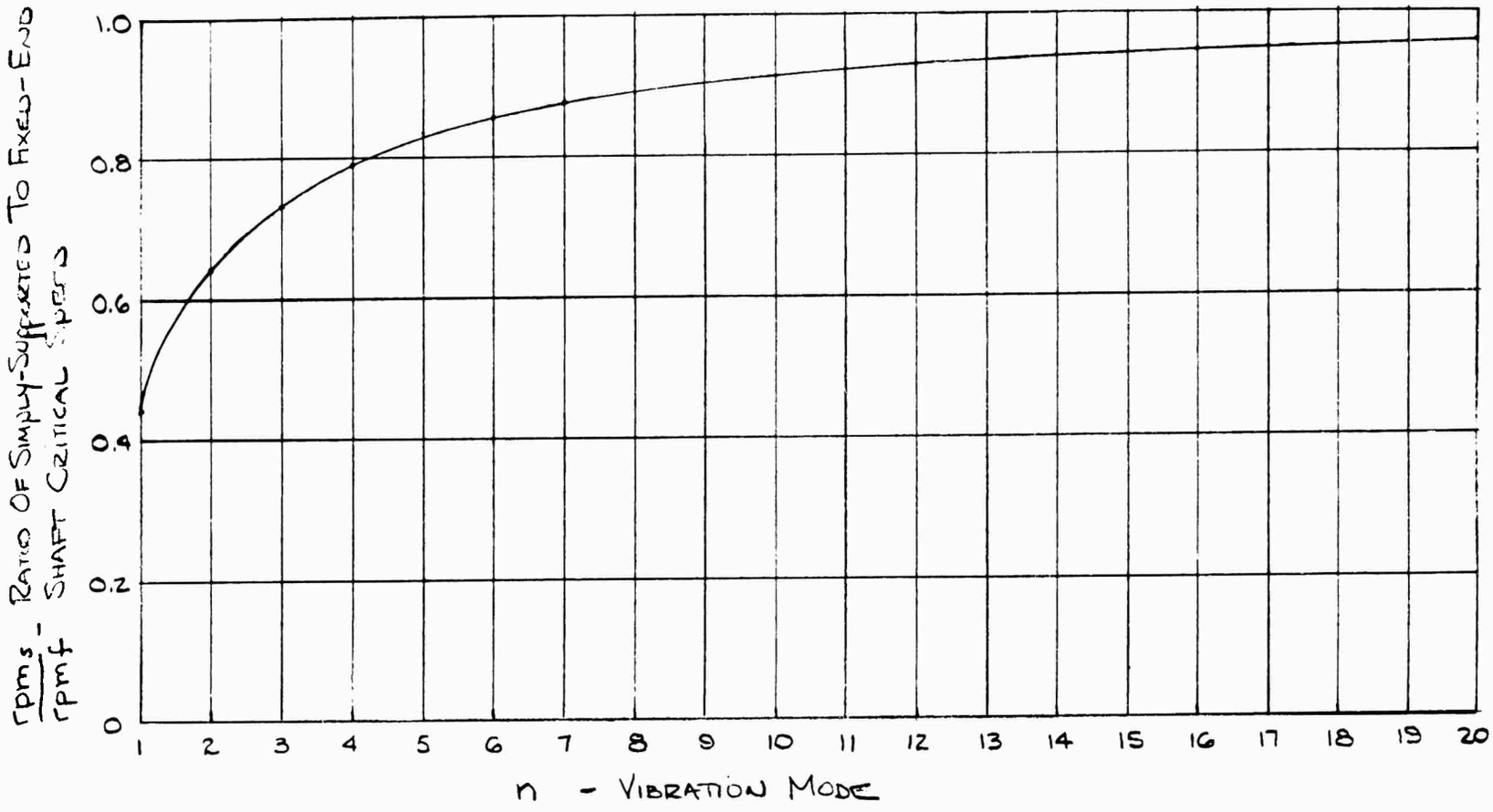

FIGURE 3. CRITICAL-SPEED COMPARISON BETWEEN SIMPLY SUPPORTED AND FIXED-END SHAFTS FOR VARIOUS VIBRATION MODES

The 0.5-inch-diameter 70-inch-long steel shaft with simple ends vibrates at its tenth critical when turning at 50,000 rpm. The same shaft with fixed ends must turn at 50,000/0.9 = 55,600 rpm to achieve the tenth critical speed. Figure 2 shows that the same 0.5-inch-diameter 70-inch-long shaft simply supported runs at its first critical speed ($n^2D = 0.5$) at about 500 rpm. The critical-speed ratio from Figure 3 for the first vibration mode is approximately 0.44. Then the first critical speed of the same shaft, but with clamped ends is 500/0.44 = 1137 rpm.

Tubular Shafts

Tubular power-transmission shafts have some very attractive advantages when compared to solid shafts. These advantages can be easily understood with the aid of graphs which are developed in this section.

Equation (1) gives the torque transmission ability versus solid shaft diameter for a certain torsional stress level. Equation (10) presents the same relationship for a tubular shaft:

$$T = \frac{\pi S_s (D^4 - d^4)}{16D}, \tag{10}$$

where

D = shaft outside diameter, in.

d = shaft inside diameter, in.

If solid and tubular shafts are compared on the basis of transmitting equal torque which develops the same stress levels at the surfaces of the shafts, Equations (1) and (10) reduce to:

$$D_s = \left(\frac{D^4 - d^4}{D} \right)^{1/3}, \tag{11}$$

where

D_s = diameter of a solid shaft which is torsionally of equal strength as a tubular shaft of given dimensions, in.

Figure 4 shows a plot of Equation (11) which compares the outside-diameter ratio of equally stressed solid and tubular shafts with equal torque capacity to the ratio of tubular shaft inside to outside diameters. For instance the 0.5-inch-diameter solid steel shaft was capable of transmitting nearly 1000 horsepower. If an equally stressed tube of 0.8-inch outside diameter were substituted to carry the same power at the same speed, the tube inside diameter could be easily calculated from Figure 4. The ratio of solid to tubing outside diameter is 5/8, or 0.625. From the curve the inside to outside tube-diameter ratio is read to be about 0.93. Then a tube of 0.744-inch bore and 0.8-inch outside diameter can handle the same torque at the same stress level as can the 0.5-inch solid shaft.

Equation (12) shows the relationship between critical speed and shaft length for tubular steel shafts with simply supported ends:

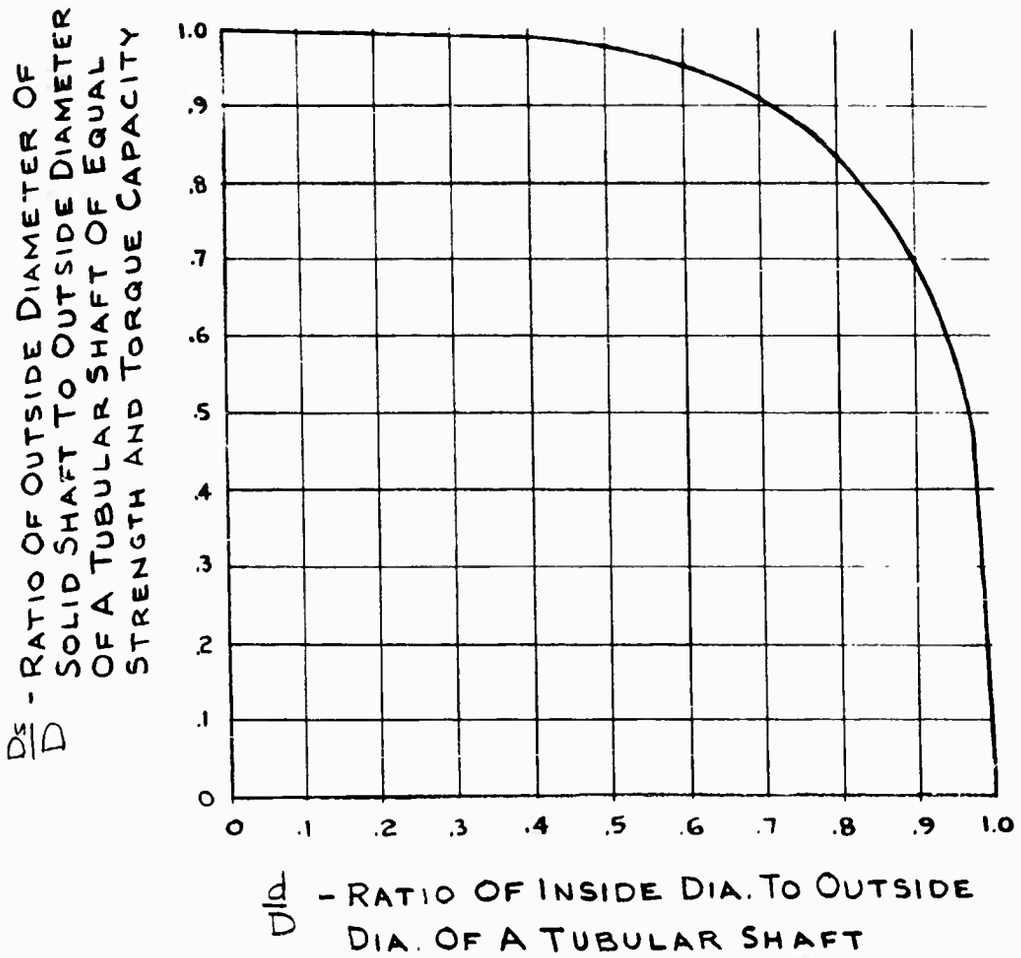

FIGURE 4. RATIO OF OUTSIDE DIAMETER OF SOLID SHAFT TO OUTSIDE DIAMETER OF TUBULAR SHAFT OF EQUAL STRENGTH AND TORQUE CAPACITY VERSUS DIAMETER RATIO OF TUBULAR SHAFT

$$\text{rpm} = \frac{4.8 \times 10^6}{\ell^2} \sqrt{D^2 + d^2}. \tag{12}$$

Dividing Equation (12) by Equation (6) shows the critical-speed relation between tubular and solid shafts for the same shaft length:

$$\frac{\text{rpm}_{\text{tube}}}{\text{rpm}_{\text{solid}}} = \frac{\sqrt{D^2 + d^2}}{D}. \tag{13}$$

Substituting Equation (11) produces the relation between tubular and solid-shaft critical speeds for shafts which can transmit the same torque at the same stress level.

$$\frac{\text{rpm}_{\text{tube}}}{\text{rpm}_{\text{solid}}} = \frac{\sqrt{D^2 + d^2}}{\frac{3}{\sqrt{D^4 - d^4}}}. \tag{14}$$

Equation (14) is plotted in Figure 5.

The 0.5-inch solid shaft and the tube with 0.8- and 0.744-inch outside and inside diameters both can transmit nearly 1000 horsepower at 50,000 rpm. The torsional stress levels of both shafts are equal. Figure 5 shows that the critical-speed ratio of the tube to the solid section is 2.218. In other words for the same vibration mode the critical speed of the tube is 2.218 times that of the solid shaft.

Previously it was seen that for the 0.5-inch-diameter 70-inch-long solid steel shaft the first critical speed was 500 rpm. The first critical speed of the equal-strength tube = 2.218 x 500 = 1109 rpm. Obviously there is an advantage to the use of tubing since fewer intermediate supports are needed. Reference to Figure 2 shows graphically the advantage in number of intermediate supports needed when tubular rather than solid shafts are used.

In Figure 2 the intersection of 70-inch span and 1109 rpm occurs at an n^2D value slightly greater than 1.1. Actually the value of n^2D is 1.113, which can be calculated exactly from Equation (7). This value, when divided by $n^2 = 1$, provides a solid shaft diameter of 1.13 inches which is equivalent from the critical-speed standpoint to the 0.8-inch-diameter tube of the same length. Since the vibration speeds of the tube and 1.13-inch-diameter equivalent solid shaft are identical, the vibration mode of the tube occurring at 50,000 rpm can be calculated easily from Figure 2. At this speed and with a shaft length of 70 inches the n^2D value is 50. Dividing 50 by the equivalent 1.13 diameter shows n to be equal to 6.65. This means that the tube operates between the sixth and seventh vibration modes. To determine the span between intermediate supports necessary to permit operation of the tube at the first critical speed find the intersection of the line equal to 1.13 and 50,000 rpm. The span length ℓ for this point is 11 inches. At 50,000 rpm the introduction of six intermediate supports permits operation of the 0.8-inch-diameter 70-inch-long tube below its first mode of vibration, while it is necessary to include ten intermediate supports along the 0.5-inch-diameter 70-inch-long solid shaft to provide operation below the first critical speed. Both the tube and solid shaft can transmit the same horsepower at the same level of stress in the shafts.

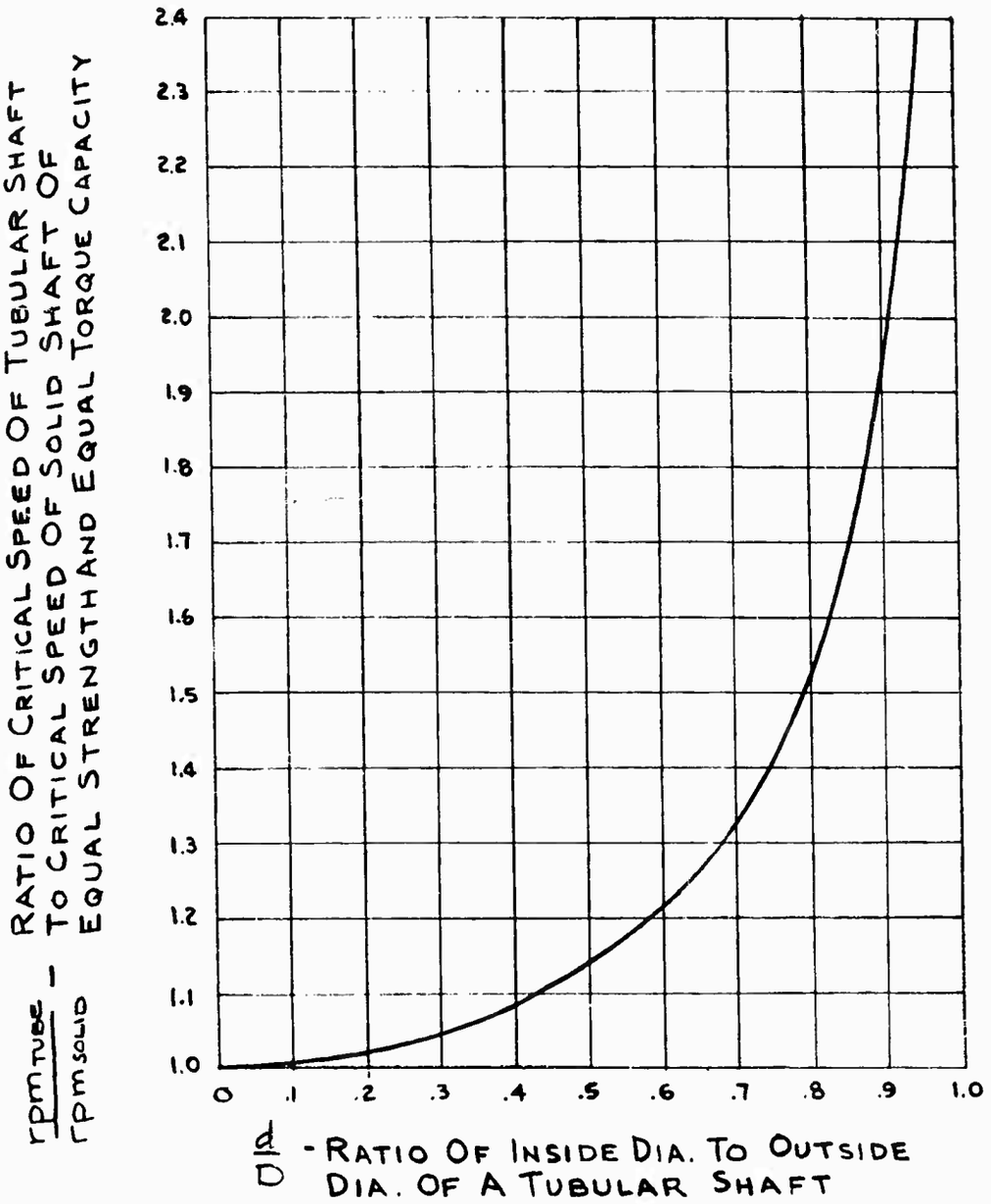

FIGURE 5. RATIO OF FIRST CRITICAL SPEED OF TUBULAR SHAFT TO SOLID SHAFT VERSUS DIAMETER RATIO OF TUBULAR SHAFT

Another advantage of tubular shafts over their solid counterparts is the reduction in shaft weight necessary to transmit the same level of power. Figure 6 shows the curve of the following equation which permits calculation of the weight ratio of equal strength tubes to solid shafts:

$$\frac{w_{tube}}{w_{solid}} = \frac{D^2 - d^2}{\left(\frac{D^4 - d^4}{D}\right)^{2/3}}, \tag{15}$$

where

w_{tube} = weight of a unit length of tubular shaft, lb

w_{solid} = weight of a unit length of solid shaft, lb.

Checking Figure 6 for the ratio of inside to outside diameter of 0.93 we find a ratio of tube to solid weight of about 0.33. For similar torque-transmission ability the tube weighs one-third that of the solid shaft.

Tubular shafts may of course be run with fixed rather than simply supported ends. The first critical speed of the 70-inch-long tube with simply supported ends was found to be 1109 rpm with an n^2D value of 1.13. Reference to Figure 3 shows the critical speed of a simply supported shaft to be about 0.44 that of a fixed-end beam. The first critical speed of the tube with fixed ends is approximately 2520 rpm. Other fixed-end critical speeds can be calculated in a similar manner.

When damped support bearings are provided to permit shaft operation through several critical speeds, the tubular shaft will have to pass through fewer critical speeds than an equivalent solid shaft in the same application. More effective damper design should therefore be possible for use with tubular shafts, since fewer design compromises would result from dealing with a smaller number of critical speeds.

Shaft Modeling Procedure

Numerous successful high-speed-shaft experiments have been made with damped intermediate supports. For instance, with one damped support bearing included on a 0.25-inch-diameter, 89.3-inch-long steel shaft, successful vibration suppression was obtained at all shaft critical speeds up to the twelfth mode. This is a remarkable accomplishment, but it must be possible to extract broader implications from this experiment to permit the design of successful shafts of different materials, lengths, and diameters. To make it possible to achieve similar performance with other shafts a set of modeling equations is needed.

Modeling Equations Relating Dynamically Similar Shafts

The following relationships between dynamic shaft parameters were developed to define the basic properties of all circular shafts of uniform cross section:

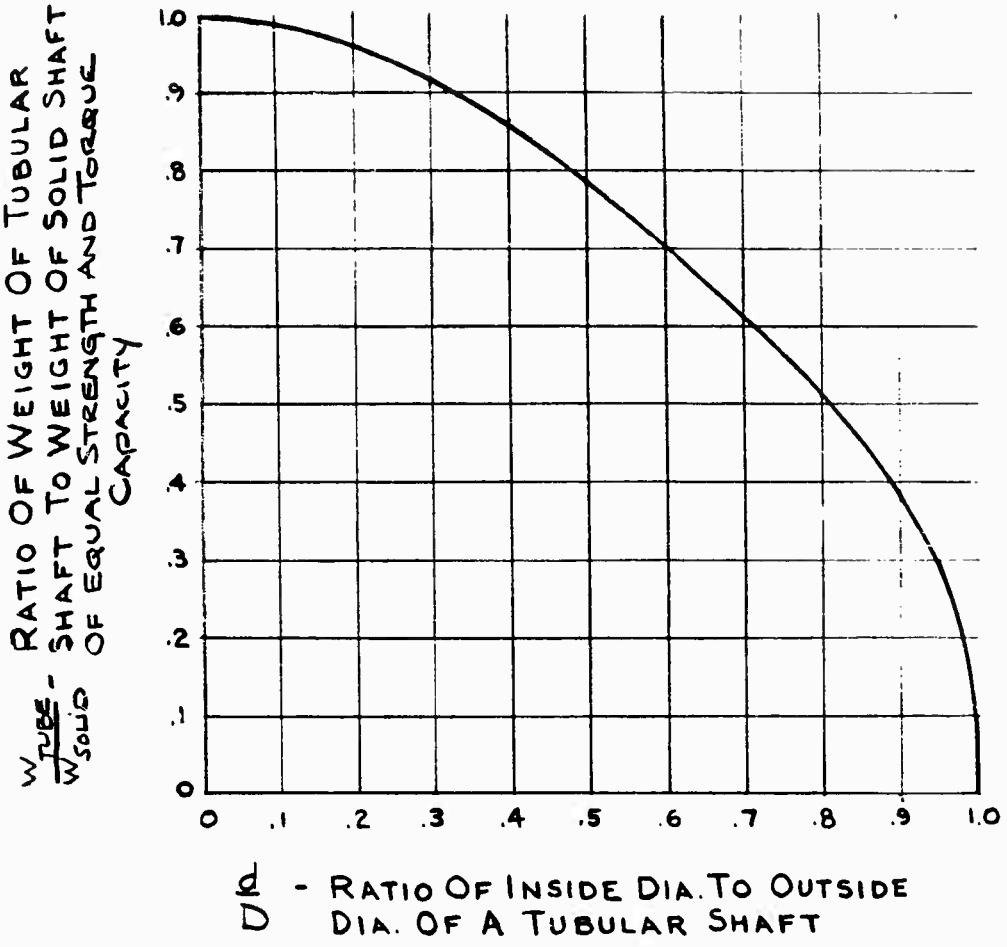

FIGURE 6. RATIO OF WEIGHT OF TUBULAR SHAFT TO SOLID SHAFT VERSUS DIAMETER RATIO OF A TUBULAR SHAFT

Characteristic Shaft Weight, $W_s = \frac{\pi}{4}(D^2 - d)^2 LP$, lb. (16)

Characteristic Shaft Lateral Stiffness, $K_s = \frac{3\pi(D^4 - d^4)E}{L^3}$, lb/in. (17)

Characteristic Shaft Natural Frequency, $\omega_s = \sqrt{\frac{K_s g}{W_s}}$, rad/sec (18)

Characteristic Shaft Critical Damping Value, $C_s = 2\sqrt{\frac{W_s K_s}{g}}$, lb-sec/in. (19)

where

D = shaft outside diameter, in.

d = shaft inside diameter, in.

L = shaft over-all length, in.

P = shaft density, $lb/in.^3$

E = shaft modulus of elasticity, $lb/in.^3$

g = 386 $in./sec^2$

The following symbols refer to the intermediate support bearing:

W = weight of bearing plus 1/3 the weight of each support spring, lb

K = combined spring rate of damper springs, lb/in.

C = support damping coefficient, lb-sec/in.

$$X = \frac{\text{distance between support and shaft end, in.}}{\text{over-all shaft length, L, in.}}$$

Four dynamic scaling ratios exist which relate parameters of shafts and their intermediate supports for similar dynamic behavior. Let subscript 1 refer to a shaft configuration of known behavior, and subscript 2 refer to a shaft of different dimensions which is to be dynamically similar to the first shaft.

$$\frac{W_1}{W_{s1}} = \frac{W_2}{W_{s2}} \quad (20)$$

$$\frac{K_1}{K_{s1}} = \frac{K_2}{K_{s2}} \quad (21)$$

$$\frac{C_1}{C_{s1}} = \frac{C_2}{C_{s2}} \quad (22)$$

$$X_1 = X_2. \quad (23)$$

Knowing the support-to-shaft ratios of Equations (20) through (23) for Shaft 1, all that remains is calculating the necessary damper characteristics W_2, K_2, and C_2, for the diameter, length, and materials of the second shaft.

To illustrate the modeling procedure let us say that a 114.2-inch-long 0.5-inch-diameter aluminum tubular shaft of 20-gage wall thickness is needed to transmit power between driving and driven components. The shaft ends are to be clamped tightly in the spindles of the driving and driven elements, and shaft speed is to be 30,000 rpm. Using Equations (16) through (19) the characteristic aluminum-shaft parameters are:

$$W_{s2} = 0.572 \text{ lb}$$

$$K_{s2} = 1.848 \text{ lb/in.}$$

$$C_{s2} = 0.1048 \text{ lb-sec/in.}$$

$$\omega_{s2} = 35.35 \text{ rad/sec.}$$

Now it is necessary to know if the vibration mode at the operating speed of the aluminum shaft is within the range of successful vibration suppression of one of the damped test shafts. This information can be obtained easily with a fifth relation given by Equation (24):

$$\frac{\omega_1}{\omega_{s1}} = \frac{\omega_2}{\omega_{s2}} , \tag{24}$$

where the subscripts are as before.

The 0.25-inch-diameter, 89.3-inch-long solid steel shaft with clamped ends and one damped support has been successfully run to the twelfth vibration mode, which occurs at approximately 22,000 rpm. The parameters of this shaft are as follows:

$$W_{s1} = 1.260 \text{ lb}$$

$$K_{s1} = 1.550 \text{ lb/in.}$$

$$C_{s1} = 0.142 \text{ lb-sec/in.}$$

$$\omega_{s1} = 21.8 \text{ rad/sec.}$$

Substituting values in Equation (24):

$$\omega_2 = \omega_{s2} \frac{\omega_1}{\omega_{s1}} = \frac{35.35 \times 22,000}{21.8} = 35,700 \text{ rpm} .$$

This calculation shows that the aluminum shaft could operate at speeds as high as 35,700 rpm without encountering severe vibrations, and that a speed of 30,000 rpm is well within the range of good operation.

To establish the damped support characteristics of the aluminum shaft it is necessary to know the support characteristics used with the 0.25-inch-diameter steel shaft. They are as follows:

$$W_1 = 0.609 \text{ lb}$$

$$K_1 = 11.6 \text{ lb/in.}$$

$$C_i = 1.736 \text{ lb-sec/in.}$$

$$X_1 = 0.05.$$

The aluminum-shaft support characteristics are calculated as follows from Equations (20) through (23):

$$W_2 = W_{s2} \frac{W_1}{W_{s1}} = \frac{0.572 \times 0.609}{1.260} = 0.276 \text{ lb.}$$

$$K_2 = K_{s2} \frac{K_1}{K_{s1}} = \frac{1.848 \times 11.6}{1.550} = 13.83 \text{ lb/in.}$$

$$C_2 = C_{s2} \frac{C_1}{C_{s1}} \quad \frac{0.1048 \times 1.736}{0.142} = 1.28 \text{ lb-sec/in.}$$

$$X_2 = X_1 = 0.05$$

The aluminum tubular shaft equipped with one damper with the above calculated parameters and located 5.71 inches from a shaft end would transmit power satisfactorily at 30,000 rpm.

Since damped shafts related to each other by the modeling Equations (20) through (23) have similar vibration characteristics when operated at speeds defined by Equation (24) they may be said to be dynamically similar. No matter how physically dissimilar are the shafts, dynamic similarity can be achieved with the proper selection of support parameters. The use of these modeling equations permits scaling the satisfactory operational characteristics of a known shaft configuration to any physically dissimilar situation.

Modeling Equations Relating Vibration Amplitude

If vibration amplitudes of a certain shaft configuration are known, then it is possible to predict vibration amplitudes of a dynamically similar second shaft configuration. If both shafts have an exactly similar distribution of shaft runout, vibration amplitudes for both will be proportional to their maximum shaft eccentricities when run at dynamical similar speeds. This may be seen by defining the following shaft parameter:

$$\text{Characteristic Shaft Unbalance, } F_s = \frac{W_s \, e \, \omega_s^2}{g} \text{ , lb ,.} \qquad (25)$$

where

e = maximum shaft runout or eccentricity, -in.

Shaft deflection, y, is proportional to the force, F_s, trying to deflect it, and inversely proportional to the shaft stiffness, K_s. Then:

$$y \propto \frac{F_s}{K_s} = \frac{W_s \, e \, \omega_s^2}{g K_s} , \tag{26}$$

but

$$\omega_s^2 = \frac{K_s \, g}{W_s} , \tag{18}$$

$$\therefore \; y \propto e, \tag{27}$$

and

$$\frac{Y_{s1}}{e_{s1}} = \frac{Y_{s2}}{e_{s2}} \quad \frac{y_1}{e_1} = \frac{y_2}{e_2} \tag{28}$$

It must be remembered that Equation (28) is true only if Shafts 1 and 2 are modeled according to Equations (20) through (24); the deflections, y_1 and y_2, are measured at the same relative position along each shaft; and the shaft runouts are exactly similar in distribution.

Modeling Equations Relating Shaft Power Transmission

Full-scale transmission shafts will be called upon to carry power in the range from 250 to 2500 horsepower. Simulation of the effects of torsion in the laboratory using much smaller horsepower levels is highly desirable, since the equipment necessary to transmit low horsepower is less expensive.

The following defines the relative horsepower transmission ability of a circular shaft of uniform cross section:

$$\text{Characteristic Shaft Power-Transmission Ability, } hp_s = \frac{(D^4 - d^4) S_{se} \omega}{D} \tag{29}$$

where S_{se} = torsional endurance stress, psi. The following equation permits scaling down of horsepower from full-scale to model values with the same percentage of torsional operating stress to torsional yield stress maintained:

$$\frac{hp_1}{hp_{s1}} = \frac{hp_2}{hp_{s2}} \tag{30}$$

where hp_1 = the actual horsepower transmitted by the shaft.

As an example a steel tube of 1.5-inch outside and 1.372-inch inside diameter is capable of transmitting 2500 horsepower at 17,000 rpm with a resulting torsional operating stress of 50,000 psi. This can be calculated using Equations (19) and (26) in the report section entitled, Relationships Between Power, Speed, Torque, Shaft Size, and Critical Speed. If it were desired to test a model shaft at the same relative stress level, application of Equation (30) would show the necessary value of model shaft horsepower.

Suppose it were convenient to test at 4,700 rpm a 0.25-inch-diameter solid shaft of the same material as the full-scale tubular shaft. The model shaft characteristic horsepower transmission ability equals:

$$hp_{s2} = \frac{(0.25^4 - 0^4)S_{se} \times 4,700}{0.25} = 73.6\ S_{se}\ .$$

The full-scale shaft characteristic equals:

$$hp_{s1} = \frac{(1.5^4 - 1.372^4)S_{se} \times 17,000}{1.5} = 17,000\ S_{se}\ .$$

Applying Equation (30)

$$hp_2 = hp_1 \frac{hp_{s2}}{hp_{s1}} = \frac{2500 \times 73.6\ S_{se}}{17,000\ S_{se}} = 10.84\ hp.$$

Transmitting 10.84 horsepower through the model shaft produces the same relative torsional stress level as 2500 horsepower carried in the full-scale tubular shaft.

Experimental Modeling Tests

Seven tests were made in the laboratory using shafts with support characteristics which fulfilled the requirements of Equations (16) through (19). Shafts were of steel, aluminum, and brass, with various lengths and diameters. Two of the shafts tested were tubes. The critical-speed ratio of the test shaft with the highest first critical speed to the shaft with the lowest was 4.75. The diameter ratio of the largest to the smallest test shaft was 2.67, and the ratio of the longest to the shortest length was 2.62. In brief, the dimensions and critical speeds of the shafts tested were distinctly dissimilar.

Figure 7 shows a plot of all the ratios of actual shaft critical speeds to characteristic shaft speed plotted versus the order of the vibration mode. The test speeds all fall within the solid-line envelope. As can be noted from the figure, the shaft critical speeds determined experimentally show good agreement with each other.

Five of the seven shafts became excessively noisy or developed excessive vibration at the fourth critical, a fairly good experimental agreement. Accurate similarity was not achieved in the amplitude versus vibration mode curves of the seven shafts. Three reasons are responsible for this fact. The intermediate support has a nonlinear moment-restraint versus shaft-angle curve. Second, some unavoidable inaccuracy occurs in adjusting damping. But probably most important in preventing precise modeling procedure verification was the shaft straightness. The shafts were bought commercially and were subject to bending in manufacture and in handling. The tubing was subject to an additional error in mass eccentricity, since the inside diameter was probably not concentric with the outside diameter. Considering these variables we concluded that similar dynamic behavior was obtained for a majority of the shafts. The critical speeds were in good agreement in spite of the test variables, which indicates that critical speeds are not particularly sensitive to shaft runout, damping tolerance, or varied intermediate support moment restraint.

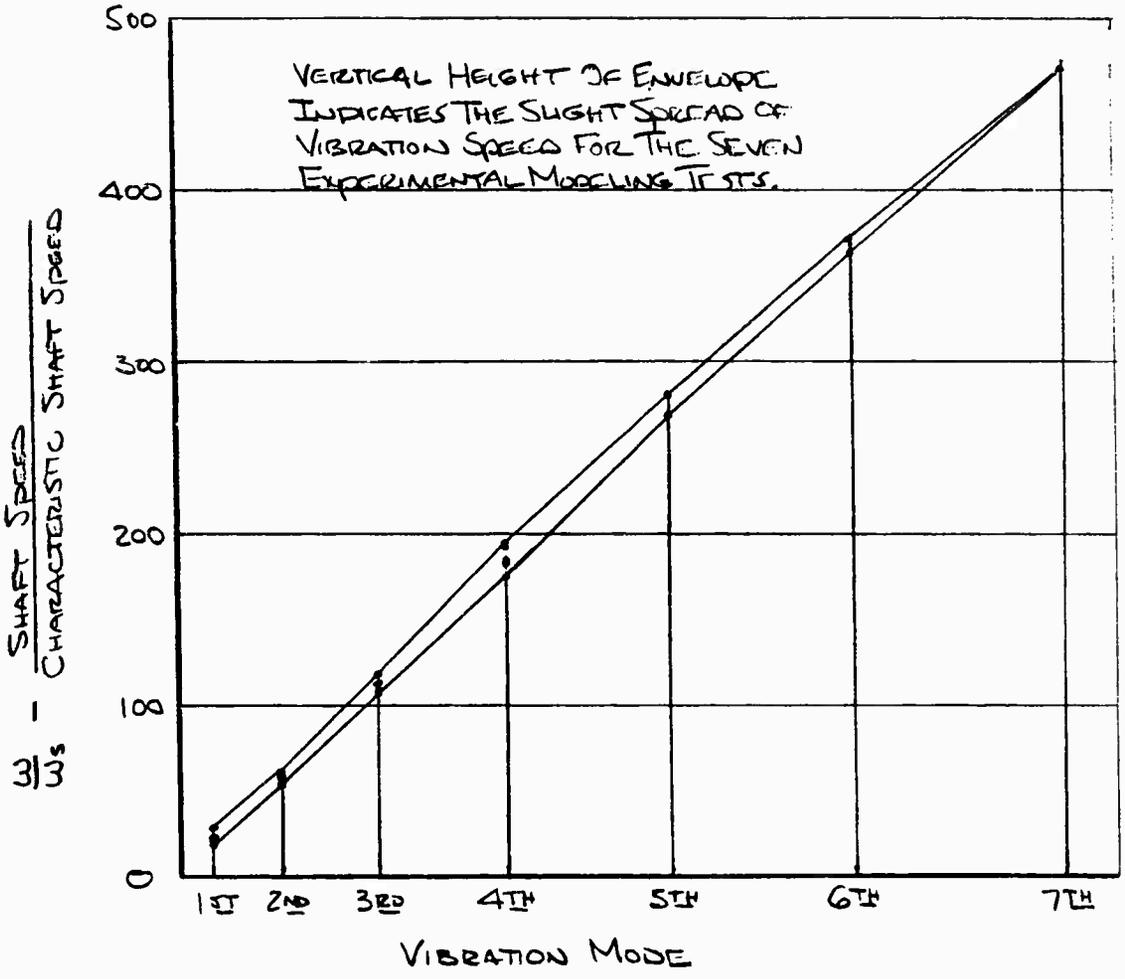

FIGURE 7. VIBRATION SPEED RANGE OF THE SEVEN EXPERIMENTAL MODELING TESTS

Computed Modeling Tests

In order to eliminate the difficulties encountered in the experimental verification of modeling, it was decided to use the computer. In the computer program, calculation of shaft deflection is carried out using the exact same damping factor as indicated on the input cards. The program dictates zero moment restraint at the intermediate support bearing. And, of major importance, the shaft straightness or mass eccentricity is controlled exactly and is also one of the computer inputs.

Two dimensionally dissimilar shafts were selected and the intermediate support parameters adjusted to conform to the modeling equations. Table 1 shows the shaft dimensions, support parameters, and values of the four modeling relations. Eccentricity was the same for both shafts. Referring to Equation (28), the ratio of vibration amplitude to eccentricity, the amplitudes were predicted to be equal since the eccentricities were equal. The computed amplitude of the large aluminum shaft was 0.059 inch and for the small steel shaft 0.060 inch at the same location. The mode shape of both shafts was similar. These two computer calculations are indicated as Runs 35 and 36 on the tabulation of runs in the computer section.

TABLE 1. PARAMETERS OF THE TWO COMPUTER MODELING TESTS

Computer Test	D, in.	L, in.	Material	W_s, lb	K_s, lb/in.	C_s, lb-sec/in.	W, lb	K, lb/in.	C, lb-sec/in.	$\frac{W}{W_s}$	$\frac{K}{K_s}$	$\frac{C}{C_s}$	ω_s
35	0.25	89.3	Steel	1.260	1.550	0.142	0.701	66	0.868	0.556	42.6	6.11	21.8
36	2.218	174.1	Aluminum	68.3	432	17.4	37.9	18,300	106.3	0.556	42.6	6.11	49.4

Note: Both shafts calculated at the second critical; 2580 rpm for the steel shaft and 5850 rpm for the aluminum shaft. Eccentricity, e, and support location, X = 0.416, were the same for both shafts. Amplitudes were measured at the same position for both shafts, and equaled 0.060 in. for the steel shaft and 0.0592 in. for the aluminum shaft.

Conclusions

From the experimental tests it is safe to say that the modeling procedure relates shaft and support parameters so that critical speeds for other modeled shafts can be predicted with accuracy. This in itself is reasonable proof that the modeling relations are correct. From the computer calculations there can be no doubt that the relations are correct, because mode shapes, amplitudes, and critical speeds can be predicted accurately between modeled shafts.

Digital-Computer Calculation Procedure, and Computed Shaft Speed and Deflection Results

Development of design criteria for high-speed power transmission shafts will rely on analytical procedures for verifying design predictions. These analytical procedures are adaptable to high-speed computation equipment, and adaptation of the problem for solution by digital computer will be presented, as well as will a discussion of the digital

computer programs. Shaft critical speeds and the deflection curves were computed for various shaft configurations, and results are discussed.

Digital-Computer Calculation Procedure

The Vibrating-Shaft Equation. The problem of determining the vibration of elastic bodies requires an infinite number of coordinates for specifying its position since it has an infinite number of degrees of freedom. Consider a shaft mounted in rigid bearings as shown in Figure 8. The first critical speed is determined by calculating the natural frequency of lateral vibration for the equivalent fixed-end beam. The differential equation of the vibrating shaft is:

$$\frac{\partial^4 y}{\partial x^4} = - \frac{PA}{386.4EI} \frac{\partial^2 y}{\partial t^2} . \tag{31}$$

where

y = shaft lateral deflection, in.

x = distance along shaft, in.

t = unit of time, sec

P = shaft density, lb/in.^{3}

A = shaft cross-sectional area, in.^{2}

E = shaft modulus of elasticity, lb/in.^{2}

I = shaft moment of inertia, in^4.

With the boundary conditions for the fixed-end shaft given in Equation (32) below:

$$y = 0 \text{ and } \frac{dy}{dx} = 0 \text{ at } x = 0 \tag{32}$$

$$y = 0 \text{ and } \frac{dy}{dx} = 0 \text{ at } x = L,$$

where

L = over-all shaft length, in.

the solution for the critical speed and deflection curve may be obtained. [Ref. (2)]

With introduction of an intermediate support having a damping coefficient and a spring rate, as shown in Figure 9, Equation (31) is written for each span of the shaft. In order to solve this equation, the boundary conditions at the intermediate support must be written. The number of constants of integration to be evaluated is increased to eight. It can be seen that for all but the most simple support systems the mathematical work increases tremendously. The digital computer has been utilized in the solution of the problem of vibration of high-speed shafts, by formulating the problem in a manner adaptable to solution by computer techniques.

(a) Physical Arrangement

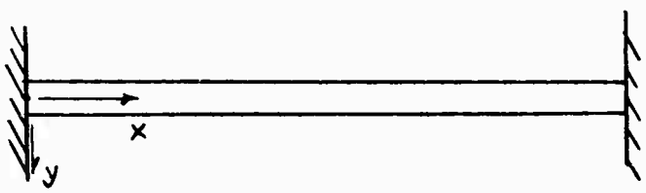

(b) Assumed Arrangement For Theoretical Problems

FIGURE 8. SHAFT WITH FIXED-END SUPPORTS

Digital-Computer Solution of the Vibrating-Shaft Equation. If the distributed-mass system shown in Figure 9 is replaced by a lumped-parameter system of many masses, as shown in Figure 10, the solution of the lumped-parameter system will approximate that of the distributed-mass system. The larger the number of masses, the better the approximation of the solution of the original problem.

In order to determine shaft behavior using the digital computer, the uniform shaft was approximated by a large number of masses by dividing it into a convenient number of equal intervals. Next, the mass of each section was calculated and divided in half, and these halves concentrated at the two ends of the interval. The shaft between intervals was assumed to possess stiffness, but not weight.

In the determination of shaft behavior there are four quantities to be evaluated at each cut; the deflection y, the slope $\phi = \frac{dy}{dx}$, the bending moment $M = EI \frac{d^2y}{dx^2}$, and the shear force $V = EI \frac{d^3y}{dx^3}$. It is necessary to find the relation between these quantities for adjacent intervals. Figure 11 shows the interval between the kth and the k+ 1st cut and the quantities acting. The following equations are written for the interval of length ℓ_c:

$$V_{k+1} = V_k + \beta_{ck} (y_k + e_k), \text{ lb}, \tag{33}$$

$$M_{k+1} = M_k + \ell_c V_{k+1}, \text{ in-lb}, \tag{34}$$

$$\phi_{k+1} = \phi_k - f_c V_{k+1} - q_c M_k, \text{ rad}, \tag{35}$$

$$y_{k+1} = y_k - \ell_c \phi_k + h_c S_{k+1} + f_c M_k, \text{ in.}, \tag{36}$$

where

$V_{k, k+1}$ = shear force, lb

e_k = eccentricity, in.

$y_{k, k+1}$ = deflection, in.

β_{ck} = inertia force constant, lb/in.

$M_{k, k+1}$ = moment, in-lb.

ℓ_c = shaft length, in.

$\phi_{k, k+1}$ = slope, rad

f_c = influence coefficient for a moment, 1/in-lb

q_c = slope influence coefficient for a moment, 1/in-lb

h_c = deflection influence coefficient for shear force, in./lb

where the first two are the equilibrium equations of the interval subject to the inertia force, or centrifugal force $m_k \omega^2 (y_k + e_k)$ at the chosen frequency ω^2. The last two equations are deduced from geometric configurations.

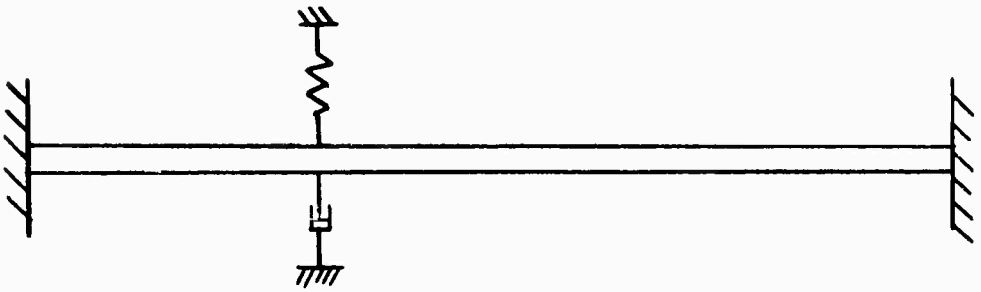

FIGURE 9. SCHEMATIC OF FIXED-END SHAFT WITH SINGLE INTERMEDIATE SUPPORT BEARING

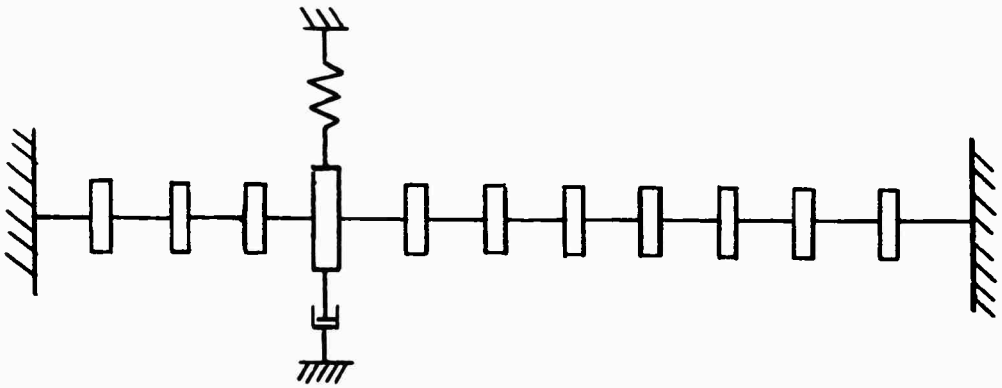

FIGURE 10. SCHEMATIC OF APPROXIMATION OF A FIXED-END SHAFT WITH SINGLE INTERMEDIATE SUPPORT BEARING

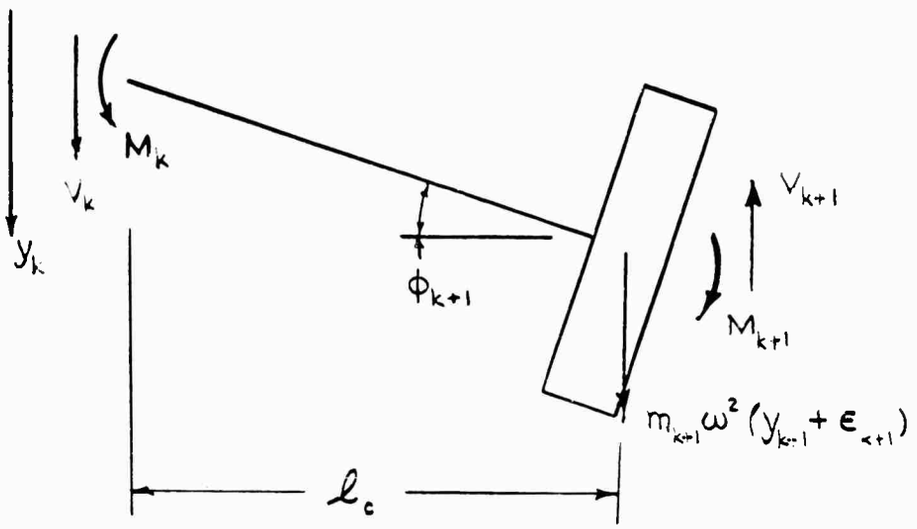

FIGURE 11. SHAFT SECTION BETWEEN STATIONS OF THE DIGITAL-COMPUTER PROGRAM WITH FORCES SHOWN

The coefficients of Equations (33) through (36) are defined in terms of the input parameters as follows:

$$a_c = \frac{\ell_c D^2 N^2 P}{386.4} \frac{\pi}{4} \left(\frac{\pi}{30}\right)^2, \text{ lb/in.}, \tag{37}$$

$$b_c = CN \frac{\pi}{30}, \text{ lb/in.}, \tag{38}$$

$$I = \frac{\pi D^4}{64}, \text{ in.}^4, \tag{39}$$

$$f_c = \frac{\ell_c^2}{2EI}, \text{ 1/lb}, \tag{40}$$

$$q_c = \frac{\ell_c}{EI}, \text{ 1/lb-in.}, \tag{41}$$

$$h_c = \frac{\ell_c^3}{6EI}, \text{ in./lb}, \tag{42}$$

$$p_c = \frac{WN^2}{386.4} \left(\frac{\pi}{30}\right)^2, \text{ lb/in.}, \tag{43}$$

$$\beta_{ck} = a_c - Q\left[\left(K + b_c\sqrt{-1}\right) - p_c\right], \text{ lb/in.}, \tag{44}$$

where

a_c = centrifugal force constant, lb/in.

ℓ_c = shaft length between computer stations, in.

D = shaft diameter, in.

N = shaft speed, rpm

P = shaft density, lb/in.^{3}

b_c = damping constant, lb/in.

C = support damping coefficient, lb-sec/in.

I = section moment of inertia, in.^{4}

f_c = influence coefficient, 1/lb

E = modulus of elasticity, lb/in.^{2}

q_c = slope influence coefficient for a moment, 1/lb-in.

h_c = deflection influence coefficient for a shear force, in./lb

p_c = support weight constant, lb/in.

W = weight of intermediate support bearing, lb

β_{ck} = inertia force constant, lb/in.

Q = index: Q = 1 indicates presence of a support;
Q = 0 indicates no support at that station

K = intermediate support spring rate, lb/in.

Equations (33) through (36) constitute a set of linear recursion relations among the four r quantities S_k, M_k, ϕ_k, y_k. The problem is to determine these quantities for a fixed-end shaft; i.e., subject to the boundary conditions that the deflection and slope are equal to zero at both ends of the shaft. Expressing the boundary conditions mathematically yields:

$$y_k = \phi_k = y_r = \phi_r = 0 . \tag{45}$$

Digital-Computer Shaft-Deflection Program. The problem of determining the deflection of a high-speed power-transmission shaft in fixed-end bearings is the determination of y_k from Equation (36). This problem becomes the solution of the four r quantities from Equations (33) through (36) for the boundary given in Equation (45). Battelle's Digital Computer Program Library contained an IBM 650 computer program which calculated the dynamic deflection of shafts. This program was for a shaft with one end fixed and the other end simply supported. Modification of this program to include fixed ends yielded the desired deflection information.

The resultant IBM 650 double-precision computer program calculates the deflection curve for a fixed-end shaft with damped, flexible intermediate supports. These supports are located at a mass point, and a support may be located at each mass. A restriction on the program is that the number of intervals or masses selected must be larger than 3 and less than 50. Since it was found that the coefficients grew very large in magnitude, equations were calculated starting from each end of the shaft and solved near the middle of the shaft. A double-precision routine (utilizing 18 digits) was used to decrease the effect of round-off error. This enabled the computer to calculate the deflection curve up to approximately the thirteenth mode of vibration. Equation (44) necessitates the use of complex algebra.

Shaft parameters substituted into the computer are the shaft diameter, length of shaft interval, shaft speed, specific weight and modulus of elasticity of the shaft material. Intermediate-support-bearing information required for the computation includes the spring constant, the damping coefficient, and the weight of the support bearing. Additional information required is the number of stations into which the shaft is divided, and the station number where the shaft is broken for computational purposes. Another item required as an input to the computer program is the initial deviation of the shaft from the center of rotation, or mass eccentricity. The results obtained from the computer program for the deflection of shafts are the shear force and moment at the ends of the shaft, the force at the intermediate support bearing, and the deflection at each station. If these values of deflection are plotted along the length of the shaft, a shaft-deflection curve results. Figure 12 shows the deflection curve calculated for a specific set of conditions.

Initial computer calculations showed the importance of the mass eccentricity on the calculation of shaft deflection. If a constant mass eccentricity was assumed, it would not excite the even mode shapes and the computer would give incorrect deflection shapes. Substitution was made of an assumed parabolic mass eccentricity distribution with a maximum of 0.010 inch at one end. In order to correlate calculated shaft deflections and measured shaft deflections, it was necessary to use measured values of shaft eccentricity. Some typical measured values of the shaft eccentricities are shown in Appendix C.

The computer program for the deflection of high-speed power-transmission shafts was utilized to determine the critical speed of the shaft. A particular critical speed could be determined by performing various computer shaft-deflection calculations at small intervals of speed on either side of the estimated critical speed. The amplitude of a particular station was plotted versus the speed of rotation. Figure 13 shows such a plot. The critical speed was determined to be the speed at which the amplitude of shaft deflection was a maximum. Although the shaft-deflection computer program allowed the critical speed to be determined from a series of runs, a separate critical-speed computer program was prepared to do the job with a series of calculations in just one run.

Digital-Computer Shaft-Critical-Speed Program. In preparing a program to determine the shaft critical speed, extensive use was made of the computer program previously described. This program determines a shaft speed in a given speed interval by maximizing the values of shear force and moment at the fixed ends. The input information concerning the shaft configuration is identical to that of the deflection program. Additional input information consists of an initial shaft speed, a final shaft speed, and

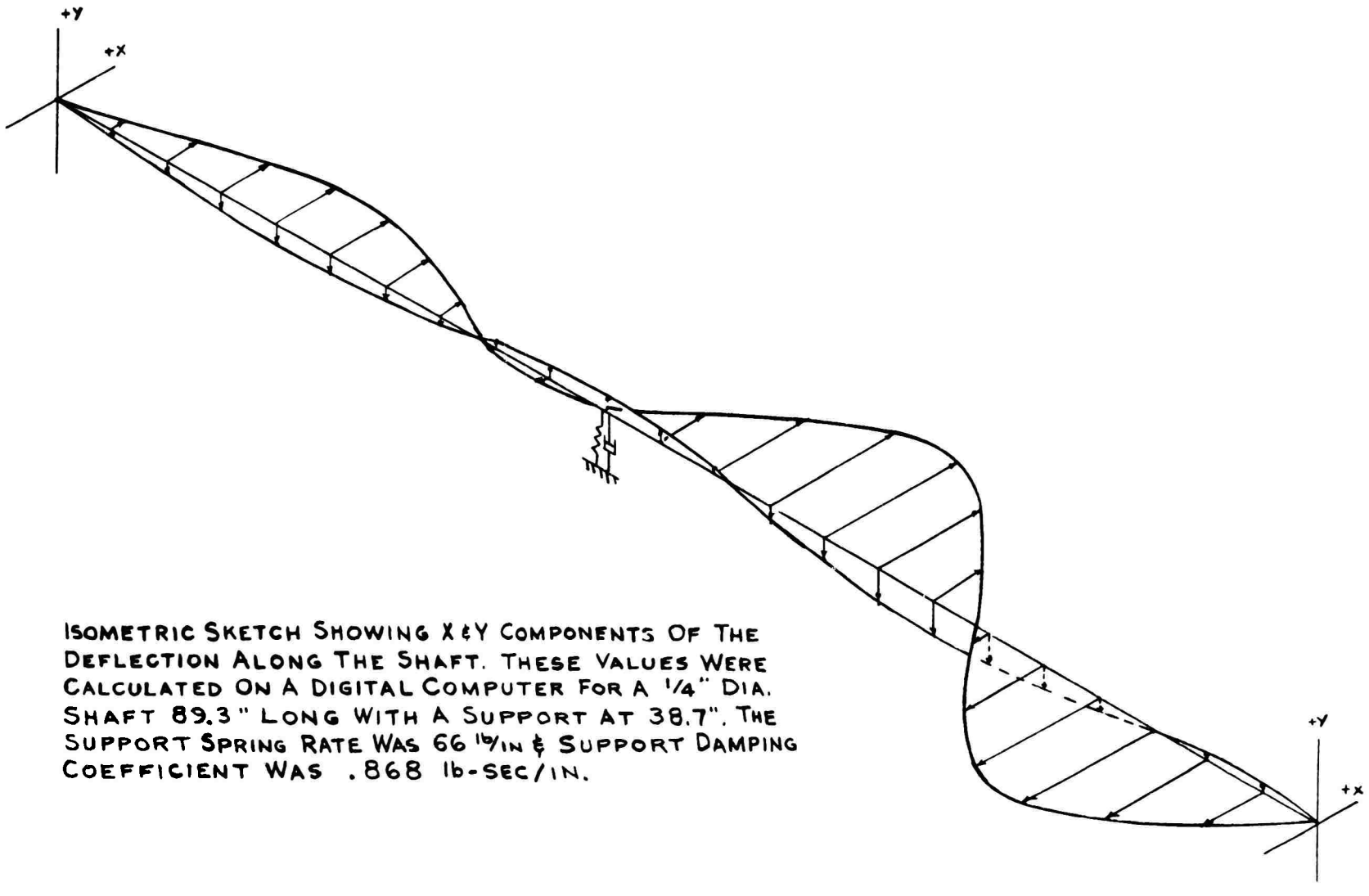

ISOMETRIC SKETCH SHOWING X & Y COMPONENTS OF THE DEFLECTION ALONG THE SHAFT. THESE VALUES WERE CALCULATED ON A DIGITAL COMPUTER FOR A 1/4" DIA. SHAFT 89.3" LONG WITH A SUPPORT AT 38.7". THE SUPPORT SPRING RATE WAS 66 lb/IN & SUPPORT DAMPING COEFFICIENT WAS .868 lb-SEC/IN.

FIGURE 12. DEFLECTION CURVE CALCULATED AT 2530 RPM WITH A SINGLE SUPPORT

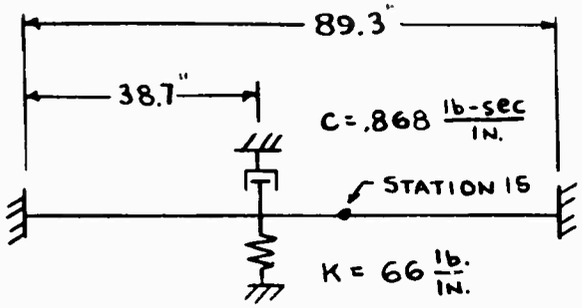

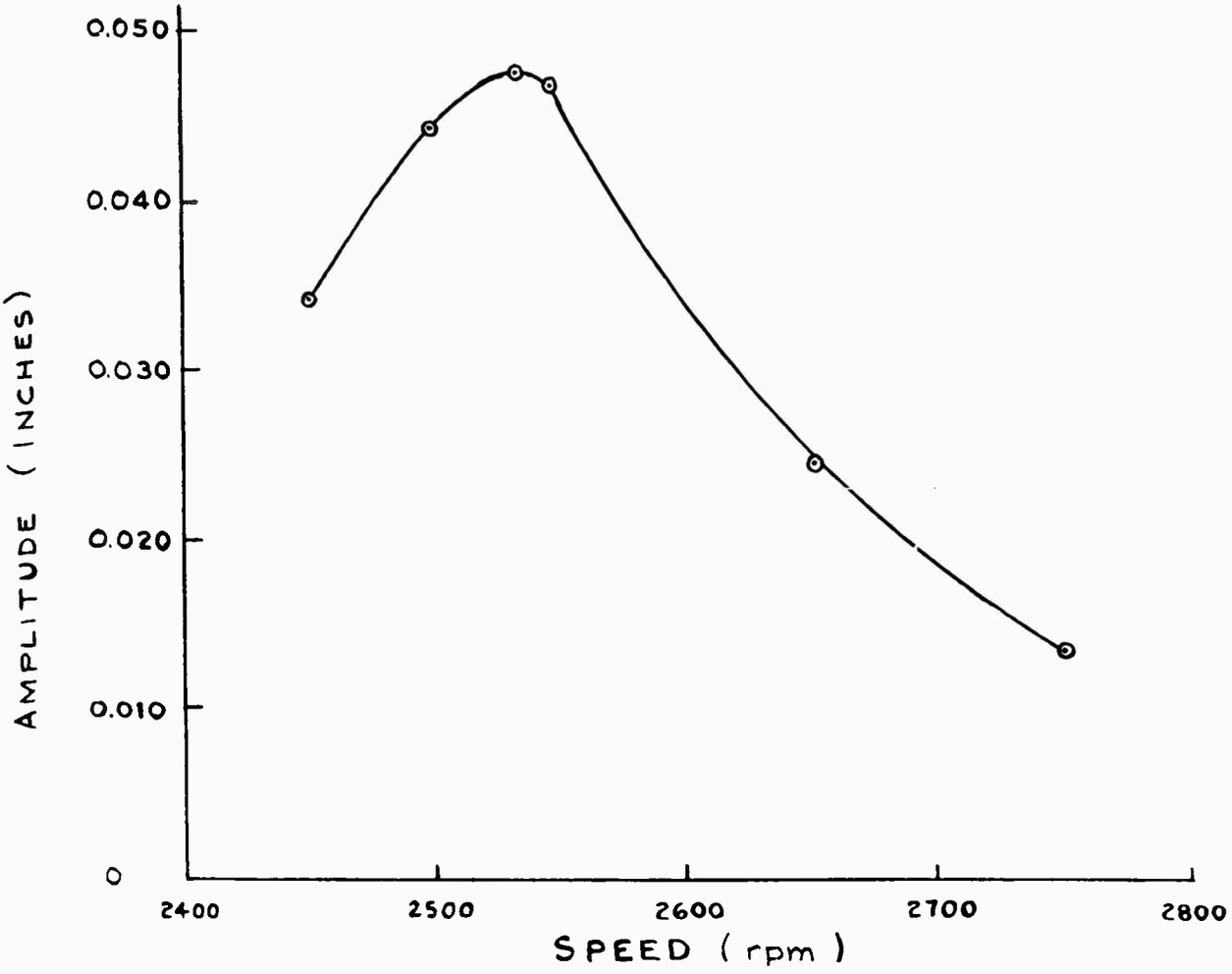

FIGURE 13. PLOT OF AMPLITUDE VERSUS SPEED FOR STATION 15 OF COMPUTER SOLUTION FOR 1/4-INCH-DIAMETER SHAFT 89.3 INCHES LONG WITH ONE INTERMEDIATE SUPPORT

an incremental shaft speed. An indicator is also included which indicates which of the four values is to be maximized.

Successful determination of the critical speed has been obtained by maximizing the fixed-end moment at the last station. The output consists of the calculated values of all of the four factors. When it is determined that the desired factor has been maximized, the computer will automatically stop calculating. The speed which produces the maximum value of the complex moment is the critical speed.

Computer Shaft-Critical-Speed and Deflection Results

Successful operation of the two computer programs described above has augmented the experimental work considerably, and has been utilized to perform calculations to substantiate the modeling theory. Table 2 presents a tabulation of computer results in this research program.

Importance of Mass Eccentricity Distribution to Calculate Shaft Deflection. To determine the suitability of the computer program in computing critical-speed shaft deflections, Runs 1 and 2 in Table 2 were conducted with an undamped shaft vibrating at its first and third critical speeds, respectively. A shaft unbalance or mass eccentricity constant along the shaft was used as the forcing function to excite critical-speed vibrations. The shaft-deflection curves were as expected in these two runs; one loop was present at the first critical, and three at the third. However, when shaft deflection was computed at the second critical, there was no change in amplitude across the shaft. Presuming that constant mass eccentricity would not excite the even numbered modes of vibration, a parabolic eccentricity was tried.

Recalculation of the third critical speed, Run 3, with parabolic eccentricity showed the program to function correctly at this speed. The amplitude was less than in Run 2, as was the averaged value of mass eccentricity. Run 4 was conducted at the second critical with the same eccentricity as in Run 3, and this time calculated the correct two-loop shaft deflection.

From these tests we concluded the necessity of using a forcing function which varies in value across the shaft length. All subsequent computer runs were made with varied mass eccentricity distribution.

Further Validation of Computer Program. Numerous computer calculations were performed for fixed-end shafts with three equally spaced rigid intermediate supports. Critical speeds were first calculated by hand for particular vibration modes and then used as a computer input. Calculated shaft deflections of sizable value showed the correctness of the input speed, and shaft-deflection shape indicated the validity of the computer program. As explained in the section discussing prediction of critical speeds and mode shapes of equally supported continuous beams, there are as many first-vibration-mode critical speeds as there are span lengths between bearings. The computed deflection curves were of the same shape as predicted.

TABLE 2. TABULATION OF COMPUTER RESULTS

Computer Run	Shaft Diameter, in.	Shaft Length, in.	Number of Supports	Support Spacing	Speed, rpm	Mode Shape	K Support	C Support	Amplitude of Vibration, in.
1	1/2	120	0	--	369	1st	--	--	0.432
2	1/2	120	0	--	2,029	3rd	--	--	0.829
3	1/2	120	0	--	2,029	3rd	--	--	0.340
4	1/2	120	0	--	1,035	2nd	--	--	0.553
5	1/2	120	3	Equal	4,120	2nd of 1st G.	49,400	0	1.15
6	1/2	120	3	Equal	4,120	2nd of 1st G.	1×10^8	0	0.55
7	1/2	120	3	Equal	3,070	1st	49,400	0	0.223
8	1/2	120	3	Equal	3,070	1st	1×10^8	0	0.19
9	1/8	126	3	Equal	703	1st	49,400	0	0.106
10	1/8	126	3	Equal	703	1st	49,400[a]	0	0.106
11	1/8	126	3	Equal	702	1st	49,400	0	0.129
12	1/8	126	3	Equal	940	2nd of 1st G.	49,400	0	0.121
13	1/8	126	3	Equal	1,213	3rd of 1st G.	49,400	0	0.187
14	1/8	126	3	Equal	1,367	4th of 1st G.	49,400	0	0.084
15	1/8	126	3	Equal	697.5	1st	49,400	0	2.827
16	1/4	89.3	1	Equal	933.8	1st	1.33	0.0868	1.68
17	1/4	89.3	1	45.8% L	933.8	1st	1.33	0.0868	0.0611
18	1/8	126	0	--	745	4th	--	--	[b]
19	1/8	126	0	--	756	4th	--	--	[b]
20	1/8	126	3	Equal	700	1st	49,400	0	[b]
21	1/4	89.3	1	41.6% L	2,530	2nd	66.	0.868	[b]
22	1/4	89.3	1	41.6% L	2,545	2nd	66.[a]	0.868	[b]
23	1/4	89.3	1	41.6% L	2,530	2nd	66.[a]	0.868	0.047
24	1/4	89.3	1	41.6% L	2,545	2nd	66.[a]	0.868	0.047
25	1/4	89.3	1	41.6% L	2,530	2nd	66.[a]	0.868	0.1072[c]
26	1/4	89.3	1	41.6% L	2,530	2nd	66.[a]	0.868	0.091[c]
27	1/4	91	1	14.3% L	7,860	6th	11.6[a]	0.372	[b]
28	1/4	91	1	14.3% L	7,860	6th	11.6[a]	0.372	0.1819[c]
29	1/4	89.3	1	41.6% L	2,530	2nd	66.[a]	0.868	0.1981[c]
30	1/4	57.5	1	14.3% L	14,500	6th	100.[a]	1.56	[b]
31	1/4	89.3	1	41.6% L	2,530	2nd	66.[a]	0.868	0.0436[c]

TABLE 2. (Continued)

Computer Run	Shaft Diameter, in.	Shaft Length, in.	Number of Supports	Support Spacing	Speed, rpm	Mode Shape	K Support	C Support	Amplitude of Vibration, in.
32	1/4	89.3	1	41.6% L	2,530	2nd	66.[a]	0.868	0.0643[c]
33	1/4	89.3	1	41.6% L	2,530	2nd	66.[a]	0.868	0.223[c]
34	1/4	89.3	1	41.6% L	2,530	2nd	66.[a]	0.868	0.0637[c]
35	1/4	89.3	1	41.6% L	2,580	2nd	66.[a]	0.868	0.000
36	2.218	174.1	1	41.6% L	5,850	2nd	18,300	106.3	0.0592

Note: All computer runs for steel shafts except No. 36, which was aluminum.

(a) Bearing weight added at support.
(b) Critical-speed program.
(c) Different values of mass eccentricity used as forcing function.

A number of computer calculations were made with a single damped intermediate support. As before, the shaft-deflection curves were similar to those expected; in this case to experimentally observed deflections. Shaft critical speeds were also quite similar. However, difference in vibration amplitude was noted between computed and experimental runs.

The amplitude variation in computed and experimental runs stems from the difficulty in adjusting damping exactly, variations in shaft runout, and shaft moment absorbing ability of the damper plate. In the computer these items are inputs and not subject to variation. For these reasons the computer was used to obtain absolute proof of modeling procedure validity.

Effect of Shaft Mass Eccentricity on Vibration Amplitude. Computer Runs 31, 23, 26, and 25 were made with identical input conditions with the exception of shaft mass eccentricity. Table 3 shows the maximum shaft mass eccentricity and the vibration amplitude. This calculated vibration amplitude was found to increase with increasing mass eccentricity. Amplitude was not proportional to eccentricity because of different eccentricity distribution along the shafts, but amplitude did increase with increasing mass eccentricity.

TABLE 3. TABULATION OF COMPUTED VIBRATION AMPLITUDE FOR VARIOUS VALUES OF SHAFT MASS ECCENTRICITY

Computer Run	Maximum Mass Eccentricity, in.	Vibration Amplitude, in.
31	0.0079	0.0436
23	0.010	0.047
26	0.0192	0.091
25	0.0344	0.1072

Computed Modeling Procedure Tests. Since mass eccentricity affects vibration amplitude it was decided to calculate the deflection of two dynamically modeled shafts using the same distribution and maximum value of shaft mass eccentricity. Computer Runs 35 and 36 refer to the dynamically similar model shafts. As noted in Table 2 the shaft dimensions are quite apart from each other, not to mention the larger being of aluminum and the smaller of steel.

Using the procedures found in the section discussing modeling, support parameters were adjusted to provide dynamically similar operation. Rotation speeds were also scaled. Since the distribution and maximum value of shaft eccentricity were equal it was predicted that amplitudes would be also. The computed amplitudes differed by less than 2 per cent (0.001 inch), proof enough of the validity of both the modeling procedure and the computer program.

Conclusions

The computer program has been shown to calculate shaft critical speeds correctly, as well as correct shaft-deflection curves. It is necessary to use a forcing function or shaft mass eccentricity which varies with respect to shaft length, however. Otherwise the even-numbered vibration modes cannot be computed.

The two computer runs of dynamically similar shafts have shown both the modeling procedure and the computer program to be correct in all respects.

High-Speed Shafting Design by Electrical Analogy

Conventional methods of analysis of high-speed shaft behavior have been used with considerable success in the digital-computer analyses conducted throughout this research program. Although the conventional analysis procedures permitted accurate calculation of critical speeds and shaft deflections, they are somewhat cumbersome as aids to high-speed shafting design. An analytical approach to high-speed shafting design was therefore sought which would provide more insight into the manner in which shaft vibration is related to the dynamic parameters of the shaft and its intermediate support bearings.

The possibility that an analogy might exist between high-frequency electrical transmission lines and high-speed shafts lead us to perform a detailed study of the similarities between the two types of problems. A particularly attractive feature of such an electrical analogy is the fact that exhaustive investigation and analysis of electrical transmission lines has developed extensive technology and analysis techniques for the solution of the electrical problems.

As a result of this work an analogy has been developed between high-speed shafting and high-frequency electrical transmission lines. As this analogy was developed late in the Phase I research program it must be emphasized that exhaustive checks and verifications are not yet completed. The extreme promise of the technique, which has resulted in the successful high-speed operation of an experimental shaft, justifies further detailed study during the second phase of the research program.

Theoretical Verification of Transmission-Line Analogy

The analogy between the bending vibrations of high-speed shafting and the standing waves in an electrical transmission line is valid if the displacements of the shaft are strictly sinusoidal functions of position along the shaft. This is shown by writing the differential equation for bending vibrations in the form

$$EI \frac{\partial^2}{\partial x^2}\left(\frac{\partial^2 y}{\partial x^2}\right) + \frac{PA}{g}\frac{\partial^2 y}{\partial t^2} = 0 \ , \qquad (46)$$

where

A = cross-sectional area, $in.^2$

E = modulus of elasticity, $lb/in.^2$

I = section moment of inertia, $in.^4$

P = density, $lb/in.^3$

g = acceleration of gravity, 386 $in./sec^2$

y = deflection, in.

x = distance along the shaft, in.

t = time, sec.

Now, if $\partial^2 y/\partial x^2 = -k^2 y$, we obtain

$$EIk^2 \frac{\partial^2 y}{\partial x^2} = \frac{PA}{g} \frac{\partial^2 y}{\partial t^2} , \tag{47}$$

where

k = constant, 1/in.

which is the ordinary wave equation with a phase velocity equal to $(EIk^2 g/PA)^{1/2}$. The condition $\partial^2 y/\partial x^2 = -k^2 y$ implies that the bending moment is everywhere proportional to the displacement, which results in $y = B_1 \sin kx + B_2 \cos kx$. The hyperbolic function terms vanish in the general solution of the bending wave equation,

$$y = B_1 \sin kx + B_2 \cos kx + B_3 \sinh kx + B_4 \cosh kx, \tag{48}$$

where

$B_{1, 2, 3, 4}$ = constants.

The transmission-line analogy is a useful one because the shape of the bending shaft is approximately sinusoidal for all modes of vibration of interest, except near the ends of the shaft, where the condition $\partial^2 y/\partial x^2 = -k^2 y$ is not valid for either simply supported or fixed-end conditions. Consequently, the analogous transmission-line computations are not carried out to the ends of the shaft. A portion of the shaft near each fixed end is replaced by the equivalent impedance of a short cantilever beam in the manner described in the following section of this report.

Electrical Analogy of High-Speed Shafting

The general arrangement of the high-speed shafts and their supports studied in this program is shown in Figure 14A. As indicated in the figure the ends of the shafts were rigidly supported in the spindles of the testing machine. For the purposes of developing a suitable analogy this shaft configuration was considered equivalent to the configuration

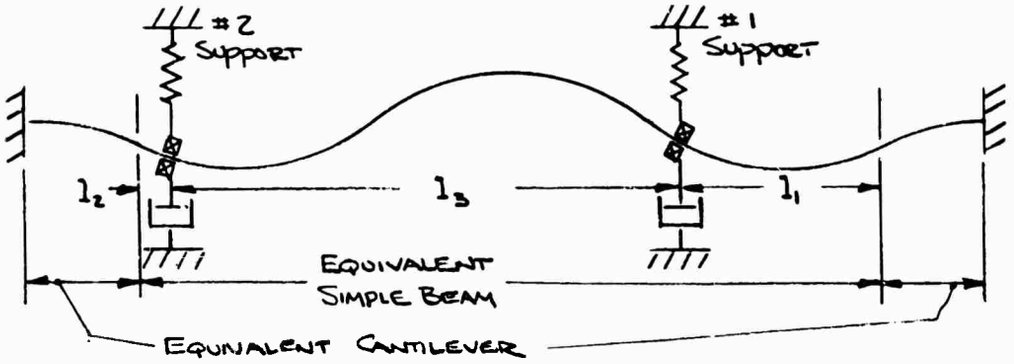

A. General Arrangement Of High-Speed Shafts Studied

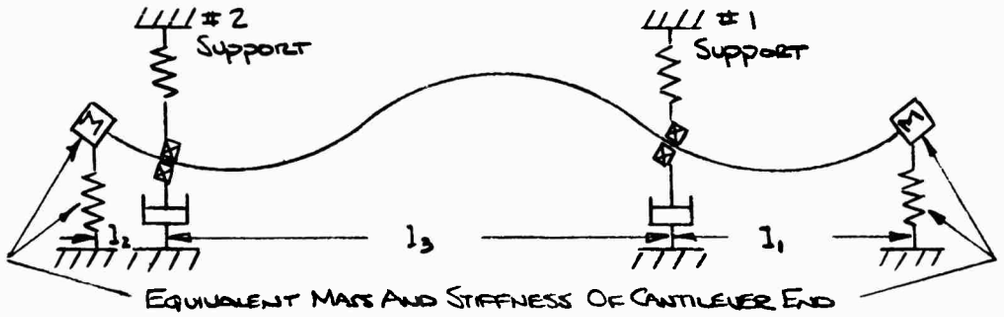

B. Equivalent Mechanical Representation Of High-Speed Shafts

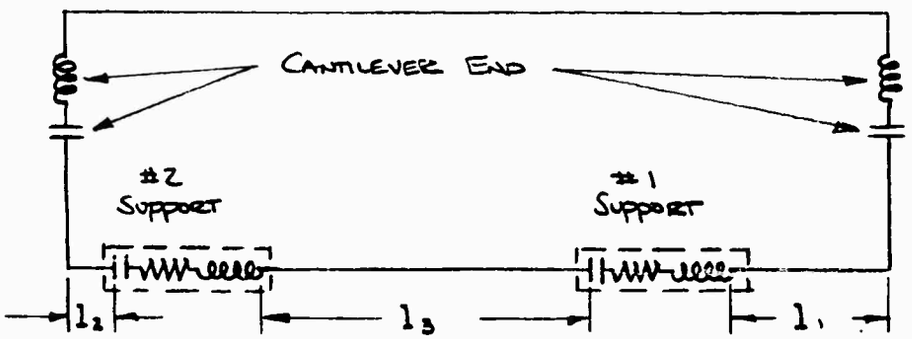

C. Electrical Analogy Of High-Speed Shafts

FIGURE 14. DEVELOPMENT OF AN ANALOGY BETWEEN A HIGH-SPEED SHAFT AND AN ELECTRICAL TRANSMISSION LINE

shown in Figure 14B, where the rigidly clamped shaft ends are replaced by a spring-mass combination. To make this change valid, the following reasoning was employed: for each critical speed of the fixed-ended shaft a shorter shaft having simply supported ends can be found which has the same critical speed. The fixed-ended shaft is therefore considered equivalent to a simply supported shaft joined at each end to a short cantilever beam. The springs and masses shown in Figure 14B attached to the ends of the shaft are equivalent to the effective masses and spring rates of the short cantilevered ends of the shaft in Figure 14A.

The mechanical system shown in Figure 14B is considered equivalent to the electrical system shown in Figure 14C for the purposes of the transmission-line analogy. In Figure 14C the spring-mass combination representing the fixed ends of the shaft has been replaced by a capacitance and inductance combination. At an equivalent distance in wave lengths down the transmission line from the end, a combination of capacitance, resistance, and inductance is placed in series with the line to represent the dynamic characteristics of the shaft support bearing. Each additional shaft support bearing is replaced by its analogous resistance, capacitance, and inductance at the correct distance in wavelengths from the end of the transmission line. It should be noted here that for purposes of wavelength measurements along the line, the end of the mechanical shaft is considered to lie at the juncture between the equivalent simple beam and the equivalent cantilever as shown in Figure 14A.

For efficient energy transfer in high-frequency power-transmission lines the load on the transmission line is designed to appear purely resistive at the operating frequency, and to have a resistance value equal to the characteristic impedance of the transmission line. In the case of the high-speed shaft the load to which vibratory energy is to be delivered is the damper located at the intermediate support bearing. One, two, or more intermediate support bearings may be used. Figure 14 shows two bearings for purposes of illustration only. The dampers at these two bearings represent the loads on the shaft insofar as vibratory energy is concerned. The intention of the design procedure is to select proper values and locations for the intermediate supports to match the impedance of the transmission line, or in this case the shaft, at the desired operating frequencies.

Relationships Between Mechanical and Electrical Quantities

The first critical speed of a simply supported beam is given by the expression

$$f = 1.57 \left[\frac{EIg}{w\ell^4} \right]^{1/2}, \tag{49}$$

where

f = critical speed, cycles or rev/sec

E = modulus of elasticity, psi

I = section moment of inertia, in.^{4}

g = acceleration due to gravity, 386 in./sec^2

w = unit weight of beam, lb/in.

ℓ = beam span length, in.

The moment of inertia of a tubular or solid shaft is given by the expression

$$I = \frac{\pi(D^4 - d^4)}{64} , \tag{50}$$

where

D = outside diameter, in.

d = inside diameter, in.

The weight per inch of a tubular or solid shaft is given by the expression

$$w = \frac{\pi(D^2 - d^2)}{4} P , \tag{51}$$

where

P = density of shaft material, lb/in.^{3}

Substituting (50) and (51) in (49) gives

$$f = \frac{7.76}{\ell^2} \left[\frac{E(D^2 + d^2)}{P} \right]^{1/2} . \tag{52}$$

For steel shafting, where $E = 3 \times 10^7$ psi and P = 0.283 lb/in.^{3}, Equation (52) reduces to

$$f = \frac{80,000 (D^2 + d^2)^{1/2}}{\ell^2} . \tag{53}$$

For solid steel shafting, Equation (53) becomes

$$f = \frac{80,000 D}{\ell^2} . \tag{54}$$

In the case of a simply supported shaft, the length between supports or between nodes of a vibrating shaft is equal to one-half a wavelength. That is,

$$\ell = \frac{\lambda}{2} , \tag{55}$$

where

λ = the vibration wavelength, in.

Substituting Equation (55) in Equation (54) gives the following:

$$f = \frac{320,000 D}{\lambda^2} . \tag{56}$$

Equation (56) may be rewritten in the following form for convenient use later.

$$\lambda = \frac{565 (Df)^{1/2}}{f} . \tag{57}$$

In the case of a lossless, high-frequency electrical transmission line, the velocity of propagation of an electrical impulse is equal to the velocity of light. It is called the velocity of phase propagation, and is independent of frequency. In the case of a lossless transmission line [Ref. (3)],

$$v = \frac{1}{(L_e C_e)^{1/2}}, \tag{58}$$

where

v = velocity of phase propagation

L_e = inductance per unit length of line

C_e = capacitance per unit length of line

Also, for the transmission line

$$\lambda = \frac{v}{f} \tag{59}$$

Substituting equation (58) in equation (59) gives

$$\lambda = \frac{1}{f(L_e C_e)^{1/2}} \tag{60}$$

Equation (60) for the wavelength on the electrical transmission line corresponds to Equation (57) for the wavelength on the high-speed shaft.

Mechanical equivalents of inductance and capacitance per unit length of line are needed for the development of the analogy. Mass per unit length of shaft is clearly analogous to inductance per unit length of transmission line.

$$L_e = m_u \tag{61}$$

$$m_u = \frac{\pi(D^2 - d^2) P}{4g}, \tag{62}$$

where

m_u = mass of shaft per unit length, lb-sec^2/in.^{2}

For a solid steel shaft

$$m_u = 5.76 \times 10^{-4} D^2. \tag{63}$$

Capacitance per unit length of the transmission line is analogous to compliance per unit length in the mechanical shaft.

$$C_e = \frac{1}{K}. \tag{64}$$

Therefore, from Equations (61) and (64),

$$L_e C_e = \frac{m_u}{K}. \tag{65}$$

From Equations (57) and (60),

$$\lambda = \frac{565\,(Df)^{1/2}}{f} = \frac{1}{f(L_e C_e)^{1/2}}$$

or

$$320{,}000\ Df = \frac{1}{L_e C_e} . \tag{66}$$

Substituting (63) and (65) in (66) gives

$$K = 184\ D^3 f . \tag{67}$$

A basic parameter of the electrical transmission line is the characteristic impedance of the line. This is the impedance that would be offered by a transmission line of infinite length. A line of any finite length, connected at one end of a resistance equal to the line's characteristic impedance, would appear at the other end to present the same impedance as an infinitely long line. An electrical impulse introduced at one end of the line would be completely dissipated in the resistive load at the other end. Thus, no reflection of energy would occur from the end of the line, and there would be no standing waves of voltage on the line. In such a case, the transmission line is said to be "matched" to the load. The voltage standing wave ratio, or ratio of maximum to minimum voltages along the line, equals one in the matched case, as there are no standing waves, and equal voltages would be measured at all points.

The characteristic impedance of the transmission line is given by the following expression [Ref. (3)]:

$$Z_s = \left(\frac{L_e}{C_e}\right)^{1/2} , \tag{68}$$

where

Z_s = characteristic line impedance.

Substituting (61) and (64) in (68) gives

$$Z_s = (m_u K)^{1/2} . \tag{69}$$

Substituting (63) and (67) in (69) gives the characteristic impedance of a solid steel shaft as

$$Z_s = 0.325\ D^2 (Df)^{1/2} . \tag{70}$$

A limited time was available at the end of Phase I for experimental verification of this analogy. Nevertheless, several tests were completed, and highly satisfactory high-speed operation was obtained. During the course of this experimental work it was determined that adjustment of the constant term in Equation (70) from 0.325 to 1.0 gave apparently superior results in actual high-speed shaft tests. This fact was actually discovered by accident, as a mistake of this magnitude was made in the original development of the analogy relationships. When the dampers of the test machine were readjusted to "correct" the mistake, however, smoothness of shaft operation suffered. Pending further experimentation, therefore, the following expression for characteristic shaft impedance will be used:

$$Z_s = D^2 (Df)^{1/2} . \tag{71}$$

The Smith Chart as a Design Tool

A valuable aid to electrical engineers in the study of high-frequency electrical transmission lines is the Smith chart [Ref. (3)] shown in Figure 15. The chart is a complex plot of load impedance on a transmission line as seen from various points along the line. So that a single plot may be used for studies of transmission lines having various characteristic impedances, all impedances are normalized, that is, divided by the characteristic line impedance. A resistive load equal in magnitude to the impedance of the line would therefore appear at the very center of the chart, at the point marked 1.0. A resistive load equal in magnitude to three times the characteristic impedance of the line would be plotted along the straight horizontal center line of the chart at the point designated 3.0. Purely reactive loads, that is, loads containing no resistive component, are plotted around the outer perimeter of the chart. Loads composed of both resistance and reactance are plotted at the intersection on the chart of lines representing the correct resistive and reactive magnitudes.

For loads that are not perfectly matched to the line impedance, that is, not purely resistive and equal to the characteristic line impedance, the load offers different characteristics when the line length is changed. Point A on Figure 15 is shown to illustrate this. The normalized impedance of Point A is 0.3 + j0.5. This means that the resistance component of the load impedance is equal to 0.3 times the characteristic line impedance, while the inductive reactance of the load is equal to 0.5 times the characteristic line impedance. If the reactive component had been negative, that is, capacitive, the load would have been represented by Point B, having a value of 0.3 - j0.5.

The radius drawn from the center of the chart through Point A crosses the outer wavelength reference circle of the chart at Point C, equal to 0.078 wavelength. This particular number of wavelengths has no significance in itself but is useful as a reference from which other wavelength measurements may be made. If measurements are made of load impedance from a location down the line from the load toward the generator, the circle drawn through Point A and having its center at the chart center is the locus of all measured values of load impedance. For example, if a measurement of load impedance were made from a point 0.172 wavelength toward the generator from the load, the measured impedance would be represented by Point D. The original load impedance was located at 0.078 wavelength. Adding 0.172 wavelength gives 0.250 wavelength. When this position is located along the outer circle of the Smith chart, and a radius drawn to that point from the center of the chart, the radius crosses the circle representing the locus of load impedance at Point D. Thus, from this location, the load would appear to be a pure resistance equal in magnitude to 4.2 times the characteristic line impedance. At a location 1/4 wavelength from the load at Point A the apparent load impedance would be represented by Point E where the normalized impedance is 0.88 - j1.48.

Another important piece of information obtained from the Smith chart is the voltage standing wave ratio, abbreviated VSWR. This quantity, often called simply the standing wave ratio, is given by the intersection of the impedance locus with the right-hand section of the Smith chart center line. In the example given, therefore, the standing wave ratio would be 4.2 as indicated at Point D.

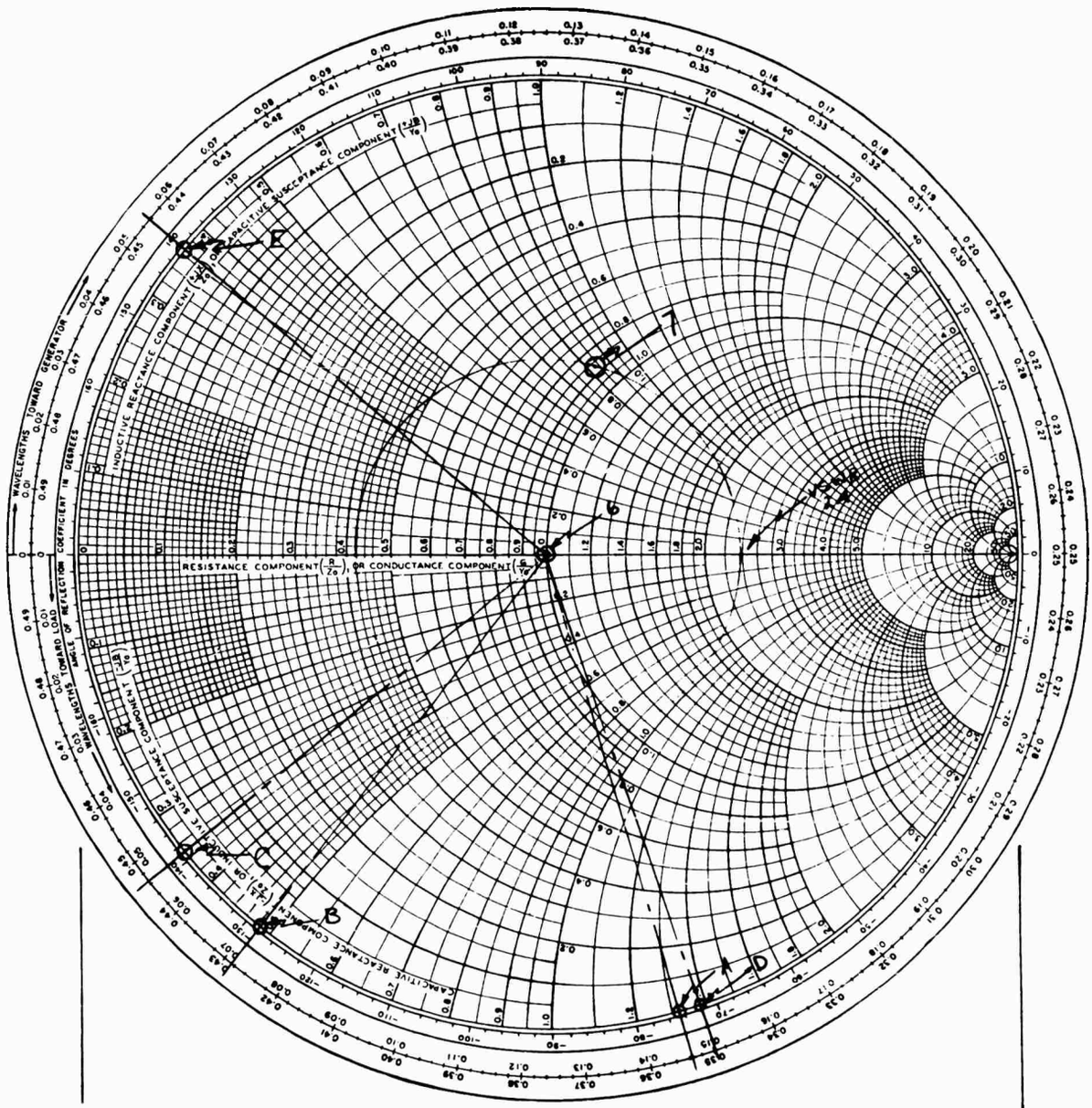

FIGURE 15. SMITH CHART FOR STUDIES OF IMPEDANCE MATCHING ON HIGH-FREQUENCY ELECTRICAL TRANSMISSION LINES

Smith chart published with permission of P. H. Smith and Kay Electric Co.

Example of High-Speed Shafting Design Procedure Using Smith Chart

As a preliminary verification of the transmission-line analogy of high-speed shafting, it was decided to design and test a damped support system. Examination of 15 combinations of variables already tested experimentally proved to be enlightening. Studying these cases with the use of the electrical analogy and the Smith chart showed that high-standing wave ratios were predicted, corresponding to large vibration amplitudes. It became apparent that standing wave ratio is a measure of the severity of shaft vibration in the examples studied. It was also apparent that the high standing wave ratios resulted primarily from the high inductive reactance (high mass) of the support bearing relative to the shaft. For this reason it was decided that the largest shaft that could be accommodated by the high-speed testing machine would be used, so that the support bearings would appear less massive relative to the shaft.

The shaft selected was of solid steel, 1/2 inch in diameter and 138 inches long. An arbitrary decision was made to design a damped support bearing for correct impedance matching at the sixth critical speed, and to determine the resulting standing wave ratios at other critical speeds. A different starting point for design could have been chosen, but for purposes of a first demonstration this choice was considered suitable.

It was decided that behavior of the shaft would be examined at the first nine critical speeds. Voltage standing wave ratio as determined from the Smith chart was selected as the parameter to be minimized for smooth operation of the high-speed shaft.

A large number of rather elementary calculations were involved in carrying out the design of the damped support bearings. The essential results of these calculations are given in Table 4. The first 11 items in the table are basic parameters of the 138-inch-long, 1/2-inch-diameter, solid steel shaft.

Line 1 in Table 4 lists the critical speeds of the shaft. These critical speeds were calculated from the following equation:

$$\text{cpm} = \frac{3.07\,(1.25n + 0.637)^2 D \times 10^6}{L^2} \tag{8}$$

where

n = order of critical speed

D = shaft diameter, in.

L = shaft length, in.

cpm = critical speed, cycles per minute.

Line 2 lists the length of a simple beam which would have the same speed for its critical speed as does a 138-inch-long beam having rigidly fixed ends. These simple beam lengths were calculated from the expression

$$L = n\left(\frac{80{,}000\,D}{f}\right)^{1/2}, \tag{72}$$

TABLE 4. PARAMETERS CALCULATED AND DETERMINED FROM THE SMITH CHART IN DESIGNING DAMPED SUPPORTS FOR A 138-INCH-LONG, 1/2-INCH-DIAMETER SOLID STEEL SHAFT FOR OPERATION UP THROUGH AND BEYOND THE SIXTH CRITICAL SPEED

Parameters of 138-In.-long, 1/2-In.-Diameter Shaft	Order of Critical Speed								
	1	2	3	4	5	6	7	8	9
1 - Critical Speed, rpm	286	790	1540	2560	3820	5330	7060	9060	11300
2 - Equivalent Simple Beam Length, in.	91.7	110.4	118.4	122.7	125.5	127.5	129.2	130.4	131.4
3 - Equivalent Length of Cantilever Ends, in.	23.15	13.8	9.8	7.65	6.25	5.25	4.4	3.8	3.3
4 - λ, Vibration Wavelength, in.	183.4	110.4	78.94	61.36	50.2	42.5	36.92	32.6	29.2
5 - Z_s Characteristic Impedance = $D^2(Df)^{1/2}$	0.39	0.64	0.90	1.15	1.41	1.67	1.92	2.17	2.43
6 - Measured Cantilever Stiffness, lb/in.	21	89	238	475	833	1316	2083	--	--
7 - Effective Mass at End of Cantilever, lb-sec^2/in.	0.000803	0.000478	0.000340	0.000265	0.000217	0.000183	0.000153	--	--
8 - Reactance of Cantilever Stiffness	-j0.700	-j1.076	-j1.470	-j1.774	-j2.083	-j2.359	-j2.818	--	--
9 - Reactance of Cantilever Mass	+j0.024	+j0.040	+j0.055	+j0.071	+j0.087	+j0.102	+j0.113	--	--
10 - Total Reactance of Cantilever	-j0.676	-j1.036	-j1.415	-j1.703	-j1.996	-j2.257	-j2.705	--	--
11 - Normalized Reactance of Cantilever	-j1.71	-j1.58	-j1.54	-j1.44	-j1.38	-j1.32	-j1.38	Est-j1.4	Est-j1.4
Support Optimized for Sixth Critical Speed									
12 - Normalized Support Damping	4.31	2.60	1.86	1.44	1.18	1.00	0.87	0.77	0.69
13 - Reactance of Support Bearing Mass	j0.044	j0.12	j0.24	j0.39	j0.58	j0.81	j1.07	j1.38	j1.72
14 - Normalized Reactance of Support Mass	+j0.1	j0.2	j0.27	j0.34	j0.40	j0.485	j0.55	j0.62	j0.70
15 - Reactance of Support Stiffness	-j4.00	-j1.45	-j0.74	-j0.45	-j0.30	-j0.22	-j0.16	-j0.13	-j0.10
16 - Normalized Reactance of Support Stiffness	-j10.1	-j2.2	-j0.82	-j0.391	-j0.21	-j0.135	-j0.09	-j0.06	-j0.05
17 - Total Normalized Support Reactance	-j10.0	-j2.0	-j0.55	-j0.051	+j0.19	+j0.35	+j0.46	+j0.56	+j0.65
18 - Reactance of Cantilever Seen from Support	-j1.0	-j0.06	+j0.77	+j5.0	-j1.76	-j0.35	+j0.37	+j1.67	-j5.25
19 - Combined Normalized Load Reactance	-j11	-j2.06	+j0.22	+j4.95	-j1.57	j0	+j0.83	+j2.23	-j4.6
20 - Inches from Simple Beam End to Support	7.32	16.67	20.67	22.82	24.22	25.22	26.07	26.67	27.17
21 - Wavelengths from Simple Beam End to Support	0.0399	0.151	0.262	0.372	0.4825	0.5932	0.7060	0.818	0.931
22 - Wavelength Reading at Cantilever Reactance	0.3343	0.3396	0.3420	0.3467	0.3496	0.3535	0.3496	0.3490	0.3490
23 - Wavelength Reading at Support Location	0.3742	0.4906	0.104	0.2187	0.3321	0.4467	0.0556	0.167	0.280
24 - Voltage Standing Wave Ratio	29	4.5	1.96	19	3.8	1.0	2.4	8.5	33

TABLE 4. (Continued)

Support Optimized for Fourth Critical Speed	Order of Critical Speed								
	1	2	3	4	5	6	7	8	9
25 - Normalized Support Damping	3.0			1.00				0.53	0.47
26 - Reactance of Support Bearing Mass	j0.040			j0.354				j1.25	j1.56
27 - Normalized Reactance of Support Mass	j0.10			j0.3				j0.56	j0.63
28 - Reactance of Support Stiffness	0			0				0	0
29 - Normalized Reactance of Support Stiffness	0			0				0	0
30 - Total Normalized Support Reactance	j0.1			j0.3				j0.56	j0.63
31 - Reactance of Cantilever Seen from Support	-j0.306			-j0.3				j0.82	-j6.50
32 - Combined Normalized Load Impedance	3-j0.206			1+j0				0.53+j1.38	0.47-j5.87
33 - Inches from Simple Beam End to Support	21.75			37.25				41.1	41.6
34 - Wavelengths from Simple Beam End to Support	0.1186			0.107				1.26	1.425
35 - Wavelength Reading at Cantilever Reactance	0.3343			0.347				0.349	0.349
36 - Wavelength Reading at Support Location	0.4529			0.454				0.109	0.274
37 - Voltage Standing Wave Ratio	3			1.0				5.9	80

where

L = simple beam length, in.

D = shaft diameter, in.

f = critical speed, cps

n = order of critical speed.

Line 3 lists the equivalent length of what is here termed the cantilevered ends of the fixed-ended shaft. This length is equal to one-half the difference in length between the total shaft length of 138 inches and the equivalent simple beam lengths listed under Item 2.

Line 4 gives the wavelength of the vibrations on the equivalent simple beam, and is equal to twice the distance between vibration nodes.

Line 5 lists the characteristic shaft impedance calculated from the equation

$$Z_s = D^2(Df)^{1/2} . \tag{71}$$

Line 6 lists the stiffness measured at the ends of cantilever beams having the lengths listed in Line 3. If the spindles and bearings of the test machine were perfectly rigid the stiffness values in Line 6 could have been computed from standard beam formulas. Because of the finite stiffness of the testing machine spindles and bearings, however, it was considered more accurate to determine the effective cantilever stiffness experimentally. Lengths of 1/2-inch shaft equal to the values given in Line 3 were installed in the testing-machine spindles, and the deflection at their ends was measured with loads applied at their ends.

Line 7 lists the effective mass that could be considered concentrated at the end of the cantilevered section of the shaft. This effective mass was determined by first computing the theoretical stiffness of the cantilever, next computing the theoretical natural frequency of vibration of the cantilever by itself, and finally computing the mass which, together with the stiffness first computed would produce the same natural frequency for the cantilever beam. The expression for cantilever stiffness is as follows:

$$K = \frac{3EI}{L^3} , \tag{73}$$

where

K = stiffness of cantilever, lb/in.

E = modulus of elasticity, psi

I = section moment of inertia, $in.^4$

L = cantilever length, in.

The natural frequency of a cantilever is given by

$$f = 0.56 \left[\frac{EIg}{wL^4} \right]^{1/2} , \tag{74}$$

where

g = acceleration due to gravity, 386 in./sec^2

w = unit weight of shaft, lb/in.

f = lowest natural frequency of vibration, cps.

Since the natural frequency of any vibratory system is given by

$$f = \frac{1}{2\pi} \left(\frac{K}{m} \right)^{1/2} , \tag{75}$$

an expression for effective mass at the end of the cantilever can be derived by combining Equations (73), (74), and (75). By this means the effective cantilever mass is found to be equal to

$$m = \frac{0.242\ wL}{g} . \tag{76}$$

For a solid steel shaft this expression becomes

$$m = 0.000139 D^2 L , \tag{77}$$

where

L = length of cantilever section of shaft, in.

D = shaft diameter, in.

Line 8 gives the reactance offered by the stiffness of the cantilever beam ends. This reactance is equal in magnitude to the stiffness in pounds per inch divided by the angular frequency in radians per second. Like capacitive reactance in electrical circuits this reactance is multiplied by -j to give the correct phase angle.

Line 9 gives the reactance offered by the effective mass of the cantilever beam ends. This quantity is equal to the mass given in Line 7 multiplied by the frequency in radians per second. The quantity is multiplied by +j to indicate the correct phase angle.

Line 10 is the algebraic sum of Lines 8 and 9.

Line 11 is equal to the value in Line 10 divided by the corresponding characteristic impedance given in Line 5.

The section of Table 4 listing Items 12 through 24 is based upon the arbitrary decision to optimize the damped support bearing for operation of the shaft at its sixth critical speed. Involved in the design procedure is the assumption that the critical speeds are only slightly changed by the presence of the damped support bearings. Experience has shown this assumption to be sufficiently accurate for practical design

purposes. Design of the damped support bearing will therefore be carried out in this case for effective operation at the sixth critical speed of 5330 rpm.

Line 12 lists the normalized support damping, that is, the value of the damping coefficient divided by the corresponding characteristic impedance given in Line 5. For best impedance matching at the sixth critical speed the normalized damping value must equal 1.0 at that speed. The actual damping coefficient must therefore be equal to 1.67 lb-sec/in. so that when divided by 1.67 the normalized value will equal 1.0. The normalized damping values at the other critical speeds are equal to 1.67 divided by the corresponding characteristic impedances.

Line 13 gives the reactance of the support bearing mass. The weight of the bearing assembly used on the testing machine was equal to 0.56 pounds. The reactance is given by 0.56 divided by 386, times frequency in radians per second.

Line 14 gives the normalized reactance of the support mass, equal to the values in Line 13 divided by the values in Line 5.

At this point it is convenient to refer to the Smith chart in Figure 16. Point A is plotted at the location -j1.32, equal to the normalized reactance of the cantilever given in Line 11 for the sixth critical speed. The radius drawn through Line A crosses the wavelength circle at about 0.3535 wavelength. Proper adjustment of the damped support bearing requires that it be placed at such a location that its own reactance is canceled by the reactance of the cantilevered shaft end as seen from the support location. It would be possible, therefore, to locate the damped support bearing at a position where the normalized reactance of the support mass, equal to j0.485, would be just canceled by the reactance of the cantilever seen from that location. This condition would result if the support were located 0.075 wavelength from the end of the equivalent simple beam section of the shaft. This placement of the support is illustrated by Point B in Figure 16. At this time it was decided that support placement on the test machine might be critical if an attempt were made to locate it only 0.075 wavelength from the end of the equivalent simple beam. The value of 0.075 wavelength was obtained from the Smith chart as follows: the radius drawn through Point B crosses the circle at 0.4285 wavelength. The radius through Point A crosses the wavelength circle at 0.3535 wavelength. The difference between these two values is 0.075 wavelength.

So that the support could be located as far as possible from the end of the equivalent beam section of the shaft it was decided that stiff support springs would be added at the support bearing. The stiffest springs conveniently provided on the testing machine have an effective rate equal to 120 lb/in. The reactance offered by these springs is given in Line 15, and is equal to 120 lb/in. divided by frequency in radians per second.

Line 16 lists the normalized value of reactance of the support stiffness, and is equal to the value in Line 15 divided by the corresponding value in Line 5.

Line 17 gives the total normalized reactance of the support bearing, and is equal to the algebraic sum of Lines 14 and 16.

Now that the total normalized support reactance is known, the required value of reactance to be contributed by the cantilever shaft end is fixed for correct impedance matching at the sixth critical speed. Line 18 lists the reactance of the cantilever seen from the support location, and in the case of the sixth critical speed it must be made

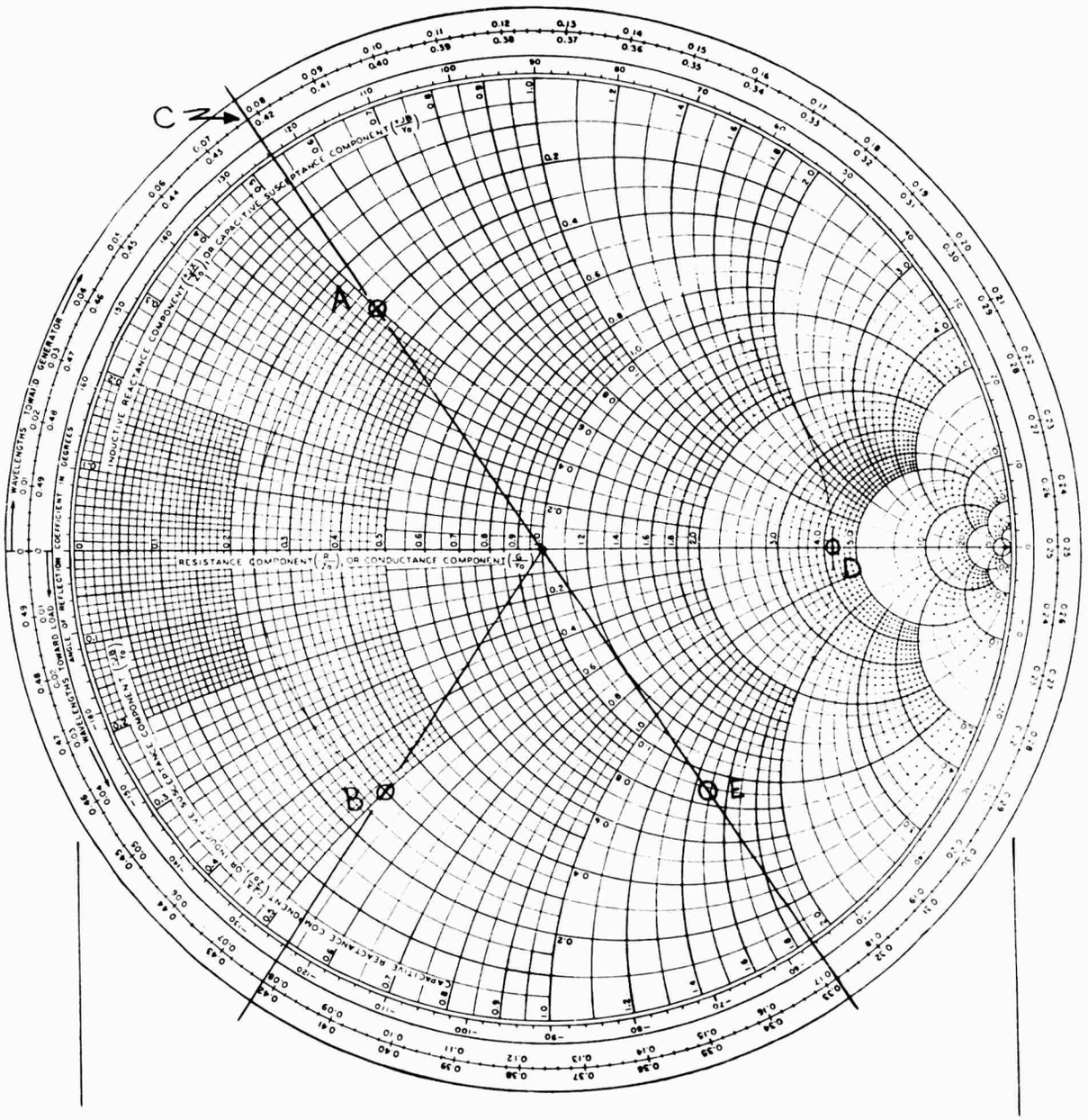

FIGURE 16. SMITH CHART SHOWING APPLICATION OF DESIGN PROCEDURE TO 138-INCH-LONG, 1/2-INCH-DIAMETER SHAFT

Smith chart published with permission of P. H. Smith and Kay Electric Co.

equal and opposite to the normalized support reactance. Therefore, for correct impedance matching at the sixth critical speed the reactance of the cantilever referenced to the support location must equal -j0.35. This value is found at Point C on the Smith chart of Figure 16. The radius through Point C crosses the wavelength circle at 0.4467 wavelength. The distance in wavelengths from Point A to Point C is therefore equal to 0.0932 wavelength.

Another property of the Smith chart can now be illustrated. It should be noted that one revolution around the chart is equal to a distance along the transmission line of 0.5 wavelength. It is possible, therefore, to obtain the same impedance match with the support bearing located 0.0932 or 0.5932 wavelength from the end of the equivalent simple beam. In this case it appeared that operation of the shaft at the lower critical speeds would be favored with the support located farther from the shaft end. The decision was therefore made to locate the support 0.5932 wavelength from the end of the equivalent simple beam.

As the wavelength at the sixth critical speed is 42.5 inches, 0.5932 wavelength equals 25.22 inches. The distance from the end of the equivalent simple beam is thus 25.22 inches, making a total distance from the end of the actual shaft to the support of 30.47 inches. This is obtained by adding the equivalent length of the cantilever end, given in Line 3 as 5.25 inches, to the value of 25.22 inches.

Now that the support location has been fixed to favor operation at the sixth critical speed, conditions at the other critical speeds may be examined. The combined normalized load reactance given in Line 19 has deliberately been made equal to j0 which, together with a normalized load resistance of 1.0, results in a voltage standing wave ratio given in Line 24 of 1.0 for the sixth critical speed. Standing wave ratios were determined for the other critical speeds to determine the effectiveness of damping at those speeds.

At the seventh critical speed, for example, the following determinations can be made. The normalized reactance of the cantilever equal to -j1.38 is shown at Point D on Figure 16. The radius through Point D crosses the wavelength circle at 0.3496 wavelength, given in Line 22. As the support is located 30.47 inches from the end of the shaft, it can be seen that it is located 26.07 inches from the end of the equivalent simple beam. This value is obtained by subtracting the equivalent length of cantilever beam in Line 3 from 30.47 inches.

In Line 21 the number of wavelengths from the simple beam end to the support is equal to the distance in Line 20 divided by the wavelength in Line 4. The wavelength reading at the support bearing location, Line 23, is obtained by adding the values in Lines 21 and 22. Integral numbers of half-wavelengths may be disregarded, as they represent identical points on the Smith chart. The value in Line 23 is therefore listed as 0.0556 wavelength, although the sum of Lines 21 and 22 equals 1.0556 wavelengths. The reactance of the cantilever seen from the support location is shown at Point E. This value equals +j0.37 and is located by a radius drawn through the wavelength circle at 0.0556 wavelength.

The total normalized support reactance in Line 17 is added to the reactance of the cantilever as seen from the support in Line 18 to give combined normalized load reactance in Line 19. The combined normalized load reactance in Line 19, together with the normalized load resistance or damping in Line 12 represents the total load impedance. For the seventh critical speed the total load impedance is therefore 0.87 + j0.83.

This value is plotted at Point 7 in Figure 16. The circle drawn through Point 7 with its center at the chart center crosses the right-hand section of the chart center line at a value of 2.4. This value is equal to the predicted voltage standing wave ratio for operation at the seventh critical speed.

This same procedure was followed for each of the other critical speeds to determine voltage standing wave ratios. It will be seen from Line 24 that high values of standing wave ratio were predicted for the first, fourth, and ninth critical speeds, with a moderately high value predicted for the eighth critical speed. The values predicted for the second, third, fifth, sixth, and seventh critical speeds are all low, predicting effective damper action at these speeds.

At this point in the design procedure it was decided that a second support should be added, designed for optimum performance at the fourth critical speed. This choice was made because previous experience had shown that vibrations at the first critical speed seldom were serious, while if conditions were optimized for the ninth critical speed bad vibrations at the fourth critical could prevent ever achieving operation at the ninth.

Lines 25 through 37 of Table 4 list parameters for the second damped support which was designed for operation at the fourth critical speed by the same procedure as that followed above. Following the design of this support, standing wave ratios were checked at the first, eighth, and ninth critical speeds. The values obtained indicated that besides controlling the fourth critical speed, the second support should be quite effective at the first and eighth criticals as well. This support, like the first one, was relatively ineffective at the ninth critical speed, so severe vibrations were anticipated at speeds around 11,000 rpm.

Experimental Demonstration of Design Procedure

The shaft testing machine was set up with two damped support bearings at the locations and having the parameters given in Table 4. The very first operation of the machine was fully successful using these values. Operation of the shaft was smooth at each of the first eight critical speeds. As the shaft speed exceeded 10,500 rpm, approaching the ninth critical speed, noise became apparent. Project personnel were reluctant to operate the shaft at or above the ninth critical speed because of the severe sound of the vibrations at that speed. This general behavior tended to support the general theory and calculations made in designing the supports.

At the encouragement of the technical monitor of the project from Wright-Patterson Air Force Base, speeds of the test machine were gradually increased during a demonstration on July 5. Vibration at the ninth critical speed was slightly noisy, though not as violent as expected. The shaft did not touch the metal guards which surrounded it at a radial clearance of only 1/8 inch. After 11,000 rpm was exceeded, speed increased smoothly with little obvious distress to the machine. In a series of runs made on July 5 the speed was gradually increased to 45,500 rpm. Some noise developed at 2 or 3 speeds in this range; however, shaft operation in general may be termed the best achieved during the course of the research program.

Because a considerable time is required for the calculations illustrated it has not yet been possible to calculate, using the newly developed procedure, the performance to

be expected of the test shaft over the entire speed range covered. Shaft speed during the tests exceeded the eighteenth critical speed. Behavior of the shaft over the speed range up to and including the ninth critical speed is closely similar to the predicted performance.

The positive results achieved in this first demonstration point to the extreme promise of the newly developed theory as a high-speed shafting design tool. Additional experimentation and analysis will be required for full confirmation of the theory.

It should be noted here that following the successful demonstration of the shaft a numerical error was found in the calculations of characteristic shaft impedance. When the damping values used in the test were changed to account for this error, shaft operation suffered. For this reason, as noted previously in the derivation of the analogy, the equation for characteristic shaft impedance was corrected by a constant factor to produce the damping values which had already been used in the successful first demonstration. Additional work with this design procedure should serve to develop the optimum correction factors and design techniques for successful high-speed shaft operation.

Of general interest is the fact that the example shaft tested has a power transmission capability of approximately 900 horsepower at the maximum speed of 45,500 rpm achieved during tests. This speed limitation was imposed not by the behavior of the shaft, but by slippage of the flat drive belts on the testing machine. The ultimate speed and power transmission capacity of this shaft are therefore not yet known.

The first demonstration of this design procedure was aimed at satisfactory shaft operation through the eighth critical speed. A far wider speed range was achieved. It is reasonable to expect that future design efforts with more ambitious objectives than this first one will achieve even more satisfactory shaft operation in the high-speed range. The most obvious trouble spot, the ninth critical speed, was identified in the design process, and presumably could have been controlled by a change of support parameters.

Determination of Shaft Lateral Critical Speeds

The design and analysis of power-transmission shafts for hypercritical-speed operation requires relatively accurate knowledge of the critical speeds. Selection of the dynamic parameters of the damped supports is dependent upon the discrete speeds at which vibration must be suppressed.

Critical Speeds and Vibration Node Position of Shafts Supported Only at Their Ends

The first section following the heading Technical Work presents formulas and curves to predict critical speeds of shafts supported only at their ends. Both simply supported and fixed-end shafts are discussed. Indication from the Sponsoring Agency has been that fixed-end shafts represent more closely the configuration to be expected in the majority of practical installations. Hence, research has been directed toward shafts with this type of end fixity.

The critical-speed formula for any circular shaft with both ends built-in is:

$$\text{cpm} = \frac{298c}{L^2}\sqrt{\frac{E\,(D^2 + d^2)}{P}}\,, \tag{78}$$

where

D = shaft outside diameter, in.

d = shaft inside diameter, in.

L = shaft length, in.

P = shaft density, lb/in.^{3}

E = shaft modulus of elasticity, lb/in.^{2}

c = proportionality constant

$= (1.250n + 0.637)^2$

n = number of the vibration mode.

Most work has been done, in both the digital-computer program and experimentally, with solid steel shafts. The resulting simplified critical speed formula for solid steel shafts with both ends built-in is:

$$\text{cpm} = \frac{3.07c\ D \times 10^6}{L^2}\,. \tag{79}$$

An important aspect of shafts vibrating at critical speeds is the position of the vibration node. A vibration node is characterized by absence of vibration amplitude, while an antinode is termed the position along the shaft of the maximum vibration. For instance at the first critical speed the antinode falls half-way between the shaft ends, and the nodes at each shaft end. At the third critical speed three vibration loops appear and there are three antinodes – one at each vibration loop. There are four nodes however; two appear at the shaft ends and the other two at 35.9 per cent of the shaft length from each end. The shaft length between nodes is the length of a vibration loop.

The formulas which describe node position along the shaft are given below.

For the position of the node nearest the shaft end:

$$X_1 = \frac{1.25}{n + 0.5} \quad \text{for } n \geq 4 \tag{80}$$

$$X_1 = 0.359 \quad \text{for } n = 3 \tag{81}$$

$$X_1 = 0.50 \quad \text{for } n = 2. \tag{82}$$

For the position of the node second from the shaft end:

$$X_2 = \frac{2.25}{n + 0.5}\,. \tag{83}$$

For the position of the node third from the shaft end:

$$X_3 = \frac{3.25}{n + 0.5}, \tag{84}$$

and so on where:

$$X = \frac{\text{Distance between the node in question and the shaft end}}{\text{Over-all shaft length}}.$$

Table 5 lists the critical-speed proportionality constant, c, and node location, X, through the first 20 critical speeds for any shaft with fixed ends. The formulas for c and and X were derived from a reference table in a vibrations textbook [Ref. (1)].

Critical Speeds of Fixed-End Shafts With Simply Supporting Equally Spaced Rigid Intermediate Supports

When rigid equally spaced intermediate supports are included along a shaft with fixed ends, the determination of critical speeds becomes more involved. One difficulty stems from the different moment absorbing ability of the bearings, when a fixed-end shaft is supported between ends by bearings of the self-aligning type. Another difficulty is occurrence of critical speeds not predicted by the simple formulas included elsewhere in this report. These difficulties have been discussed and solved in an article entitled, Natural Frequencies of Continuous Beams of Uniform Span Length. [Ref. (4)]

Consider a fixed-end shaft with three equally spaced simple bearings included along its length. Since lateral shaft stiffness is greater at the end spans, the first critical speed is a compromise between the fixed-hinged end spans and the simply supported center spans. As the number of supports increases, or higher critical speeds are encountered, the number of simple vibration loops overshadows the two fixed-hinged loops adjacent to the shaft ends. The shaft critical speed for many vibration loops begins to approximate that of a continuous beam with as many equally spaced intermediate supports and with the shaft ends simply supported.

Discussing the example given before with three equally spaced intermediate supports there are not one but four critical-speed vibrations which correspond to the first mode of vibration. Figure 17 shows the deflection shapes of this shaft for the first two groups of natural modes, and the four critical speeds occurring in each group.

The first critical speed of the first group of natural modes has a deflection curve with simple vibration loops at the center and fixed-hinged loops at each end. From the aspect of lateral shaft stiffness, this is the least stiff arrangement of the loops and therefore it appears at the lowest critical speed. The second speed occurs at the loop orientation to present the next higher over-all shaft stiffness. In this situation the center support bearing acts as would a fixed or moment-absorbing member. The third speed occurs at the next higher over-all shaft stiffness with a total of four of the five shaft bearings acting as moment-absorbing members. At the fourth speed of the first group of natural modes all support bearings act as built-in shaft supports, and provide the highest critical speed which can occur with one vibration loop per span between bearings. In the second group of natural modes the sequence repeats itself with the basic difference that there are two instead of one loop between support bearings. The number, h, in Figure 17 refers to the number of shaft span lengths between bearings.

TABLE 5. CRITICAL-SPEED PROPORTIONALITY CONSTANT c AND NODE LOCATION X THROUGH THE FIRST TWENTY CRITICAL SPEEDS OF A SHAFT WITH FIXED ENDS

n	c	X_1	X_2	X_3	X_4	X_5	X_6	X_7	X_8	X_9	X_{10}
1	3.56	--	--	--	--	--	--	--	--	--	--
2	9.82	0.500	--	--	--	--	--	--	--	--	--
3	19.27	0.359	--	--	--	--	--	--	--	--	--
4	31.75	0.278	0.500	--	--	--	--	--	--	--	--
5	47.4	0.227	0.409	--	--	--	--	--	--	--	--
6	66.2	0.192	0.348	0.500	-	--	--	--	--	--	--
7	88.1	0.167	0.300	0.433	--	--	--	--	--	--	--
8	113	0.147	0.265	0.382	0.500	--	--	--	--	--	--
9	141	0.132	0.237	0.342	0.447	--	--	--	--	--	--
10	172	0.119	0.214	0.309	0.405	0.500	--	--	--	--	--
11	207	0.109	0.196	0.283	0.370	0.457	--	--	--	--	--
12	244	0.100	0.180	0.260	0.340	0.420	0.500	--	--	--	--
13	285	0.0926	0.167	0.241	0.315	0.389	0.462	--	--	--	--
14	329	0.0862	0.155	0.224	0.293	0.362	0.431	0.500	--	--	--
15	376	0.0807	0.145	0.210	0.274	0.339	0.403	0.467	--	--	--
16	426	0.0757	0.136	0.197	0.258	0.318	0.379	0.439	0.500	--	--
17	479	0.0714	0.128	0.186	0.243	0.300	0.357	0.414	0.471	--	--
18	535	0.0676	0.122	0.176	0.230	0.284	0.338	0.392	0.446	0.500	--
19	595	0.0641	0.115	0.167	0.218	0.269	0.320	0.372	0.423	0.474	--
20	657	0.0609	0.110	0.158	0.207	0.256	0.305	0.354	0.402	0.451	0.500

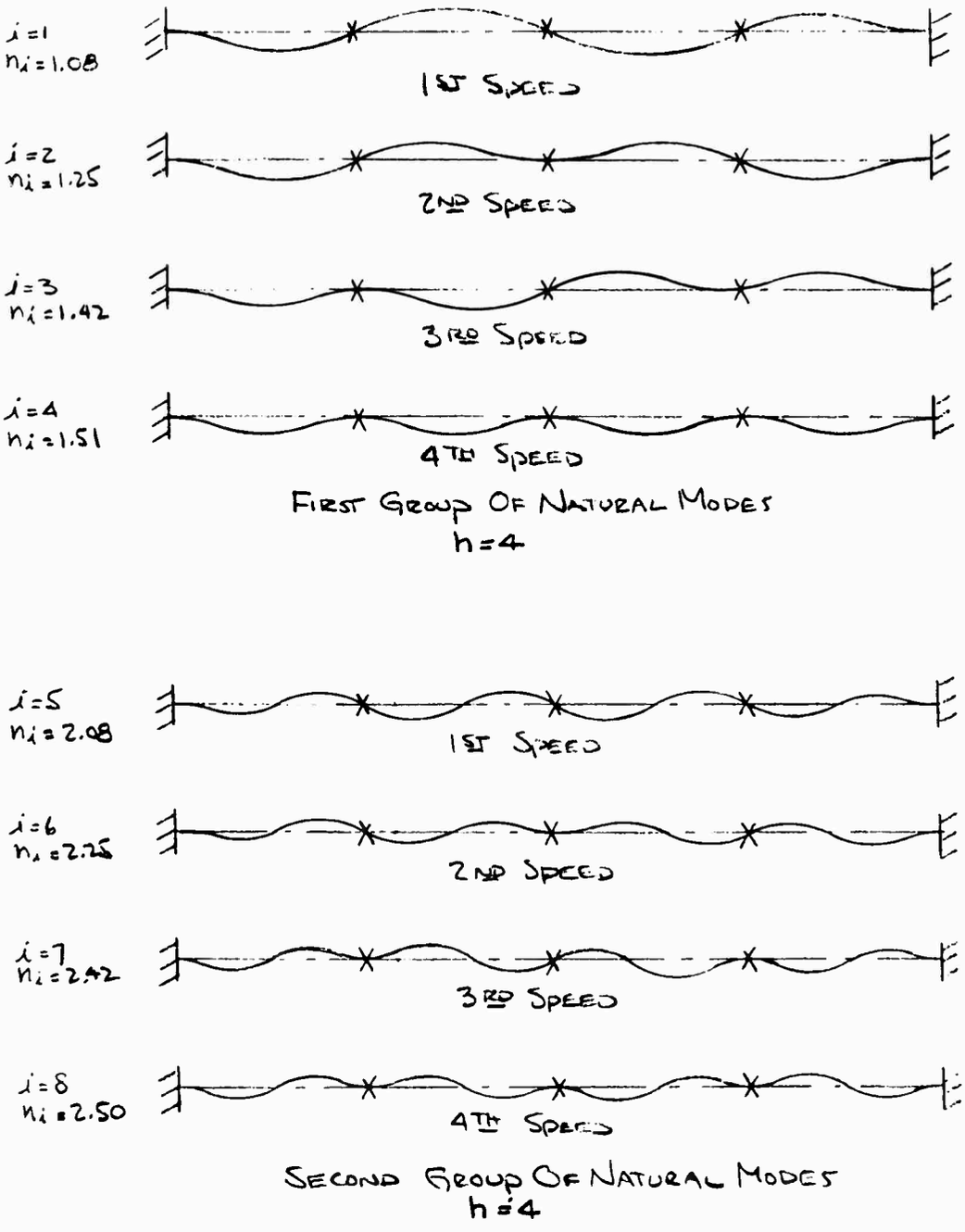

FIGURE 17. SHAFT-DEFLECTION CURVES FOR A CONTINUOUS FIXED-END SHAFT WITH THREE EQUALLY SPACED RIGID INTERMEDIATE SUPPORTS

The number, h, also indicates the number of critical speeds for each group of natural modes. The number i refers to the position in the vibration sequence. The number n_i is a proportionality constant used in critical-speed calculations.

The critical speed for any round shaft with fixed ends can be found from the following formula:

$$\text{cpm} = \frac{466(n_i)^2}{\ell^2}\sqrt{\frac{E(D^2 + d^2)}{P}} , \tag{85}$$

where

ℓ = span length between supports, in.

n_i = proportionality constant

other symbols as before.

Converting the equation for use with solid steel shafts gives the more simple relation:

$$\text{cpm} = \frac{4.8 \times 10^6 (n_i)^2 D}{\ell^2} . \tag{86}$$

Table 6 lists values of the critical-speed proportionality constant, n_i, with respect to number of spans between supports, h, and vibration speed number, i. With these values critical speeds can be calculated, and applied to the appropriate shaft-deflection curve adapted from Figure 17.

Table 7 lists comparative values of critical speeds calculated using the above equations, determined experimentally, and calculated by the digital-computer program, of fixed-end shafts with equally spaced rigid support bearings. In the experimental work critical speeds were determined by averaging the speeds at which the test shaft first contacted the shaft guards as shaft speed increased and decreased through the critical. In the computer tests the speed at which shaft amplitudes were computed to be substantial, was chosen as the critical speed. The tabulation shows reasonably good correlation of calculated and observed speeds, indicating that calculation procedure is correct.

Critical Speeds of Fixed-End Shafts With One Intermediate Support Not Centrally Located

Numerous experimental tests have been conducted with one intermediate support positioned away from the shaft center. Critical-speed vibrations have been successfully controlled only when the spans are unequal in length, which complicates the critical-speed problem. Determination of critical speed with various support positions has been made experimentally both with one rigid and one damped intermediate support.

Using a steel test shaft of 1/4-inch diameter 89.3 inches long, a rigid support was positioned at many locations between the shaft end and mid-point. At each rigid support location, shaft speed was increased through critical speeds until the noise of the shaft meeting the shaft guards became highly objectionable. Lateral-vibration mode shape and critical speed were recorded versus support location. Figure 18 shows a

TABLE 6. VALUES OF n_i VERSUS h AND i FOR FIXED-END SHAFTS WITH EQUALLY SPACED SIMPLE INTERMEDIATE BEARINGS

i \ h:	1	2	3	4	5	6	7	8	9	10
1	1.51	1.25	1.13	1.08	1.05	1.04	1.03	1.02	1.02	1.02
2	2.50	1.51	1.37	1.25	1.18	1.13	1.10	1.08	1.06	1.05
3	3.50	2.25	1.51	1.42	1.32	1.25	1.20	1.16	1.13	1.11
4	4.50	2.50	2.13	1.51	1.45	1.37	1.30	1.25	1.21	1.18
5	5.50	3.25	2.37	2.08	1.51	1.46	1.40	1.34	1.29	1.25
6	6.50	3.50	2.50	2.25	2.05	1.51	1.47	1.42	1.37	1.32
7	7.50	4.25	3.13	2.42	2.18	2.04	1.51	1.48	1.44	1.39
8	8.50	4.50	3.37	2.50	2.32	2.13	2.03	1.51	1.49	1.45
9	9.50	5.25	3.50	3.08	2.45	2.25	2.10	2.02	1.51	1.49
10	10.50	5.50	4.13	3.25	2.50	2.37	2.20	2.08	2.02	1.51
11	11.50	6.25	4.37	3.42	3.05	2.46	2.30	2.16	2.06	2.02
12	12.50	6.50	4.50	3.50	3.18	2.50	2.40	2.25	2.13	2.05
13	13.50	7.25	5.13	4.08	3.32	3.04	2.47	2.34	2.21	2.11
14	14.50	7.50	5.37	4.25	3.45	3.13	2.50	2.42	2.29	2.18
15	15.50	8.25	5.50	4.42	3.50	3.25	3.03	2.48	2.37	2.25
16	16.50	8.50	6.13	4.50	4.05	3.37	3.10	2.50	2.44	2.32
17	17.50	9.25	6.37	5.08	4.18	3.46	3.20	3.02	2.48	2.39
18	18.50	9.50	6.50	5.25	4.32	3.50	3.30	3.08	2.50	2.45
19	19.50	10.25	7.13	5.42	4.45	4.04	3.40	3.16	3.02	2.48
20	20.50	10.50	7.37	5.50	4.50	4.13	3.47	3.25	3.06	2.50

TABLE 7. HAND-CALCULATED VERSUS EXPERIMENTAL AND COMPUTER-CALCULATED CRITICAL SPEEDS OF FIXED-END STEEL SHAFTS WITH EQUALLY SPACED RIGID SUPPORTS

			First Group of Modes				Second Group of Modes			
d, in.	L, in.	h	1st	2nd	3rd	4th	1st	2nd	3rd	4th
			Critical Speed - Calculated, rpm / Experimental, rpm							
1/4	89.3	3	1740/1900	2555/2550	3105/2975	None	5660/6300	7640/7450	8490/8300	None
1/8	63	4	2830/2772	--	4900/4960	--	--	--	--	--
1/4	89.3	4	2810/3095	3770/3850	4870/4800	--	--	--	--	--
1/4	126	4	1410/1470	1890/1951	2445/2448	2675/2738	5240/5275	6120/6125	7090/7000	--
1/2	126	4	2830/2935	3790/3820	4900/4850	5550/5445	--	--	--	--
			Critical Speed - Calculated, rpm / Computed, rpm							
1/8	126	4	708/702	948/940	1225/1213	1387/1367	--	--	--	--
1/2	120	4	3110/3070	4180/4120	--	--	--	--	--	--

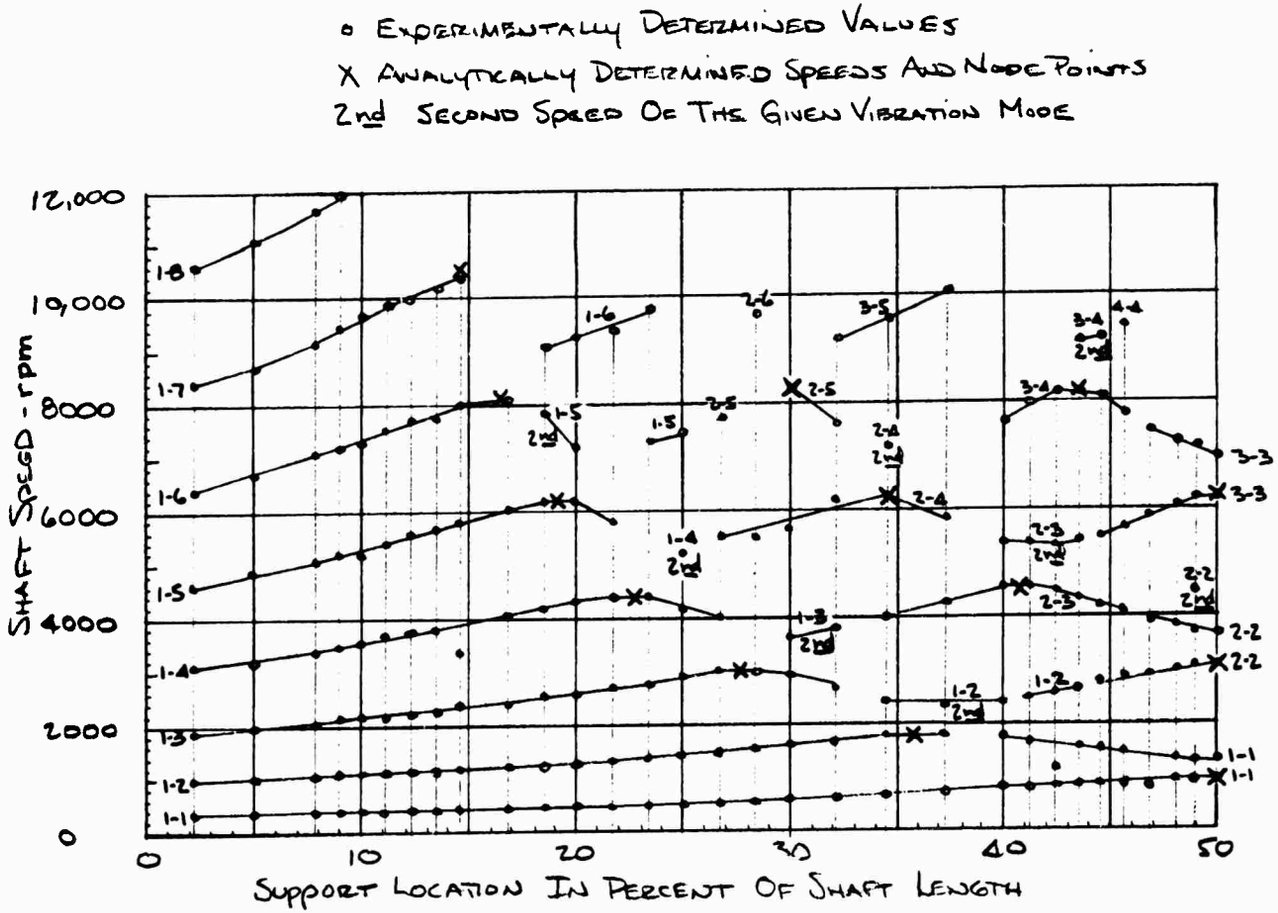

FIGURE 18. EXPERIMENTALLY DETERMINED SHAFT SPEED VERSUS SINGLE-RIGID-SUPPORT LOCATION SHOWING MODE SHAPES OF CRITICAL SPEEDS AND CORRELATION WITH ANALYTICALLY DETERMINED CRITICAL SPEEDS AND NODE POINTS FOR A 1/4-INCH-DIAMETER 89.3-INCH-LONG STEEL SHAFT WITH CLAMPED ENDS

summary of the data collected. Observed speeds are noted, and for the same vibration modes the speeds generally fall in a smooth curve as shown in the figure. The curve marked 1-4 means that one vibration loop occurs in the shorter span, while four loops are seen in the longer span.

The lower left portion of Figure 18 shows speed of each vibration mode to increase as support location progresses toward shaft mid-point. Since, as observed in the tests, the vibration of the loops in the longer section of the shaft is more severe than that of the single loop in the shorter span, the vibrations in the longer span are the more dominant. This is evident from a glance at the lower left portion of the figure, which shows the critical speed of each vibration mode to increase as the long span becomes shorter.

However, as support location proceeds toward mid-point, a point is reached where the vibration amplitudes in both spans are equal. This support location is coincident with a vibration node point. Then as the support is again moved toward shaft mid-point, the short span vibration becomes predominant and speed of the particular vibration mode decreases.

The x's shown on Figure 18 refer to predicted speed and location of vibration nodes. The tabulation of node position, X, and critical speed constant, c, is listed as Table 5 in this section. There is good agreement between predicted and measured speeds, as well as predicted and measured node locations. The experimentally determined node position occurs at the point of maximum speed for any certain mode of vibration.

For the various single damped support tests critical speeds followed the same pattern and occurred at the same approximate speed as for the rigid single support test. Curves of critical speeds versus support location for damped supports can be found in the section discussing high-speed shaft operation. Results of the single damped tests showed that good vibration control might be secured if the damper were not located at a vibration node point. Since the damper is active only when shaft vibration occurs at the damper, it must be positioned away from vibration nodes. Figure 19 shows a series of curves which represent the data of Table 5. The curves connect node positions which have similar characteristics, and the ordinate plots vibration speed for a 1/4-inch-diameter 89.3-inch-long steel shaft with clamped ends. It can be seen from the figure that damper locations other than toward a shaft end will eventually be positioned at or close to a node. This is undoubtedly the reason the single damped support tests have shown consistently better operation with the damper close to a shaft end, rather than toward shaft mid-point.

Critical Speeds of Fixed-End Shafts With Damped Multiple Intermediate Supports

One Support Fixed Close to Shaft End and Other Varied. A series of tests using two damped intermediate supports produced the critical-speed pattern shown in Figure 20. One damped support retained its position close to a shaft end, while the other was varied between the shaft mid-point and the other end. Comparison of Figures 19 and 20 shows a very similar orientation of vibration modes and speeds at which they occur. Figure 20 terminology is the same as previously used; for instance, the curve

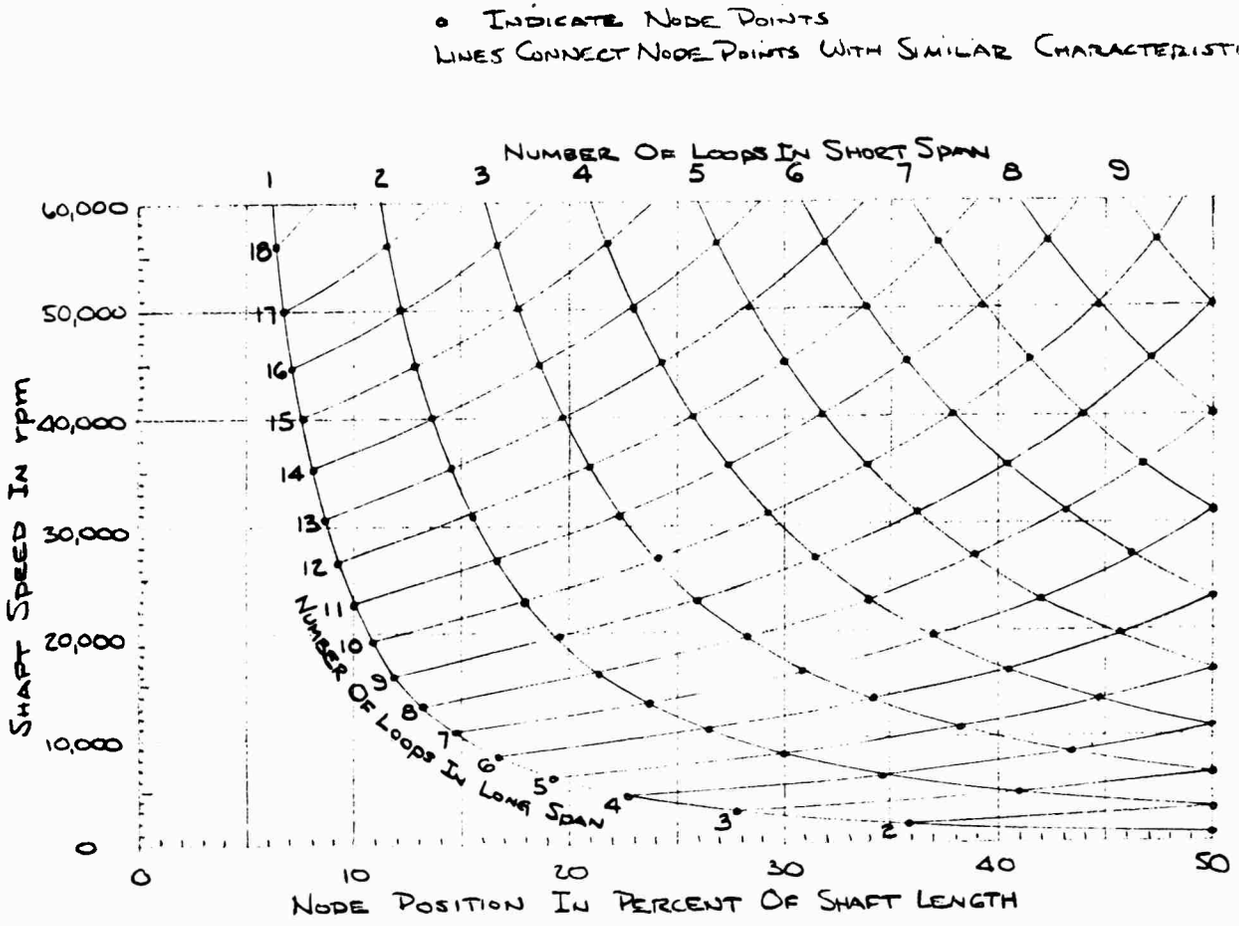

FIGURE 19. ANALYTICALLY DETERMINED SHAFT SPEED VERSUS NODE POSITION FOR VARIOUS MODES OF VIBRATION OF A 1/4-INCH-DIAMETER 89.3-INCH-LONG STEEL SHAFT WITH CLAMPED ENDS

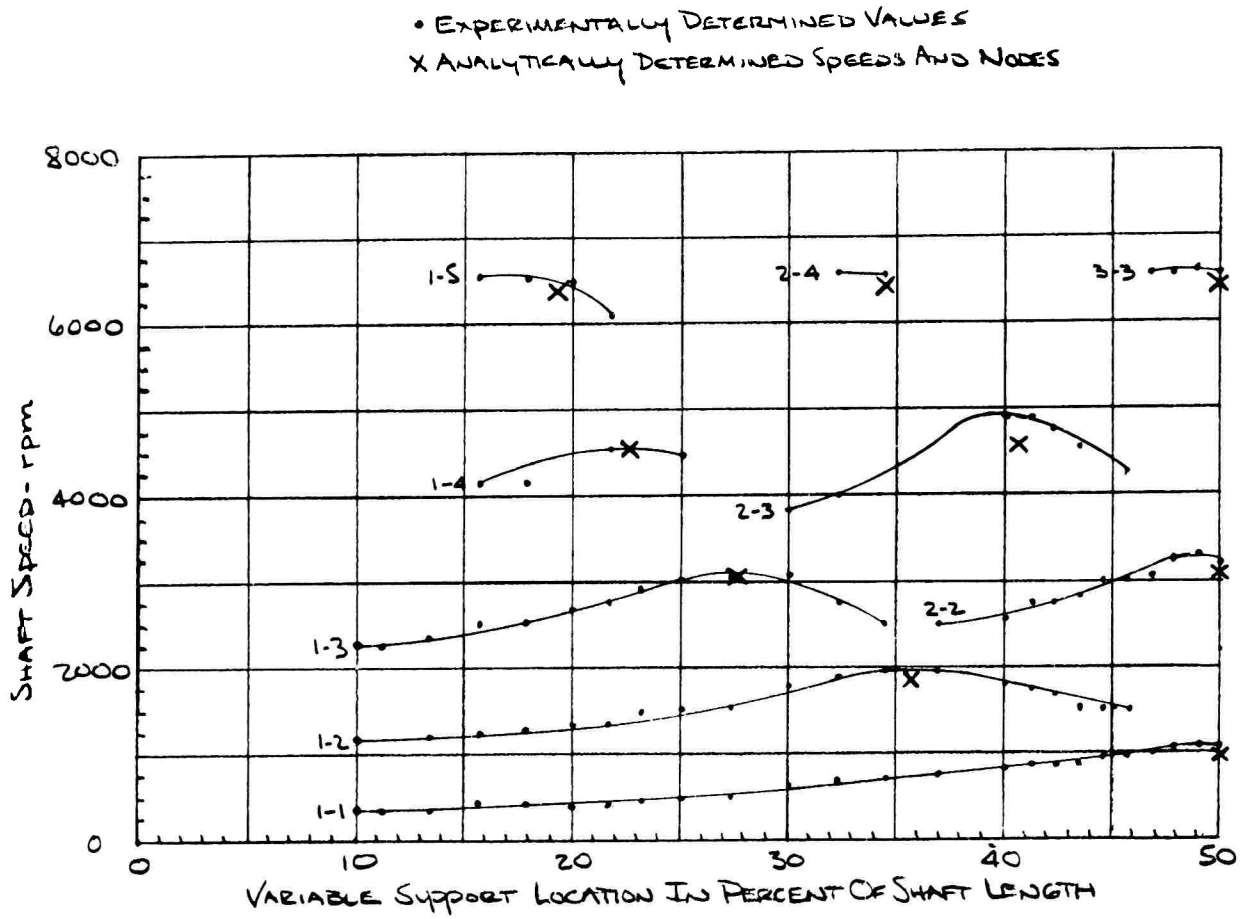

FIGURE 20. CRITICAL SPEED VERSUS SUPPORT LOCATION WITH ONE SUPPORT FIXED AT 3.36 PER CENT FROM ONE END AND OTHER SUPPORT VARIED FROM OTHER END TOWARD SHAFT MID-POINT FOR 1/4-INCH-DIAMETER STEEL SHAFT 89.3 INCHES LONG WITH FIXED ENDS

Support characteristics: K = 11.6 lb/in.; C = 1.736 lb-sec/in.

described by 1-3 means that one vibration loop is present in the shorter span side of the movable support, and three loops occur in the long span between supports.

The x's again indicate critical speeds and node locations of the same size shaft, but without intermediate supports. There is good agreement between peaks of the curves and x's, indicating that the presence of the second damper fixed close to one shaft end did not materially alter vibration speeds with respect to those of an unsupported shaft, or a shaft with one variably positioned damper.

Two and Three Variably Positioned Supports. Figures 21 and 22 show curves of tests with two and three damped supports, respectively. The positions of the supports are defined by the number, k, which is the ratio of the shortest span length between dampers to the next longer span length. A value of k equal to 1.0 means that the spans are divided evenly, while k = 0.8 means that the shortest span is 0.8 the length of the next longer, and so on. In these two test series span orientation was such that the shorter spans were adjacent to the shaft ends. More detail on this subject is included in the section discussing high-speed shaft operation.

Figures 21 and 22 indicate shaft critical speed and vibration mode with respect to support position. The numbers next to the vibration-speed points refer to the number of vibration loops along the total shaft length. There is no ovbious pattern in the critical speeds and vibration modes as was seen in Figures 19 and 20. Critical speeds of an unsupported fixed-end shaft of the same size are indicated on the curves by dashed lines. The only pattern which emerges from these plots is that shaft critical speed generally occurs at a different value than indicated by the dashed lines.

Conclusions

Lateral vibration critical speeds of transmission shafts with simple and fixed-end supports can be calculated accurately. The positions of vibration nodes can also be predicted with accuracy. Knowing the critical speeds of unsupported shafts is necessary so that suitable means can be applied to limit vibration in hypercritical-speed applications.

Critical speeds of continuous shafting with equally spaced rigid supports can also be predicted. Reference (4) has indicated, and experiment has shown, that there are as many critical speeds of each order as there are equal spans in a continuous beam with equally spaced rigid supports. That is, with three equally spaced rigid supports between the end supports, making four shaft spans, there will be four first critical speeds, four second criticals, and so on.

In tests with one rigid support positioned at various locations along the shaft there are consistent changes in critical speeds of the various vibrations modes. As the support progresses toward the shaft mid-point, critical speeds increase to a peak and then start to decrease. The peak speed occurs at the node position for the particular vibration mode, and indicates that vibration frequencies of the shaft sections on either side of the support are equal and matched. From the numerous single damped support tests made, it is safe to say that shafts with single supports, whether damped or rigid, perform identically so far as critical speed is concerned.

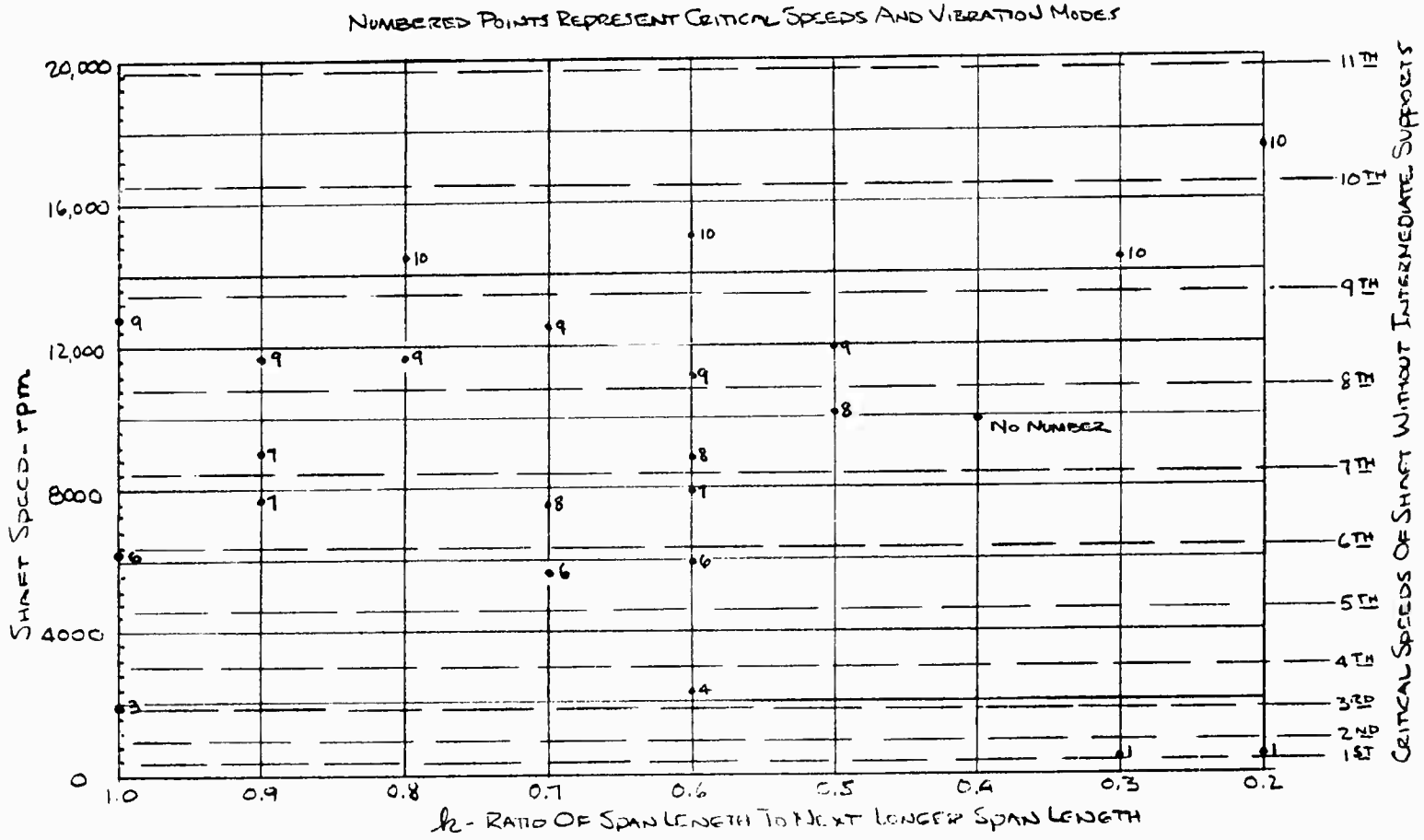

FIGURE 21. CRITICAL SPEED VERSUS SUPPORT LOCATION WITH TWO VARIABLY POSITIONED DAMPED SUPPORTS FOR 1/4-INCH-DIAMETER STEEL SHAFT 89.3 INCHES LONG WITH FIXED ENDS

Support characteristics: K = 11.6 lb/in.; C = 0.744 lb-sec/in.

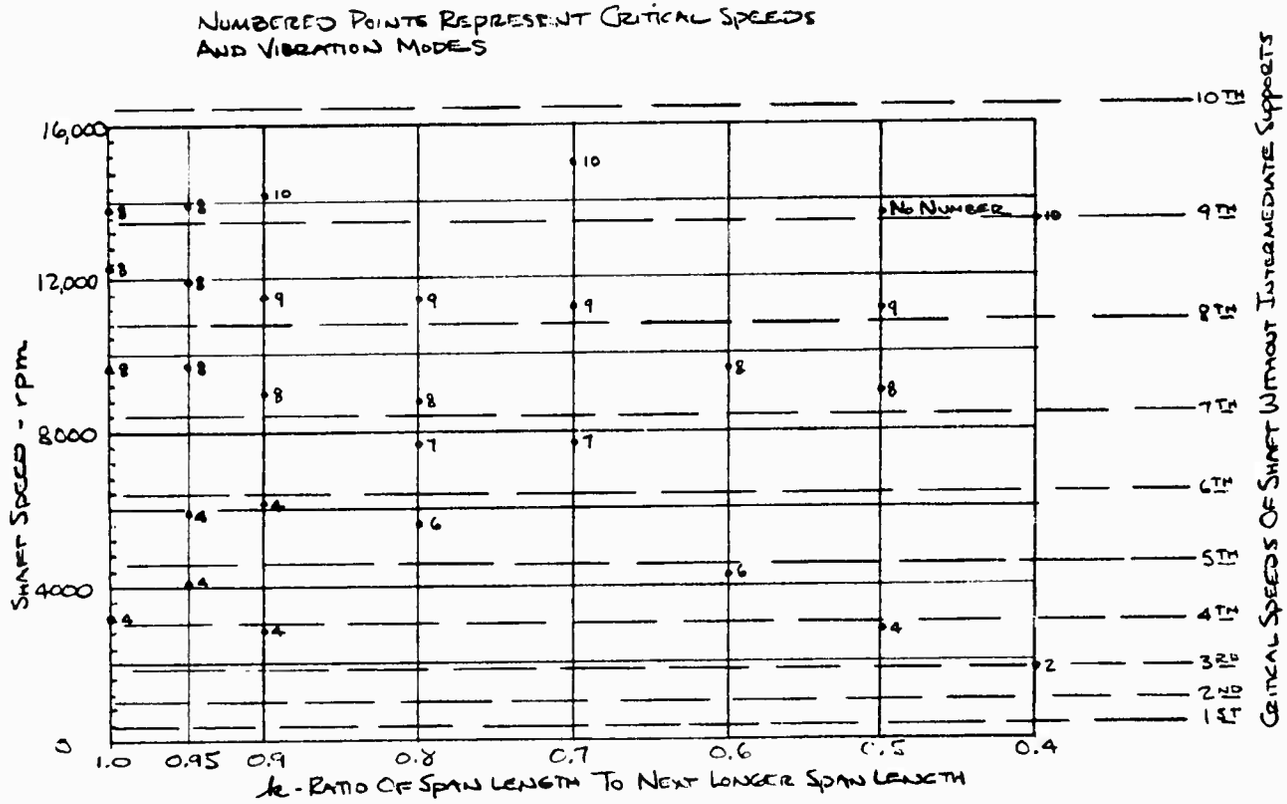

FIGURE 22. CRITICAL SPEED VERSUS SUPPORT LOCATION WITH THREE VARIABLY POSITIONED DAMPED SUPPORTS FOR 1/4-INCH-DIAMETER STEEL SHAFT 89.3 INCHES LONG WITH FIXED ENDS

Support characteristics: K = 11.6 lb/in.; C = 0.744 lb-sec/in.

A test of two damped supports with one fixed quite close to a shaft end showed similar critical speeds and mode-shape curves. However, in tests of two and three dampers variable in location and considerably away from the shaft ends, the pattern of critical speeds was not apparent.

Effects of Axial Shaft-End Force and Torque on Shaft Critical Speeds

The problem of determining the shaft critical speed for various shaft end loading conditions of axial force and torque is important to the development of design criteria for power-transmission shafts. Work on this problem consisted of the investigation of the effect on critical speeds as predicted by theoretical work, and investigation by experimental tests. The theoretical results were compiled from a search of the literature on shaft critical speeds, while the experimental tests were performed in the high-speed shaft test machine. The effect of each external load upon the shaft critical speed was investigated separately. Inasmuch as these loads will interact when applied to a shaft simultaneously, the effect of combined loads was also investigated. A comparison of the theoretical and experimental results is presented toward the end of this section.

Theoretical Work

Effect of Axial Force. The problem of determining the frequency of lateral vibration of a beam subjected to an axial compressive force has been solved [Ref. (5)]. This problem is identical to the problem of determining the critical speed of a shaft subjected to an axial compressive force [Ref. (6)]. A vibrating beam subjected to an axial compressive force, F, has a deflection curve, see Figure 23, under static lateral load given by the following equation:

$$EI \frac{d^2y}{dx^2} = - M - Fy , \tag{87}$$

where

E = modulus of elasticity, lb/in.^{2}

F = axial force, lb

I = moment of inertia, in.^{4}

M = bending moment caused by lateral load, in-lb

y = deflection, in.

x = distance along shaft, in.

FIGURE 23. DEFLECTION CURVE OF VIBRATING BEAM SUBJECTED TO AN AXIAL FORCE

By differentiating twice the following equation is obtained.

$$\frac{d}{dx^2}\left(EI \frac{d^2y}{dx^2}\right) = w - F\frac{d^2y}{dx^2}, \tag{88}$$

where

w = lateral load on beam, lb/in.

Substitution of the inertia force for w gives the equation for the lateral vibration of the beam.

$$\frac{\partial^2}{\partial x^2}\left(EI \frac{\partial^2 y}{\partial x^2}\right) + F\frac{\partial^2 y}{\partial x^2} = -\frac{AP}{g}\frac{\partial^2 y}{\partial t^2}, \tag{89}$$

where

A = cross sectional area, $in.^2$

g = acceleration of gravity, 386 $in./sec^2$

P = density, $lb/in.^3$

t = time, sec.

Assuming that the beam is prismatic and that the beam performs one of the natural modes of vibration, the solution is in the form

$$y = X(B_5 \cos \omega t + B_6 \sin \omega t), \tag{90}$$

where

$B_{5,\ 6}$ = constants

X = function of x

ω = frequency, rad/sec.

Substitution of Equation (90) into Equation (89) yields

$$EI\frac{d^4X}{dx^4} + F\frac{d^2X}{dx^2} = \frac{AP}{g}\omega^2 X. \tag{91}$$

The solution of this equation for the natural frequency of lateral vibration for a simply supported beam yields

$$\omega_* = \frac{\pi^2}{\ell^2}\sqrt{\frac{EIg}{AP}}\sqrt{1 - \frac{F\,\ell^2}{\pi^2 EI}} \quad , \tag{92}$$

where

ℓ = length of beam, in.

ω_* = natural frequency of lateral vibration of a beam with an axial force, rad/sec.

As can be seen from Equation (92), the frequency of vibration is reduced as the axial compressive force is increased. The frequency of vibration is determined by the value of the ratio of $F\,\ell^2/\pi^2\,EI$, which is the ratio of the axial compressive force to the Euler critical load. If the value of this ratio approaches one, the frequency of vibration of the first mode approaches zero, and lateral buckling of the beam results.

If the beam is subjected to an axial tensile force, F, the natural frequency of lateral vibration increases and the value may be obtained by substituting -F for F in Equation (92). This substitution yields

$$\omega_* = \frac{\pi^2}{\ell^2}\sqrt{\frac{EIg}{AP}}\sqrt{1 + \frac{F\,\ell^2}{\pi^2 EI}} \quad . \tag{93}$$

Equations (92) and (93) present the equations for the natural frequency of lateral vibration of a simply supported beam subjected to an axial force. These equations are also the equations for the critical speeds of a simply supported shaft subjected to an axial force. The first term in each equation is the first critical speed of a shaft without an axial force, as shown below

$$\omega = \frac{\pi^2}{\ell^2}\sqrt{\frac{EIg}{AP}} \quad . \tag{94}$$

Substituting Equation (94) into Equation (93) yields

$$\omega_* = \omega\sqrt{1 + \frac{F\,\ell^2}{\pi^2 EI}} \quad . \tag{95}$$

Dividing both sides of this equation by ω yields

$$\frac{\omega_*}{\omega} = \sqrt{1 + \frac{F\,\ell^2}{\pi^2 EI}} \quad . \tag{96}$$

This critical-speed ratio including the effect of the axial force is plotted as the function of the axial force to the Euler critical-load ratio in Figure 24. For axial compressive forces, the critical-speed ratio is less than one, and for axial tensile forces, the critical-speed ratio is greater than one.

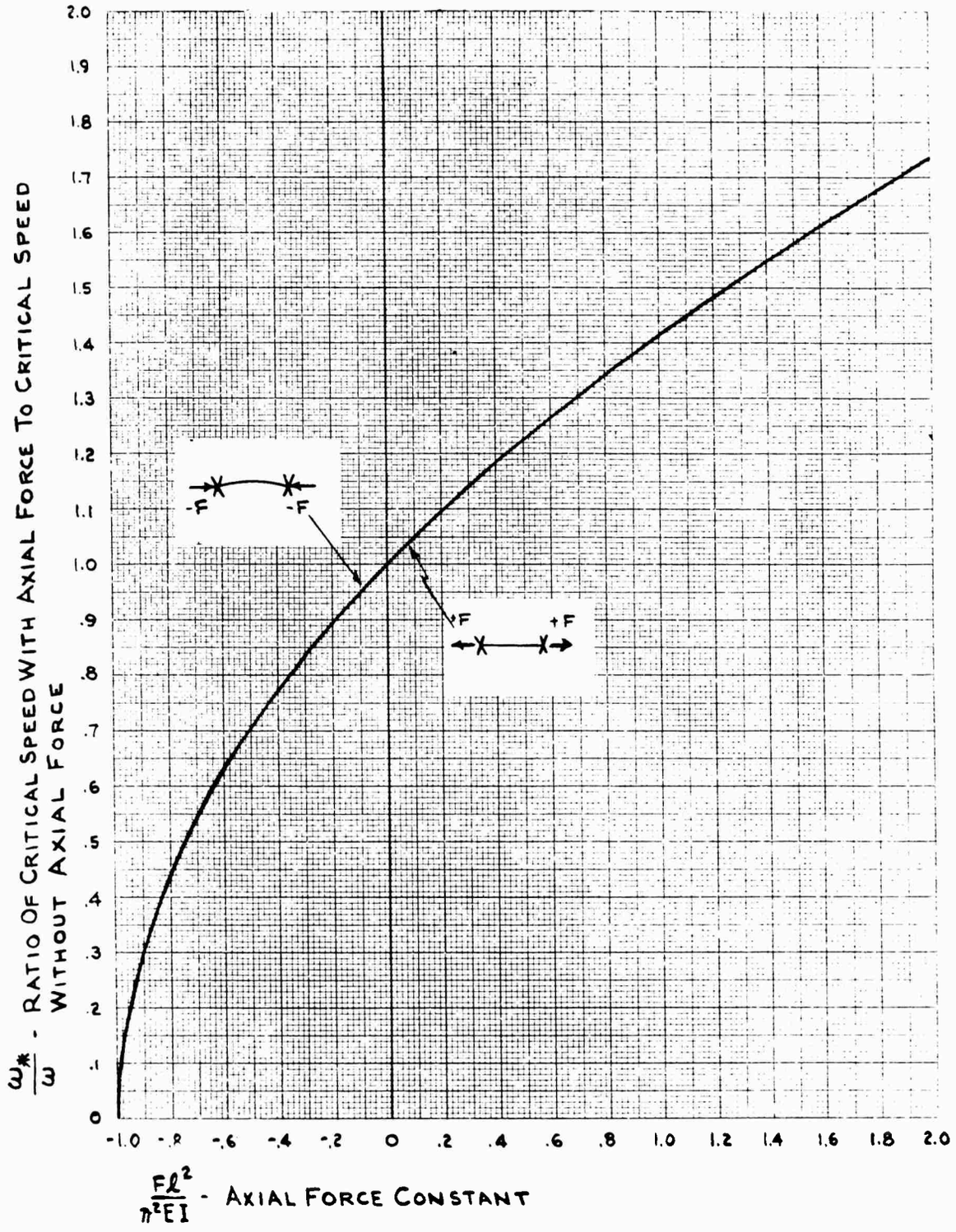

FIGURE 24. CRITICAL-SPEED RATIO INCLUDING EFFECT OF AXIAL FORCE VERSUS AXIAL FORCE CONSTANT FOR A SHAFT WITH SIMPLY SUPPORTED ENDS

The theoretical effect of axial forces upon the shaft critical speed has been presented in a graphical form to assist in the development of a design criteria for high-speed power-transmission shafts. In the development of this criteria the effect of axial torque upon shaft critical speed must also be considered.

Effect of Axial Torque. The problem of determining the critical speeds of shafts subjected to axial torque has been investigated thoroughly in the development of a design criteria, since the primary purpose of the power-transmission shaft is to transmit torque. A search of the technical literature indicated that the problem has been solved previously. Greenhill [Ref. (7)] solved the related problem of the influence of axial torque on the buckling load of an Euler column. Approximate solutions of the problem based on the work of Greenhill are presented in standard textbooks on strength of materials [Ref. (8), Ref. (9)]. The problem of determining the critical speeds of a rotating shaft of uniform cross section, which is subjected to an axial torque was solved by Rosenberg [Ref. (10), Ref. (11)].

The problem is treated by formulating a differential equation from the equations of motion which balance the force components in the two perpendicular planes whose intersection is the x-axis and the center line of the undeflected shaft. Substitution of the boundary conditions for shafts with simply supported ends and fixed ends yields two boundary value problems. The solution of the boundary value problems employs elegant mathematical techniques which are interesting, but will not be presented in this report because of the length and complexity of the problem. This solution yields numerical results for the effect of torque on the critical speed of shafts in simply supported and fixed-end bearings.

This investigation of the theoretical treatment of the influence of axial torque on the shaft critical speed indicates that the critical speed always decreases with increasing torque. The decrease in critical speed is greater for shafts mounted in simply supported or self-aligning bearings than for shafts mounted in rigid bearings. An additional conclusion is that the reduction in critical speed is less for higher critical speeds than that for lower speeds. This information is expressed graphically in Figure 25.

Figure 25 is a plot of the frequency function, β, versus the torque function, α, for shafts with simply supported ends and fixed ends. Both of these functions are defined in terms of physical dimensions of the shaft. As defined in the theoretical work, the frequency function may be expressed as:

$$\beta = \frac{\omega^2 \ell^4 m_u}{16EI} \tag{97}$$

where

E = modulus of elasticity, lb/in.^{2}

I = moment of inertia, in.^{4}

ℓ = shaft length, in.

m_u = mass per unit length of the beam, lb-sec^2/in.^{2}

β = frequency function, dimensionless

ω = frequency, rad/sec.

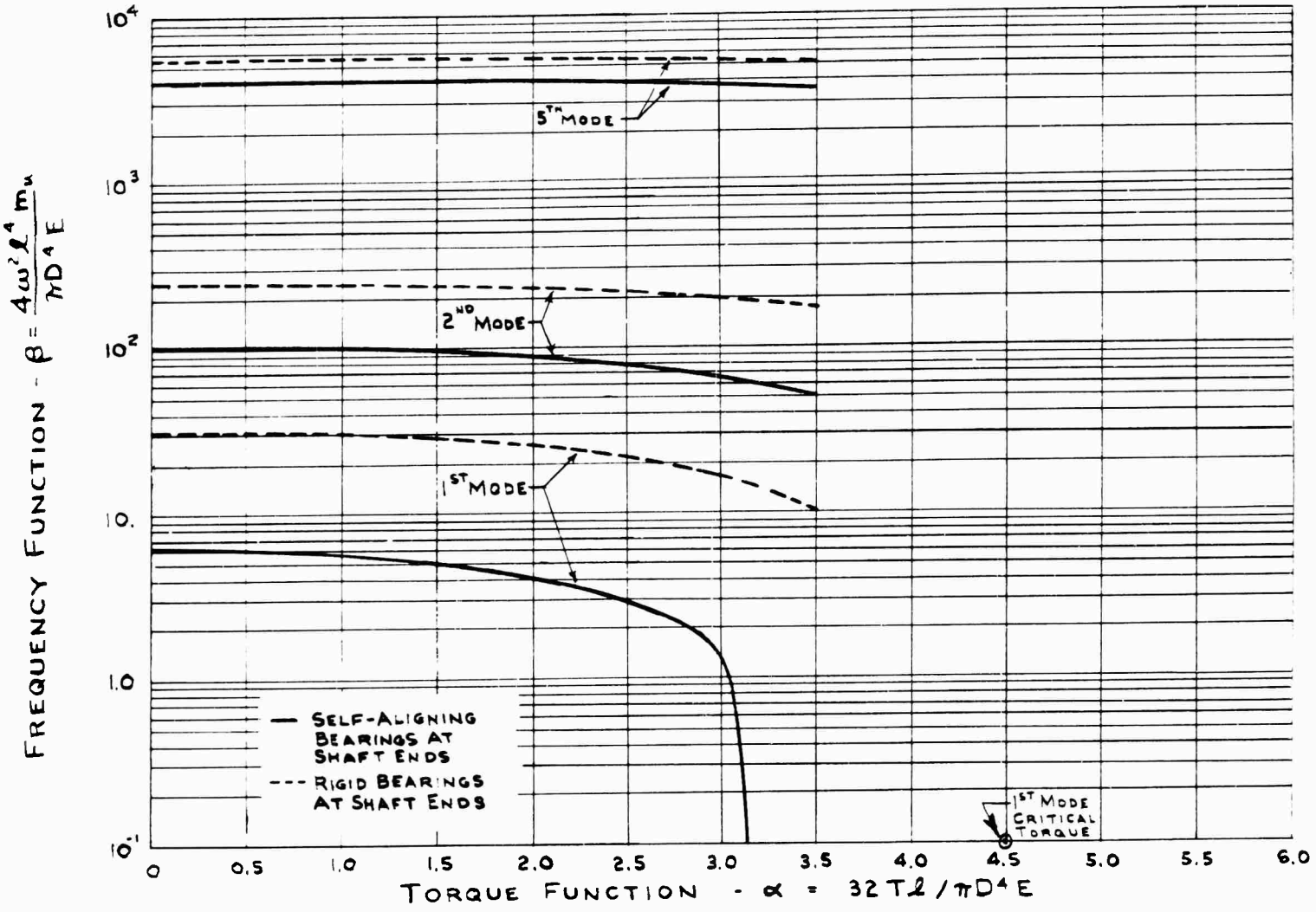

FIGURE 25. PLOT OF FREQUENCY FUNCTION VERSUS TORQUE FUNCTION SHOWING THE EFFECT OF TORQUE ON CRITICAL SPEED

and the torque function may be expressed as

$$\alpha = \frac{T\ell}{2EI} , \tag{98}$$

where

T = axial torque, in-lb

α = torque function, dimensionless.

Values for the frequency function and the torque function are represented by the solid lines in Figure 25.

This theoretical work also predicts the existence of a critical torque with each critical vibration mode. Critical torques are sufficient to cause instability of the non-rotating shaft; i. e. , sufficient to reduce the corresponding critical speed to zero. The equation for the critical torque for a shaft with simply supported ends is

$$T_k = k \frac{2\pi}{\ell} EI , \tag{99}$$

where

T_k = critical axial torque for the kth mode, lb-in.

k = index corresponding to the mode number.

Figure 25 shows the torque function $\alpha_1 = 3.14$ for the first critical torque for a shaft with simply supported ends.

For a shaft mounted in fixed-end bearings, the equation for the critical torque is

$$T_k = \alpha_k \frac{2EI}{\ell} , \tag{100}$$

where

α_k = critical torque function for the kth mode, dimensionless.

The value of α_k is determined from the following transcendental equation

$$\tan \alpha_k = \alpha_k . \tag{101}$$

The solution of this equation may be visualized by rewriting it as two equations. Rewriting Equation (101) as

$$H = \tan \alpha_k \tag{102}$$

and

$$h = \alpha_k \tag{103}$$

where H = dimensionless parameter and plotting these equations results in Figure 26. The values of α at the intersections of the two curves are solutions of Equation (101).

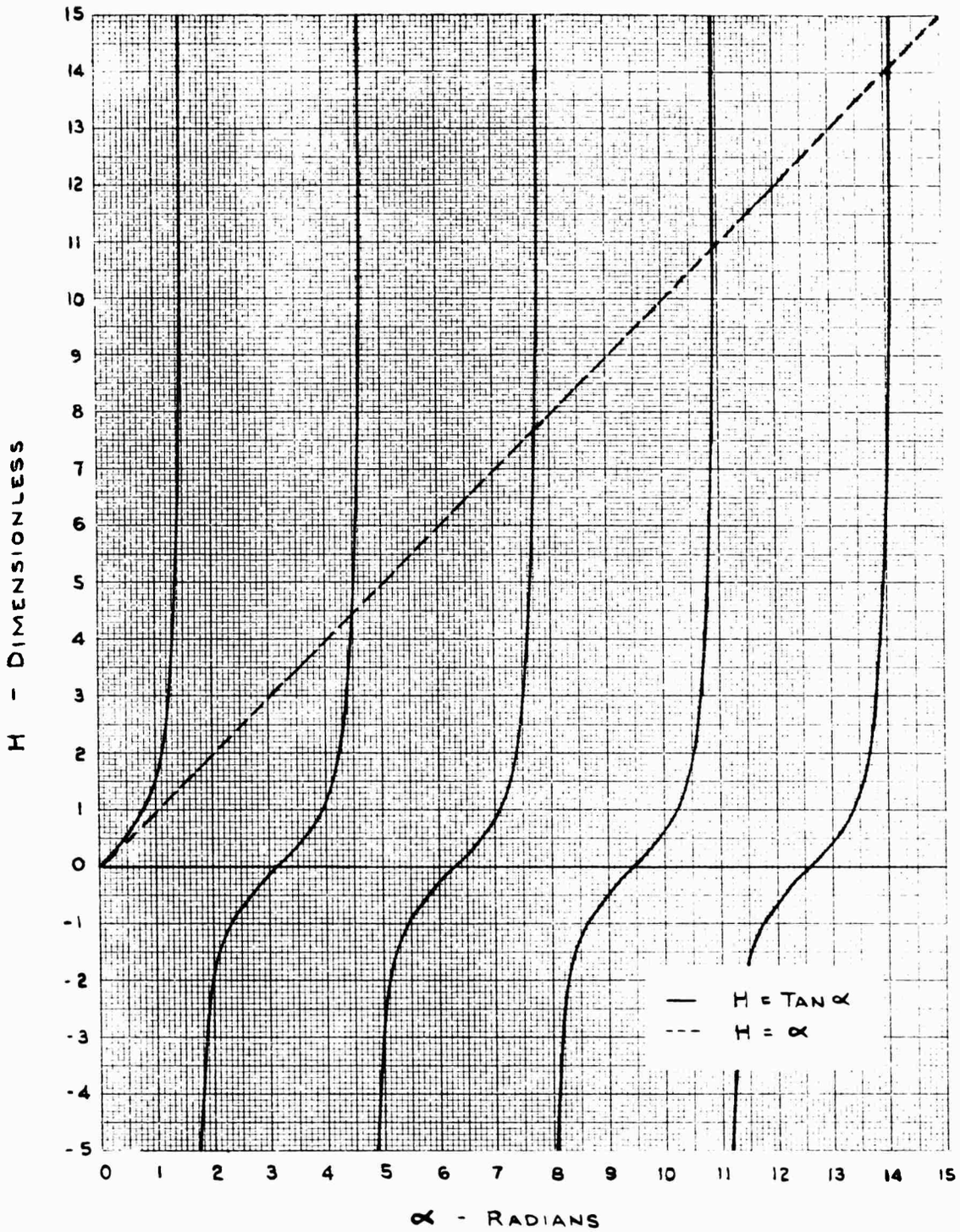

FIGURE 26. PLOT ILLUSTRATING SOLUTION OF TAN $\alpha = \alpha$ FOR THE FIRST FOUR MODES

For the first vibration mode, the torque function, α_1, equals 4.495 satisfies Equation (101). Figure 25 shows this value of the critical torque for the first mode of a shaft mounted in fixed-end bearings.

Figure 25 is a graphical summary of the solution of the problem of the theoretical effect of axial torque on the critical speed of a shaft. From this figure, it is concluded that a shaft will become unstable at a lower speed as the torque is increased; and that a critical torque exists for each vibration mode which is sufficient to cause instability of the nonrotating shaft.

As in all cases of buckling or instability, it is necessary to answer the question of the range in which this result applies; i.e., find out the region in which the shaft will buckle before it will yield. Examination of Equations (99) and (100) indicates that the critical torque for instability or lateral buckling is directly proportional to the shaft diameter and the modulus of elasticity of the shaft material and inversely proportional to the shaft length. The expression for the torque required to yield a circular shaft subjected to an axial torque is

$$T_y = S_{sy} Z^* , \tag{104}$$

where

S_{sy} = shear yield stress, lb/in.^{2}

Z^* = polar section modulus = $\frac{4I}{D}$, in.^{3}

Substituting the value α_k for the first mode critical torque and equating Equations (100) and (104), rearranging yields

$$\frac{\ell}{D} = 4.495 \frac{E}{S_{sy}} , \tag{105}$$

where

D = outside diameter, in.

This equation represents the boundary between the region of lateral buckling and yielding of a shaft as a result of the axial torque. Defining a new quantity

$$N = \frac{E}{S_{sy}} , \tag{106}$$

where

N = ratio of modulus of elasticity to shear yield stress, dimensionless

and substituting Equation (106) into Equation (105) indicates that a shaft will buckle before it will yield if

$$\frac{\ell}{D} > 4.495 \, N . \tag{107}$$

Figure 27 shows the value of the ℓ/D ratio for various values of N for the inequality of Equation (107).

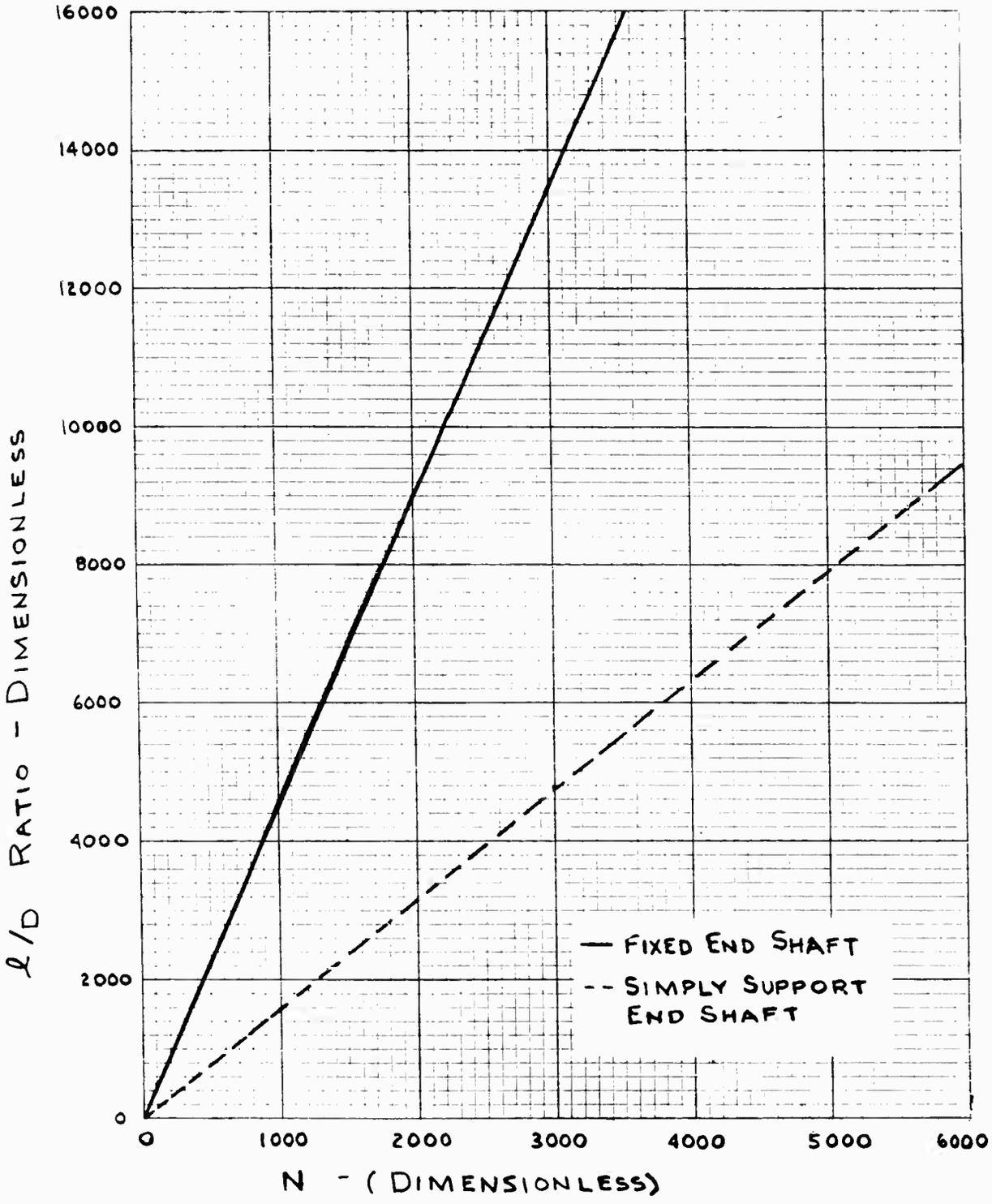

FIGURE 27. REGION OF LATERAL BUCKLING AND TORSIONAL YIELDING

If the point for the ℓ/D ratio versus N is above the boundary curve, the shaft will buckle laterally; however, if the point is below the curve, the shaft will yield in torsion. A curve separating the two regions is shown in Figure 27 for the shaft mounted with simply supported ends, as well as for fixed ends. The information in Figure 27 supplements the information in Figure 25.

The effect of the axial torque and axial force on the critical speeds of shafts has been considered separately. Since it is impossible to anticipate the type of external loads acting on the shaft as a result of the design geometry; i. e., flexible couplings, supports, etc., it is considered essential to present an investigation of the combined effect of axial force and axial torque on the critical speed of shafts.

Effect of Combined Axial Force and Torque. The general problem of determining the critical speeds of a shaft subjected to simultaneous axial force and axial torque has been solved by Southwell and Gough [Ref. (12)]. This theoretical work presents a stability criterion for a shaft subjected to a rotational speed, an axial force, and an axial torque. The solution of the problem is carried out by writing the equations of neutral equilibrium and solving the resulting differential equations by classical mathematical techniques. The solution is extremely complicated, but the authors have made the results usable by representing the solution in the form of diagrams. Figures 28 and 29 exhibit the stability criteria graphically by means of curves which connect values of the frequency factor and the axial force factor for various values of the torque factor. The stability criterion for a shaft with simply supported ends is diagrammed in Figure 28, and for a shaft with fixed ends in Figure 29.

The coordinates of Figures 28 and 29 are nondimensional quantities. The quantities A^*, B^*, and C^* relate to the dimensions and material of the shaft and the axial torque, axial force, and the critical speed, respectively:

$$A^* = \frac{T\ell}{2EI} \tag{108}$$

$$B^* = \frac{F\ell^2}{4EI} \tag{109}$$

$$C^* = \frac{m_u \omega^2 \ell^4}{16EI} \tag{110}$$

where

A^* = torque constant, dimensionless

E = modulus of elasticity, lb/in.^{2}

I = section moment of inertia, in.^{4}

ℓ = shaft length between supports, in.

T = torque, in-lb

B^* = force constant, dimensionless

F = force, lb

C^* = frequency constant, dimensionless

m_u = mass per unit length of shaft, lb-sec^2/in.^{2}

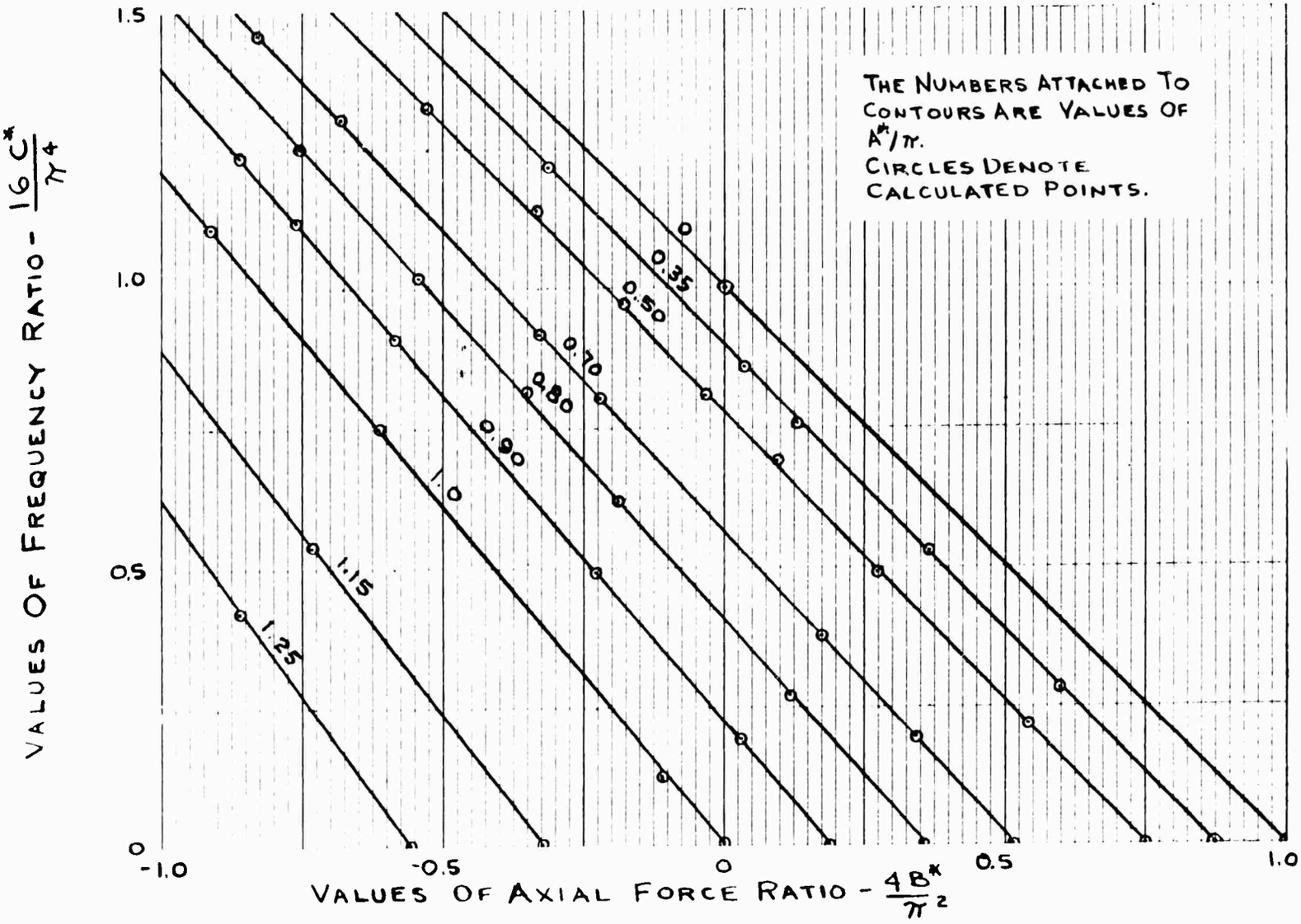

FIGURE 28. FREQUENCY RATIO VERSUS AXIAL FORCE RATIO FOR VARIOUS VALUES OF TORQUE RATIO FOR A SHAFT WITH SIMPLY SUPPORTED ENDS

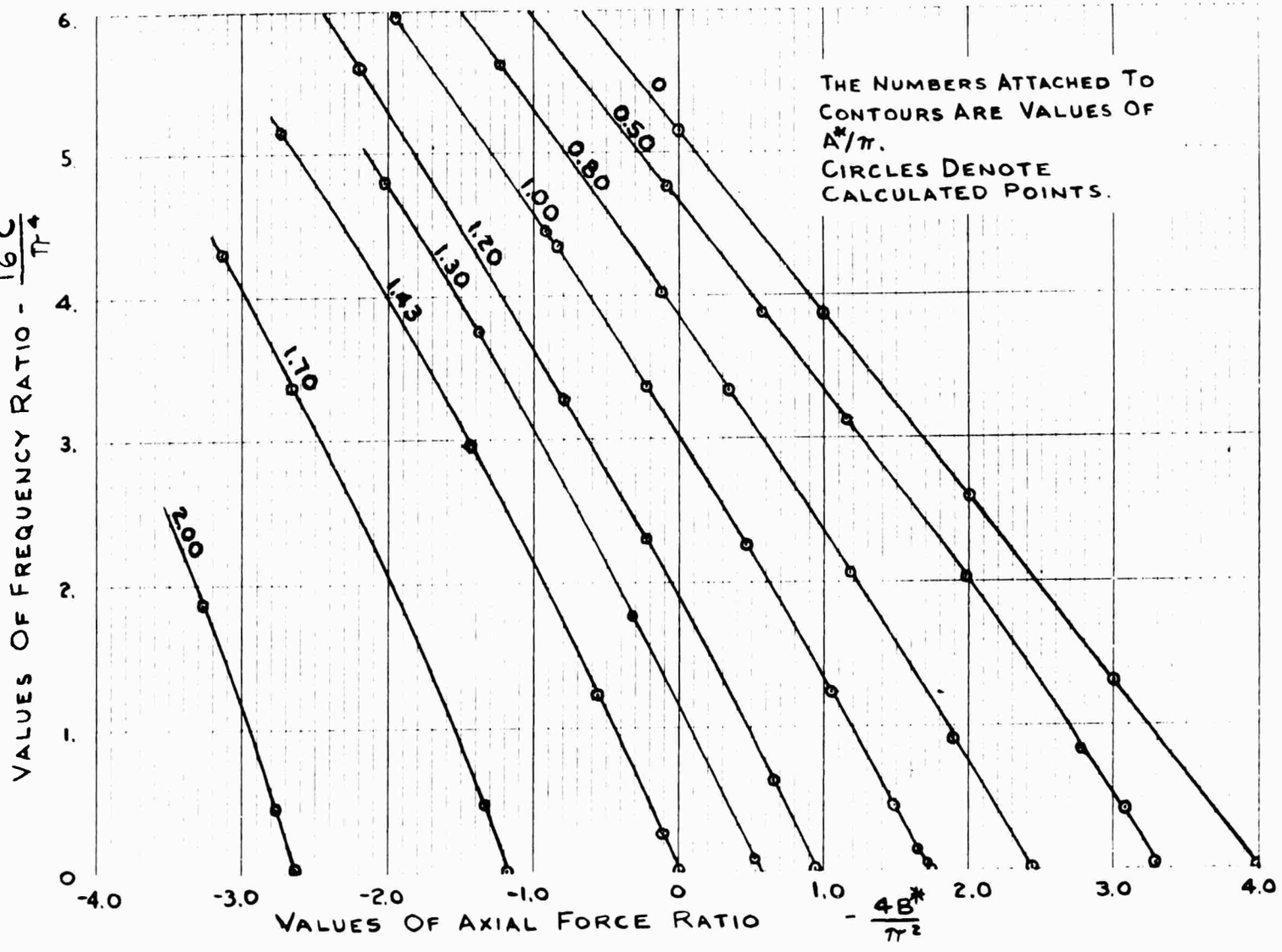

FIGURE 29. FREQUENCY RATIO VERSUS AXIAL FORCE RATIO FOR VARIOUS VALUES OF TORQUE RATIO FOR A SHAFT WITH FIXED ENDS

These diagrams illustrating the solution of the problem have been extended to the negative B^* region. It should be pointed out that this analysis considers the negative B^* region as the region of axial tensile force. Examination of Figures 28 and 29 indicates that the axial tensile force maintains stability, i. e. , the frequency factor increases for a constant torque factor in the negative B^* region. In the positive B^* region, corresponding to an axial compressive force, instability will occur at lower rotational speeds for a constant torque factor. Thus the critical speed is said to be reduced. These diagrams indicate that axial force, axial torque, and rotation are equally important in causing instability; i. e. , reducing the critical speed, when they act simultaneously.

Figures 28 and 29 may be used to investigate the stability of a shaft subjected to a single external load while rotating. Investigating the stability of a fixed-end shaft subjected only to an axial torque means that the value of the axial force factor, $\frac{4B^*}{\pi^2}$, must equal zero. The diagram reduces to points of the frequency factor, $\frac{16C^*}{\pi^4}$, where the values of the axial torque factor cross the axis at $\frac{4B^*}{\pi^2}$ equal to zero. A plot of these values of frequency factor versus the values of the axial torque factor is shown in Figure 30.

If the ordinate of Figure 30, $\frac{16C^*}{\pi^4}$, is multiplied by $\frac{\pi^4}{16}$; and the abscissa of Figure 30, $\frac{A^*}{\pi}$, is multiplied by π, and the calculated points are plotted, a curve is obtained as shown in Figure 31. This is a plot of frequency function versus torque function showing the effect of axial torque on the critical speed. Comparison of Figure 31 and Figure 25 shows good correlation between the calculated curves. This indicates identical results for the effect of axial torque on the critical speeds of shafts based on the two theories presented.

Using the general solution in the graphical form by Southwell, it is possible to prepare a curve for the effect of axial force on the critical speed of a shaft with fixed ends. In Figure 29, the calculated points on the contour of A^*/π equal to zero will yield the desired curve. These results can be transformed into a curve of critical-speed ratio versus the axial force constant. Rearranging the values of $\frac{16C^*}{\pi^4}$ in terms of the critical speed, and dividing by the expression for critical speed without axial force yields the ordinate of the curve as plotted in Figure 32. Thus Figure 32 is the critical-speed ratio including the effect of the axial force versus the axial force constant for a shaft with fixed ends, and Figure 24 is the same curve for a shaft with simply supported ends.

This section has presented the results of theoretical work on the effects of external loads on the shaft critical speeds. It has been found, theoretically that an axial compressive force and an axial torque reduce the critical speeds. Each type of loading has a critical value which causes lateral buckling; i. e. , reduces the critical speed to zero. Axial compressive force and axial torque are equally important in causing instability when they act simultaneously.

Experimental Study of Torque Effects

The effect of axial torque on the shaft critical speed has been studied in the shaft test machine. Tests were conducted with a steady torque and with a transient torque

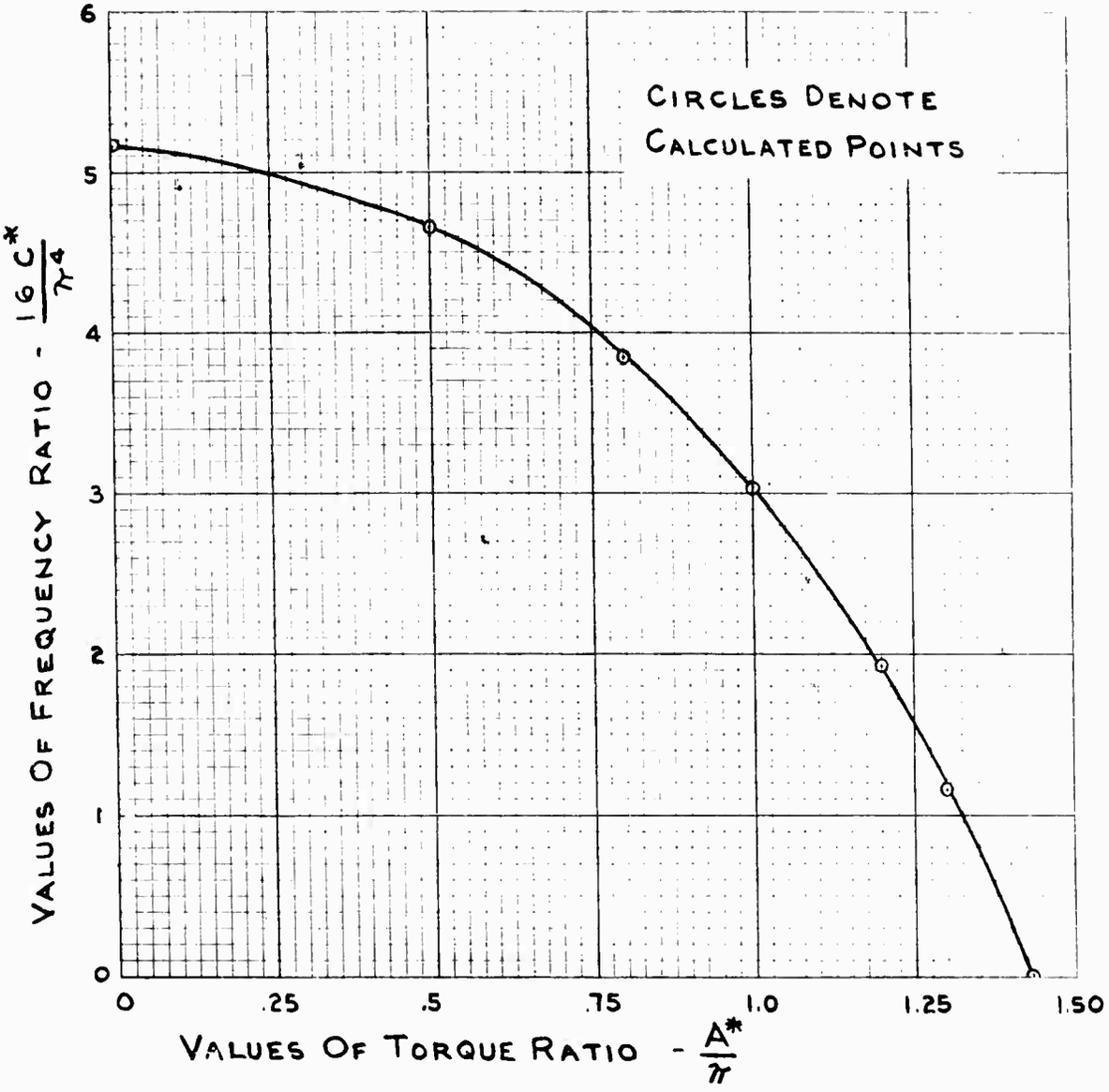

FIGURE 30. FREQUENCY RATIO VERSUS TORQUE RATIO FOR AN AXIAL FORCE RATIO EQUAL TO ZERO

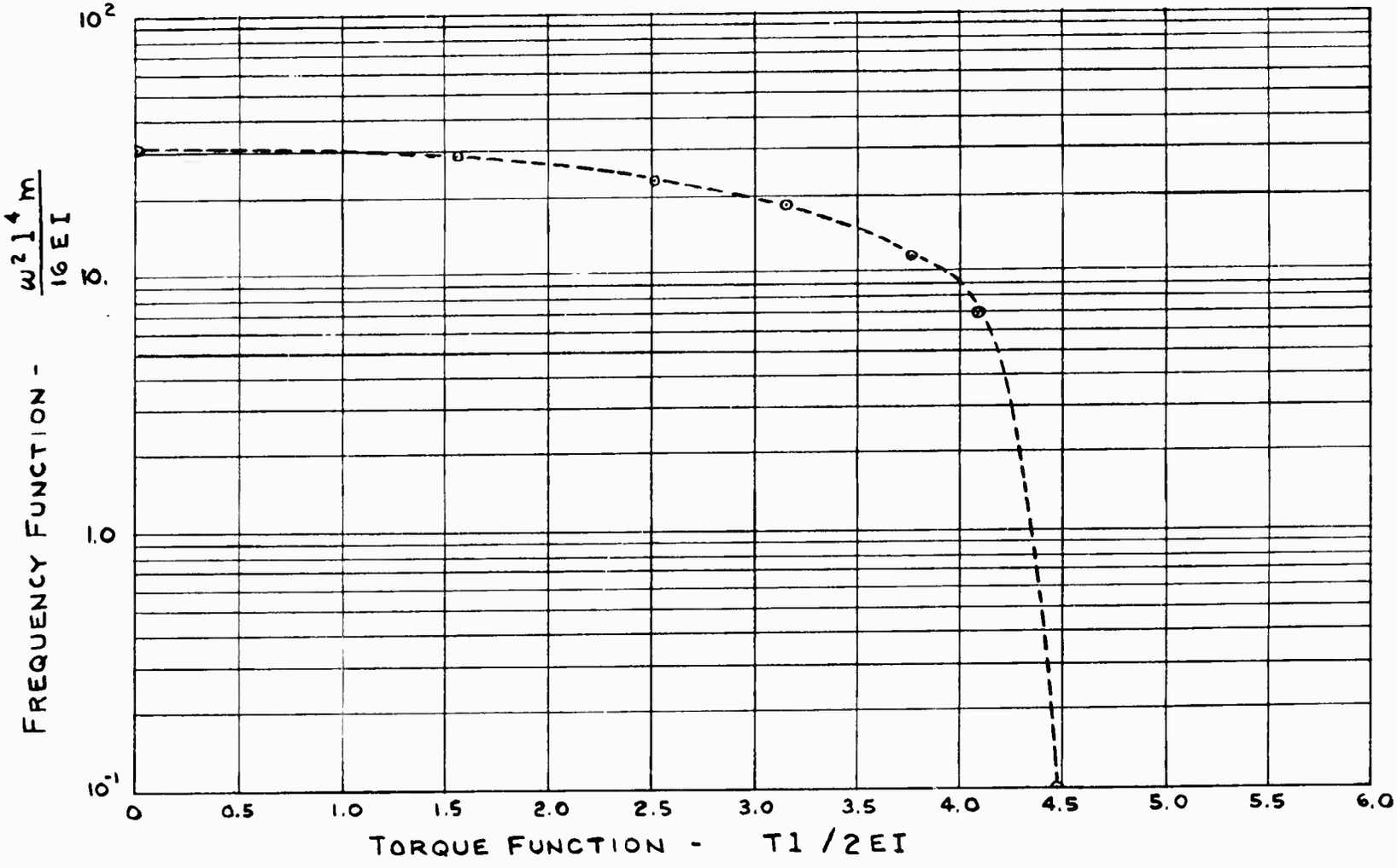

FIGURE 31. CALCULATED FREQUENCY FUNCTION VERSUS TORQUE FUNCTION

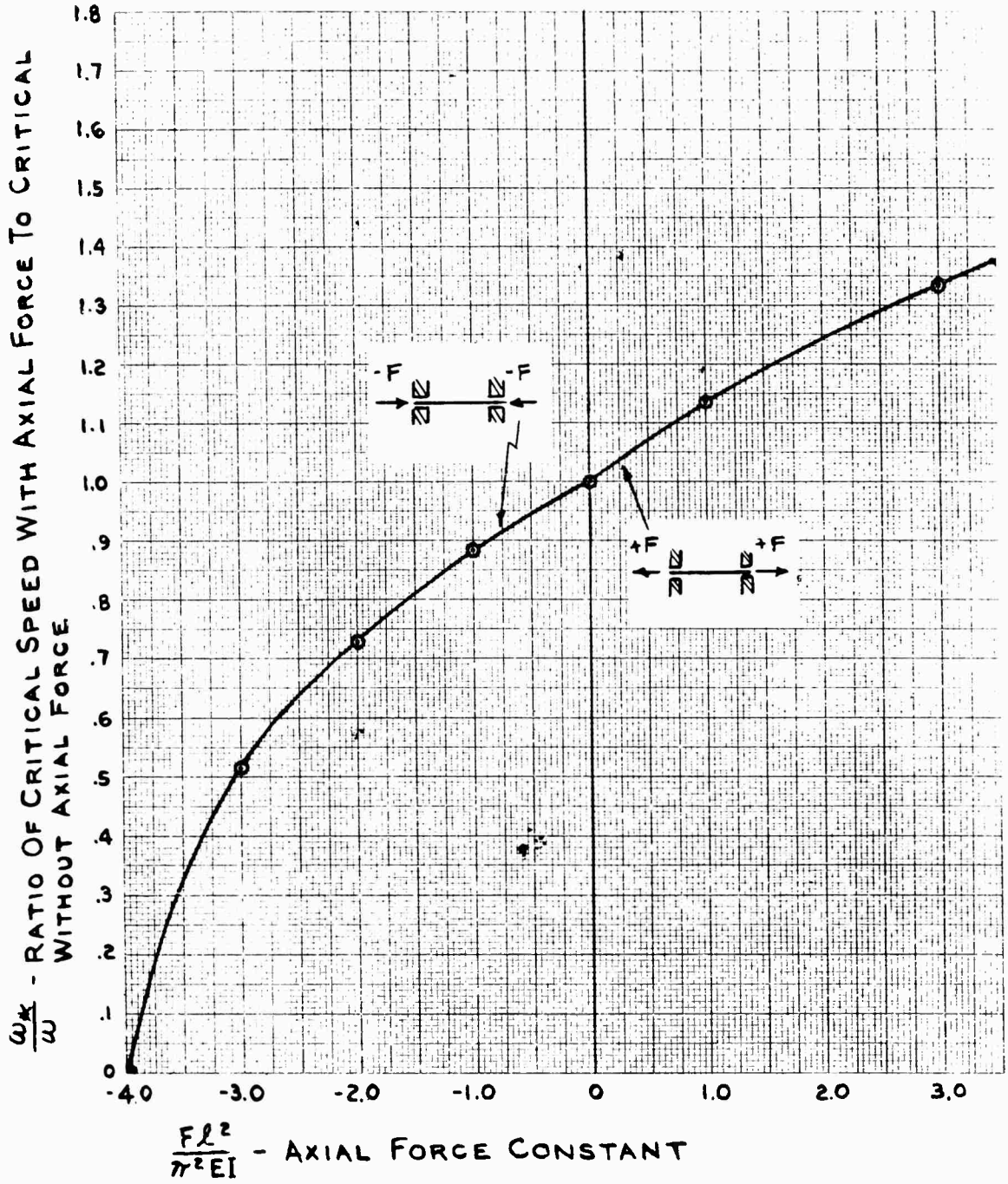

FIGURE 32. CRITICAL-SPEED RATIO INCLUDING EFFECT OF AXIAL FORCE VERSUS AXIAL FORCE CONSTANT FOR A SHAFT WITH FIXED ENDS

applied as the shaft was rotating. In addition the influence of axial torque and of axial force was observed with the shaft stationary. The results of these tests are discussed in this section.

Data on the effect of torque on the critical speeds of shafts are summarized in the following tables. Table 8 shows the critical speeds obtained in rotational tests for the second and fifth critical speeds for a 1/8-inch-diameter and 1/4-inch-diameter shaft. The deviation of the measured speed and the calculated speed is attributed to induced shaft-end tension or compression obtained during setup. The 1/8-inch-diameter shafting was loaded with a torque of 13. 78 in-lb which caused a torsional shearing stress of 36,000 psi. This magnitude of stress is approximately the torsional yield strength of the drill rod steel. The tests were repeated with shorter lengths of 1/8-inch-diameter shafting. These tests showed a very small reduction in the second and fifth critical speeds with the application of torque.

In order to obtain more definite information about the reduction of the critical speed caused by axial torque, the tests were repeated using commercial music spring wire as the shaft material. The hardness of this material was Rockwell C 47, which corresponds to an approximate yield strength in shear of 92,000 psi. Tests performed with the high strength material are presented in Tables 9 and 10.

Table 9 lists experiments conducted with constant sag and varied torque. Tests 9 and 10 note a negligible difference in measured critical speed with applied torque increased from 0 to 26. 45 in-lb (sufficient to cause a shearing stress of 69,000 psi in the test shaft). Consequently critical speed appeared insensitive to torque change. Since the initial shaft deflection or sag was nominal, indicating tensile shaft-end forces, measured critical speed was higher than that calculated for a shaft without axial force or torque shaft-end effects.

Experiments 11 and 12, and 13 and 14 produced negligible change in critical speed with change in torque. There was again, however, a difference between the measured and calculated critical speeds. The nominal sag of Tests 11 and 12 produced a measured critical speed nearly three times as high as the calculated value. In Tests 13 and 14 the shaft was adjusted to be in compression and the measured value was somewhat lower than calculated for the shaft without applied axial shaft-end force and torque. For the shaft in Tests 13 and 14 the adjusted sag of the test shaft was 1. 44 inches greater than its natural sag of 3 inches.

In Tests 15 through 22 the shaft was adjusted with 1. 6 inches initial deflection – equal to the natural sag. As applied torque was increased beyond the levels of the previous six tests, measured critical speed increased. However, with increasing torque, the shaft became horizontally deformed in an "S" shape – inducing tensile effects at the shaft ends. At very high torsional stress critical speed dropped perhaps caused by axial slip between the shaft ends and the gripping collets.

In Table 10 tests were conducted with torque held constant, and with initial deflection or sag varied. The first group beginning with Test 13 and ending with 29 shows the effect of sag on critical speed when the shaft was untorqued. As sag was decreased from the beginning value producing shaft-end compression to the value of least sag denoting shaft-end tension, critical speed changed from a value below to considerably higher than calculated for the shaft without axial shaft-end force or torque. The second and third groups of tests in Table 9 showed a similar sensitivity of critical

TABLE 8. SHAFT CONFIGURATIONS TESTED WITH APPLIED TORQUE

Test	Shaft Configuration		Second Critical Speed				Fifth Critical Speed			
	Diameter, in.	Length, in.	Measured Value, rpm	Calculated Value, rpm	Torque Applied, in-lb	Shear Stress, psi	Measured Value, rpm	Calculated Value[a]	Torque Applied, in-lb	Shear Stress, psi
1	1/4	89.3	888	938	26.3	8,570	4412	4530	18.92	6,170
2	1/4	89.3	888	938	0	--	4412	4530	0	--
3	1/8	63.2	1100	938	3.24	8,450	4750	4530	2.54	6,630
4	1/8	63.2	1025	938	13.78	36,000	4650	4530	13.78	36,000
5	1/8	51.4	1700	1408	3.24	8,450	6800	6830	2.54	6,630
6	1/8	51.4	1675	1408	13.8	36,000	6700	6830	13.8	36,000
7	1/8	44.6	2100	1870	3.25	8.470	8850	9060	2.54	6.630
8	1/8	44.6	1950	1870	13.78	36,000	8800	9060	13.78	36.000

Note: Shaft torsional yield strength = 36,000 psi.

(a) Calculated critical speed of shaft without applied axial shaft-end force or torque.

TABLE 9. SHAFT CONFIGURATIONS TESTED WITH VARIED TORQUE AND CONSTANT SAG

Test	Length, in.	First Mode Critical Speed: Measured Value, rpm	First Mode Critical Speed: Calculated Value(a), rpm	Torque Applied, in-lb	Shear Stress, psi	Initial Deflection, in.	Lateral Displacement, in.
9	50	812	532	0	--	--	--
10	50	800	532	26.45	69,000	--	--
11	132	200	76	0	--	--	--
12	132	212	76	22.4	58,400	--	--
13	110	100	116	0	--	4.44	--
14	110	100	116	22.4	58,400	4.44	--
15	89.3	175	167	0	--	1.60(b)	--
16	89.3	174(c)	167	20.15	50,260	1.60(b)	(d)
17	89.3	189(c)	167	27.6	72,000	1.60(b)	1/4
18	89.3	198(c)	167	35.1	91,500	1.60(b)	5/16
19	89.3	212(c)	167	40.4	105,200	1.60(b)	11/32
20	89.3	240(c)	167	47.1	123,000	1.60(b)	11/32
21	89.3	219(c)	167	48.7	126,200	1.60(b)	11/32
22	89.3	167(c)	167	47.1	123,000	1.60(b)	(d)

Note: All shafts 1/8 inch in diameter. Shaft torsional yield strength = 92,000 psi.

(a) Calculated critical speed of shaft without applied axial shaft-end force or torque.

(b) Approximately equal to the sag of the shaft without applied axial shaft-end force

(c) Natural frequency of lateral vibration.

(d) Lateral displacement not measured.

TABLE 10. SHAFT CONFIGURATIONS TESTED WITH VARIED SAG AND CONSTANT TORQUE

Test	Length, in.	First Mode Critical Speed: Measured Value, rpm	First Mode Critical Speed: Calculated Value[a], rpm	Torque Applied, in-lb	Shear Stress, psi	Initial Deflection, in.	Lateral Displacement, in.
13	110	100	116	0	--	4.44	--
15	89.3	175	167	0	--	1.60[b]	--
23	89.3	170	167	0	--	1.60[b]	--
26	89.3	485[c]	167	0	--	0.187	3/32
27	89.3	480	167	0	--	0.187	--
29	89.3	410	167	0	--	0.187	--
14	110	100	116	22.4	58,400	4.44	--
24	89.3	170	167	22.4	58,400	1.60[b]	--
28	89.3	462	167	22.4	58,400	0.187	--
30	89.3	430	167	22.4	58,400	0.187	--
19	89.3	212[c]	167	40.4	105,200	1.60[b]	11/32
25	89.3	388[c]	167	40.6	106,000	0.437	(d)
31	89.3	770[c]	167	42.3	110,400	0.062	(d)

Note: All shafts 1/8 inch in diameter. Shaft torsional yield strength = 92,000 psi.

(a) Calculated critical speed of shaft without applied axial shaft-end or torque.

(b) Approximately equal to the sag of the shaft without applied axial shaft-end force

(c) Natural frequency of lateral vibration.

(d) Lateral displacement not measured.

speed to axial shaft-end forces. From the results of Tables 8 and 9 critical speed is quite dependent upon axial shaft-end forces, but is relatively insensitive to torque change.

Table 11 presents the results of tests conducted to determine the effect of axial torque on the natural frequency of lateral vibration for various conditions of critical installation and axial force. Tests 32 through 36 show no significant change in the frequency of lateral vibration even though the torque was sufficient to begin yielding the shaft. This test group was performed with an initial mid-point deflection of 1.67 inch and the bearing preload springs undeflected. In Tests 37 through 42, conducted with the bearing preload springs undeflected, the natural frequency of vibration did not change until the torsional shear stress exceeded the yield strength by a substantial amount. Tests 45 through 48 were conducted with the bearing preload springs deflected substantially; i.e., developing an axial tension, and showed an increase in natural frequency of lateral vibration. The natural frequency of lateral vibration was reduced as the shaft mid-point deflection was increased as shown by Tests 49 through 54.

Data on the effect of axial torque on the natural frequency of lateral vibration of a 1/4-inch-diameter shaft for two distinct installation methods are presented in Table 12. Tests 57 through 64 present the results of natural-frequency tests as torque is increasing for the shaft installed with the spindle bearing preload springs undeflected. As can be seen no change was observed in the natural frequency of lateral vibration as axial torque was applied. Tests 68 through 75 were to be conducted with the bearing preload springs deflected the same amount as in Tests 45 through 48; however, it was impossible to install the 1/4-inch-diameter shaft in the same manner as the 1/8-inch-diameter shaft. The stiffness of the 1/4-inch-diameter shaft is 8 times as large as the 1/8-inch-diameter shaft and cannot be subjected to the mid-point deflection and the axial force conditions. These tests show that the natural frequency of lateral vibration is reduced as the mid-point deflection increases.

Additional tests on the transient torque were conducted along with the testing program of shafts on two supports. This consisted of testing a damped 1/4-inch-diameter shaft 89.3 inches long with the first support located at 3.36 per cent of shaft length from one end and the second support varied from 10 to 50 per cent of shaft length from the opposite end. The eddy-current brake was energized by interruption of the current to excite a transient torque. This testing was conducted at the second critical speed of the longest span, with approximately 3.6 amperes of current. In all the tests no change was observed in the critical speed or the amplitude of vibration with application of transient torques.

A 1/8-inch-diameter shaft 89.3 inches long with an axial torque of 40.4 inch-pounds applied developed a large amount of lateral displacement. Figure 33 shows the lateral and mid-point deflection curve of a nonrotating shaft with applied torque. All shafts tested at zero speed which were 89.3 inches or longer assumed a lateral deflected position similar to Figure 33. This deflected shape began to occur when the applied torque was less than the calculated critical torque. Shafts with smaller amounts of sag developed smaller amounts of lateral displacement. It was not possible to observe lateral instability at rotational speeds.

It is thus apparent that steady or transient axial torque applied to a shaft installed in the shaft test machine does not reduce the critical speed, or the natural frequency of lateral vibration. Increasing the axial tension reduces the mid-point deflection of the shaft and increases the natural frequency of lateral vibration.

TABLE 11. SHAFT CONFIGURATIONS TESTED WITH APPLIED TORQUE AND CONTROLLED AXIAL FORCE

Test	First Mode Critical Speed: Measured Value[a], cpm	First Mode Critical Speed: Calculated Value[b], rpm	Torque Applied, in-lb	Shear Stress, psi	Initial Deflection, in.	Axial Displacement, in.	Remarks
32	174	167	0	0	1.67[c]	0	
33	172	167	21.15	55,100	1.67[c]	0	
34	168	167	27.95	73,000	1.67[c]	0	
35	169	167	35.8	93,500	1.67[c]	0.00573	Sag reduced slightly
36	175	167	42.3	110,500	1.67[c]	0.008	Ditto
37	175	167	21.1	55,100	1.67[c]	0	
38	177	167	27.6	72,000	1.67[c]	0.001	
39	176	167	35.8	93,500	1.67[c]	0.001	
40	176	167	42.3	110,500	1.67[c]	0.002	
41	192	167	48.7	127,700	1.67[c]	0.002	
42	195	167	52.0	136,400	1.67[c]	0.003	
43	180	167	0	0	1.67[c]	--	
44	220	167	0	0	1.67[c]	--	Sag reduced slightly
45	175	167	17.88	46,600	1.67[c]	0	
46	188	167	32.5	85,000	1.67[c]	0	
47	202	167	42.2	110,000	1.67[c]	0.0005	
48	204	167	50.4	132,000	1.67[c]	0.0008	
49	215	167	50.4	132,000	1.0625	0	
50	202	167	50.4	132,000	1.25	0.022	External axial force applied to the bearings
51	200	167	50.4	132,000	1.31	0.0304	
52	190	167	50.4	132,000	1.37	0.0374	
53	180	167	50.4	132,000	1.43	0.0454	
54	180	167	50.4	132,000	1.50	0.0590	

Note: All shafts tested are 1/8-inch diameter and 89.3 inches long. Shaft torsional yield strength = 92,000 psi.

(a) Natural frequency of lateral vibration.
(b) Calculated critical speed of shaft without applied axial shaft-end force or torque.
(c) Approximately equal to the sag of the shaft without applied axial shaft-end force.

TABLE 12. SHAFT CONFIGURATIONS TESTED WITH APPLIED TORQUE AND CONTROLLED AXIAL FORCE

Test	First Mode Critical Speed: Measured Value[a], rpm	First Mode Critical Speed: Calculated Value[b], rpm	Torque Applied, in-lb	Shear Stress, psi	Initial Deflection, in.	Axial Displacement, in.
55	334	333	0	--	0.468	--
56	337	333	28.4	9,250	0.468	--
57	334	333	0	--	--	--
58	332	333	29.2	9,550	--	0.001
59	334	333	42.2	13,800	--	0.001
60	333	333	60	19,540	--	0.001
61	332	333	80	26,050	--	0.001
62	332	333	100	32,600	--	0.001
63	332	333	120	39,100	--	0.0013
64	332	333	140	45,600	--	0.0016
65	400	333	0	--	--	
66	368	333	0	--	--	
67	331	333	0	--	0.468	
68	405	333	0	--	0.312	
69	397	333	29.3	9,500	0.312	
70	397	333	42.3	13,800	0.312	
71	397	333	60.0	19,540	0.296	
72	385	333	80	26,050	0.328	
73	382	333	100	32,600	0.328	
74	376	333	120	39,100	0.343	
75	376	333	140	45,600	0.343	
76	395	333	0	--	0.312	
77	400	333	0	--	0.343	

Note: All shafts tested are 1/4 inch in diameter, 89.3 inches long. Shaft torsional yield strength = 36,000 psi.

(a) Speed is natural frequency of lateral vibration with the exception of Test 56.

(b) Calculated critical speed of shaft without applied axial shaft-end force or torque.

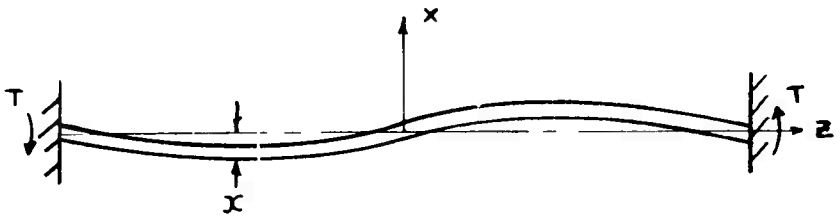

DISPLACEMENTS FOR
40.4 IN.-LB OF TORQUE

$x = 3/8"$

$y = 1\ 7/16"$

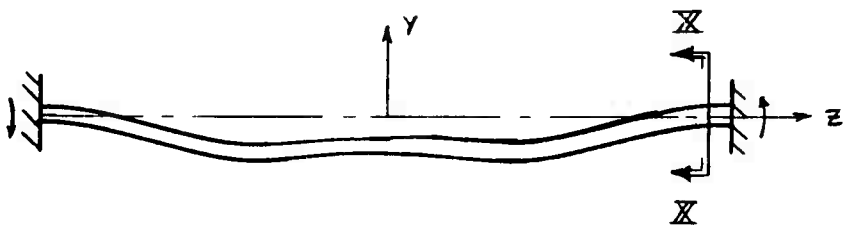

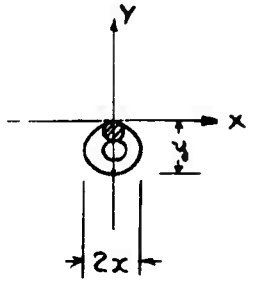

SECTION XX

FIGURE 33. DEFLECTED POSITION OF NONROTATING SHAFT WITH APPLIED TORQUE EXCEEDING THE CRITICAL TORQUE

Comparison of Experimental and Theoretical Results

The results of the theoretical work to determine the effect of axial torque on shaft critical speed were expressed graphically in Figure 25. Figure 34 repeats the information; the theoretical-torque versus critical-speed functions, α and β, respectively, for first, second, and fifth critical speed of a shaft with built-in ends are shown by dashed lines.

Table 13 summarizes the experimental work conducted to determine torque effect upon critical speed. Values of the frequency and torque functions, β and α, were calculated for most of the tests in Table 13. Equations (97) and (98) relate the physical dimensions of the test shafts to β and α; the frequency function, β, is proportional to the square of the experimentally observed critical speed and the torque function, α, proportional to the experimentally applied torque.

Following calculation the α and β functions were entered on Figure 34 to enable a graphic comparison of theoretical and experimental torque effects on critical speed. The plotted experimental points were scattered, so they were represented as forming the double-line envelopes of the figure. Rather than lower with increased torque as theory predicted, the experimental critical speeds increased m value. Consequently, the theoretical and experimental correlation of torque effects upon critical speed was not obtained.

Experimental observation of the lateral buckling of shafts does verify the theoretical results predicted. The deflected shape of the shaft as shown in Figure 33 was similar to results presented in Ref. (7).

The theoretical effect of increased axial force, as determined by a reduction in mid-point deflection on the critical speed was verified by the experimental work. Thus an axial tensile force increased the natural frequency of lateral vibration.

Conclusions Regarding Torque Effects

The major conclusions from this section of the report may be summarized as follows:

(1) Experimental work indicated that both constant and intermittent axial torque applied to fixed-end shafts does not reduce the critical speeds of shafts.

(2) Axial tensile force increases the critical speed of rotating shafts.

(3) Axial torque produces lateral buckling of the stationary shaft as predicted theoretically.

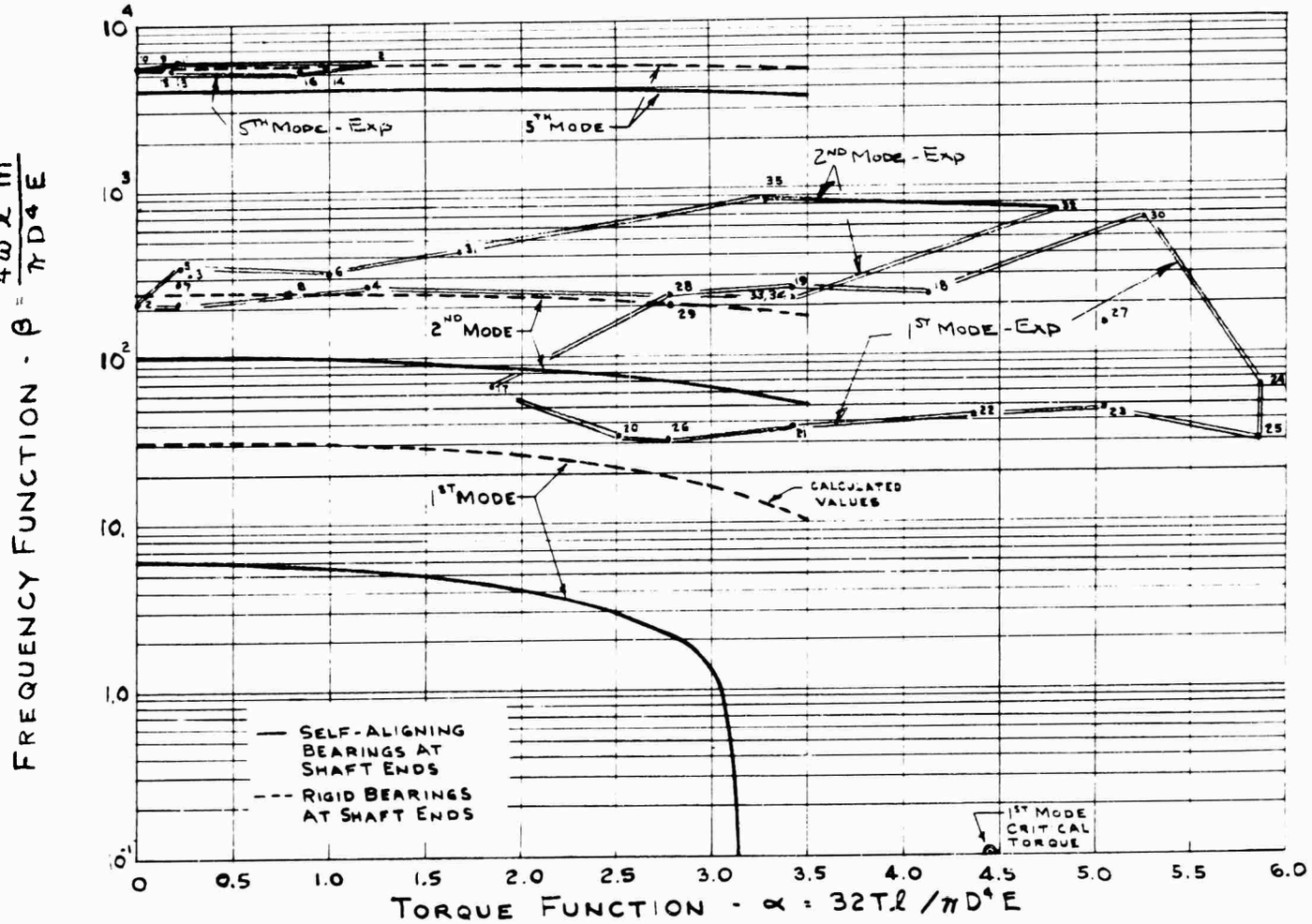

FIGURE 34. PLOT OF FREQUENCY FUNCTION VERSUS TORQUE FUNCTION SHOWING THE EFFECT OF TORQUE ON CRITICAL SPEED

TABLE 13. FREQUENCY FUNCTION AND TORQUE FUNCTION FOR SHAFTS TESTED WITH APPLIED TORQUE

	Shaft Configuration							
	Diameter, in.	Length, in.	Frequency Function	Torque Function	Point No. Plotted in Figure 34	Frequency Function	Torque Function	Point No. Plotted in Figure 34
			Second Mode			Fifth Mode		
1	1/4	89.3	215.5	0.204	1	5320.	0.147	9
2	1/4	89.3	215.5	0	2	5320.	0	10
3	1/8	63.2	332.	0.287	3	6170.	0.225	11
4	1/8	63.2	287.	1.21	4	5920.	1.21	12
5	1/8	51.4	347.	0.232	5	5550.	0.182	13
6	1/8	51.4	335.	0.988	6	5370.	0.988	14
7	1/8	44.6	299.	0.202	7	5320.	0.158	15
8	1/8	44.6	259.	0.856	8	5260.	0.856	16
			First Mode			Second Mode		
9	1/8	50.	70.7	0	--(a)	439.	0	--
10	1/8	50.	68.4	1.84	17	429.	1.675	31
11	1/8	132.	209.	0	--	1172.	0	--
12	1/8	132.	234.	4.12	18	714.	4.79	32
13	1/8	110.	251.	0	--	--	--	--
14	1/8	110.	251.	3.43	19	219.	3.42	33
15	1/8	89.3	33.4	0	--	238.	0	--
16	1/8	89.3	33.0(b)	2.51	20	--	--	--
17	1/8	89.3	38.9(b)	3.43	21	--	--	--
18	1/8	89.3	42.4(b)	4.36	22	--	--	--
19	1/8	89.3	49.0(b)	5.03	23	--		--
20	1/8	89.3	62.6(b)	5.86	24	--	--	--
21	1/8	89.3	52.0(b)	6.06	--(c)	--	--	--
22	1/8	89.3	30.4(b)	5.86	25	--	--	--
23	1/8	89.3	31.5	0	--	240.	0	--
24	1/8	89.3	31.5	2.78	26	225.	3.42	34
25	1/8	89.3	163.8(b)	5.05	27	--	--	--
26	1/8	89.3	256. (b)	0	--	--	--	--
27	1/8	89.3	250	0	--	--	--	--
28	1/8	89.3	233	2.78	28	--	--	--
29	1/8	89.3	183	0	--	854.	0	--
30	1/8	89.3	202	2.78	29	881.	3.28	35
31	1/8	89.3	646 (b)	5.26	30	--	--	--

(a) Torque function values of zero are not plotted in Figure 34.

(b) Frequency function calculated with natural frequency of lateral vibration.

(c) Value not plotted.

Intermediate Support Characteristics Providing Suitable High-Speed Shaft Operation

Numerous experimental shaft tests have been conducted to determine damped intermediate support characteristics necessary for high-speed shaft operation. Earlier in the research program before the "High Speed Shafting Design by Electrical Analogy" had been formulated, suitable damper parameters were sought by trial and error. Inasmuch as more data per research dollar could be obtained experimentally, rather than with use of the computer program, laboratory work comprised most of this phase of research.

Single Damped Support Tests

A single damped intermediate support was used in the first series of tests to determine suitable support parameters. The damping coefficients and support flexibilities were established for the first three tests by a simple calculation procedure as follows:

$$C_c = 2\frac{WK}{g}, \tag{111}$$

where

C_c = support critical damping coefficient, lb-sec/in.

W = shaft weight, lb

K = support spring constant, lb/in.

A standard steel test shaft size of 0.25-inch diameter and 89.3 inches long had been chosen as one which could be easily manipulated in the shaft test machine. The weight of the standard shaft was 1.260 pounds. The spring rate of the shaft at mid-span with no intermediate supports equaled 1.550 pounds per inch. Three support spring constants were chosen and corresponding damping coefficients were calculated, with the lowest valued spring constant approximately equal to the shaft mid-span spring rate.

During the test program it was discovered that the actual support damping coefficients were equal to about twice the calculated values for the damping fluids used in these tests. The following lists the support spring constants, K; calculated critical damping coefficients, C_c; and the actual damping values, C, used in the first three tests:

K, lb/in.	C_c, lb-sec/in.	C, lb-sec/in.
1.33	0.180	0.360
11.6	0.372	0.744
66	0.868	1.736

Figures 35, 36, and 37 show the shaft operating speed range versus intermediate support location for the support damping and flexibility values listed above. For each support location in a test series the shaft speed was increased through a rather wide

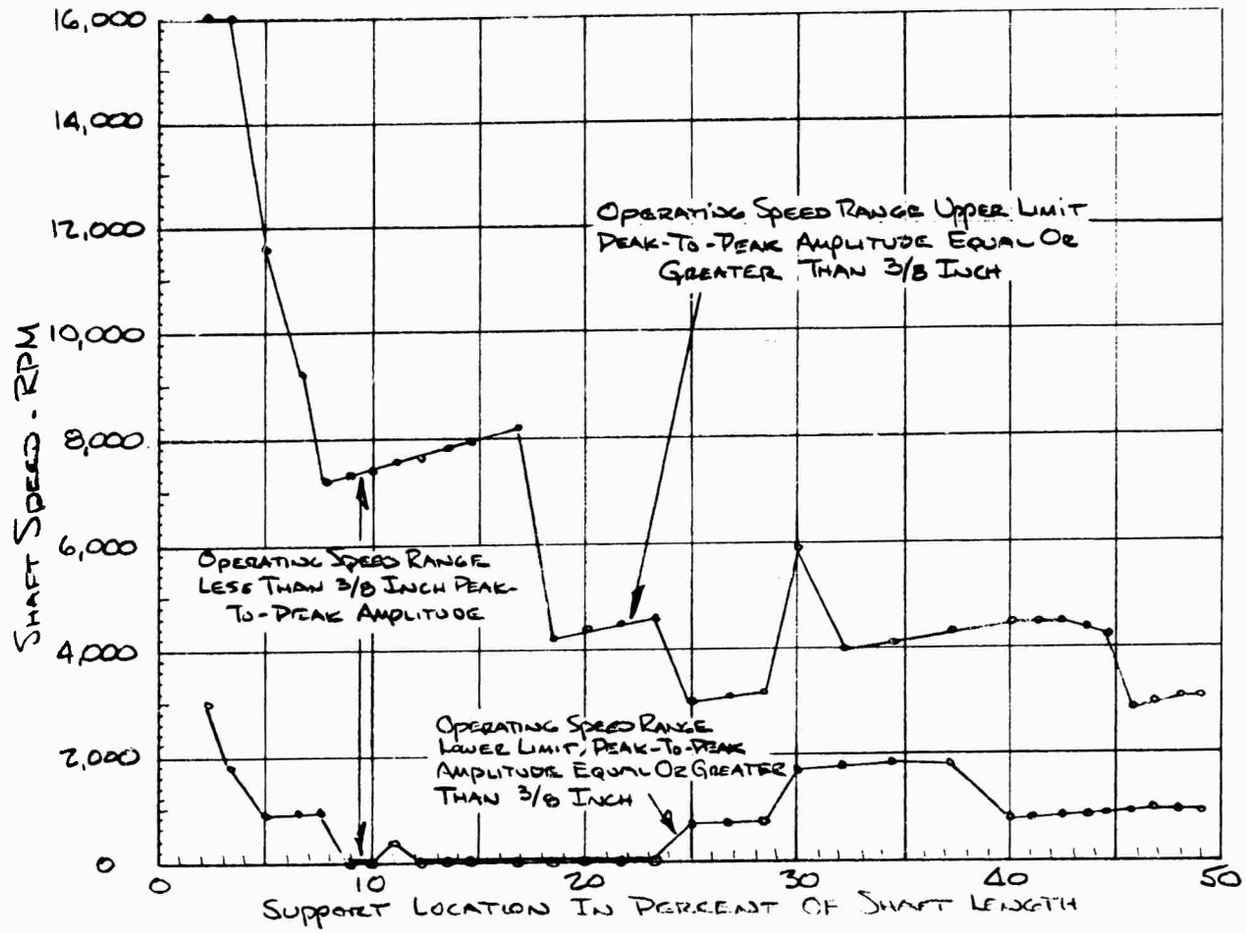

FIGURE 35. SHAFT SPEED VERSUS SINGLE DAMPED SUPPORT LOCATION FOR A 1/4-INCH-DIAMETER 89.3-INCH-LONG STEEL SHAFT WITH CLAMPED ENDS (SUPPORT CHARACTERISTICS: K = 1.33 LB/IN.; C = 0.360 LB-SEC/IN.)

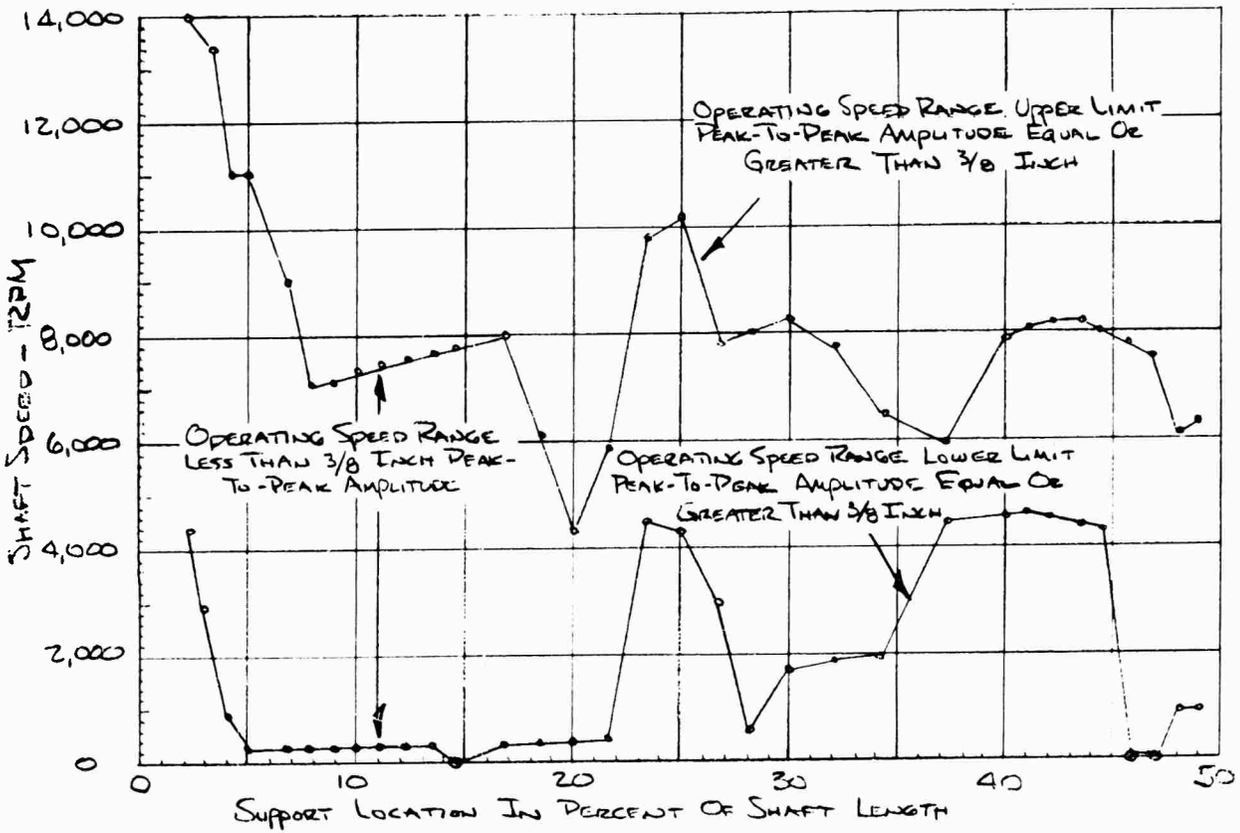

FIGURE 36. SHAFT SPEED VERSUS SINGLE DAMPED SUPPORT LOCATION FOR A 1/4-INCH-DIAMETER 89.3-INCH-LONG STEEL SHAFT WITH CLAMPED ENDS (SUPPORT CHARACTERISTICS: K = 11.6 LB/IN.; C = 0.744 LB-SEC/IN.)

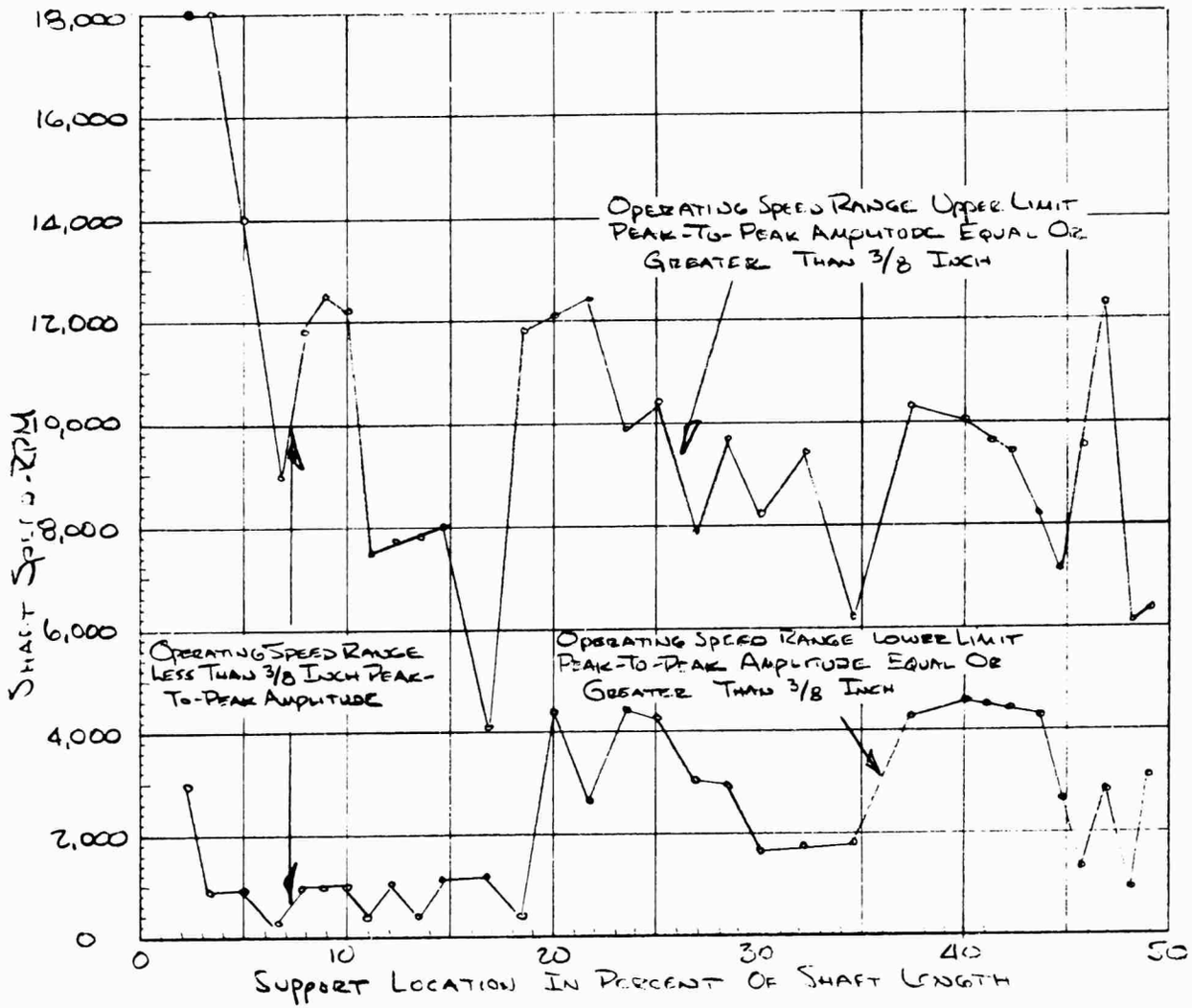

FIGURE 37. SHAFT SPEED VERSUS SINGLE DAMPED SUPPORT LOCATION FOR A 1/4-INCH-DIAMETER 89.3-INCH-LONG STEEL SHAFT WITH CLAMPED ENDS (SUPPORT CHARACTERISTICS: K = 66 LB/IN.; C = 1.736 LB-SEC/IN.)

range. Generally there was a speed range evident through which vibration amplitudes were well controlled, and less then 3/8-inch peak to peak. For some tests the effectiveness of the damped support was sufficient to limit shaft vibration amplitude to less than 3/8 inch from zero speed to nearly 8000 rpm, more than 23 times the first critical speed of 340 rpm.

Examination of Figures 35, 36, and 37 shows the best operating speed range (shaft vibration amplitude less the 3/8-inch peak to peak) to be obtained with the support located toward a shaft end. Consequently further test series were made with the support in the region between 2.24 and 11.2 per cent of shaft length from the shaft end. To find a better combination of support flexibility and damping to permit a wide shaft operating speed range, various combinations of K and C values were chosen for testing. Figures 38 through 42 show plots of operating speed range versus support location for various support damping and flexibility values.

The best support situation is shown in Figure 39. With the support located at 5.05 per cent of shaft length from one end, damper vibration control allowed satisfactory shaft operation from zero speed to 22,000 rpm. This corresponds approximately to the twelfth critical speed of an unsupported shaft. Moving the support to 3.36 per cent of shaft length from one end increased the satisfactory top speed to 26,000 rpm, but with diminished low-speed vibration control. Damper characteristics in this test series were K = 11.6 lb/in. and C = 1.736 lb-sec/in.

Thinking that such successful shaft vibration control as achieved with one damper might yet be improved, a series of tests were scheduled with two damped intermediate supports.

Tests With Two Damped Supports

Two Damped Supports Symmetrically Located. Since excellent high-speed shaft operation was obtained with one damper located close to a shaft end, four tests were made with two dampers located symmetrically near each shaft end. Damper parameters were as before in the best single support test series, with K = 11.6 lb/in. and C = 1.736 lb-sec/in. As before to limit extreme amplitude, and to signal 3/8-inch peak-to-peak vibration, 5/8-inch-diameter shaft guards were used.

In two or three preliminary runs with the two symmetrically located supports, shaft operation seemed extremely violent and noisy. For this reason, in the four series of tests shaft speed was brought up rather quickly and data were consequently less complete than with the single support tests.

In Test 1 with dampers located at 2.24 per cent of the shaft length from each end, vibration amplitude equal to 3/8-inch peak-to-peak occurred somewhere over 20,000 rpm. Then at 31,000 rpm vibration was so violent that one of the flexure plates was broken.

In Test 2 with parts renewed and dampers at 3.36 per cent from each end, vibration was mild until 28,000 rpm. At this speed damper parts were loosened by extreme vibration.

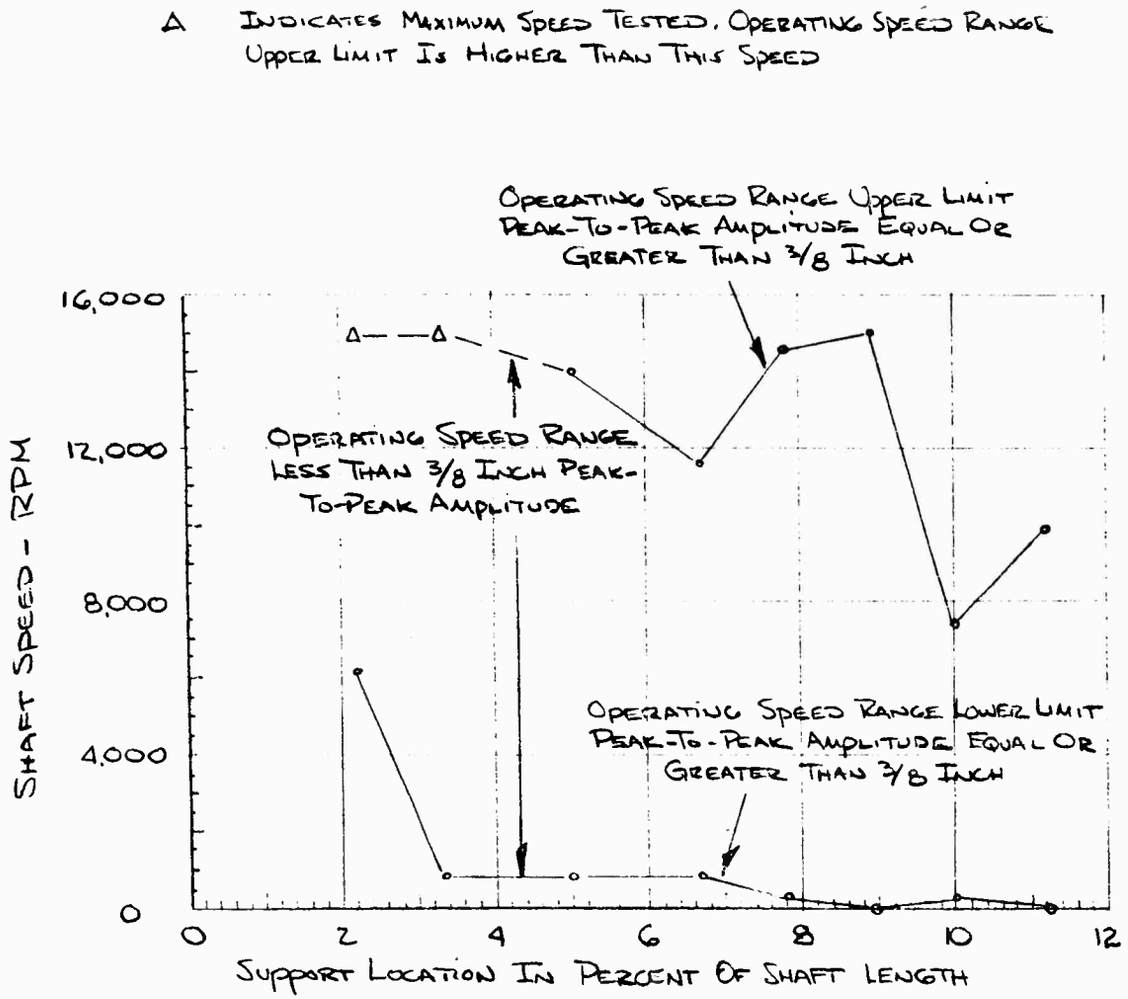

FIGURE 38. SHAFT SPEED VERSUS SINGLE DAMPED SUPPORT LOCATION FOR A 1/4-INCH-DIAMETER 89.3-INCH-LONG STEEL SHAFT WITH CLAMPED ENDS (SUPPORT CHARACTERISTICS: K = 11.6 LB/IN.; C = 0.360 LB-SEC/IN.)

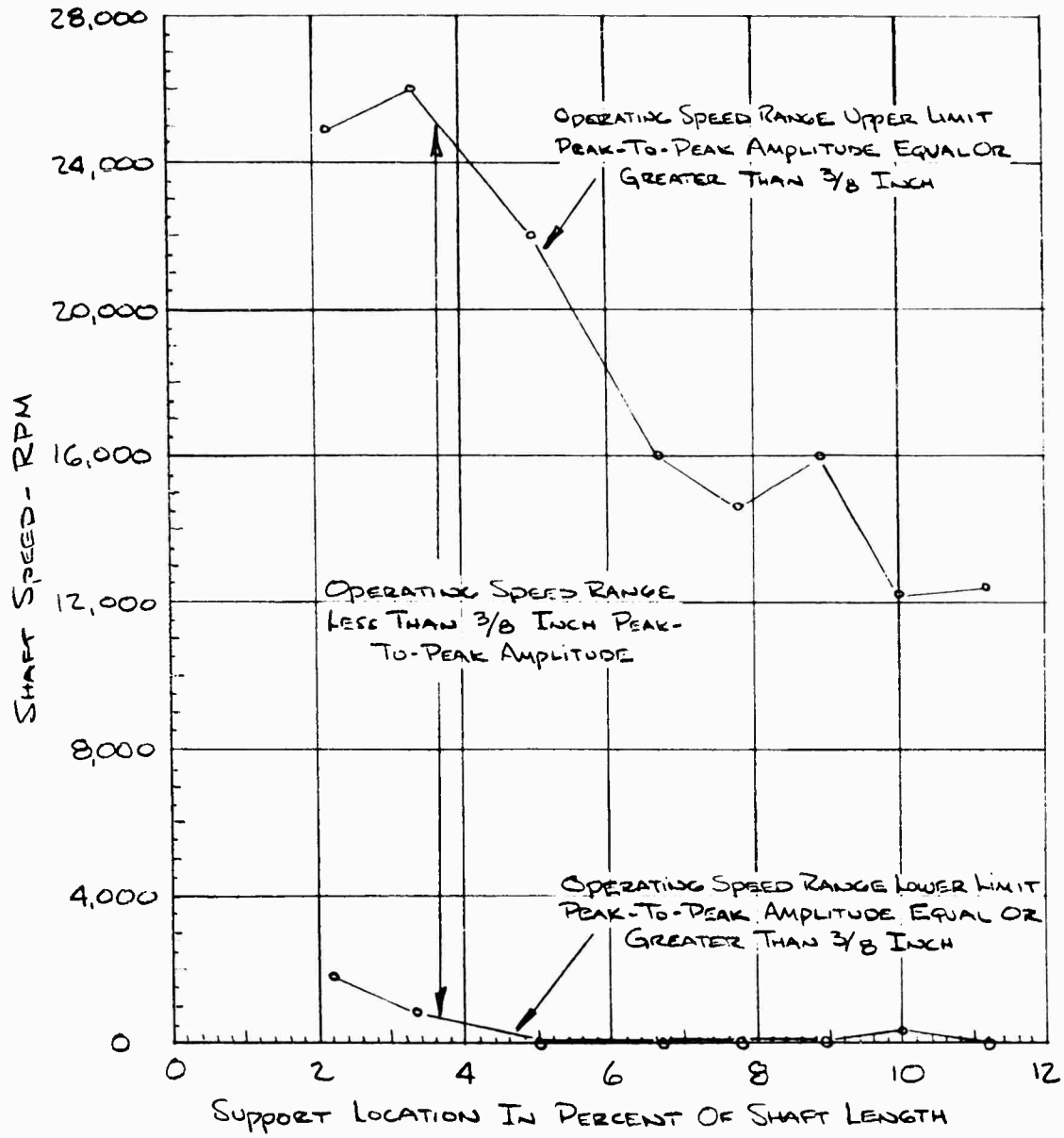

FIGURE 39. SHAFT SPEED VERSUS SINGLE DAMPED SUPPORT LOCATION FOR A 1/4-INCH-DIAMETER 89.3-INCH-LONG STEEL SHAFT WITH CLAMPED ENDS (SUPPORT CHARACTERISTICS: K = 11.6 LB/IN.; C = 1.736 LB-SEC/IN.)

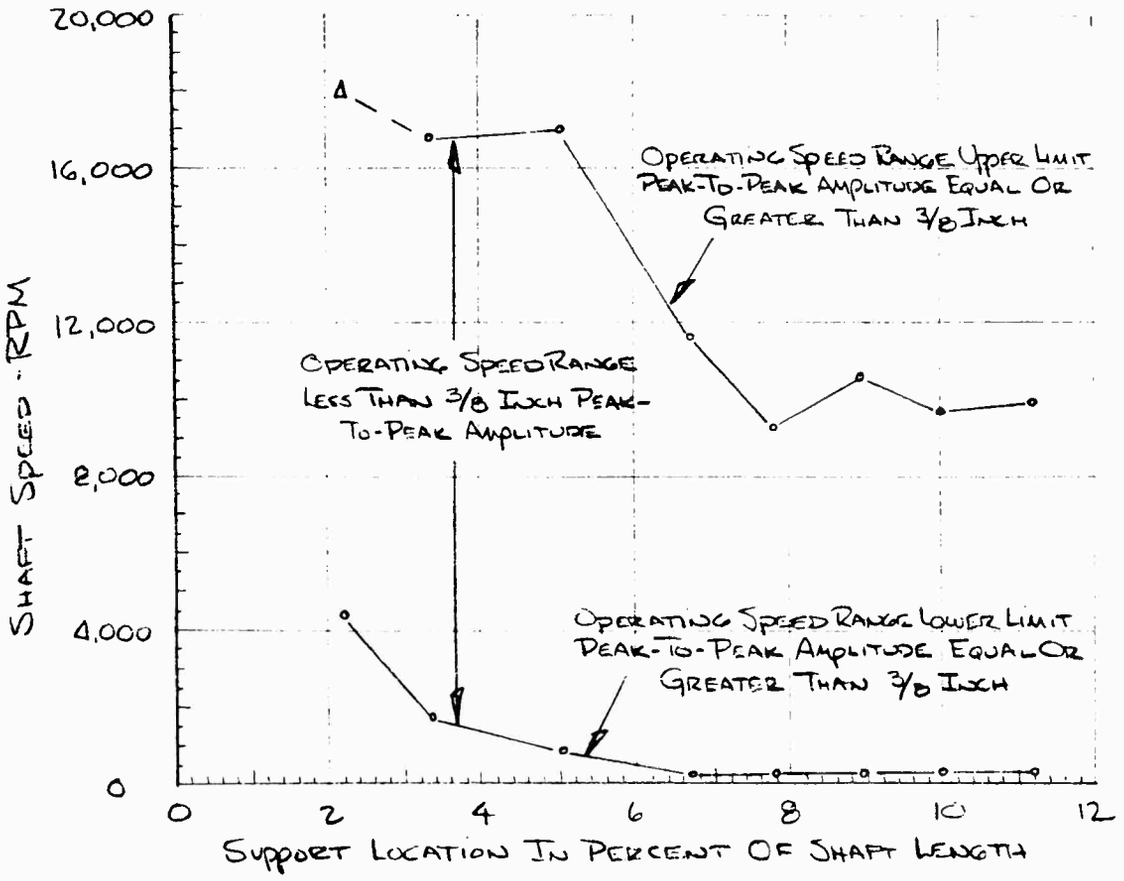

FIGURE 40. SHAFT SPEED VERSUS SINGLE DAMPED SUPPORT LOCATION FOR A 1/4-INCH-DIAMETER 89.3-INCH-LONG STEEL SHAFT WITH CLAMPED ENDS (SUPPORT CHARACTERISTICS: K = 1.33 LB/IN.; C = 0.744 LB-SEC/IN.)

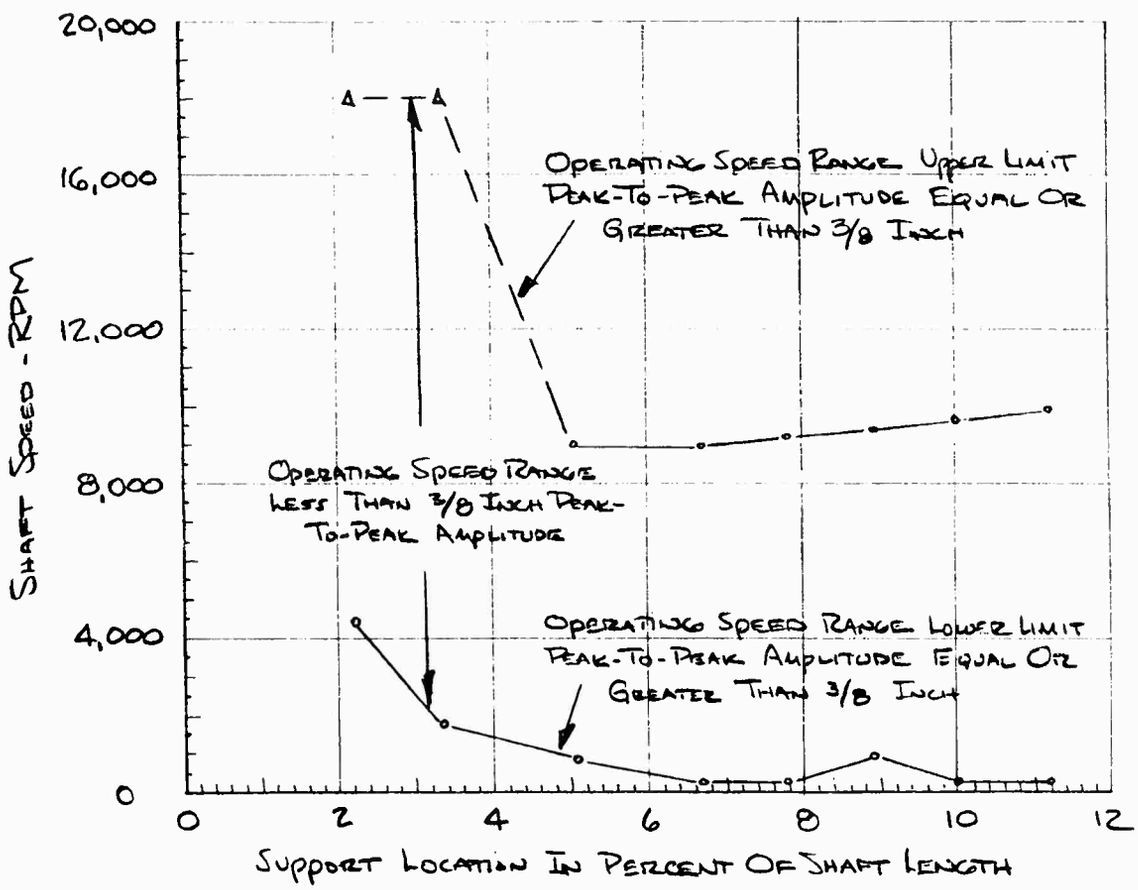

FIGURE 41. SHAFT SPEED VERSUS SINGLE DAMPED SUPPORT LOCATION FOR A 1/4-INCH-DIAMETER 89.3-INCH-LONG STEEL SHAFT WITH CLAMPED ENDS (SUPPORT CHARACTERISTICS: K = 66 LB/IN.; C = 0.744 LB-SEC/IN.)

Δ INDICATES MAXIMUM SPEED TESTED. OPERATING SPEED RANGE IS HIGHER THAN THIS VALUE.

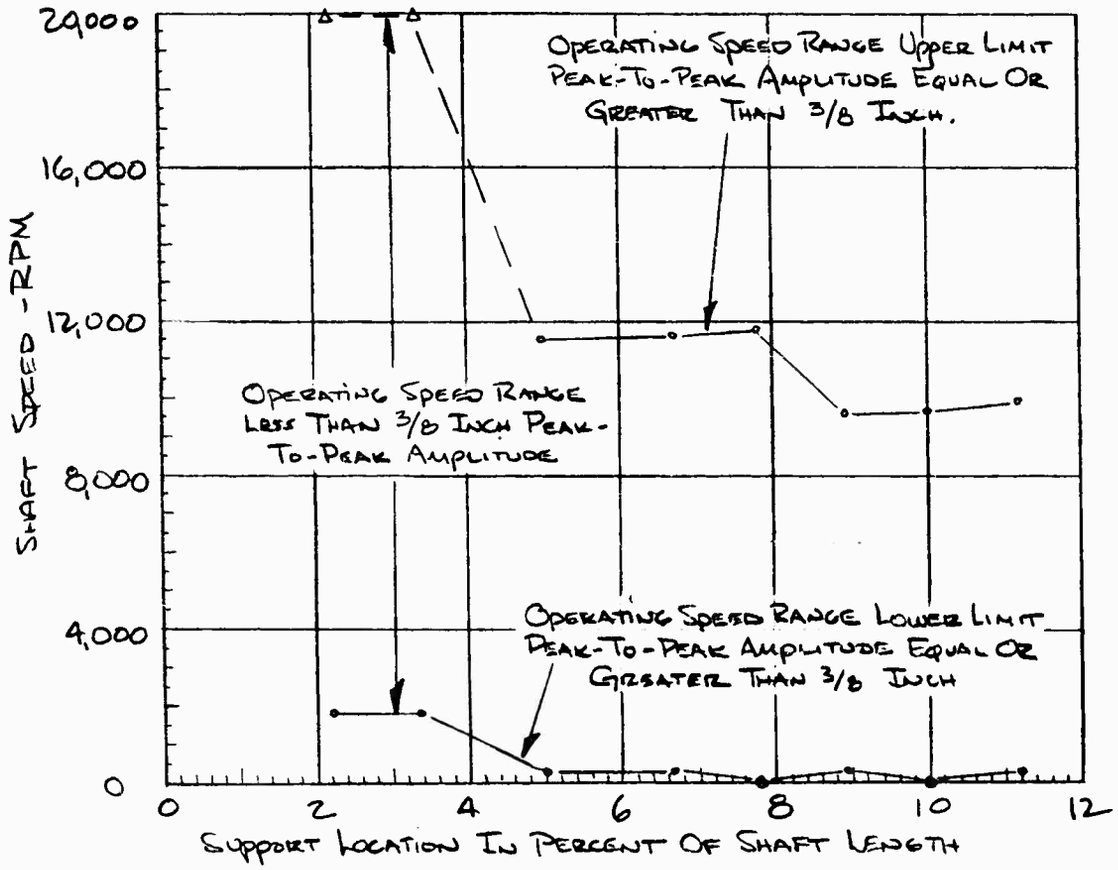

FIGURE 42. SHAFT SPEED VERSUS SINGLE DAMPED SUPPORT LOCATION FOR A 1/4-INCH-DIAMETER 89.3-INCH-LONG STEEL SHAFT WITH CLAMPED ENDS (SUPPORT CHARACTERISTICS: K = 1.33 LB/IN.; C = 1.736 LB-SEC/IN.)

In Test 3 with all parts retightened and dampers at 5.05 per cent from each end a speed of 34,000 rpm was attained. There were two critical speeds below 34,000 rpm that produced vibration amplitude equal to 3/8-inch peak to peak but the speeds were not recorded. At 34,000 rpm vibration was sufficient to loosen damper parts and to cause a permanent set in the shaft.

After replacing the shaft and retightening parts in Test 4, operation to 18,000 rpm was attained with dampers located at 6.72 per cent from each end. As the upper limiting speed of the operating speed range was seen to be decreasing another two-support test was scheduled.

Two Damped Supports - One Fixed and the Other Variably Positioned. Since previous tests had indicated the 3.36 per cent support location to be a good compromise between low- and high-speed vibration control, a series of tests was conducted with one damper fixed at this position. The other damper was variably positioned, starting near the other shaft end and moving toward the shaft mid-point as testing progressed. Support damping and spring rate were as before; C = 1.736 lb-sec/in. and K = 11.6 lb/in. Use of the 5/8-inch-diameter shaft guards was continued.

Figure 43 shows the resulting operating speed range obtained as the movable damper was repositioned in small increments from the shaft end toward mid-span. The largest operating speed range was obtained with both supports located symmetrically at 3.36 per cent of shaft length from the shaft ends. At this location there were no amplitudes as large as 3/8-inch peak to peak until 28,000 rpm was reached. However, in the varied support location region between zero and 8.95 per cent, vibration at the highest operating speeds was sufficient to loosen damper parts three times and to deform the test shaft permanently twice. To avoid these difficulties, 1/2-inch bushings were inserted in the shaft guards to reduce peak-to-peak amplitude from 3/8 to 1/4 inch. Subsequent testing of varied support location in the region from 10 to 50 per cent of shaft length from the end was conducted with these 1/2-inch-diameter shaft guards, and the highest-speed shaft vibrations were more effectively limited. Loosening of parts and permanent deformation of test shafts was eliminated.

It is interesting to note from Figure 43 that location of one support close to a shaft end with another very close to the shaft mid-point produces an excellent operating speed range. Although low-speed vibration control is diminished, both the lower and upper limits defining the operating speed range envelope are rather flat with respect to the location of the varied support. Speed range is not so sensitive to slight changes in support location.

Up to this point in the test program, no extensive experimental work had been accomplished with two supports both varied with each test. A geometric relationship describing positions of the two damped supports with a single number was devised, which enabled still another two-support test to be scheduled.

Two Damped Supports - Both Variably Positioned. Figure 44 shows a curve which denotes the position of each of two intermediate supports with one number, k. For any value of k there is but one position of each support along the test shaft length. For instance at k = 1, two supports were located such that the three spans between shaft ends and dampers were of equal length. At k = 0.5, the smallest span was one-half the

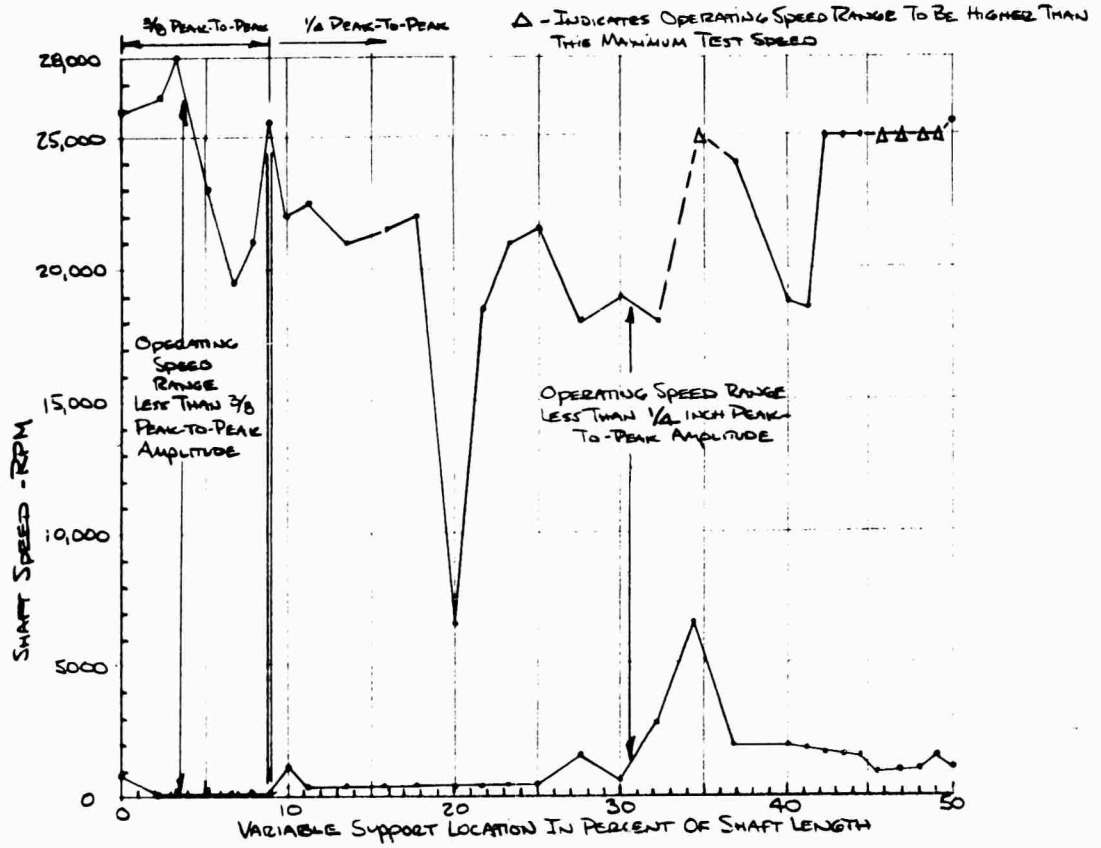

FIGURE 43. SHAFT SPEED VERSUS SUPPORT LOCATION WITH ONE SUPPORT FIXED AT 3.36 PER CENT FROM ONE END AND OTHER SUPPORT VARIED FROM OTHER END TOWARD SHAFT MIDPOINT FOR 1/4-INCH-DIAMETER STEEL SHAFT 89.3 INCHES LONG WITH FIXED ENDS

Support Characteristics: K = 11.6 lb/in.; C = 1.736 lb-sec/in.

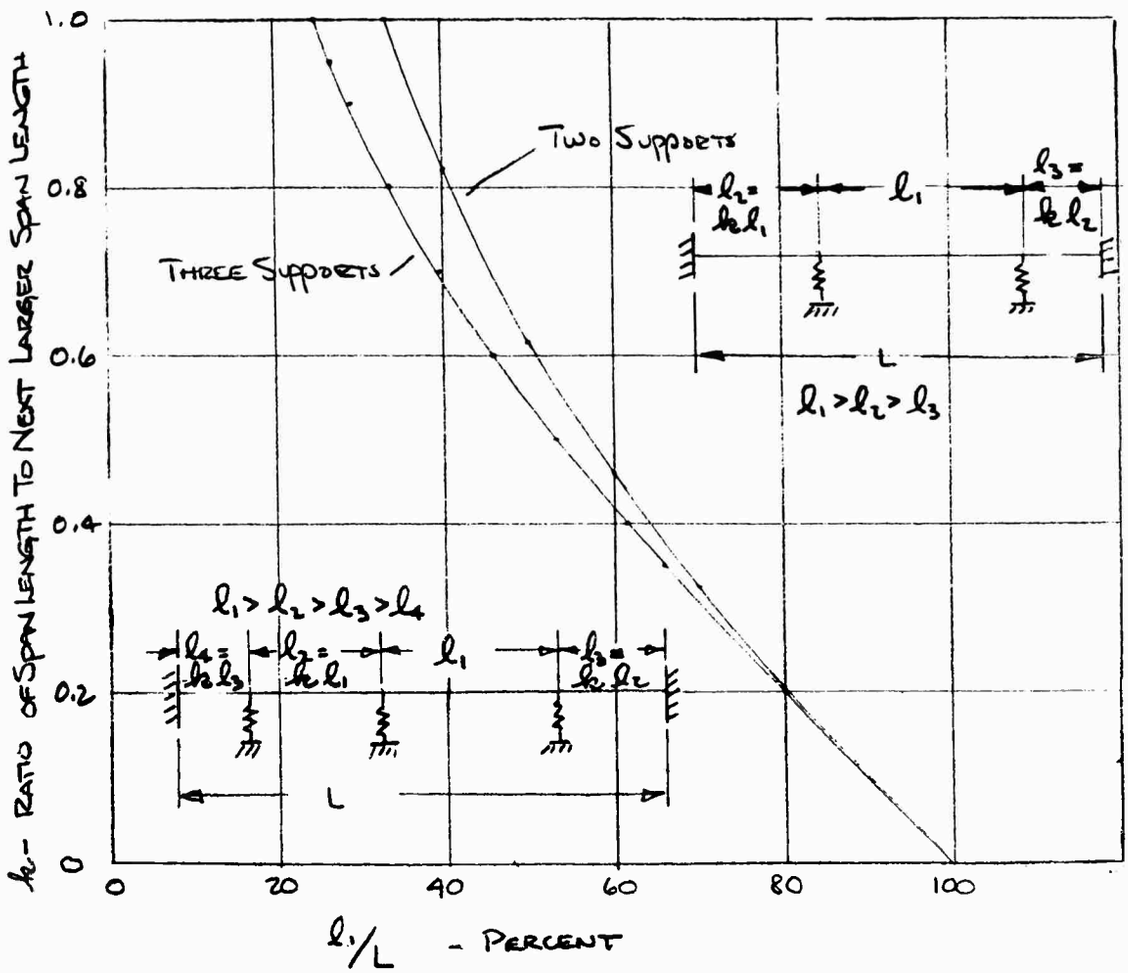

FIGURE 44. k VERSUS $\frac{l_1}{L}$ FOR A SHAFT WITH TWO OR THREE INTERMEDIATE SUPPORTS

middle-sized span, and the middle-sized span one-half the length of the longest span. The series of tests shown in Figure 44 was made with supports spaced to position the longest span in the center, with the shorter spans adjacent to the shaft ends.

Damping in this test series was reduced to 0.736 lb-sec/in., but support flexibility remained at 11.6 lb/in. Use of the 1/2-inch diameter shaft guards was continued. Figure 45 shows that the greatest operating speed range occurred at k = 0.2 with the two supports close to the shaft ends. A maximum speed of 17,500 rpm was reached before peak-to-peak vibration amplitude reached 1/4 inch.

For comparative purposes damper locations can be calculated easily from Figure 44. From the figure, at k = 0.2, ℓ_1/L = 80.7 per cent of the total shaft length. The longer end span equals 0.2 times the length of the longest span or 16.08 per cent of shaft length from one end. The shortest span at the other shaft and equals 0.2 squared times the longest span or 3.21 per cent of total shaft length.

Referring to the test of Figure 43 we can see a similar distribution of supports with one located at 3.36 per cent and the other at 15.7 or 17.9 per cent of shaft length from the other end. All shaft dimensions, support locations, and parameters of the test in which k = 0.2 are similar, with the exception of damping. Damping equal to 1.736 lb-sec/in. controlled shaft speed to approximately 21,750 rpm, while the smaller damping value of 0.744 lb-sec/in. used in the test with k = 0.2 permitted operation to just 17,500 rpm. Low-speed operation was the same in both cases. The conclusion may be drawn that with two dampers, each located close to a shaft end, vibration will be better controlled at higher speeds with the higher support damping value.

Tests With Three Damped Supports

Three Damped Supports – All Variably Positioned. It was also desired to evaluate use of three variably positioned dampers. A series of tests was conducted with the same support parameters as used in the variably positioned two-support test series. Figure 44 shows the relation of span lengths to one another with respect to the value k, and also the span position along the shaft. Span orientation begins with the shortest adjacent to one shaft end, then the next to the longest, the longest, and the next to the shortest at the other shaft end.

Figure 46 shows test results of this series. Contrary to the similar series with two dampers, all low critical speeds are sufficiently controlled by three dampers to limit vibration amplitude to less than 1/4 inch peak to peak. However, peak operating speed reached only 13,600 rpm at k = 0.5.

Since project emphasis has been toward developing ultrahigh-speed shaft support data, investigation with three variably positioned dampers was discontinued. Previous tests have shown two dampers, and even a single damped intermediate support to provide better shaft vibration control at the higher speeds.

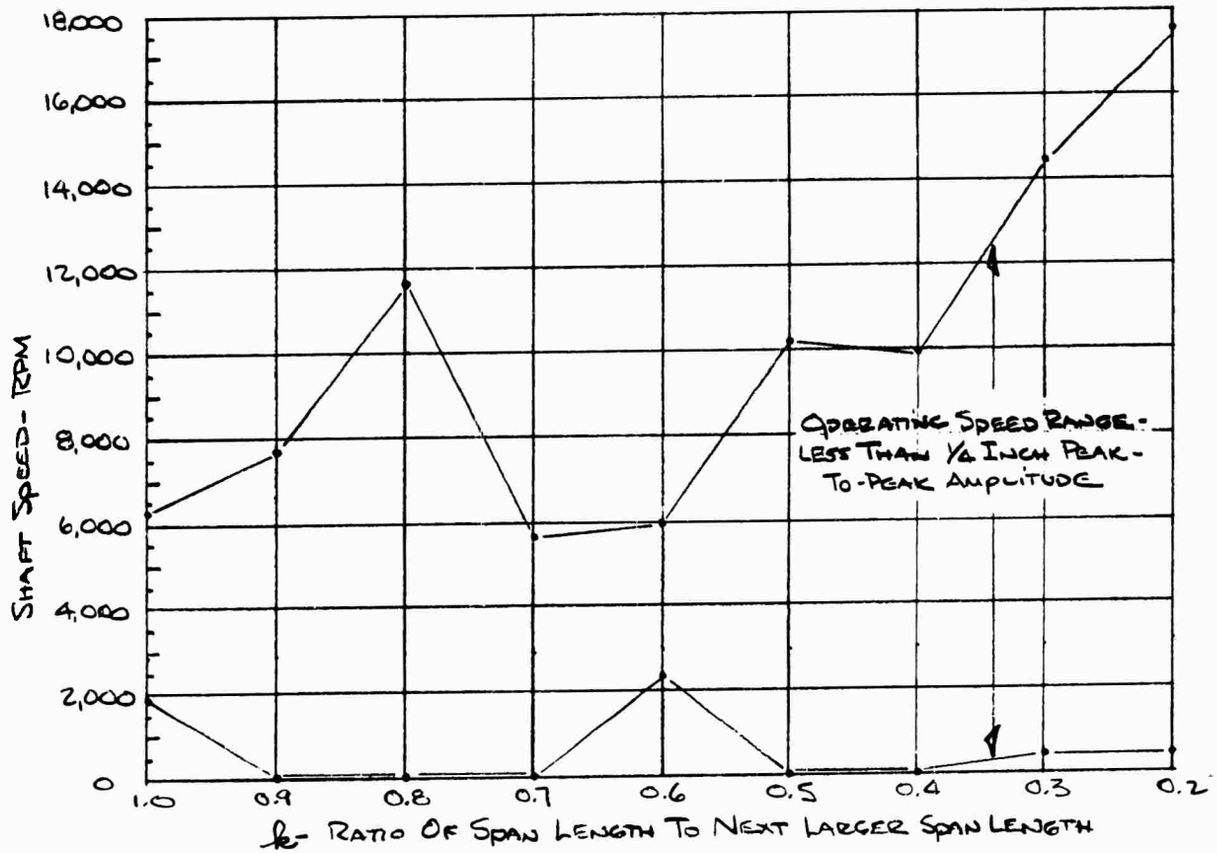

FIGURE 45. SHAFT SPEED VERSUS SUPPORT LOCATION WITH TWO DAMPED SUPPORTS VARIABLY POSITIONED FOR 1/4-INCH-DIAMETER STEEL SHAFT 89.3 INCHES LONG WITH FIXED ENDS (SUPPORT CHARACTERISTICS: K = 11.6 LB/IN.; C = 0.744 LB-SEC/IN.)

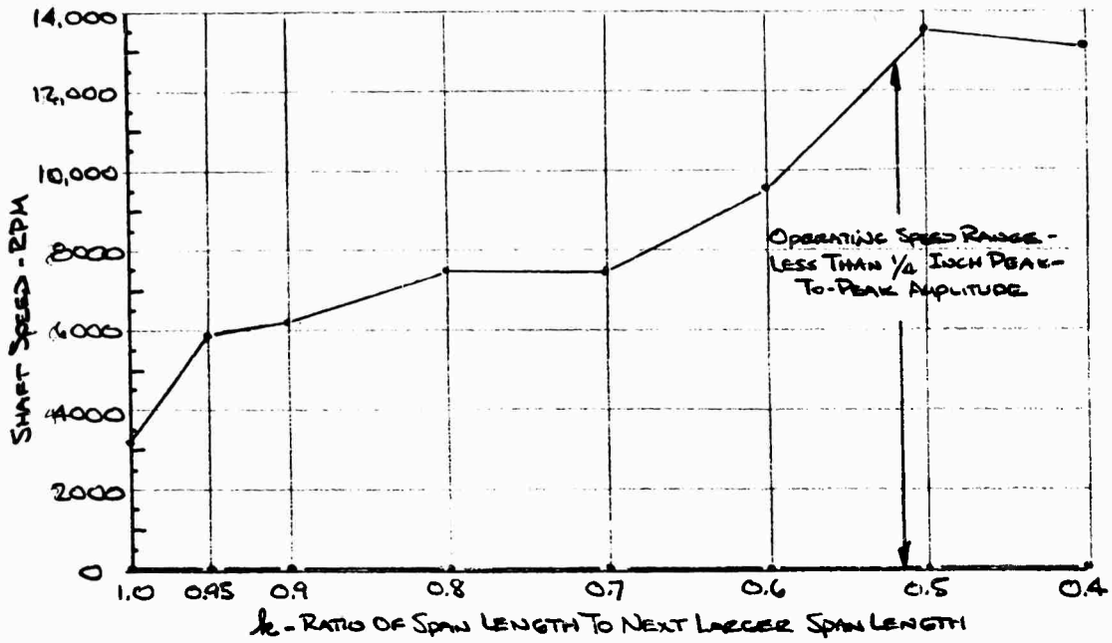

FIGURE 46. SHAFT SPEED VERSUS SUPPORT LOCATION WITH THREE VARIABLY POSITIONED DAMPED SUPPORTS FOR 1/4-INCH-DIAMETER STEEL SHAFT 89.3 INCHES LONG WITH FIXED ENDS (SUPPORT CHARACTERISTICS: K = 11.6 LB/IN. ; C = 0.744 LB-SEC/IN.)

Three Damped Supports – Stefano's Spacing. Early in the research program a Fairchild Aircraft Report by N. M. Stefano [Ref. (13)] was brought to our attention. The report discussed positioning of three damped intermediate supports to provide adequate vibration control through the first 300-plus critical speeds. "Stefano's positioning of intermediate supports calls for placement at 1/5, 4/9, and 4/7 of shaft length, all measured from the same shaft end.

The reference however, did not indicate what intermediate support flexibilities or damping values were required, and so the same values as indicated in Figure 35 were used: K = 1.33 lb/in. and C = 0.360 lb-sec/in. Shaft guards with 5/8-inch-diameter holes were used to contain the 1/4-inch-diameter test shaft.

When the test was run, high-speed vibration control was adequate only to 7250 rpm, at which point vibration amplitude equalled 3/8 inch peak to peak. This speed is between the sixth and seventh criticals for the shaft without intermediate supports. Since better operation was possible with just one damped support (see Figures 35 through 42), no further tests were made with this three-support orientation.

It is only fair to say that there very well may be a more suitable combination of support bearing weights in relation to shaft weight, support flexibility, and damping coefficients which would permit operation to a much higher speed than 7250 rpm. However, it was considered more in keeping with the research program objectives to strive

for high-speed shaft operation with a mimimum weight penalty imposed by the number of dampers required.

Experiment With Shaft Behavior Predicted by Electrical Analogy

Late in the research program a method of predicting shaft behavior was developed by application of modified electrical transmission line theory. Details of the theory are explained in the section entitled, High Speed Shafting Design by Electrical Analogy.

A laboratory experiment was set up using shaft and support parameters calculated by the analogy. It was predicted that two dampers spaced along a steel shaft of 1/2-inch diameter and 138 inches in length would successfully control vibration amplitudes through the first eight critical speeds of the same shaft with no supports. At the ninth critical speed operation would become unsuitable.

One damper was located 30-15/32 inches from one end, equipped with a spring constant of 120 lb/in., and a damping coefficient of 1.7 lb-sec/in. The second damper was positioned 44-29/32 inches from the other shaft end. Its damping factor was adjusted to 1.2 lb-sec/in., and the spring rate used was negligible.

The experiment showed what was predicted. The first eight critical speeds were well controlled with the seventh and eighth extremely smooth running. At the ninth critical speed shaft operation became so noisy that there was considerable doubt that the test machine would remain intact. However, Mr. Bruce Brooks of the Sponsoring Agency directed that speed be increased, with the final result that a maximum speed of 45,500 rpm was attained. Although there were shaft operating speeds above the ninth critical which produced a disturbing noise, there were also wide ranges in speed over which operation was very smooth. We are confident that the methods of damper selection provided by the electrical analogy produce an important new insight for predicting high-speed shaft operation.

Conclusions

Numerous experiments have shown that transmission shafts can be operated dependably at and above their first critical speeds. Although tests were conducted with a standard steel shaft size of 1/4-inch diameter 89.3 inches long, the modeling procedure explained previously permits similar operation to be obtained with any other shaft size and length.

In the single-damped-support tests best operation was obtained with the damper located close to one shaft end. Figure 39 shows the best of the single-damped-support test series. Damper parameters are: K = 11.6 lb/in., and C = 1.736 lb-sec/in. At a damper position 5.05 per cent of shaft length from one end, operation to 22,000 rpm was achieved before the vibration double amplitude reached 3/8 inch.

In the two-support tests highest speed operation was again attained with supports located toward each shaft end. However, during some tests vibration was so violent that in two cases shafts were bent. More dependable operation was obtained with one support close to a shaft end and the other near mid-span as indicated in Figure 43. A

noteworthy feature of this arrangement is that vibration amplitude control is not particularly sensitive to location of the center support. With one support located at 3.36 per cent of shaft length and the other positioned between 42 and 49 per cent from the other shaft end, double amplitudes were limited to less than 1/4 inch from approximately 2000 to 25,000 rpm. Damping values and spring rates were the same as used in the best single-support test: K = 11.6 lb/in. and C = 1.736 lb-sec/in.

Another two-support test conducted with the same support flexibility, K, but with 43 per cent as much damping showed the similar trend of best attainable operating speed range with dampers set close to each end. However, the highest operating speed was just 17,500 rpm. The conclusion to be reached here is that damping was not sufficiently high to provide best operation.

All of the three support tests showed decreasing ability to control vibration at high speeds. All, however, controlled low-speed amplitudes well enough. There seemed no advantage to continued three-support investigation, since single-support tests successfully controlled vibration amplitudes at higher speeds.

With the advent of high-speed shafting design by electrical analogy, experimentation will be called upon during the second-phase research program to corroborate predicted high-speed shaft operation, rather than to generate support parameter data for high-speed model shafts. A 1/2-inch-diameter, 138-inch-long steel shaft with two damped supports was predicted by the analogy to perform well through its first eight critical speeds, but to operate poorly at the ninth. Experiment has shown the predicted operation to be correct. Using the newly developed design procedure it is expected that superior damped supports can be designed for any high-speed shaft without scaling values from previous experiments.

Effect of Continuous Damping on High-Speed Shaft Operation

A method of providing suitable hypercritical-speed shaft operation by using a continuous damping coating applied to the length of a shaft was suggested in the research program proposal. This section deals with the investigation of coatings and their effect upon shaft behavior.

The requirements of a suitable continuous viscous damping coating are that it be able to absorb and dissipate a large quantity of vibration energy, and that its bonding strength to the shaft be great. For viscoelastic materials the measure of area within the hysteresis loop indicates the energy-dissipation qualities. Due to the tendency of externally applied coatings to separate from the shaft surface at high speed, a good bond between shaft and coating either by an adhesive or by "shrink fit" is essential. Viscoelastic coatings used on the shaft surface absorb energy by changing shape as the shaft surface fibers stretch and compress. Viscous damping of shaft vibrations using viscoelastic coatings forms a major part of the evaluation of continuously damped shaft behavior.

Coulomb damping provides another means of absorbing the energy of vibrating shafts. Hollow turbine blades have been damped by bundles of wires placed longitudinally inside the blades [Ref. (14)]. A similar arrangement was investigated for damping tubular shafts. In a discussion concerning damping materials, use of a woven steel

mesh fitting the shaft surface closely was suggested [Ref. (15)]. As the outside or inside surface fibers of the vibrating shaft change length, the friction of the steel wires or mesh sliding on the shaft surface would cause energy dissipation.

A two-part evaluation was made of both coulomb and viscous damping methods. A large number of coatings were first tested on nonrotating shafts which were vibrated laterally. Then the more promising coatings were applied to shafts for rotational tests in the shaft test machine.

Nonrotational Continuous-Damping Evaluation

Information concerning suitable damping coatings was obtained from various sources. Battelle's Rubber and Plastics Division was consulted, as was a coatings manufacturer, and a technical publication [Ref. (16)]. Quite a few coatings were suggested, and, to reduce the number of rotational tests necessary for actual coating evaluation, a nonrotating test procedure was devised.

Figure 47 shows a schematic diagram of the nonrotational test apparatus. Coated shaft samples were clamped at their centers to the moving element of an electrodynamic shaker. A variable-frequency alternating-current source supplied energy to power the shaker so that the cantilevered test samples could be vibrated at their natural frequencies. Table 14 indexes the details of the coatings and how they were applied to test shafts. Table 15 shows a tabulation of the relative merit of the damping coatings.

The effectiveness of continuous damping on nonrotational lateral vibration was determined by calculating the amplitude ratio of free-end vibration, y, to shaker vibration, y_s. The ratio is called amplification or amplification factor. For all tests the vibration amplitudes were noted at the test-shaft natural frequency, which varied somewhat due to the different weights of the coatings. Table 15 shows for the calibration tests of bare shafts that amplification factors range between 134 and 200. Tests 4 through 20 indicate amplification from 6.4 to 159 for the continuously coated shafts. The lower the amplification the better the damping characteristics of the shaft coating. The best coating was produced by winding rubber tape on the shaft surface. However, near the end of this test the free-end amplitude of vibration began to increase, indicating a reduction in damping after absorbing a large amount of energy. This was probably caused by an increase in temperature of the coating, which started its separation from the shaft. In the next best test, a tubular shaft filled with wires, the problems associated with temperature increase did not occur and free-end amplitude did not change.

The results show that amplitude reduction of continuously damped shaft samples is quite apparent in some cases. The four most promising continuously damped shaft configurations were chosen for rotational tests, which will be described now.

Rotational Continuous-Damping Evaluation

The four most promising damping coatings as shown by nonrotational testing were chosen for evaluation in the shaft test machine. All coatings were applied to 1/4-inch-diameter by 89.3-inch-long steel shafts. The fourth test used a tube of these dimensions with a wall thickness of 0.035 inch. Details of the coatings are shown in Table 14 and refer to Tests 10, 6, 5, and 15 of that table.

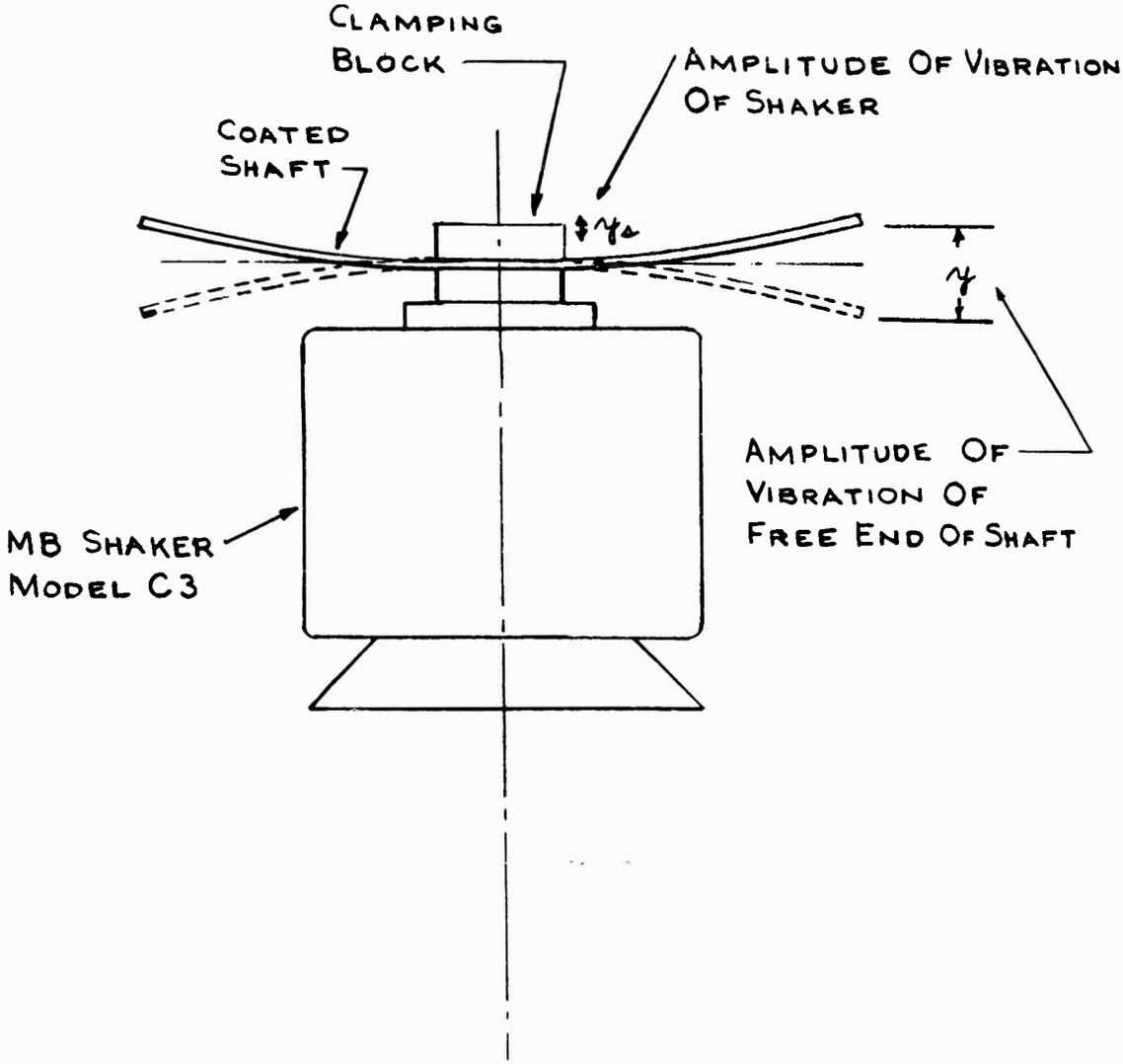

FIGURE 47. SCHEMATIC DIAGRAM OF ARRANGEMENT FOR PRELIMINARY EVALUATION OF THE EFFECTIVENESS OF SHAFT COATINGS

TABLE 14. SHAFT COATINGS TESTED

Test	Description of Shaft Preparation
1	No coating – calibration
2	No coating – calibration
3	No coating – calibration
4	Latex gum rubber (1/4-in. ID x 1/16-in.-thick wall) bonded to shaft with epoxy resin (Woodhill Chemical Co.); shaft coated with rubber tube along entire length
5	Latex gum rubber, etc., same as Test 4
6	Tygon – plasticized vinyl (1/4-in. ID x 1/16-in.-thick wall) bonded to shaft with epoxy resin (Woodhill Chemical Co.)
7	Polyolefin shrinkable tubing – FIT 275-4; shaft clamped with tubing along entire length
8	Polyolefin shrinkable tubing – FIT 275-4
9	3M Tape Adhesive No. 466 – wrapped around shaft in helix
10	P & R Splicing Compound No. 8 – 3/4 in. wide x 1/16 in. thick wrapped around shaft in helix, with 1/2-width overlap (electrical tape)
11	Shielding and bonding cable – Belden's No. 8663 – 160 wires x 34 gage (wire mesh) soldered to shaft at ends
12	Shielding and bonding cable, etc., same as Test 11 Pliobond adhesive allowed to fill wire interstices
13	No coating – 1/4-in. OD x 0.035-in.-thick wall, seamless, cold-drawn mechanical tubing
14	1/4-in.-OD x 0.035-in.-thick-wall tubing with 1/8-in.-diameter shaft cemented in place with Pro-Seal 890-B2
15	1/4-in.-OD x 0.035-in.-thick-wall tubing filled with 46 steel wires (0.022-in.-diameter)
16	Wire (0.033-in. diameter) wound on outside diameter – closely wound
17	Wire wound – same as Test 16
18	Wire (0.024-in. diameter) wound on outside diameter – closely wound
19	Wire (0.033-in. diameter) wound on outside diameter – open wind – one wire diameter between coils
20	Wire (0.024-in. diameter) wound on outside diameter – open wind – one wire diameter between coils

Note: All shafts are 1/4-in. diameter x 12 in. long, and coatings cover entire length of shaft only unless otherwise indicated. Wires were wound separate from the shaft and then assembled.

TABLE 15. TABULAR RESULTS OF SHAFT COATINGS TESTED TO DETERMINE EFFECTIVENESS OF DAMPING

Test	y_s Amplitude of Vibration of Shaker, in.	y Amplitude of Vibration at Free End, in.	Natural Frequency, cpm	Amplification, $\frac{y}{y_s}$
1	0.014	1.812	2880	134.
2	0.005	1.00	2880	200.
3	0.0125	1.75	2760	140.
4	0.016	0.875	2630	54.6
5	0.014	0.938	2720	65.5
6	0.025	1.625	2580	63.7
7	0.013	0.75	2760	59.
8	0.015	0.938	2700	62.6
9	0.014	1.625	2820	116.
10	0.271	1.75	2520	6.4
11	0.011	1.625	2700	159.
12	0.018	1.625	2720	90.
13	0.005	0.75	3360	140.
14	0.012	0.875	2700	72.9
15	0.011	0.25	2700	22.8
16	0.0148	0.3125	2330	21.2
17	0.0344	1.625	2330	47.3
18	0.0143	1.500	2400	105.
19	0.0138	1.500	2490	109.
20	0.0136	1.1875	2520	138.

Some difficulty was encountered in preparing the Number 15 rotational test specimen; the tube filled with many small-diameter wires. The wires were cut to shaft length from a coil. During installation of the wires in the tubing, they attempted to assume the coiled shape and align themselves in the same direction. This resulted in a curved tube which was not suitable for rotational test. A 3/16-inch-diameter length of sash cable was substituted for the individual wires, and the tendency toward tube curvature was eliminated. A nonrotational test was the made of this substitution for the Test 15 specimen, resulting in an amplification factor of 46.8.

Table 16 shows results of the rotational tests. Tests were run to the second or third critical without intermediate supports. Table 16 shows the speed range for the four prepared shafts. The term speed range is used to indicate the difference between the speeds at which large amplitudes of vibration were first noted as the shaft speed was increased, and as the shaft speed was decreased through the given vibration mode. For comparison, the speed range of large amplitudes of vibration for an uncoated shaft is presented in the same table.

The shafts coated with P & R splicing compound and latex gum rubber showed the best improvement in the operating speed range. This is indicated by the small difference in speed at which the large amplitudes of vibration began when increasing and decreasing speed.

The Tygon-coated shaft showed a lesser degree of vibration improvement than the two best shafts. The tube filled with sash cable proved to be a disappointment, although its nonrotational rating was better than either the Tygon- or gum-rubber coated shafts. The rotational behavior of the sash-cable-filled tube was very similar to the bare calibration shaft listed first in Table 16.

In comparing damping of filled tubes and viscoelastic coatings, consideration should be given to the change in exciting force as well as damping ability. Filling a tubular shaft with steel sash cable probably introduces more mass unbalance than coating a shaft with a thin layer of viscoelastic material. Although the filled tubular shaft may be just as effective percentagewise, in reducing the vibration amplitudes, the larger mass unbalance causes it to appear to be less effective.

Consideration must also be given to a basic difference between the preliminary shaker tests and the rotating tests of continuously damped shafts. In the shaker tests there is a cyclic change in shaft fiber length, which causes energy dissipation by alternately stretching and compressing the damping materials. In shafts rotating at their critical speeds, for the most part there is no cyclic change in shaft fiber length, if the shaft is supported symmetrically at its ends. Consequently, in rotating tests, the improvement in operation of continuously damped shafts over uncoated shafts was minor.

Conclusions

Limited experimental testing of continuous shaft damping has shown some effectiveness in reducing the speed range of large amplitudes of vibration for the lower critical speeds. Operation at the higher critical speeds was, however, totally unsatisfactory. Damping provided by shaft coatings or fillings cannot, therefore, be recommended.

TABLE 16. RESULTS OF COATINGS TESTED ON 1/4-INCH-DIAMETER SHAFTS 89.3 INCHES LONG WITH NO INTERMEDIATE SUPPORTS

Shaft Coating	Speed Range of Large Amplitude of Vibration, rpm		
	First Mode	Second Mode	Third Mode
Uncoated shaft	275-400	850-950	1725-1825
Tygon tubing (plasticized vinyl) bonded to shaft	300-325	850-875	1650-1700
P & R splicing compound (electrical tape) wound around shaft	300-300	850-875	1700-1700
Latex gum rubber bonded to the shaft	300-300	850-860	1700- --
1/4-in. -OD x 0.035-in. -thick wall tube with 3/16-in. -diameter steel sash cable	300-425	900-1025	-- --

Equipment and Calculations

Shaft Test Machine

General Description. In order to obtain useful information concerning hypercritical-speed power-transmission shaft operation it was necessary to design and build a shaft test machine. Since testing of full-scale transmission shafts would have involved excessive cost it was decided at the outset of the program to conduct tests with reduced-scale shafts and to incorporate a modeling procedure to relate information of reduced-scale tests to full-sized shafts.

Figure 48 shows a photograph of the entire test machine. Figure 49 is a schematic diagram of the test machine bed and equipment. Essentially the test machine consists of a straight bed to hold the spindle assemblies at the ends and the intermediate shaft support bearings, and an electronically governed variable-speed drive to rotate the shafts. The test bed is capable of accepting commercially available shafts 12 feet in length, and the spindles and intermediate support assemblies, accept shaft diameters 1/2 inch and smaller. The support assemblies are designed to provide adjustment of damping and spring rate with the least possible difficulty. Intermediate supports and the brake-head spindle assembly can be moved and clamped to the test bed at desired distances from the drive-head spindle assembly. Guards which limit test shaft amplitude can also be clamped at desired distances along the test bed. The brake-head assembly is capable of applying torque to the test shaft. The drive-head assembly rotates the test shaft at various speeds, and is belt driven from the variable-speed drive mechanism. Also at the drive-head assembly is a stroboscope actuator which permits observation of the test shaft by stroboscope either once or twice per shaft revolution.

Figure 50 is a schematic diagram of the test-machine drive mechanism. Two 7-1/2-horsepower motors power two eddy-current clutches. The clutches transmit power to a common shaft. Power is transmitted by belt to a speed-change mechanism consisting of two pulley assemblies, and from there to the drive-head assembly. By varying clutch output-speed and by changing speed ratio in the two pulley assemblies, drive-head spindle speed may be varied from zero to nearly 50,000 rpm with considerable horsepower available at the drive-head spindle. The highest speed achieved to date with an experimental shaft is 45,500 rpm.

Test shaft spindle speed is regulated by controlling eddy-current clutch excitation. The control box which mounts a direct reading tachometer and a potentiometer to change shaft speed may be carried by the operator to any position along the test bed. Because of the varying power requirements of test shafts as they are brought up through critical speeds, an electronic speed governor is incorporated in the speed-control system to maintain selected operating speeds with negligible drift.

Description of Test Bed and Equipment. The test bed consists of a 15-foot-long welded structural steel base with supports at each end. The supports of the bed are firmly bolted to an isolation pad in the laboratory. Pads welded to the top of the bed were machined in-line and four lathe beds were aligned, leveled, and bolted to the pads.

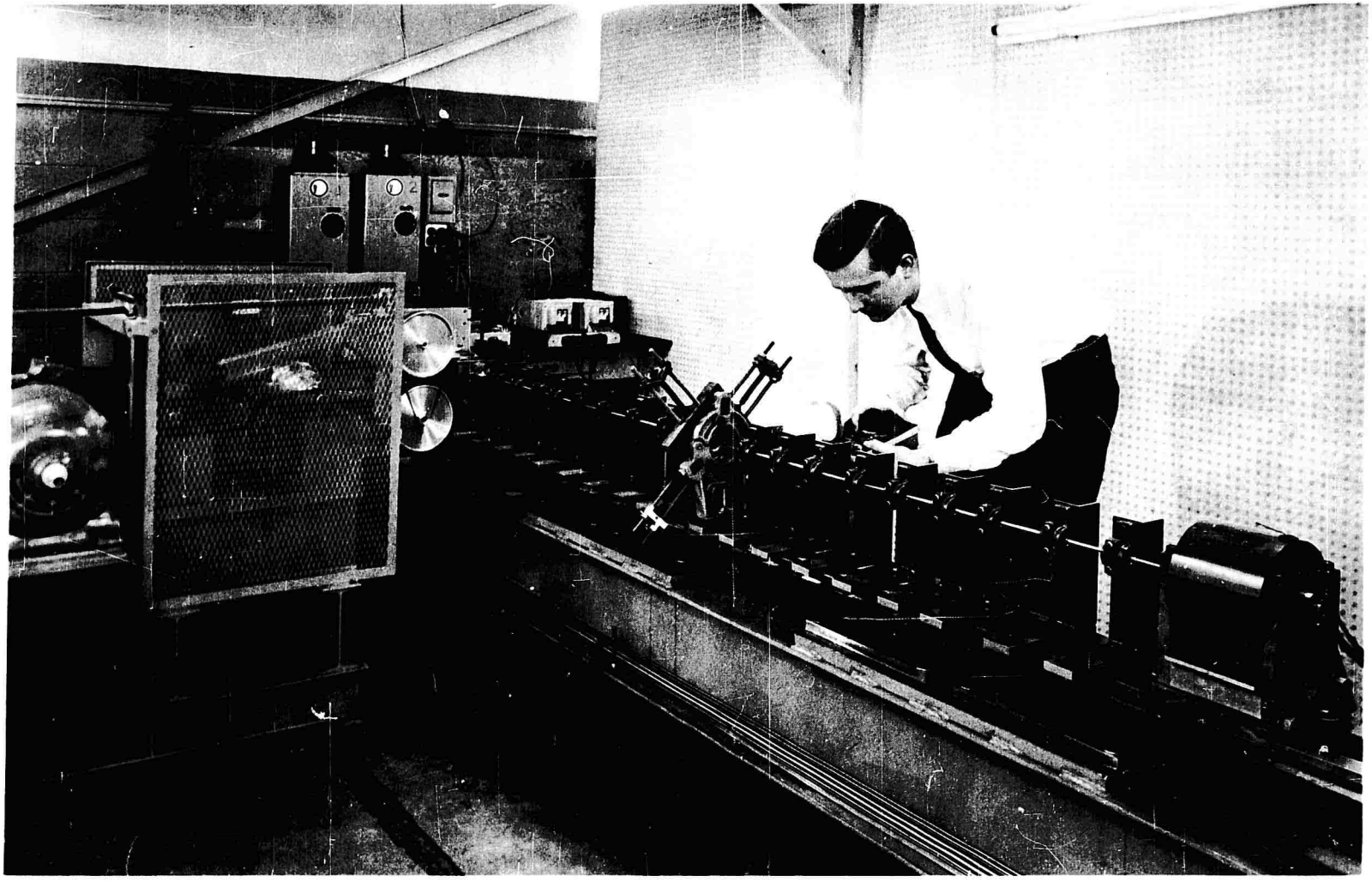

N86385

FIGURE 48. PHOTOGRAPH OF ENTIRE TEST MACHINE

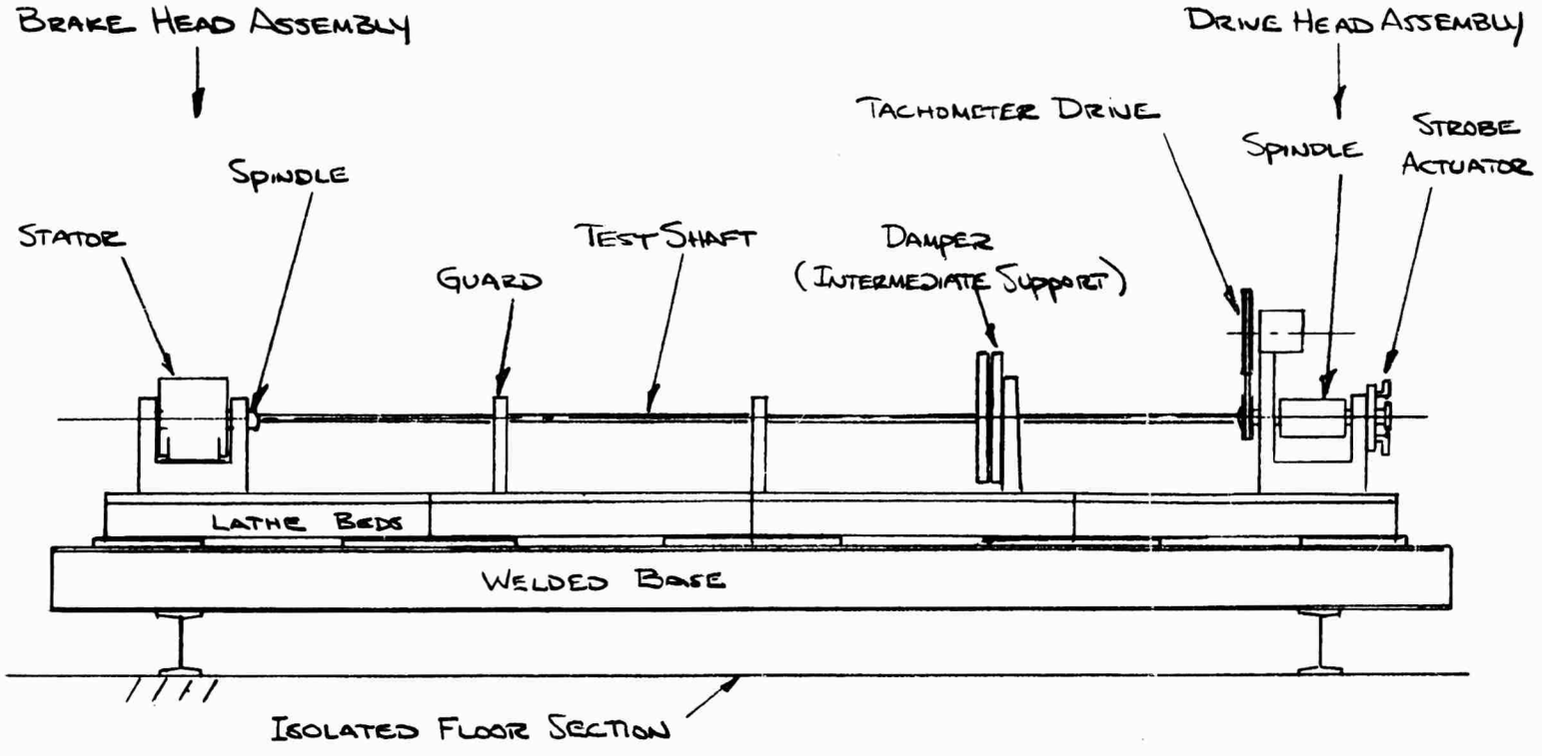

FIGURE 49. SCHEMATIC DIAGRAM OF TEST-MACHINE BED AND EQUIPMENT

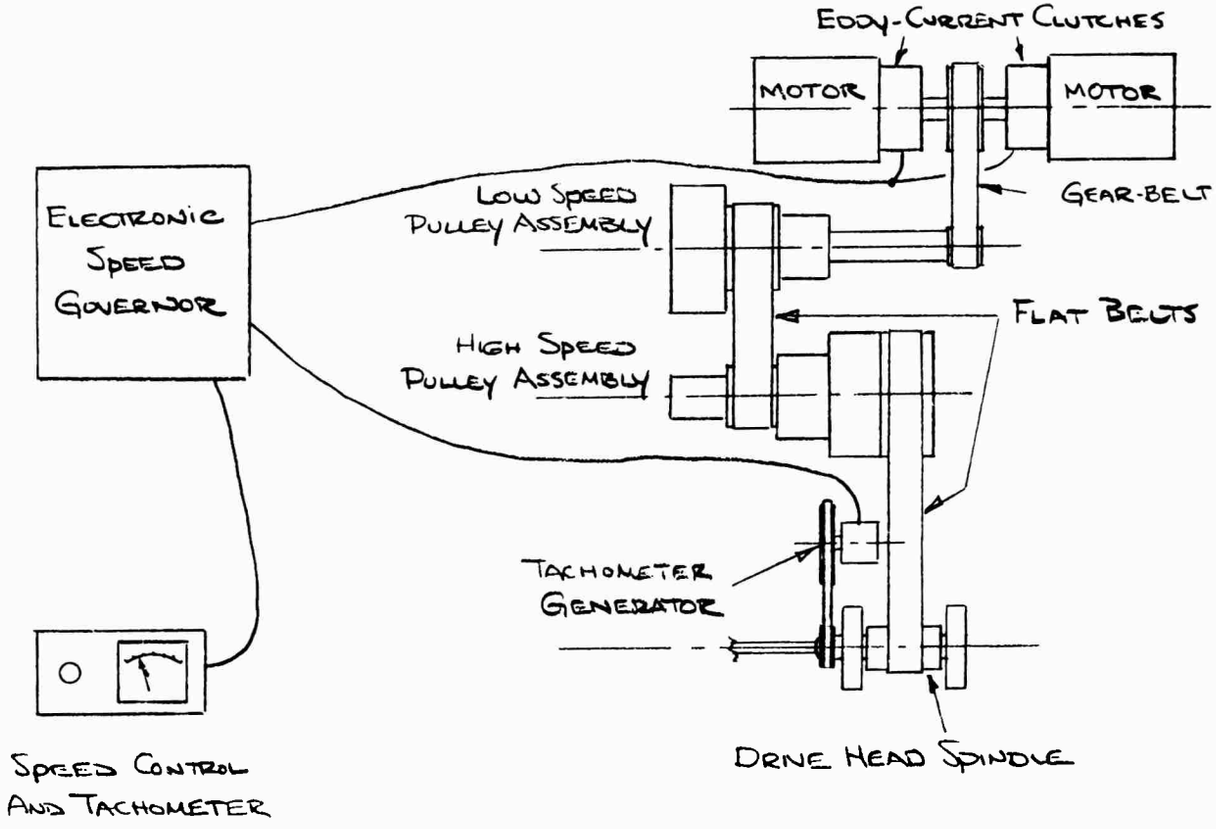

FIGURE 50. SCHEMATIC DIAGRAM OF TEST-MACHINE DRIVE MECHANISM

In effect this forms an extremely rigid 14-foot-long lathe bed with a 12-inch swing. The precision alignment of the individual lathe beds to each other permits the drive- and brake-head spindles to remain in-line no matter what position the brake head occupies. Likewise the intermediate supports are always in alignment with the spindle axes.

The drive-head and brake-head assemblies consist of reworked lathe spindles mounted to rigid bearing housings. The spindles are mounted in Barden angular-contact bearings, which are lightly preloaded to insure proper bearing life. Both spindles have a built-in capacity to move axially, since the ball-bearing outer races are a slip-fit in the bearing housings. In the drive head, however, the flat belt which transmits power to the drive spindle creates a large friction force at the bearing-to-bearing housing interface. Effectively there is no axial spindle travel at the drive head for this reason. Travel is allowed at the brake-head spindle, and the axial spring rate is plotted in a curve and shown in Appendix A.

The brake-head assembly is equipped as an eddy-current brake so that torque can be applied to the rotating test shafts. A 3-5/8-inch-diameter high-strength steel rotor is attached to the brake-head spindle. A fractional-horsepower electric motor stator is bolted to the brake-head bearing housing so that its axis is concentric with the rotor. Application of direct current from a storage battery to the stator windings produces a braking torque in the test shaft. A curve showing torque versus spindle speed is included in Appendix A.

Both drive- and brake-head spindles are hollow and machined to the same inside diameters. The method of gripping the tests shafts is similar to that used in lathe operation. Lathe collets, collet chucks, and draw-in tubes were used for test-shaft sizes up through 1/4-inch diameter. For 1/2-inch-diameter test shafts specially designed collets were machined, since the spindle bores were too small to accommodate standard draw-in tubes and collets.

Attached to the drive-head assembly are the stroboscope actuator and the tachometer generator. Figure 51 is a schematic diagram of the actuator. Fastened to one end of the spindle is a disk with an interruption at one location on its periphery. Concentric with the disk is a ring to which two magnetic pickups are mounted, 180 degrees from each other. As the slot in the disk passes a pickup, the magnetic field of the pickup is distrubed sufficiently that, with the aid of an amplifier, the stroboscope is triggered by the pulse. Use of both pickups permits observation of the lateral vibration "envelope". By rotating the pickup ring the shaft can be inspected at any angular orientation.

Figure 50 shows the location of the tachometer generator which is driven from the inboard end of the drive-head spindle. The tachometer drive uses narrow, flat, high-speed belts and incorporates a speed reduction from the spindle to the tachometer generator of either 5:1 or 25:1. The output of the generator is fed to a speed-indicating voltmeter in the control box, and to the electronic speed governor where it serves as the feedback voltage. Since most of the running has been in the high-speed range, the higher ratio of speed reduction has been used almost exclusively.

Figure 52 is a photograph and Figure 53 is a schematic diagram of the intermediate support damper. Figure 52 also shows the shaft guards which will be described later. The intermediate support consists of two heavy square plates, one of which is

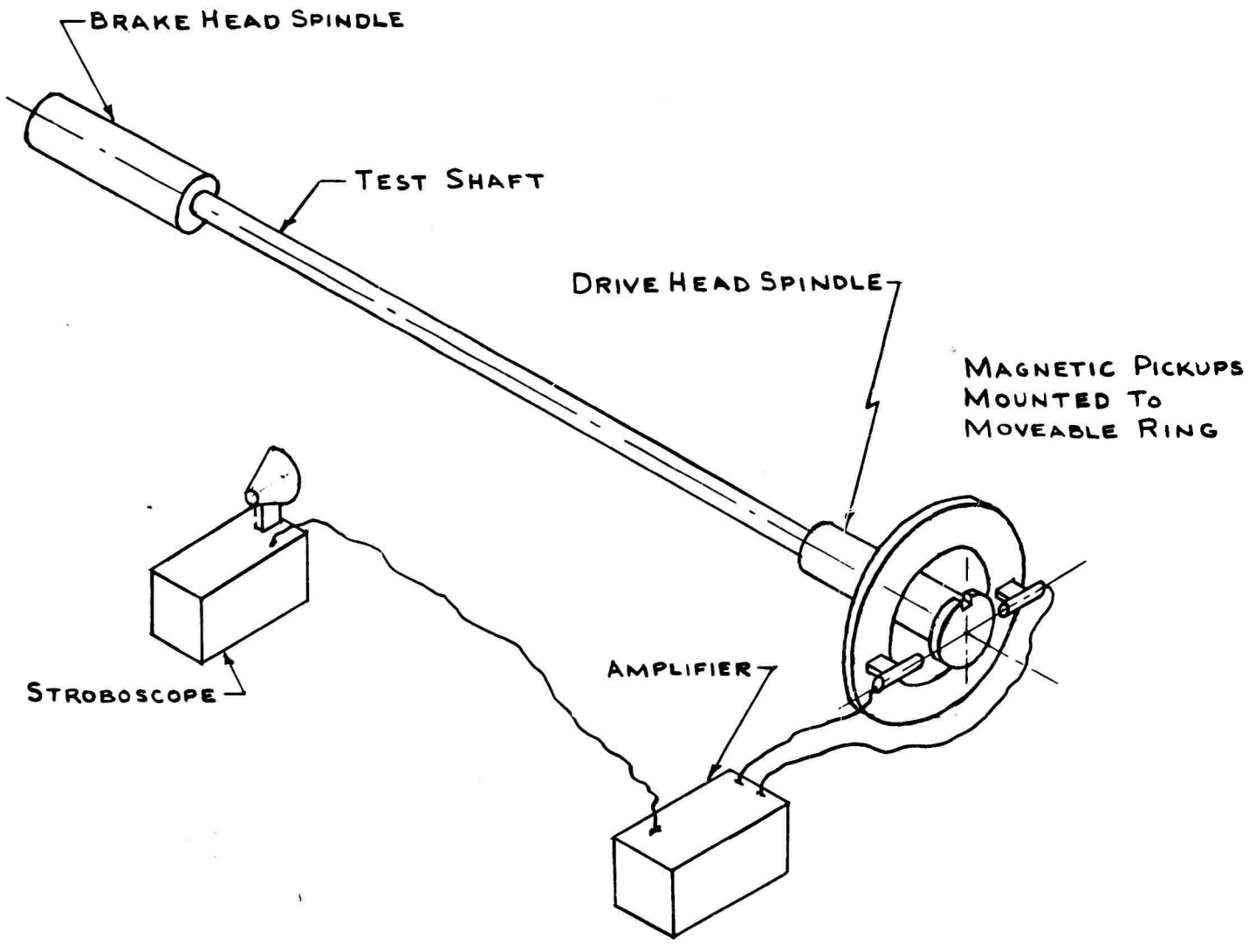

FIGURE 51. STROBOSCOPE ACTUATOR

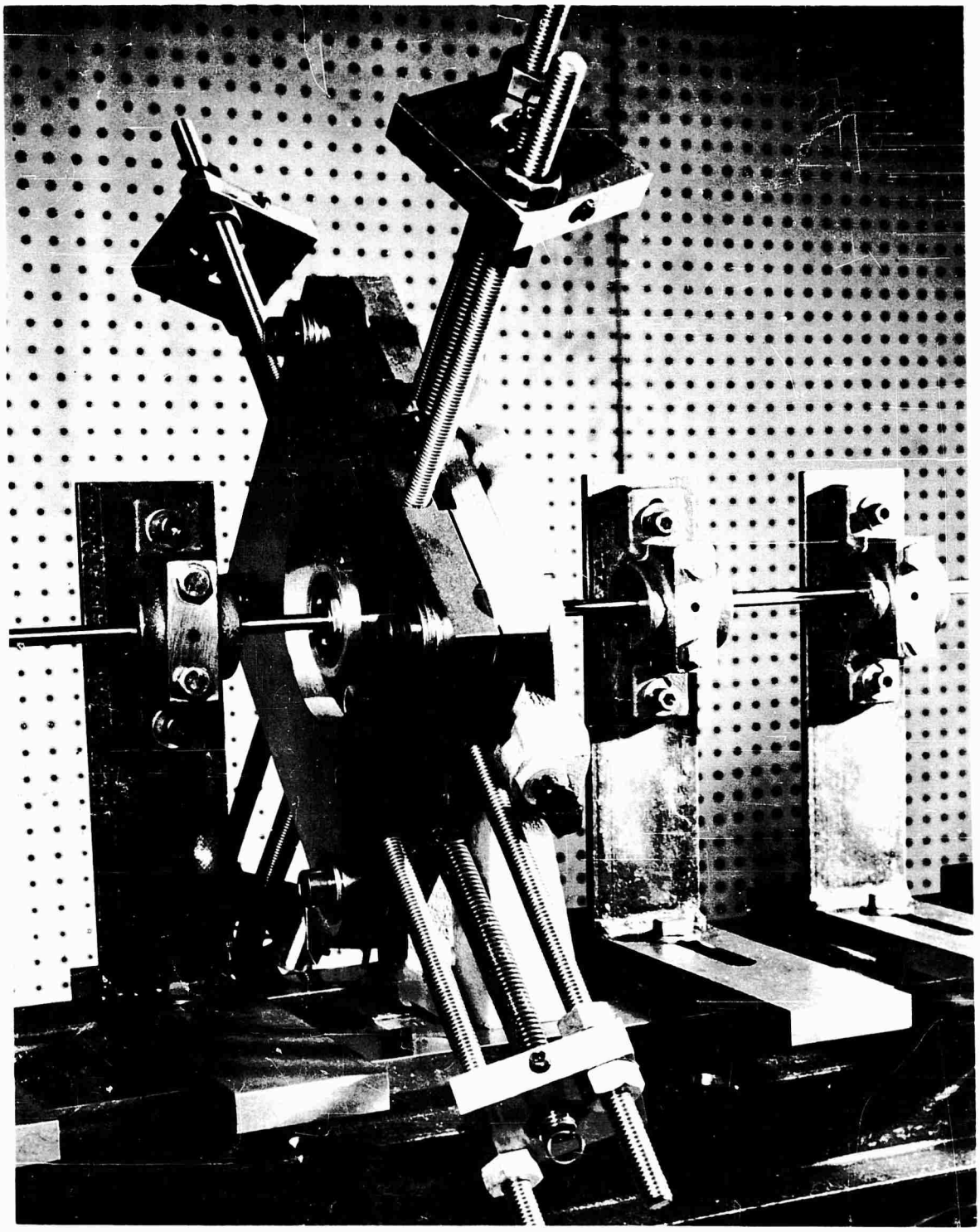

N86382

FIGURE 52. PHOTOGRAPH OF INTERMEDIATE SUPPORT DAMPER

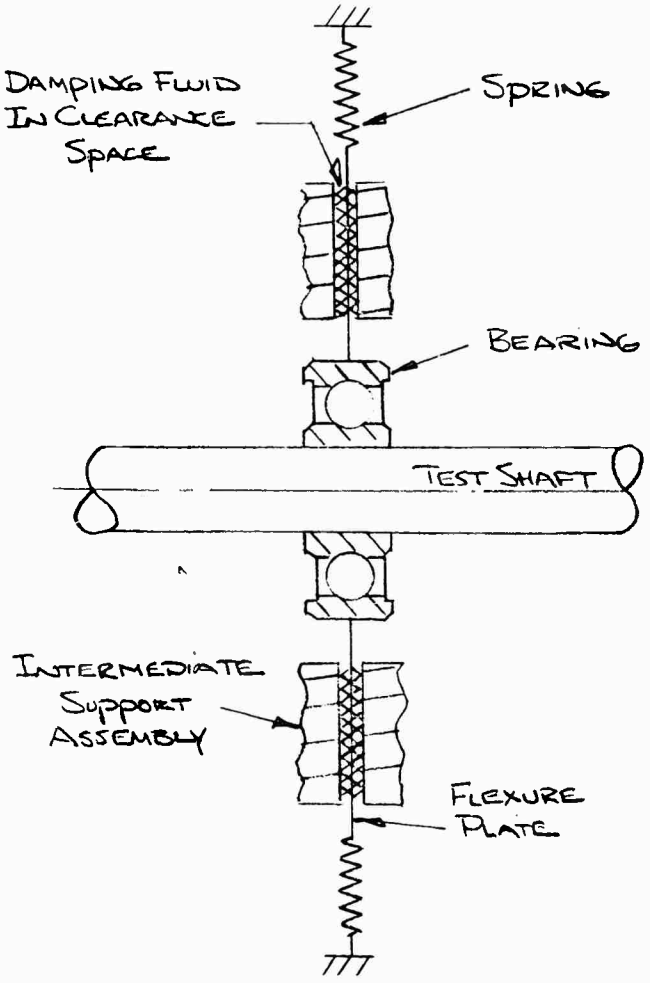

FIGURE 53. SCHEMATIC DIAGRAM OF INTERMEDIATE SUPPORT DAMPER

bolted to a lathe steady-rest. The plates are bolted together parallel to each other with ground spacers between them to provide the necessary oil-film thickness for support damping. An 0.018-inch-thick flexure plate, which mounts the support bearing, is sandwiched between the heavy outer plates. By filling the gap between the outer plates and flexure plate with a damping fluid such as oil and clamping the test shaft in the support bearing bore, viscous damping forces are generated when the vibrating shaft causes the damper assembly to move. The damping factor may be changed by inserting spacers of different thickness to alter the clearance between the outer plates and flexure plate. Likewise the damping factor may be changed by using damping fluids of different viscosities. A curve showing the difference of calculated to actual values of damping factor is included in the Appendix A.

The flexure plate to which the support bearing is fastened is laterally supported at its four corners by four springs. Adjusting the lateral flexibility of the support can be done by either changing to springs of a different spring rate or by changing the number of active coils of the springs by changing the point at which the springs are clamped.

Four circumferential slots have been cut in the flexure plate at a slightly larger diameter than the support bearing fastening. The slots reduce the bending stiffness of the flexure plate to minimize its effect on shaft behavior. Tests show that the intermediate support does not act strictly as a simple support, but has some moment-absorbing ability. The initial angular motion of the bearing is practically free from moment restraint due to the built-in radial clearance in the Barden support bearings. After the free motion is taken up in the bearing, moment restraint increased due to bending of the flexure plate. A curve of the intermediate support moment restraint is given in Appendix A.

The intermediate support assemblies are mounted on lathe steady-rests. The bottom of each steady-rest has a tongue which fits closely between the ways of the lathe beds. The close fit assures that the intermediate support bearing axis be parallel to the spindle axis.

Figure 52 is a photograph showing the guards used when testing high-speed shafting. L-shaped brackets were made which clamp to the lathe bed ways. Cast-iron pillow blocks are bolted to the vertical portion of the brackets. The pillow-block bolt-holes are oversized so the blocks can be aligned to follow the natural sag of test shafts. The pillow blocks are split and held together with screws. This feature permits installation or removal of guards without withdrawing the test shaft.

Description of Test-Machine Drive Mechanism. Figure 48 shown earlier, and Figure 54 show two views of the test-machine drive mechanism. A common shaft carries the combined output of two eddy-current clutches, each of which is driven by a 7-1/2-horsepower 1750-rpm electric motor. Each motor and clutch assembly develops approximately one-half of the needed power at any given time. Power is transmitted from the common clutch output shaft to the low-speed pulley assembly by means of a fixed-ratio gear belt and pulleys. The low-speed pulley assembly is composed of a 2-inch-diameter shaft with three flat-belt pulleys pressed on one end and the gear-belt pulley on the other. Adjacent to the low-speed pulley assembly is the high-speed pulley assembly. Its cone-pulley assembly is integrally machined with the shaft. The cone-pulley diameters on both shafts range from 2 to 6 inches, providing a total speed

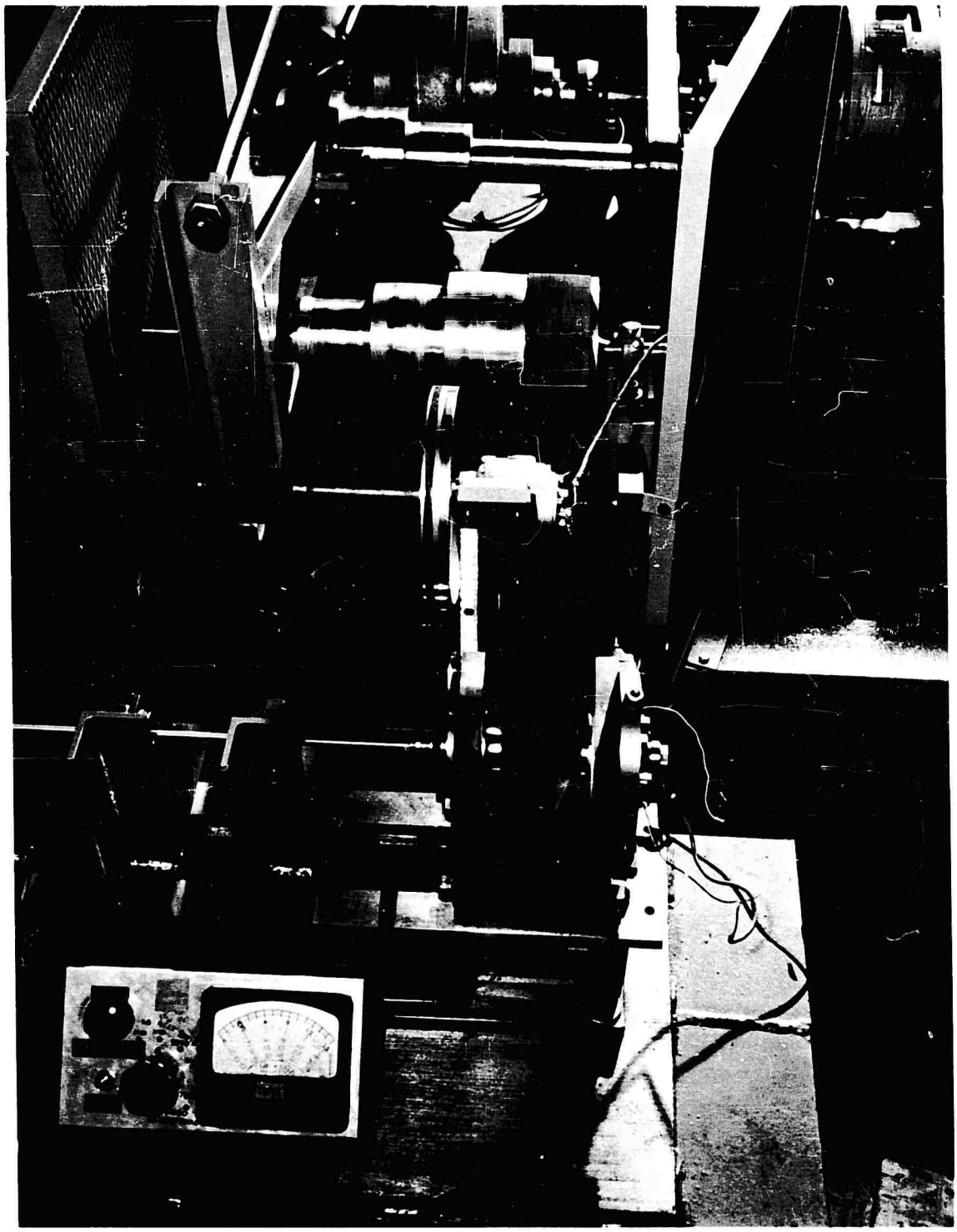

N86381

FIGURE 54. PHOTOGRAPH OF TEST-MACHINE DRIVE MECHANISM

ratio change of approximately 9:1. Power is transmitted from the high-speed pulley assembly to the drive-head spindle at a constant speed ratio by means of a flat belt. Minimum spindle-to-clutch speed ratio is approximately 4.36:1 and the maximum ratio is approximately 39.2:1. Use of the various speed ratios makes a fairly constant maximum horsepower available at the spindle regardless of speed, since clutch horsepower output varies with speed.

Due to the sensitivity of clutch output-speed to load-change it was necessary to equip the test-machine drive mechanism with an electronic speed governor. Circuit diagrams of the speed governor may be found in the Appendix B. Basically the speed governor consists of a tachometer to supply feedback voltage, amplifiers to increase the gain of the difference between feedback and signal voltage, and magnetic amplifiers to change the speed correction voltage to an output suitable to power the eddy-current clutches.

The speed governor is composed of Battelle-owned components and the circuit diagrams in Appendix B show the necessary wiring between the major assemblies. Wiring diagrams of the assemblies are not shown; instead the names and model numbers are listed.

The motor and eddy-current clutch assembly is also Battelle owned. The detail drawings of the shaft test machine show the names and model numbers of these components.

Use of Test Machine. As mentioned previously numerous high-speed shaft tests have been made. A discussion follows of the technique involved and the problems encountered.

Early in the experimental program a series of 1/8-, 1/4-, and 1/2-inch-diameter shafts were tested in the machine to obtain correlation between calculated and observed critical speeds. Good correlation was achieved with all sizes; however, the 1/8-inch-diameter-shaft critical speeds proved extremely sensitive to axial shaft-end forces encountered when installing the shaft in the machine spindles. To minimize the problem and to permit ease in handling of the many shafts used, the 1/4-inch-diameter size was chosen.

In the early period of testing manually controlled speed regulation was found to be a disadvantage. The sensitivity of the potentiometers, which controlled eddy-current clutch excitation and shaft speed, made it difficult to increase speed slowly through critical speeds. There was insufficient time to obtain accurate critical-speed vibration amplitudes. In addition without employing extra laboratory personnel it was impossible to record the speed at which maximum vibration amplitudes occurred. To relieve the problem an electronically controlled speed governor was designed and constructed to maintain selected operating speeds with negligible drift. The governor speed control was mounted in a small box which could be carried by the operator to any observation point along the test machine. For convenience to the operator a meter showing shaft speed was also included in the control box.

Methods of vibration-amplitude measurement were also a concern. Originally, a large-range dial indicator was mounted in a stand clamped to the test-machine bed. The indicator was equipped with a shoe riding on the test shaft. At shaft speeds above

the very lowest the inertia of the shoe and indicator mechanism would cause the indicator shoe to float at a position just in contact with the whirling shaft once per revolution. The amplitude reading of the indicator was zero to peak in inches. Although this scheme performed as planned, the indicator movement could not withstand such punishing service, and its use was discontinued.

Another device called a cathetometer was employed for a short time in amplitude measurement. The cathetometer is an optical telescope mounted to a graduated vertical vernier column. Use of this instrument consisted of recording the height of the upper- and lowermost edges of the vibrating shaft from which peak-to-peak amplitude was obtained by subtraction. This method produced precise values of shaft deflection, but was extremely time consuming in its operation.

Since hundreds of amplitude measurements were necessary for experimental evaluation of suitable high-speed shafting support parameters, a simpler method of amplitude measurement was chosen. A scale was mounted to the vertical leg of a combination square, and the square set on the test bed just behind the vibrating shaft. By noting the dimensional height of the shaded projection of the vibrating shaft on the scale, amplitude measurements to the nearest sixty-fourth of an inch were possible. This device was used in quite a number of tests because of its extreme portability and ease of operation.

Another amplitude-indicating device used extensively was formed by the pillow blocks mounted at intervals along the test shaft. Primarily the pillow blocks served as guards to contain the shaft should it break or become disengaged from the machine during operation. The blocks normally used were of 5/8-inch bore, providing substantial clearance with the 1/4-inch-diameter test shafts. It was found that vibration of the 1/4-inch-diameter shafts did not become severe until peak-to-peak amplitude reached 1/4 to 3/8 inch. Since 3/8 inch was the diametral clearance of the shafts and guards, noise of the shaft contacting the guards was used to indicate unsatisfactory operation.

Figure 55 shows a typical data sheet from one of the experiments. The figure contains information concerning test shaft length and diameter, and intermediate support position along the shaft, damping factor, and flexibility. At the bottom of the figure is recorded the first of the various critical speed vibrations of the shaft and support system described. For each critical speed the vibration mode of the shaft is drawn showing the relative position of the vibration loops and intermediate support. The fractions are in inches and denote peak-to-peak vibration amplitude. To the left of the diagram is recorded the speed in rpm at which maximum amplitude was observed. When vibration amplitude reached 3/8 inch peak-to-peak the speed was suffixed "hit", meaning that the shaft contacted the guards. Generally testing was continued into the higher operating speeds until, at a certain critical speed, the shaft contacted the guards. In most tests at the lowest criticals hitting occurred, but this was not considered serious because shaft bending stresses over the long spans were minor. At high speeds where shaft length between nodes is short, bending stresses become significant when shaft deflection is sufficient to contact the guards.

After operating with a certain set of damper parameters to a high speed at which the test shaft contacted the guards, the machine was shut down momentarily. Support position was then changed and a new data sheet started for the succeeding test. Following a series of tests with the support moved in small increments a plot of satisfactory

DATE _____ G-4869-1 SHEET NO. _____

TEST SETUP

	% L	INCHES FROM DRIVE END
SUPPORT 1	30	62.5
SUPPORT 2		
SUPPORT 3		

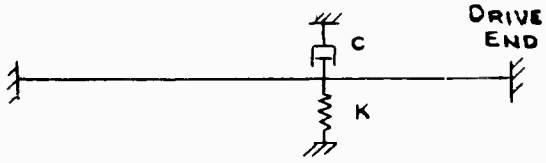

DIAMETER OF SHAFT 1/4

TOTAL LENGTH 89.3

	SPRING RATE K - lb/in.	DIA. OF SPRING WIRE	O.D. OF SPRING	DAMPING COEFFICIENT - $\frac{lb\text{-}sec}{in.}$	DAMPING FLUID	SPACER THICKNESS
SUPPORT 1	11.6	1/16	1/2	0.118	SAE 30	0.0285
SUPPORT 2						
SUPPORT 3						

REMARKS: T=70°F

RECORDED BY: _____ OBSERVED BY: _____

CONDITIONS: _____

SPEED	MODE SHAPE AND AMPLITUDES	OPERATION
550 rpm	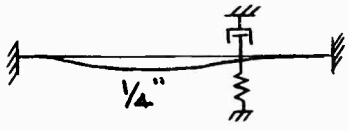	

FIGURE 55. SAMPLE LABORATORY DATA SHEET

shaft operating speed range versus support location for the particular support damping coefficient and spring rate was made. Following evaluation a different value of damping or spring rate was chosen and the test process repeated with the expectation of finding still better shaft operating behavior.

The effect of torque on the critical speed was determined by rotating the shaft with the eddy-current brake energized. Shaft action at these critical speeds was observed with a stroboscope. Steel shafts with a torsional yield strength of 36,000 psi, as well as others with 92,000 psi torsional yield, were used in the torsion experiments.

In initial tests of long slender shafts, the measured critical speeds exceeded the calculated values for shafts tested without axial torque applied. In order to compare the experimental and the theoretical torque effects, it was necessary to install the shafts with a certain value of mid-point deflection. On the longer shafts, this amounted to a significant value. The mid-point deflection is that which corresponds to the sag of a shaft caused by its own weight. When shafts were installed with the calculated values of mid-point deflection, measured and calculated critical speeds were in close agreement.

Tests to determine the effects of torque on the first critical speed were conducted below the speed range of operation of the stroboscope, and the angle-of-twist could not be observed when the shaft was rotating. In order to measure the angle of twist and to determine the critical speed accurately, the effect of torque on the natural frequency of lateral vibration was observed. The problem of determining the frequencies of lateral vibration of a uniform beam subjected to an axial torque is identical to the problem of determining the critical speeds of a rotating shaft subjected to an axial torque. With torque applied to the nonrotating shaft by means of a wrench and a spring scale, the first natural frequency of lateral vibration was excited by striking the shaft.

In certain tests of long slender shafts the measured critical speeds exceeded the calculated values. This increase was attributed to tension applied to the shaft ends when installed in the test machine. A number of torque tests were conducted to determine the effect of tension induced in the shaft during installation, and the effect of external axial force caused by the bearing preloading springs. These tests were conducted on 1/8-inch-diameter shafts and 1/4-inch-diameter shafts.

During the second phase of the research program, the effects of axial shaft-end and torque loads will be studied more fully. To implement this work, certain modifications will be made to the experimental equipment. One such change involves changing the eddy-current brake to a device capable of delivering considerably more torque to the test shaft.

Support Damping Measurement Equipment

In order to determine the actual damping factors developed in the damped intermediate supports, tests of two types were made. Lower viscosity damping fluids composed of SAE 10, 30, and 50 motor oil were tested by measuring the decay of damped free vibration at the damper. Higher viscosity damping fluids including SAE 50 motor oil and Viscasil 1000 and 10,000 silicone fluids were tested by measuring the energy required to sustain damped forced vibration at the damper.

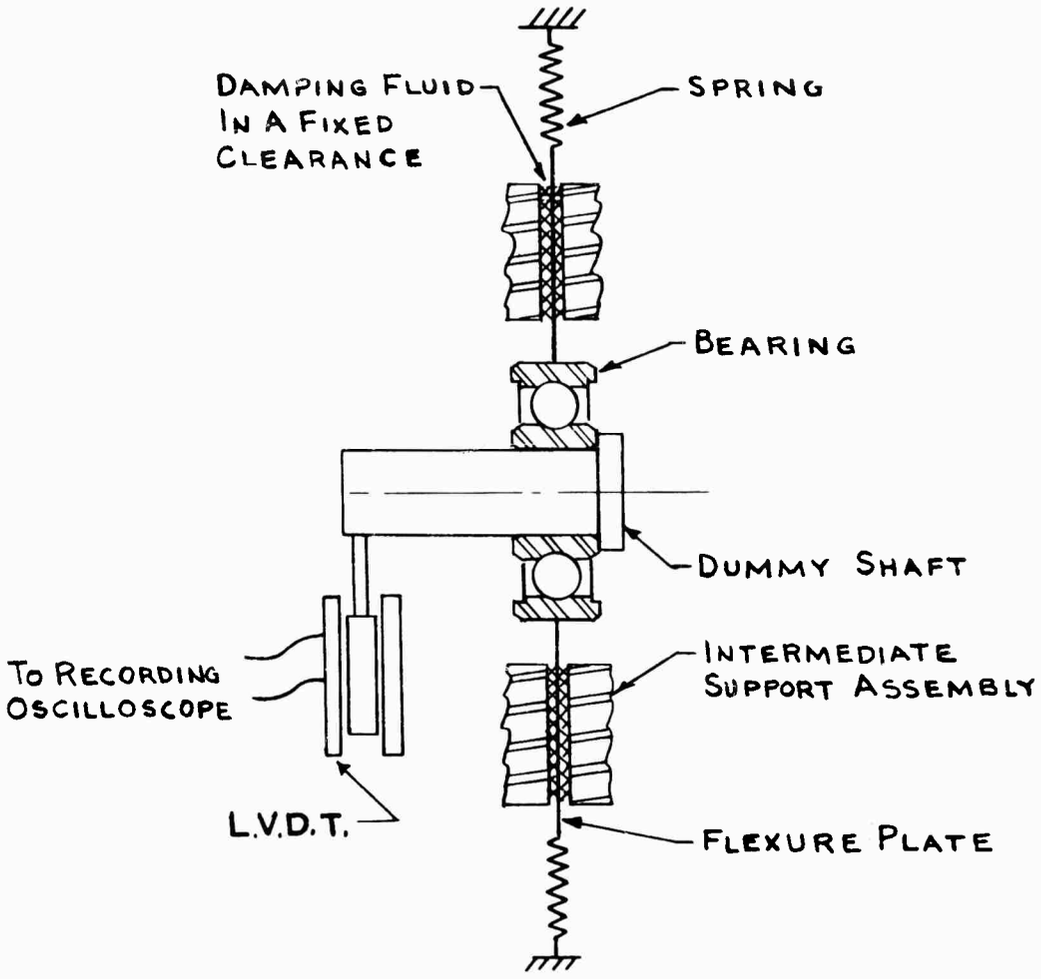

FIGURE 56. SCHEMATIC DIAGRAM OF DAMPED-FREE-VIBRATION TEST APPARATUS

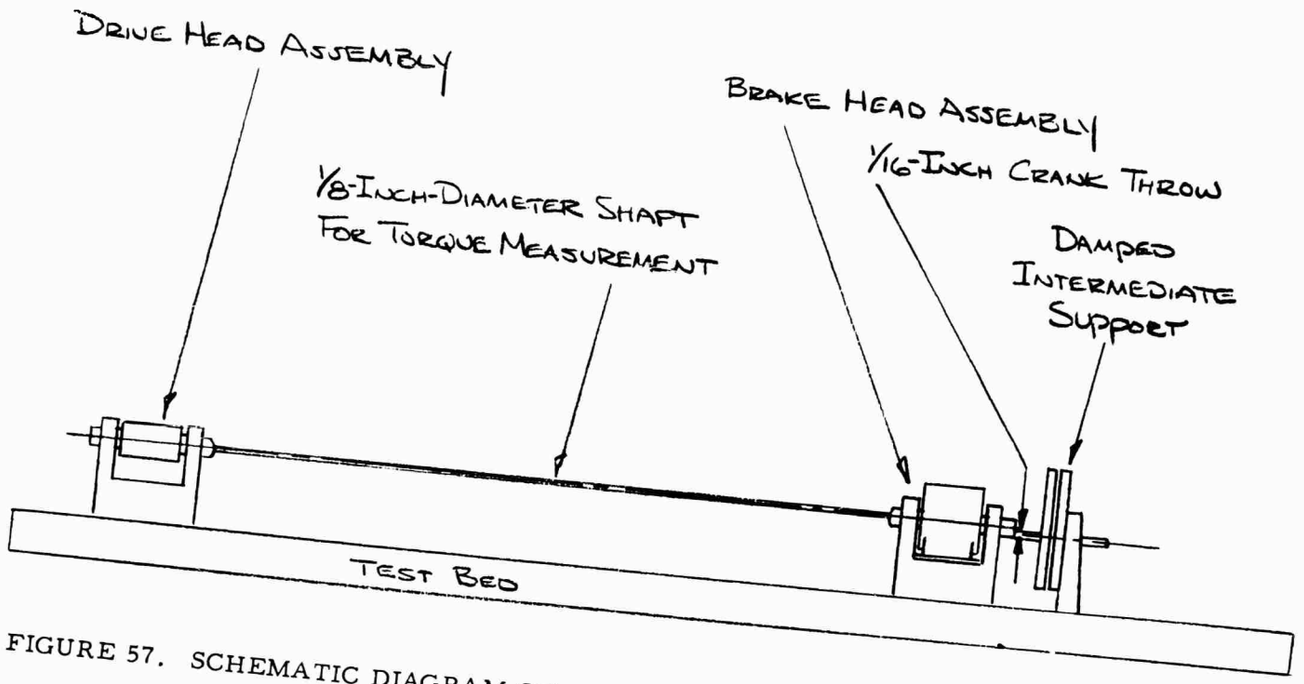

FIGURE 57. SCHEMATIC DIAGRAM OF DAMPED-FORCED-VIBRATION TEST APPARATUS

A schematic diagram of the damped-free-vibration test apparatus is given in Figure 56. With the proper mass and spring combination the damped bearing and flexure plate was caused to oscillate with lessening amplitude after first being displaced. A linear-variable-differential-transformer core connected directly to the oscillating member by means of a dummy shaft interpreted damper position as a positive or negative voltage. The voltage curve was plotted with respect to time by a Sanborn recorder. From the plots obtained calculations were made to determine the actual damping factors for the lighter viscosity oils.

A schematic diagram of the damped-forced vibration test apparatus is given in Figure 57. A 1/2-inch-diameter bar was inserted rigidly through the brake-head spindle. A 1/4-inch-diameter tang was turned on a protruding end of the bar to act as an eccentric or crank with a 1/16-inch throw. A damped intermediate support bearing was clamped to the crank just as it would fasten to a shaft under test. A 1/8-inch-diameter long rod connected the drive-head and brake-head spindles. When the test was run, the torque necessary to operate the damper at a certain speed with the fixed eccentric motion was determined from the twist of the 1/8-inch-diameter shaft. From the measured torque and speed values the damping coefficient was calculated.

Method of Free-Vibration Damping Calculation. Figure 58 is typical of the vibration-amplitude decay curves recorded to determine intermediate support damping coefficient. The flexure plate was first displaced from its position of rest, and then released to vibrate at its natural frequency. Since damping was present, vibration amplitude diminished until the system ceased to oscillate. An LVDT interpreted flexure plate position as a voltage which, when recorded, furnished a plot similar to that in the figure.

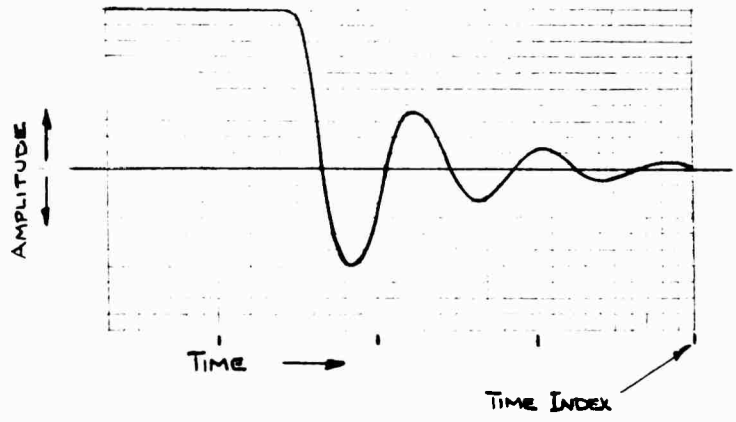

FIGURE 58. TYPICAL VIBRATION-AMPLITUDE DECAY CURVE

Calculation of flexure-plate damping was made using the following equation:

$$C = \frac{m\omega_n}{\pi} \ln \frac{y_k}{y_{k+1}} \qquad (112)$$

where

C = damping coefficient, lb-sec/in.

m = flexure-plate mass, lb-sec/in.

ω_n = natural frequency of the flexure plate assembly, rad/sec

y_k = amplitude of the kth cycle, in.

y_{k+1} = amplitude of the kth + 1 cycle, in.

This equation may be found in most vibration textbooks.

Natural frequency, ω_n, was taken directly from the decay curves. The recorder marked each decay curve in 1-second intervals, which enabled direct measurement of the number of cycles occurring in 1 second. Flexure-plate mass was determined by weighing all the vibrating parts including the LVDT core, and by adding one-third the weight of the flexure-plate support springs.

Method of Forced-Vibration Damping Calculation. Damping measurement technique described in the free-vibration damping tests was suitable for the lower viscosity fluids. However, when using the higher viscosities, flexure plate vibration diminished to zero during the second or third cycle, which prevented accurate determination of damping factors. To circumvent this problem a laboratory setup was made of a forced-vibration system, shown in Figure 57.

The flexure plate was made to oscillate in a circular path once per shaft revolution by clamping its bearing to a crank with a 1/16-inch throw. Springs attached to the four corners of the flexure plate prevented its rotation. The force required to drive the flexure plate through the circular path was determined by the angular twist of the 1/8-inch-diameter shaft driving the crank. The velocity of the flexure plate with respect to the heavy outer support plates was directly proportional to speed. Dividing force by velocity produces the coefficient of viscous damping.

Calculation of the force necessary to overcome damping is as follows:

$$T = \frac{\theta GJ}{57.3L}, \tag{113}$$

where

T = torque transmitted by 1/8-inch diameter in shaft, in-lb.

θ = angular windup in total shaft length, degrees

L = shaft length, in.

G = shear modulus of shaft material, lb/in.^{2}

J = polar moment of inertia of shaft cross section, in.^{4}

The force required to sustain forced vibration in the presence of damping was found by dividing the torque of Equation (113) by the crank throw:

$$F = \frac{T}{R} = \frac{\theta GJ}{57.3LR} \text{ lb} \tag{114}$$

where

F = force necessary to sustain vibration of the damped flexure plate, lb

R = crank throw, in.

The tangential or peripheral velocity of the circular vibration path was determined easily:

$$v = \frac{2\pi R \text{ rpm}}{60}, \tag{115}$$

where

v = tangential velocity of the circular vibration path, in./sec

rpm = rotation speed, rev/sec.

By definition the coefficient of viscous damping equals damping force per unit velocity, or:

$$C = \frac{F}{v} = \frac{60\,\theta GJ}{57.3 \times 2\pi LR^2 \text{rpm}} \tag{116}$$

where

C = damping coefficient, lb-sec/in.

Shaker-Table Equipment

To make a preliminary determination of the ability of shaft coatings to damp lateral shaft vibrations, a shaker-table test was made. The shaker consists of a moving coil of wire in a magnetic field, with a table attached to the moving coil. When alternating current is fed to the coil, it is forced to move vertically up and down to follow the excitation frequency. The current source is a variable-frequency audio-oscillator and amplifier. Clamp blocks were machined to fasten the coated shaft specimens rigidly to the shaker table. Details of the tests may be found in the section discussing shafts with continuously applied damping coatings.

Computer

The digital-computer facility at Battelle consists of Bendix G-20 units. It is an efficient machine which has satisfactorily performed many shaft-deflection calculations and has also performed critical-speed determinations. We consider the programs used to be correct in all respects.

Prior to the installation of the new, more efficient G-20 computer, an IBM Model 650 computer was in use. The computer programs used in this research project are designed primarily for the IBM 650, but have been successfully adapted to the newer facility with an approximate doubling of speed resulting.

CONCLUSIONS

In the past year, research conducted with high-speed power-transmission shafts has produced significant results. The major conclusions to be drawn are:

(1) Power transmission by shafts operating at speeds above their first critical is practical, since one or two dampers strategically located along the shaft have been shown to limit vibration very effectively.

(2) A systematic procedure for the design of shaft dampers using an electrical analogy has been developed. The initial experimental verification of the design procedure showed excellent performance. Using this procedure in a given power-transmission situation it is believed that a system of dampers can be designed to prohibit excessive and dangerous vibration amplitudes at the desired operating speeds. Added experimental verification of this design procedure is required to prove it fully.

(3) Once a suitable high-speed shaft system has been designed and demonstrated, similar operation can be achieved with shafts of other dimensions and materials by applying modeling equations developed in this program. Use of these equations can provide dynamically similar operation of dissimilar shafts by adjustment of damper parameters.

The above conclusions are basic and show that power transmission by high-speed shafting is not a whimsical notion, but is completely practical.

Many other conclusions can be drawn as a result of the research, and are discussed in the following paragraphs.

A digital-computer program has been formulated which correctly calculates the deflection shapes of shafts rotating at their critical speeds. A modified program has been used to determine the critical speeds, and has excellent ability in this regard.

Many experimental high-speed shafting tests have shown that, with just one damper, shafts can be operated at more than 60 times their first critical speed. With two dampers, operation at even higher speeds was observed, in one case reaching 159 times the first critical speed. Generally, best operation occurred with the damper or dampers positioned close to the ends of the transmission shafts.

The design and analysis of high-speed shafting by electrical analogy adds understanding to the experimental program. The analogy shows, for instance, that broad tuning of the shaft system is not only dependent upon the damping coefficient, but is also quite dependent upon the weight ratio of the damper to the shaft. The smaller the ratio the wider is the acceptable speed range of shaft operation. Description of the mechanical shaft in terms applying to high-frequency electrical transmission lines opens the door to straightforward design of hypercritical-speed shafting, since the electrical theories are so highly developed.

Standard formulas for determining shaft critical speeds have been shown to be correct by research work. For a shaft with one damper at any location along the shaft length, critical speeds are readily predictable. For multiple dampers the critical speeds are less accurately calculable by the approximate methods, but are accurately calculated by the computer program used.

Application of torque to high-speed shafting has been studied both theoretically and experimentally. Although theory predicts a lowering of shaft critical speed, experiment has not shown this to be so. The application of torque has shown a tendency, however, to cause a "corkscrew" shape at torsional shear stresses near the yield point of the material. But neither the application of steady-state or intermittently applied torque has caused a change in lateral critical speed or vibration amplitude.

Theory and experiment have shown that critical speed varies with axial shaft-end loading. Tension on the shaft ends increases critical speed, and compression decreases it.

Experimental work has been conducted using shafts coated with damping materials. An improvement was noted in shaft operation at the lower critical speeds. Operation was totally unsatisfactory, however, at higher speeds. Therefore, this does not appear to be a solution to the vibration problem.

Finally, it is concluded that hollow tubing has the ability to transmit the same degree of power but with higher critical speeds and with decreased shaft weight. Examples in the Technical Work section of this report point out that solid shafts running at high speeds are capable of tremendous horsepower transmission but that hollow shafts can do the same work with less weight, and encounter fewer critical speeds. Hence, dampers need not be so highly refined. The resulting decrease in weight for both dampers and shafts would appear highly attractive in applications to aircraft. All of the research results are equally applicable to the design of solid and tubular shafts. The only apparent reservation regarding the use of tubing is that tubing with extremely thin walls may encounter other modes of vibration in which the walls flex, in addition to critical speed vibrations. Additional investigation may identify this problem or eliminate it as a possible concern.

RECOMMENDATIONS FOR FUTURE WORK

The present Phase I research program has shown that power transmission by shafting operating above its first critical speed is quite practical. Inclusion of dampers along the transmission shaft can reduce vibration to very small and acceptable values. To extend the understanding of high-speed power-transmission shafts the following tasks are recommended for study in the Phase II research program:

I. Basic High-Speed Shafting Research

(1) A comprehensive program of testing and computation should be conducted to fully confirm the analogy developed during Phase I, relating high-speed shafting to high-frequency electrical transmission lines. The analogy should be extended to include

shaft end terminations such as flexible couplings. A systematic shaft design procedure based upon the analogy, and using graphical aids where possible, should be perfected.

(2) The effects of initial shaft crookedness should be evaluated to determine the degree of accuracy required in the production of the high-speed power-transmission shafting. In conjunction with this work, the practical advantages obtainable using tubing in place of solid shafting should be carefully investigated. Theoretical studies indicate that thin-walled tubing should have substantially higher critical speeds than solid shafting capable of transmitting the same torque. The accuracy of commercially available tubing in terms of straightness and concentricity may impose practical limitations which affect to some extent the theoretical advantages. An experimental study should be conducted to ascertain the true situation.

(3) The effect of moving the shaft supports from an aligned relationship to cause the shaft to operate around a gradual curve should be studied. This mode of operation would correspond to the conditions imposed upon a shaft if it should be mounted in a flexible structure such as an aircraft wing which might assume various static deflections. In conjunction with this work, the dynamic behavior of flexible shaft couplings should be studied both experimentally and analytically. Operation should be carried out under both aligned and misaligned conditions, and with shaft ends concentric to, and eccentric to the main section of shaft.

(4) Intermediate-shaft-support bearings capable of withstanding bending moments should be compared with intermediate-support bearings without moment-taking ability. In addition, intermediate-shaft-support bearings capable of introducing damping when located at the positions of nodes of lateral shaft vibration should be evaluated experimentally.

(5) The effects of torque upon shaft critical speed and vibration amplitude should be investigated more thoroughly. Phase I research showed that theory predicted shaft critical-speed change with application of torque, whereas experimental testing indicated neither critical speed nor vibration amplitude change.

(6) The effect upon shaft behavior of external vibrations introduced to the shaft through the shaft-support-bearing mounts should be investigated.

II. Design Studies of High Speed Aircraft Power Transmission Systems

(1) Specific current or future aircraft power transmission systems should be analyzed to establish the parameters for which some of the experimental shafts in the research program would be designed. This work should be augmented by design studies for specific applications. This would ensure the earliest application and greatest utility of the research results.

(2) Design studies should be made of damped support bearing configurations considered realistic and suitable for aircraft installations. Power dissipation to be expected at the dampers should be determined.

(3) Typical aircraft power transmission systems should be analyzed to determine the sources and effects of torsional vibrations. These effects in conventional power-transmission systems should then be compared with the effects which would be developed

in high-speed shaft installations. If objectionable torsional effects are identified in high-speed shaft systems, means for damping or otherwise eliminating these effects should be studied.

III. Preparation of a Design Manual for High-Speed Power-Transmission Shafting

The results of all of the research activities carried out during Phases I and II should be incorporated into a design manual. This design manual would relate all of the important shaft parameters such as over-all length, support spacing, shaft diameter, shaft material, allowable shaft crookedness, required stiffness of bearing supports, shaft end restraint, and necessary damping provisions, to be used in designing a shaft for any given horsepower and operating speed. Design data for shafts operating below the first critical speed would not necessarily be included. The emphasis during the entire research program and in the design manual would be placed upon shaft operation above the first critical speed and, in most cases, at very high multiples of the first critical speed.

REFERENCES

(1) Freberg, C. R., and Kemler, E. N., Elements of Mechanical Vibrations, John Wiley and Sons, Inc., New York (1949), p 142.

(2) Den Hartog, J. P., Mechanical Vibrations, Fourth Edition, McGraw-Hill Book Co., New York (1959), p 148.

(3) Koehler, Glenn., Circuits and Networks, First Edition, The Macmillian Co., New York (1955), pp 222, 232, 281.

(4) Ayre, R. S., and Jacobsen, L. S., "Natural Frequencies of Continuous Beams of Uniform Span Length", Journal of Applied Mechanics, pp 391-395 (Dec. 1950).

(5) Timoshenko, S., Vibration Problems in Engineering, Third Ediction, D. Van Nostrand Co., New York (1955), p 374.

(6) Cole, E. B., The Theory of Vibrations for Engineers, Third Edition, The Macmillan Co., New York (1957), p 323.

(7) Greenhill, A. G., "On the Strength of Shafting When Exposed Both to Torsion and to End Thrust", Proceedings of the Institute of Mechanical Engineers, pp 182-225 (1883).

(8) Den Hartog, J. P., Advanced Strength of Materials, McGraw-Hill Book Co., New York (1952), p 296.

(9) Morley, A., Strength of Materials, Eleventh Edition, Longmans, Green and Co., London (1954) p 488.

(10) Rosenberg, R. M., "The Influence of Axial Torques on the Critical Speeds of Uniform Shafts in Self-Aligning Bearings", Engineering Experiment Station Bulletin 128, University of Washington, p 88.

(11) Golomb, M., and Rosenberg, R. M., "Critical Speeds of Uniform Shafts Under Axial Torque", Proceedings First National Congress of Applied Mechanics, ASME, p 103.

(12) Southwell, R. V., and Gough, B. S., "On the Stability of a Rotating Shaft, Subjected Simultaneously to End Thrust and Twist", Report of the British Association for the Advancement of Science, pp 345-355 (1921).

(13) Stefano, N. M., "The Damping of the Critical Speeds of High Speed Shafting", Fairchild Aircraft Report Number RR-17 (November, 1955).

(14) Di Taranto, R. A., "A Blade-Vibration-Damping Device – Its Testing and a Preliminary Theory of Its Operation", Journal of Applied Mechanics, p 21 (March 1958).

(15) Meeting With Dr. Raymond Cohen, Purdue University.

(16) Ungar, E. E., and Hatch, D. K., "Your Selection Guide to High Damping Materials", Product Engineering (April 17, 1961).

RECORDS OF RESEARCH PROGRAM

Data upon which this report is based may be found in Battelle Laboratory Record Books Numbers: 18478, 18710, 18788, 18827, 18889, 18956, 18966, 18890, 18918, 18967, 18968, and 19274.

APPENDIX A

TEST-MACHINE CALIBRATION CURVES

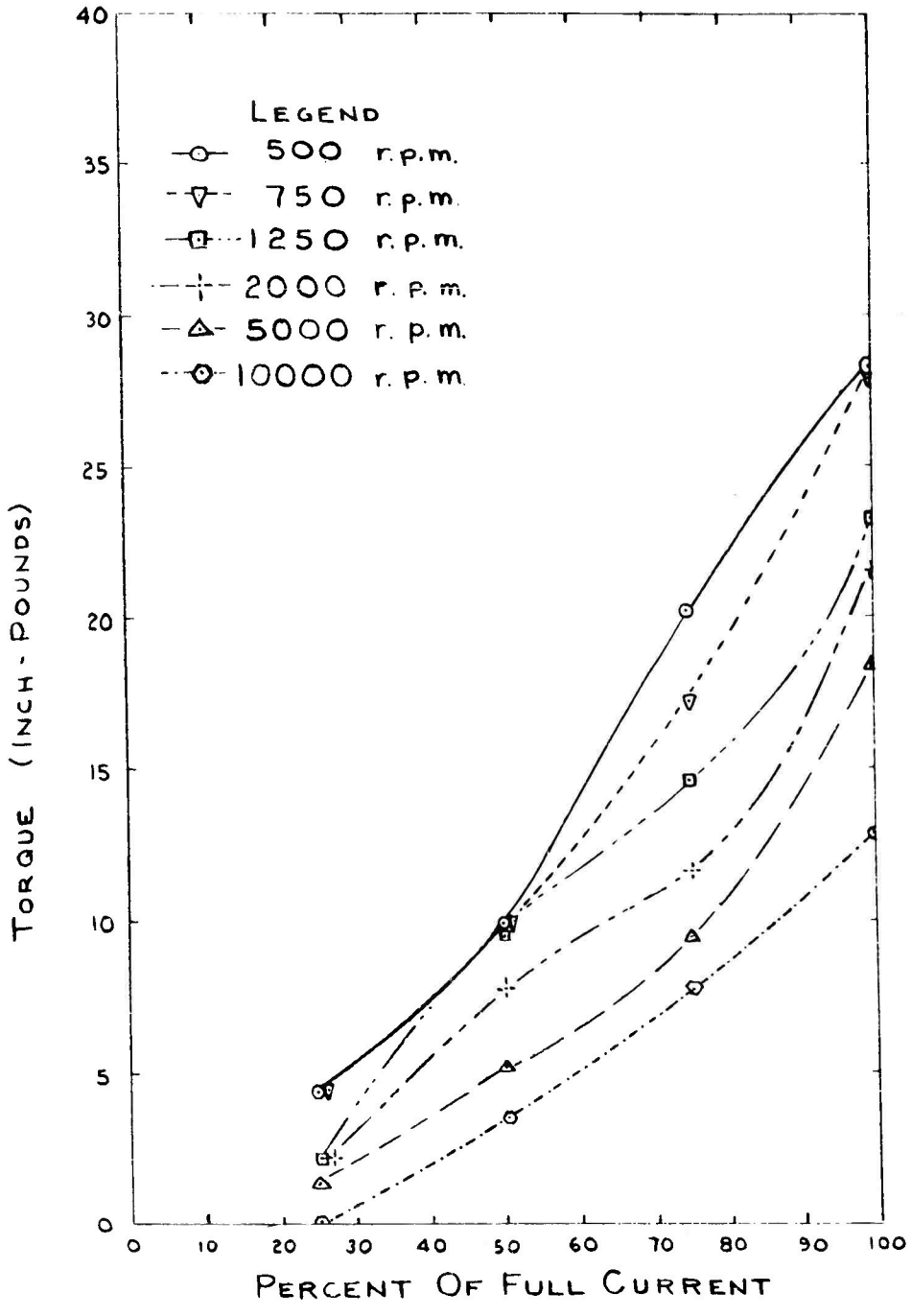

FIGURE 59. EDDY-CURRENT BRAKE TORQUE CALIBRATION – TORQUE VERSUS PER CENT OF FULL CURRENT

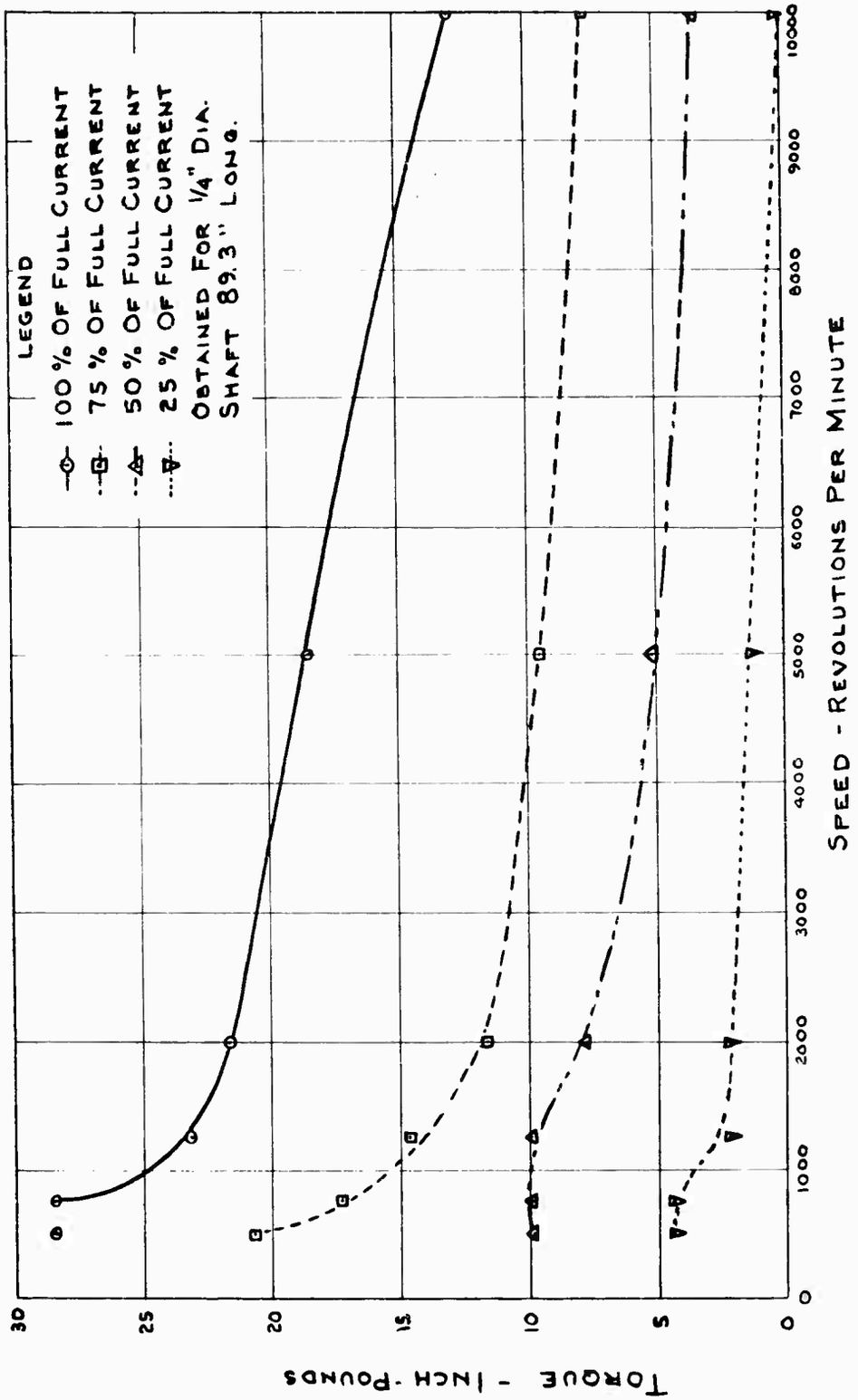

FIGURE 60. EDDY-CURRENT BRAKE TORQUE CALIBRATION - TORQUE VERSUS SPEED

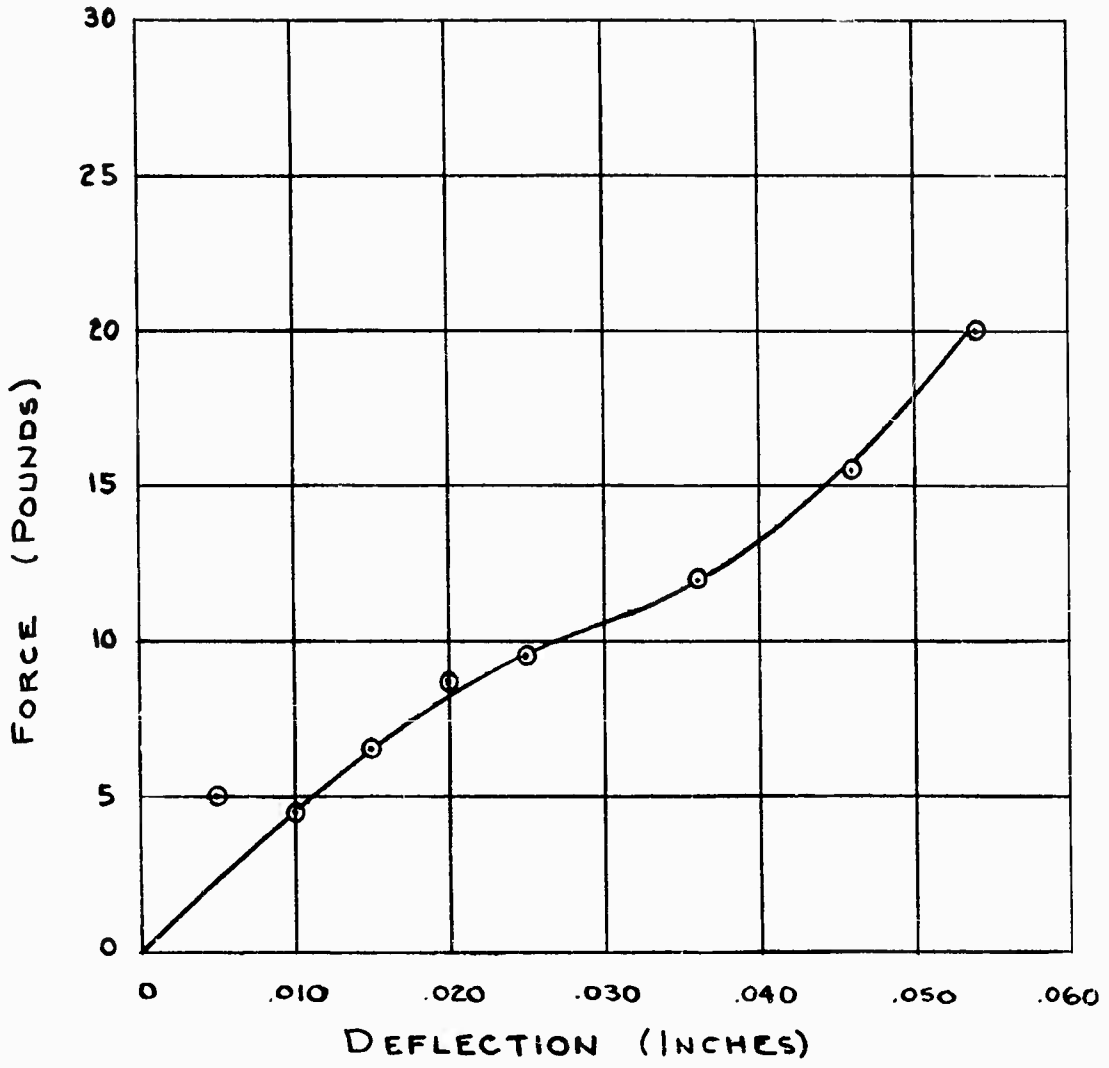

FIGURE 61. FORCE-DEFLECTION CURVE FOR BRAKE END SPINDLE

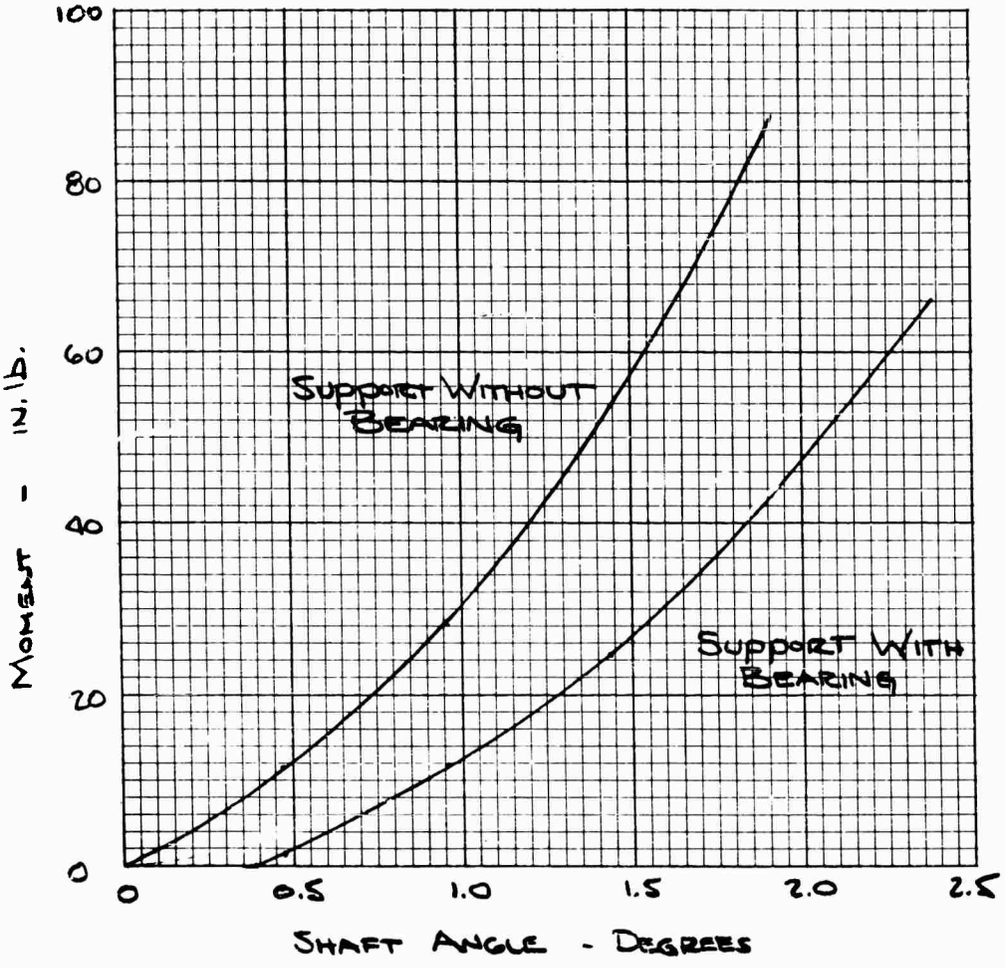

FIGURE 62. MOMENT RESTRAINT VERSUS SHAFT ANGLE AT POINT OF CONNECTION TO INTERMEDIATE SUPPORT

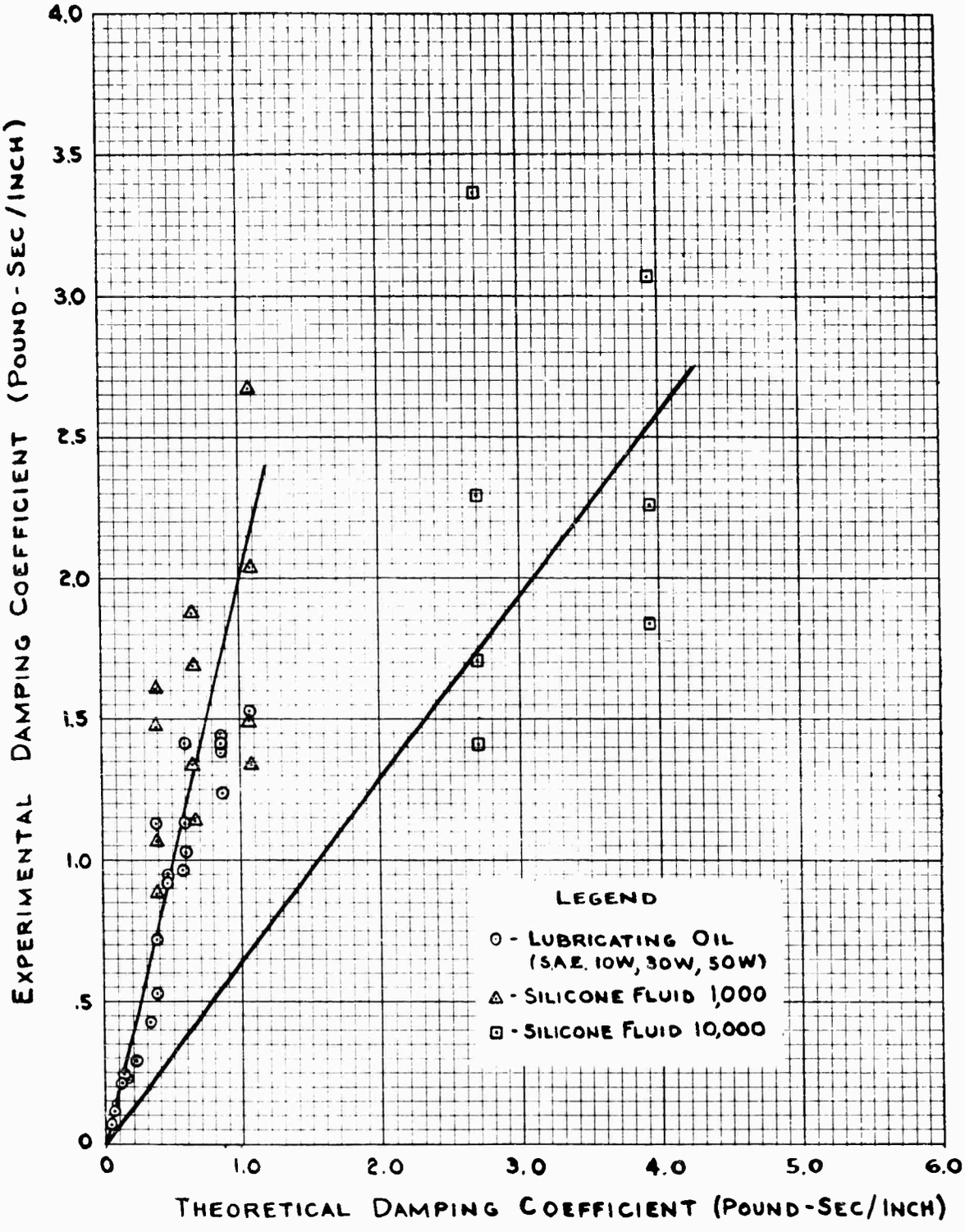

FIGURE 63. EXPERIMENTAL DAMPING COEFFICIENT VERSUS THEORETICAL DAMPING COEFFICIENT

APPENDIX B

TEST-MACHINE SPEED-GOVERNOR CIRCUITRY

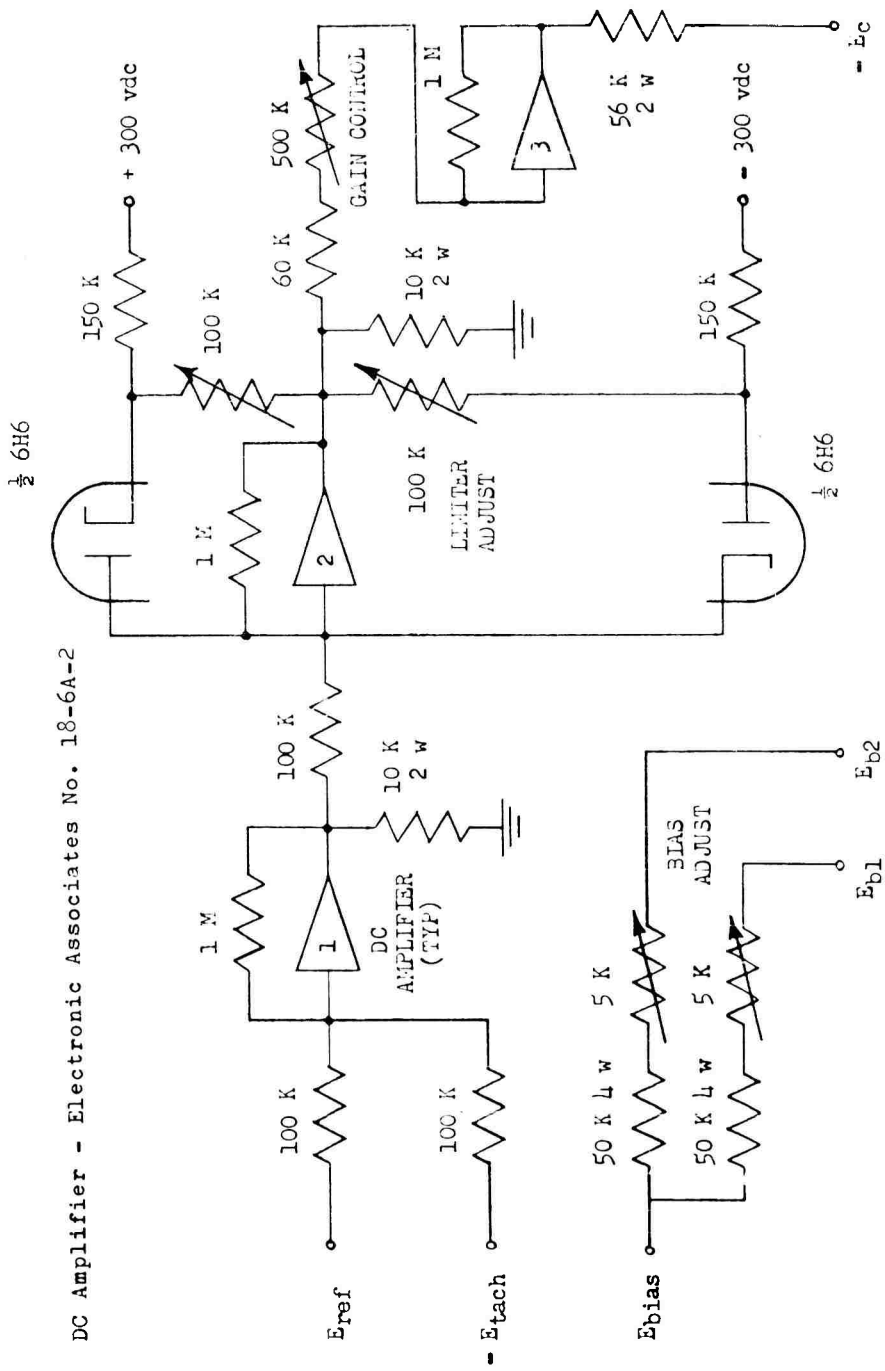

FIGURE 64. D-C AMPLIFIERS AND TERMINAL BOX SCHEMATIC

Magnetic Amplifier-
Control Division of Magnetics, Inc.
Reactor Assembly No. 3908-005

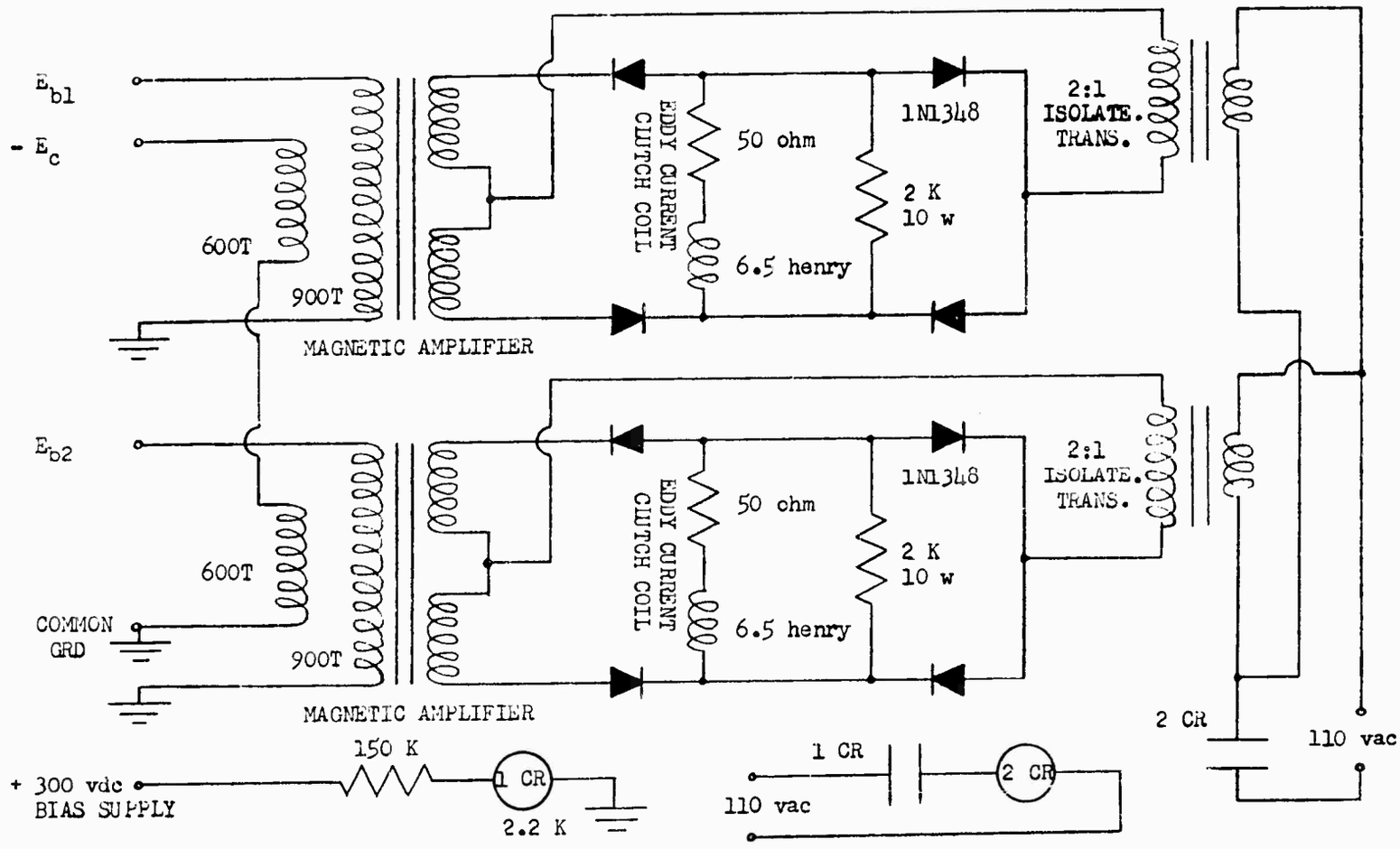

FIGURE 65. MAGNETIC AMPLIFIERS, RECTIFIERS, AND CLUTCH COIL SCHEMATIC

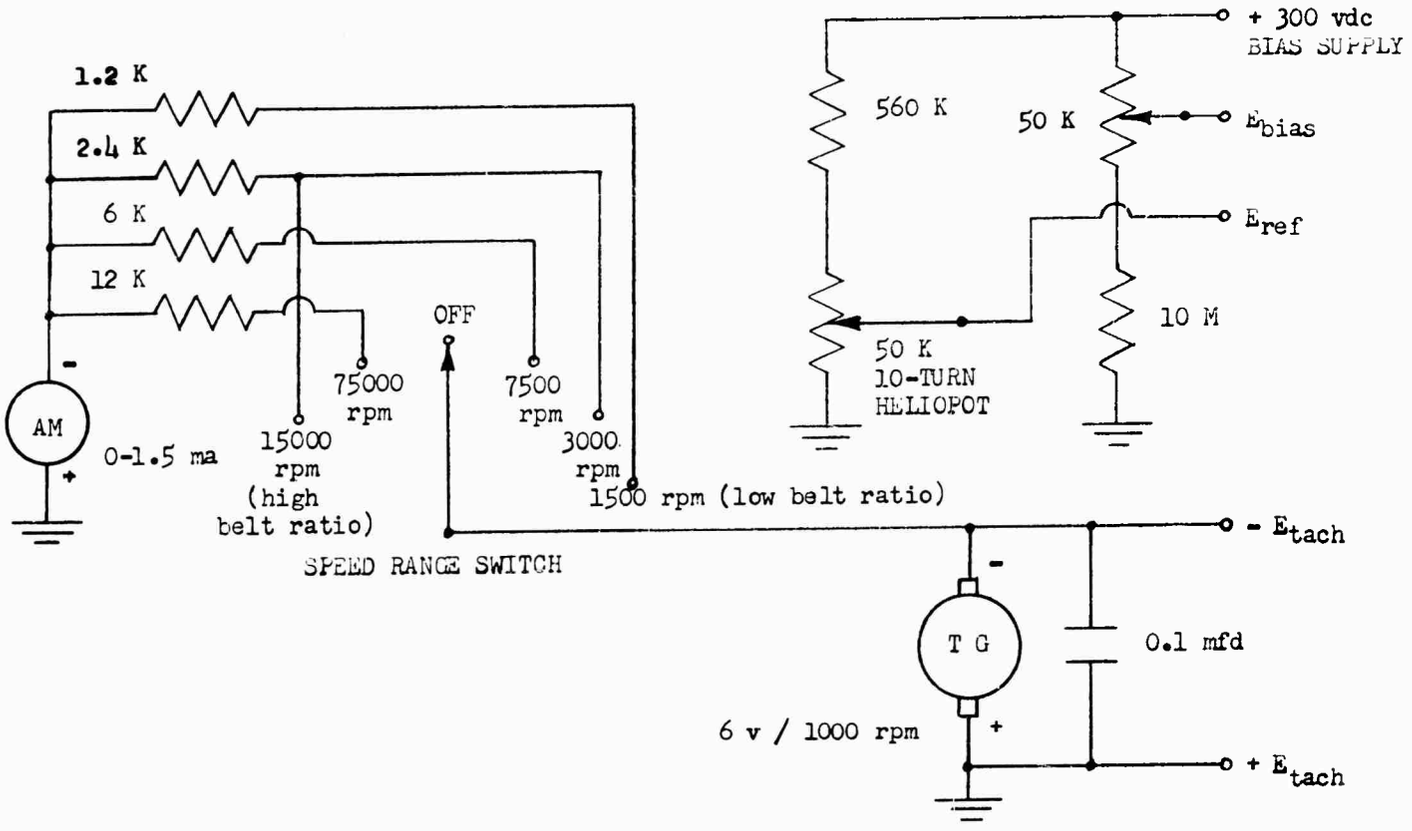

FIGURE 66. TACHOMETER AND PORTABLE SPEED-CONTROL BOX SCHEMATIC

APPENDIX C

ECCENTRICITIES OF SOME TYPICAL EXPERIMENTAL SHAFTS

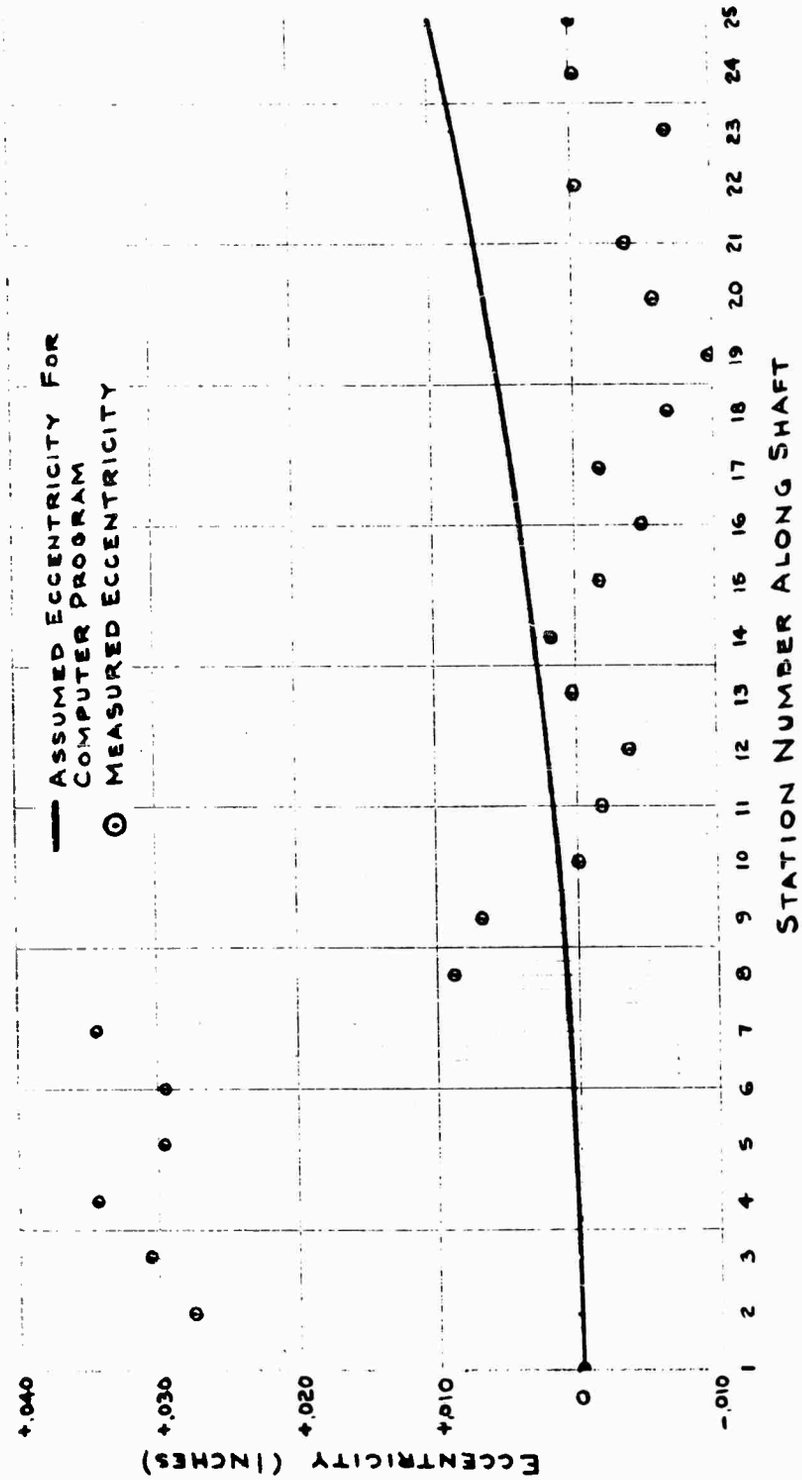

FIGURE 67. MEASURED AND ASSUMED MASS ECCENTRICITY FOR A 1/4-INCH-DIAMETER SHAFT 89.3 INCHES LONG

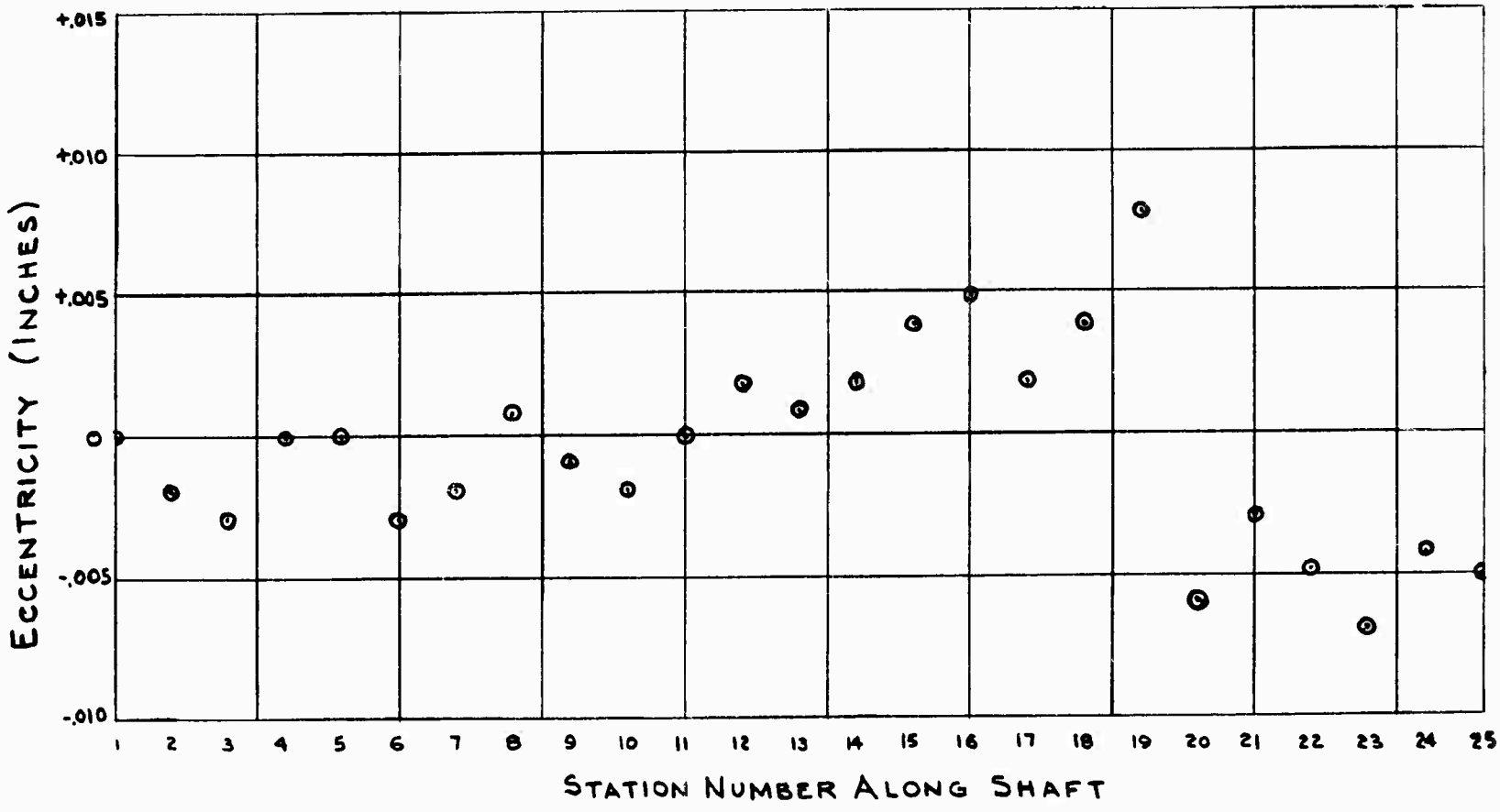

FIGURE 68. MASS ECCENTRICITY MEASURED IN PLANE OF MAXIMUM ECCENTRICITY FOR A 1/4-INCH-DIAMETER SHAFT 89.3 INCHES LONG

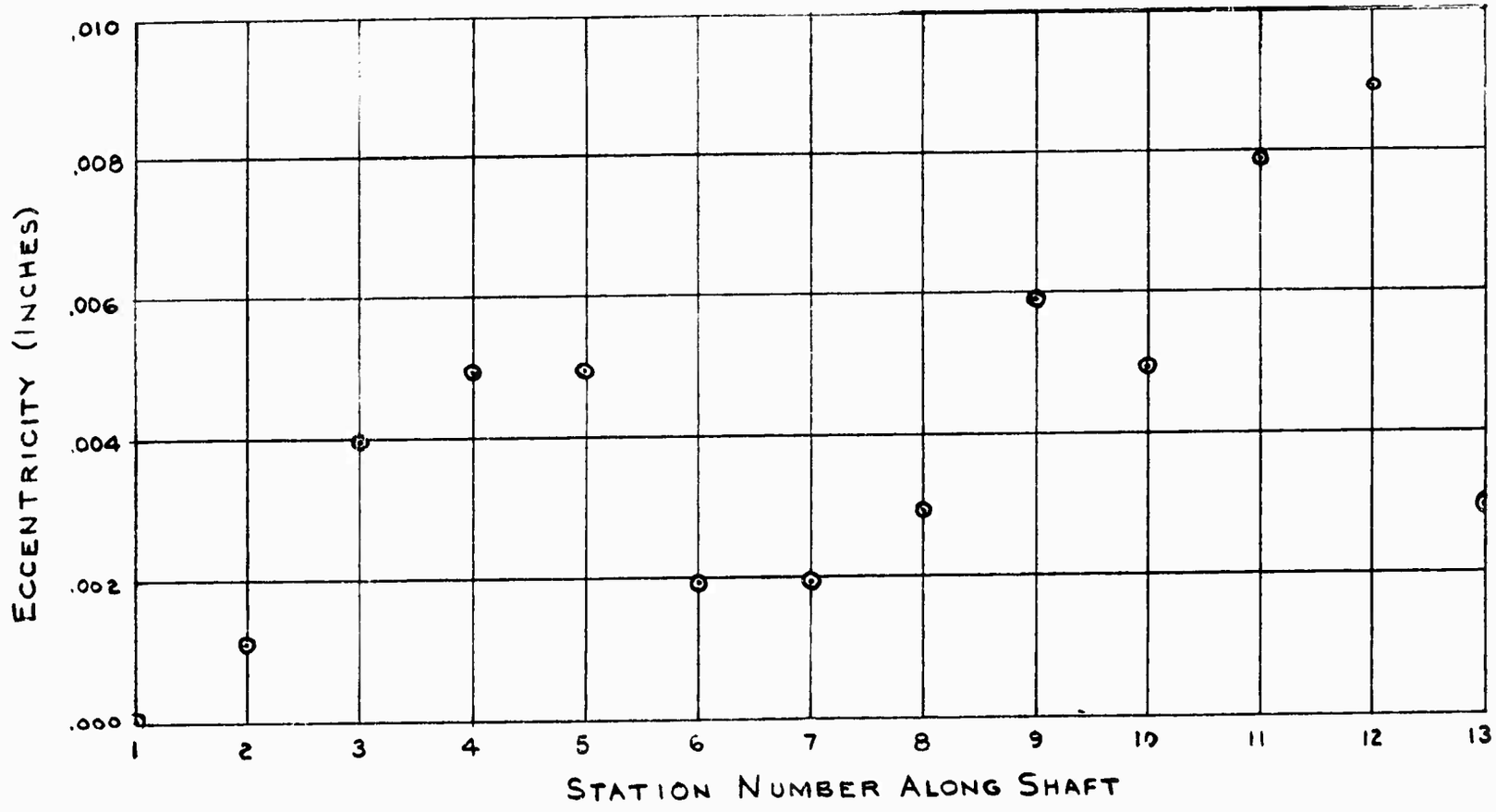

FIGURE 69. MASS ECCENTRICITY DETERMINED FROM MEASURED MAXIMUM AND MINIMUM VALUES FOR A 1/4-INCH-DIAMETER SHAFT 89.3 INCHES LONG

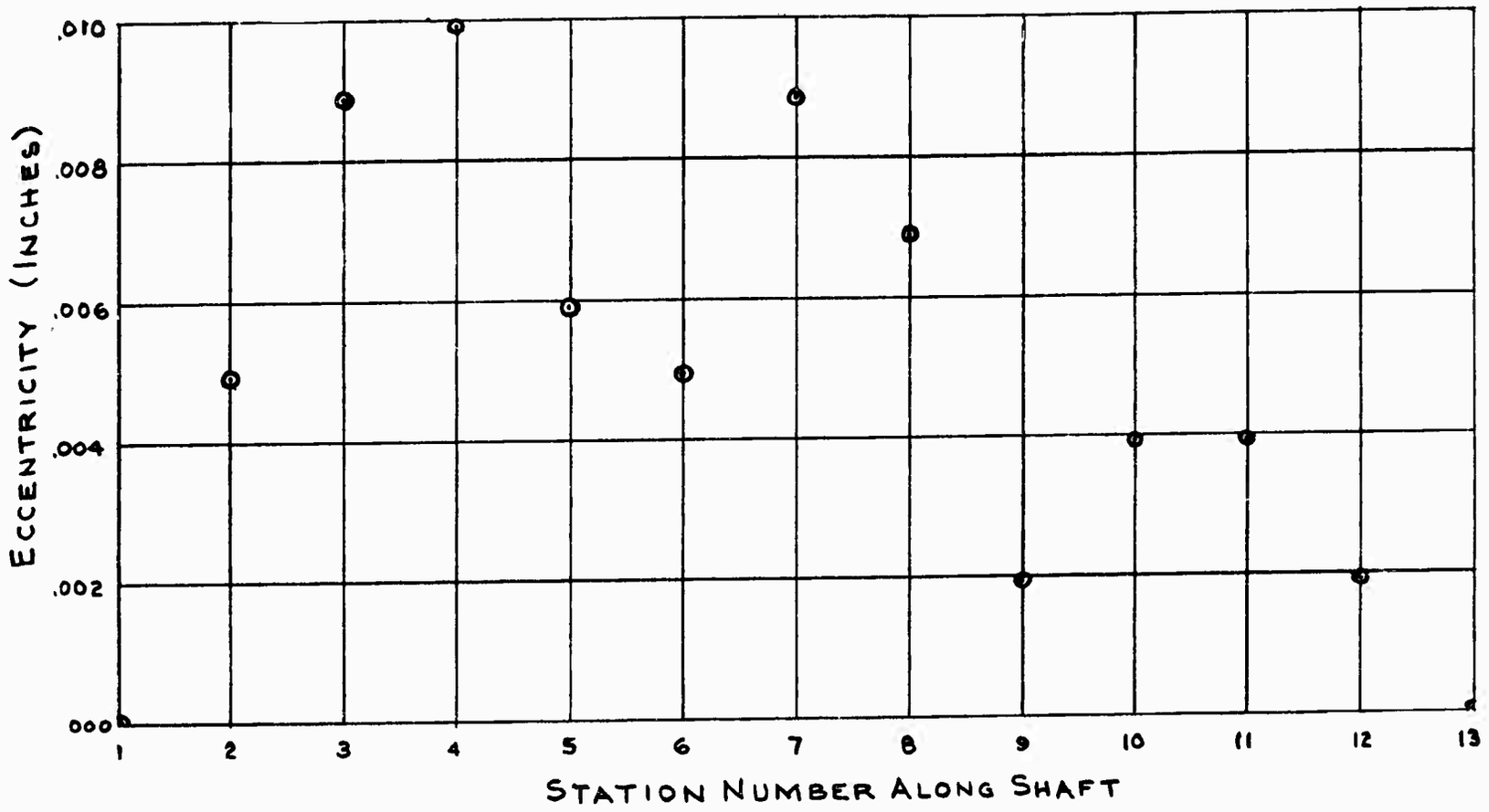

FIGURE 70. MASS ECCENTRICITY DETERMINED FROM MEASURED MAXIMUM AND MINIMUM VALUES FOR A 1/2-INCH-DIAMETER SHAFT 126.5 INCHES LONG

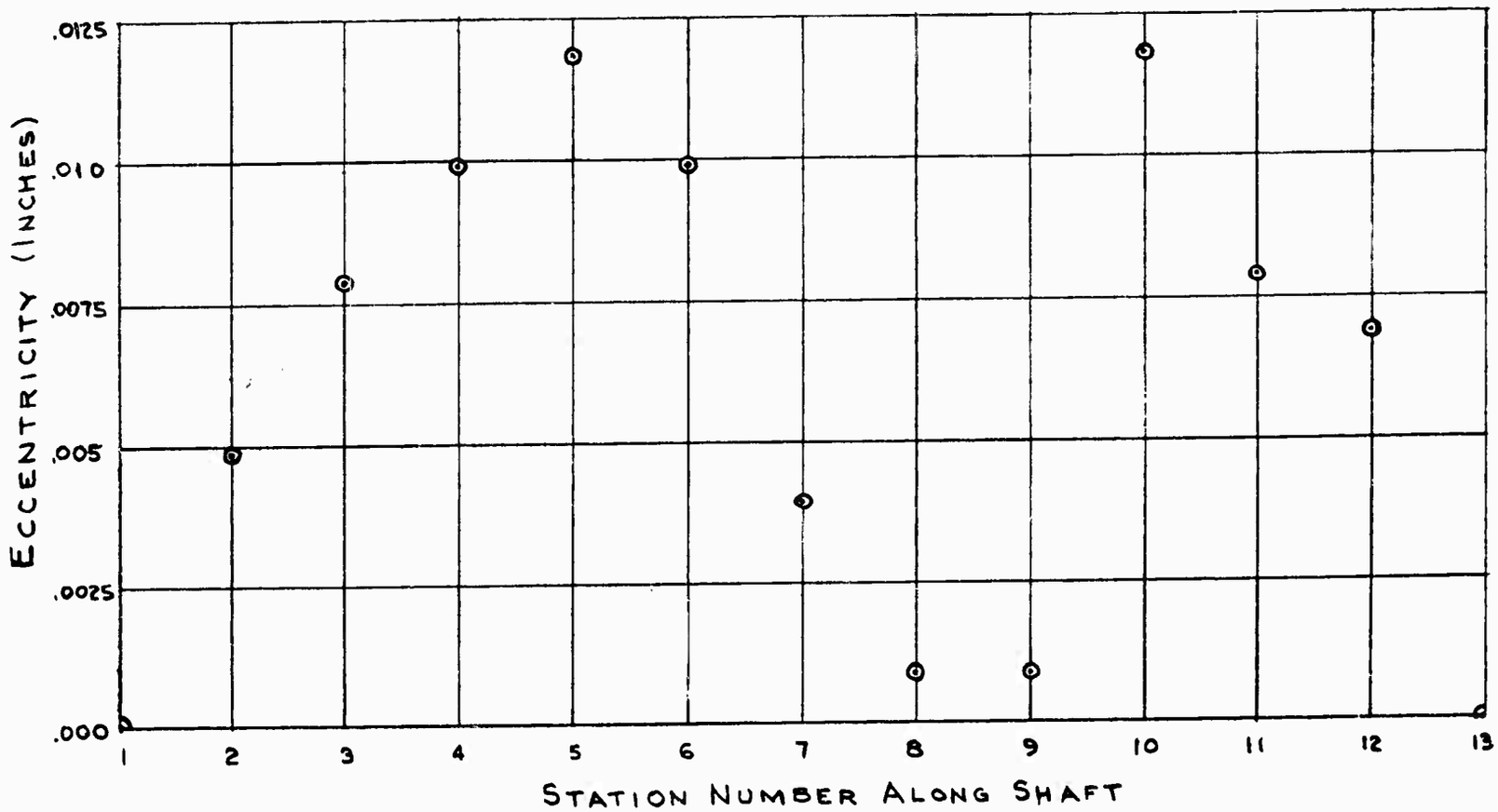

FIGURE 71. MASS ECCENTRICITY DETERMINED FROM MEASURED MAXIMUM AND MINIMUM VALUES FOR A 3/16-INCH-DIAMETER SHAFT 77.3 INCHES LONG

APPENDIX D

HYSTERESIS WHIRLING

One circumstance of interest in the experimental program was observation of hysteresis whirling. Although this type of shaft vibration occurred just once during the complete series of experiments, mention is included to complete the record.

Normal shaft vibrations occur at discrete speeds of shaft rotation. At these critical speeds the vibrating shaft whirls about its undeflected axis at the same rate as shaft rotation. In other words fibers at the surface of the shaft do not change length as rotation position changes.

Hysteresis whirling is a self-excited vibration caused by the internal damping of the shaft material. Whirl can occur during a wide speed range as long as shaft running speed is above the first critical. The frequency of the hysteresis whirl is the same as the shaft natural frequency. Since whirl frequency remains constant as shaft running speed changes, there is stress reversal in the shaft fibers.

The one instance of hysteresis whirl occurred with the shaft clamped at the ends and set up on three rigid evenly spaced intermediate supports. Whirling occurred continuously between 2570 rpm and 5000 rpm, the fourth speed of the first group of natural modes and the first speed of the second group of natural modes, respectively. Although shaft speed varied whirl frequency remained 2570 rpm.

Although hysteresis whirling produces stress reversals, it is not thought to be of importance. The phenomenon was observed only once in the numerous experiments conducted, and efforts to duplicate it at a later date proved futile. Also, it is our opinion that hysteresis whirling will not take place when damped supports are included in the system. Consequently the subject appears to be of little more than academic interest in the design of high-speed power-transmission shafts. Accounts of hysteresis whirling theory may be found in References (2) and (5).

Aeronautical Systems Division, Dir/Aeromechanics, Flight Accessories Lab, Wright-Patterson AFB, Ohio.
Rpt Nr ASD-TDR-62-728. Part I. DESIGN CRITERIA FOR HIGH-SPEED POWER-TRANSMISSION SHAFTS: Analysis of Critical Speed Effects and Damper Support Location. Final report, Jan 63, 161+ incl illus., tables, 16 refs.
Unclassified Report

Demonstrated successful operation of high-speed power-transmission shafts at and far above their first critical speeds has been achieved. A basic new analytical technique for the design and analysis of high-speed shafting has been developed using electrical

(over)

transmission line theory. Limited experimental work has shown the technique to predict successfully the damper parameters necessary to high-speed shaft operation. Equations relating full-scale and model shaft configurations to produce similar dynamic behavior have been formulated. The experimental application of torque on high-speed shafting did not change lateral critical speed. This is not in agreement with theory, which predicts a decrease in critical speed. Damping coatings applied continuously along the length of high-speed shafts controlled vibration amplitudes to a slight degree at the lowest critical speeds. At higher order criticals the coatings had no desirable effects.

1. Shafts
2. Power transmissions
I. Project 8128, Task 912802
II. Contract AF 33 (616)-8290
III. Battelle Memorial Institute, Columbus, Ohio
IV. R. G. Dubensky, C. D. Mellor, Jr., J. F. Vorhees
V. Secondary Rpt Nr 5-4869
VI. Aval fr CTS
VII. In ASTIA collection

Aeronautical Systems Division, Dir/Aeromechanics, Flight Accessories Lab, Wright-Patterson AFB, Ohio.
Rpt Nr ASD-TDR-62-728. Part I. DESIGN CRITERIA FOR HIGH-SPEED POWER-TRANSMISSION SHAFTS: Analysis of Critical Speed Effects and Damper Support Location. Final report, Jan 63, 161+ incl illus., tables, 16 refs.
Unclassified Report

Demonstrated successful operation of high-speed power-transmission shafts at and far above their first critical speeds has been achieved. A basic new analytical technique for the design and analysis of high-speed shafting has been developed using electrical

(over)

transmission line theory. Limited experimental work has shown the technique to predict successfully the damper parameters necessary to high-speed shaft operation. Equations relating full-scale and model shaft configurations to produce similar dynamic behavior have been formulated. The experimental application of torque on high-speed shafting did not change lateral critical speed. This is not in agreement with theory, which predicts a decrease in critical speed. Damping coatings applied continuously along the length of high-speed shafts controlled vibration amplitudes to a slight degree at the lowest critical speeds. At higher order criticals the coatings had no desirable effects.

1. Shafts
2. Power transmissions
I. Project 8128, Task 912802
II. Contract AF 33 (616)-8290
III. Battelle Memorial Institute, Columbus, Ohio
IV. R. G. Dubensky, C. D. Mellor, Jr., J. F. Vorhees
V. Secondary Rpt Nr 5-4869
VI. Aval fr CTS
VII. In ASTIA collection

Aeronautical Systems Division, Dir/Aeromechanics, Flight Accessories Lab, Wright-Patterson AFB, Ohio.
Rpt Nr ASD-TDR-62-728. Part I. DESIGN CRITERIA FOR HIGH-SPEED POWER-TRANSMISSION SHAFTS: Analysis of Critical Speed Effects and Damper Support Location. Final report, Jan 63, 161p incl illus., tables, 16 refs.

Unclassified Report

Repeated successful operation of high-speed power-transmission shafts at and far above their first critical speeds has been achieved. A basic new analytical technique for the design and analysis of high-speed shafting has been developed using electrical

(over)

transmission line theory. Limited experimental work has shown the technique to predict successfully the damper parameters necessary to high-speed shaft operation. Equations relating full-scale and model shaft configurations to produce similar dynamic behavior have been formulated. The experimental application of torque on high-speed shafting did not change lateral critical speed. This is not in agreement with theory, which predicts a decrease in critical speed. Damping coatings applied continuously along the length of high-speed shafts controlled vibration amplitudes to a slight degree at the lowest critical speeds. At higher order criticals the coatings had no desirable effects.

1. Shafts
2. Power transmissions
I. Project 8128, Task 812802
II. Contract AF 33 (616)-8290
III. Battelle Memorial Institute, Columbus, Ohio
IV. R. G. Dubensky, C. C. Mellor, Jr., J. F. Vorhees
V. Secondary Rpt Nr G-4869
VI. Aval fr CTs
VII. In ASTIA collection

Aeronautical Systems Division, Dir/Aeromechanics, Flight Accessories Lab, Wright-Patterson AFB, Ohio.
Rpt Nr ASD-TDR-62-728. Part I. DESIGN CRITERIA FOR HIGH-SPEED POWER-TRANSMISSION SHAFTS: Analysis of Critical Speed Effects and Damper Support Location. Final report, Jan 63, 161p incl illus., tables, 16 refs.

Unclassified Report

Repeated successful operation of high-speed power-transmission shafts at and far above their first critical speeds has been achieved. A basic new analytical technique for the design and analysis of high-speed shafting has been developed using electrical

(over)

transmission line theory. Limited experimental work has shown the technique to predict successfully the damper parameters necessary to high-speed shaft operation. Equations relating full-scale and model shaft configurations to produce similar dynamic behavior have been formulated. The experimental application of torque on high-speed shafting did not change lateral critical speed. This is not in agreement with theory, which predicts a decrease in critical speed. Damping coatings applied continuously along the length of high-speed shafts controlled vibration amplitudes to a slight degree at the lowest critical speeds. At higher order criticals the coatings had no desirable effects.

1. Shafts
2. Power transmissions
I. Project 8128, Task 812802
II. Contract AF 33 (616)-8290
III. Battelle Memorial Institute, Columbus, Ohio
IV. R. G. Dubensky, C. C. Mellor, Jr., J. F. Vorhees
V. Secondary Rpt Nr G-4869
VI. Aval fr CTs
VII. In ASTIA collection